Stony Brook University

OFFICIAL COPY

The official electronic file of this thesis or dissertation is maintained by the University Libraries on behalf of The Graduate School at Stony Brook University.

© All Rights Reserved by Author.

Computational Systems Analysis of Deterministic Pair Rule Gene Network and Stochastic Bicoid Morphogen Gradient in *Drosophila melanogaster*

A Dissertation Presented

by

Yu Feng Wu

to

The Graduate School

in Partial Fulfillment of the Requirements

for the Degree of

Doctor of Philosophy

in

Applied Mathematics and Statistics

Stony Brook University

May 2011

Stony Brook University
The Graduate School

Yu Feng Wu

We, the dissertation committee for the above candidate for the Doctor of Philosophy degree, hereby recommend acceptance of this dissertation.

Professor John Reinitz, Advisor
Department of Applied Mathematics & Statistics

Professor Alan Tucker, Committee Chairperson
Department of Applied Mathematics & Statistics

Professor Xiaolin Li, Committee Member
Department of Applied Mathematics & Statistics

Professor David Green, Committee Member
Department of Applied Mathematics & Statistics

Professor Jin Wang, Committee Member
Department of Applied Mathematics & Statistics

Professor J. Peter Gergen, Outside Committee Member
Department of Biochemistry & Cell Biology

This dissertation is accepted by the Graduate School.

Lawrence Martin
Dean of the Graduate School

Abstract of the Dissertation

Computational Systems Analysis of Deterministic Pair Rule Gene Network and Stochastic Bicoid Morphogen Gradient in *Drosophila melanogaster*

by

Yu Feng Wu

Doctor of Philosophy

in

Applied Mathematics and Statistics

Stony Brook University

2011

Computational systems biology is an emerging field built upon advances in biological experimentation, computational tools, and joint interdisciplinary efforts from physical sciences to engineering. In this thesis, I solve two important problems in the developmental genetics of *Drosophila melanogaster* by means of two different computational systems approaches, one stochastic and the other deterministic.

In the first problem I use exact simulations of a spatially extended Master Equation to analyze intrinsic fluctuations in the gradient of the Bicoid morphogen. These simulation results were in turn compared to quantitative experimental measurements of Bicoid levels performed in fixed tissue by immunostaining. We selected Bicoid for this study because different concentrations of Bicoid can trigger different developmental pathways and determine the cell fate. These properties define a morphogen gradient, and Bicoid is the best characterized such gradient at the molecular level. At the theoretical level, the Bicoid gradient is amenable to investigation by stochastic models because its formation can be described by the processes of diffusion and decay, with synthesis described by a boundary condition. I show that the intrinsic noise of Bicoid gradient is Poisson distributed. I demonstrate how experimental noise can be identified in the logarithm domain from single embryo analysis, and then separated from intrinsic noise in the normalized variance domain of an ensemble statistical analysis. I show how measurement sensitivity affects our observations, and how small amounts of rescaling noise can perturb the noise strength (Fano factor) observed. I demonstrate that the biological noise level in data can serve as a physical constraint for restricting the model's parameter space, and for predicting the Bicoid molecular number and variation range. I exhibit the predicted molecular number gradient together with measurement

effects, and make a comparison between conditions of higher and lower variance respectively.

In the second problem I use the gene circuit method, which uses coarse-grained chemical kinetic equations fitted by a data-driven optimization approach, to study the pattern formation regulatory control of pair-rule genes. The mathematical model, based on mechanisms of protein synthesis, decay and diffusion, captures the essential control of the size, location and timing of the pair-rule stripe formation process. The gene circuits were optimized in modular manner, such that two classes of circuits were found by systematically and combinatorially reducing optimization constraints. Three major circuits were selected for detailed dynamical regulatory analysis. These circuits include 5 cross-regulating pair rule genes (*eve*, *h*, *run*, *ftz*, *odd*) and 7 external input gap and maternal genes (*bcd*, *cad*, *hb*, *Kr*, *gt*, *kni*, *tll*). The circuits model a period of time from cycle 13 to gastrulation in a spatial region covering 44 nuclei from 35% to 78% EL, extending from *eve* stripe 2 to the stripe 7 anterior border. The biological conclusions were drawn in 6 levels based on a consensus among circuits and literature. The regulatory phasing analysis examines a simple phasing rule based on stripe formation and shifting constraints. The major predictions include gap gene activation on *odd*, with exceptionally strong consensus among all circuits. The complete lack of understanding and literature reference for gap gene regulations of *odd* illustrates the significance and advantage of the computational system approach. Other systems conclusions include that all gap gene regulation on *eve* is repressive, while all gap gene regulation on *odd* is activating. *h* has the least gap gene inputs in the circuits, which is strong contradiction to literature.

Contents

List of Figures

List of Tables

Acknowledgments

I thank my advisor, John Reinitz, for this opportunity and support to explore the unknown frontier in systems biology, with two outstanding projects. If I have seen further it is only by standing on the shoulders of giants. This work can not be done without the pioneer work he has done at the systems level in developing the gene circuit method, and being the authority on both the theoretical and experimental levels. I also thank him for personal assistance in my difficult time, and for all the guidance and patience along the way. The earlier days when we were still stuck in the basement of math tower, drawing master equations on the board is good memory.

This work can not be done without the strong support from my family. I thank my parents for their understanding to let me pursue the unknown journey and focus on my work without going home for 7 years. I also thank their full financial support in the first and last year, and support in my difficult times.

I thank Manu for his crucial help and friendship in my early phase of research. I thank Alexander Spirov, Johannes Jaeger, Ekaterina Myasnikova, Svetlana Surkova, Kostya Kozlov, and David Fange for their specific help on my research. I thank the members of the Reinitz Lab (Zhihao, Lena, Ahram, Carlos, Varsha, Jean) for their daily company and help in the earlier days before moving to Chicago. I also thank Jean Cadet for the heavy lifting.

I also want to thank the support from my friends, without them I wouldn't be able to survive this far on my own. I thank Steve and Joanne for their hospitality, sharing and company. I thank Xu Yan for all the listening. I thank Tong Fei for taking me to the hospital. I thank Claire and Stephen for all the good times.

I thank God for his company on this lonely journey when there is no one else around.

Chapter 1

Introduction

In the first chapter of this dissertation, I introduce the context of this work in a new and booming field of computational systems biology. I then introduce the context of computational systems approach and the two major problems I am going to solve in *Drosophila* embryo development: one to understand the stochastic signature and molecular processes underlying the gradient of the morphogen Bicoid gradient observed from immunostaining; the other to understand pair rule pattern formation regulatory mechanism and control in the segmentation gene network using a specific computational systems approach called gene circuit method.

1.1 Computational Systems Biology

Advances in the last 30 years in the field of biological science, including developmental genetics, have made tremendous progress in identifying large number of genes involved in regulating physiological and developmental processes. The basic regulatory mechanisms underlying these genes have also been recognized

to a larger extent to date. This exciting progress has made it possible for theoreticians and physical scientists to join in order to build more sophisticated quantitative and predictive models, and to pursue further complexity and meet higher challenges.

Theoreticians and physical scientists began to build fundamental mathematical models at many different levels, from molecular to orgasmic and subsets of regulatory processes. Theoretical efforts in the field of *Drosophila* embryo development include Reinitz et al. (1995); Reinitz and Sharp (1995); Reinitz et al. (1998); Sánchez and Thieffry (2003); Gursky et al. (2004). As the field of theoretical and computational biology grow, we have more computational and informational tools at hand, also more quantitative and predictive models evolving regulatory processes at many different levels and scales. This exciting progress has made possible for systems scientists and engineers to join, to begin putting the pieces together toward a more integrative and higher level systems view of the complex organism.

The timing for engineering has always relied on the maturation of tools and basic science. Today is an exciting time with the advances of life science, and the development of experimental and computational tools. The core of systems biology can be defined as systems level reverse engineering of biology. Systems scientists and engineers introduce a new concept of viewing biology as an engineering system, like a jet airplane, into the field of life science. Systems level engineering is about how millions of parts and devices, divided into subsystems, can function together in harmony. The huge amount of data is familiar to engineers, for example those designing control systems for modern passenger jets (Csete and Doyle, 2002). The paradigm shifted from the reductionist approach of identifying components, to a rigorous integration approach

of recognizing emergent system properties. Systems work involves bridging the gap between experimental biology and computational tools. A counterpart of systems biology is another emerging field of synthetic biology. The core of synthetic biology can be defined as systems level forward engineering of biology. Together systems and synthetic biology constitutes a new engineering field of molecular bioengineering, which is fundamentally different from traditional bioengineering in terms of scope, methodology, and applications.

In summary, computational systems biology is a collaboration of all three levels of work, from the experimental level, to the computational level, and to the systems engineering level (Fig. 1.1). Systems biology is also defined in a broad sense as a whole-listic (holistic), inter-disciplinary, approach to understanding complex interactions in biology (Kitano, 2002). One major objective is the modeling and discovery of emergent properties of system behaviors.

1.2 Computational Systems Approach

In the early phase of biology research, our knowledge about one particular organism and its regulatory processes is extremely limited, hence we start from drawing simple interaction diagrams and mechanism cartoons to analyze the experimental results. Later on in the research phase our knowledge grows and the diagram becomes more complicated, for example in the study of segmentation gene network (Jaynes and Fujioka, 2004), the simple diagrammatic analysis becomes limited. It is difficult to provide further insight into the complex system and to keep pace with the rapidly increasing experimental information. There were increasing amounts of complex and controversial experimental results, such as mutant and ectopic gene expression patterns,

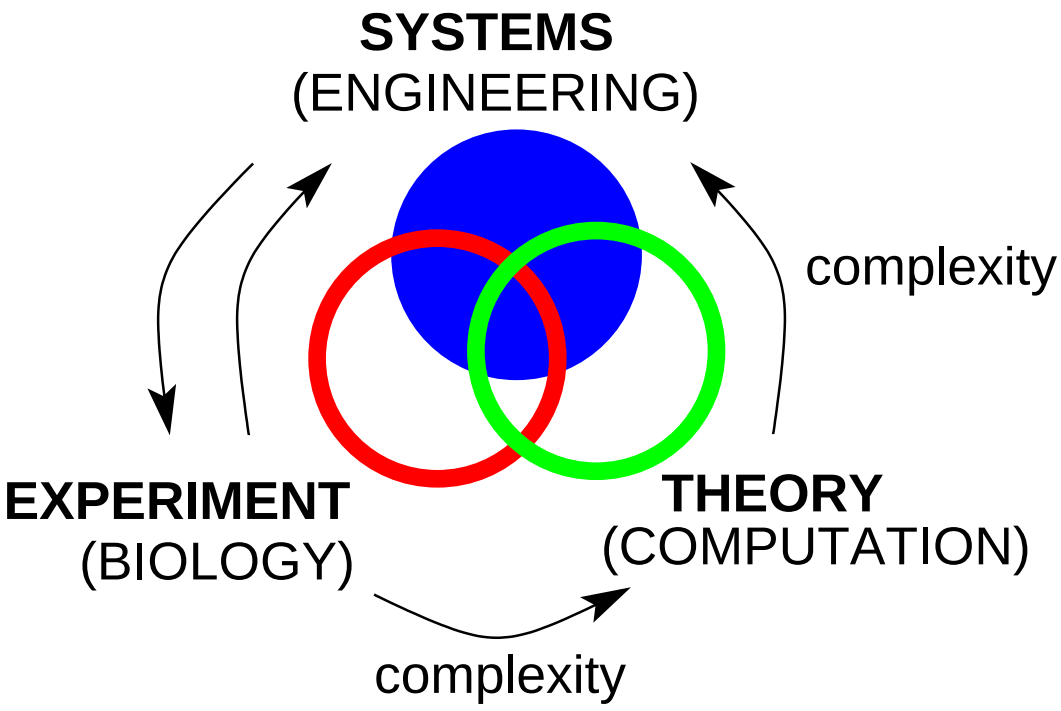

Figure 1.1: The computational systems approach is a collaboration of three levels of work, from the experimental level, to the computational and theoretical level, and to the systems engineering level, where the engineering refers to reverse engineering within the context of systems biology. The arrows indicate the information flow. The involvement and demand for theory and systems level work depends on the increase of systems complexity. One important aspect of this approach in reaching ultimate success is the ability to continuously refine and improve the model understanding through communications and feedbacks from the experimental level.

accumulating in the literature waiting to be resolved. Hence the development of a more sophisticated quantitative model is necessary to move forward.

Model development and theoretical analysis usually starts from smaller and simpler systems. For example the *bicoid* morphogen gradient is the most well studied system on the morphogen field before full theoretical characterization of the entire segmentation gene network (Gregor et al., 2005, 2007b,a; Houchmandzadeh et al., 2002, 2005). In Reinitz and Sharp (1995) and Jaeger et al. (2004b), full dynamical models were developed to analyze an upstream subset of the segmentation gene network called gap genes, and also to delineate the stripe formation mechanism of pair-rule gene *eve* regulated by gap genes. These earlier theoretical efforts, in developing and applying the gene circuit method, are the foundation and precursor for this dissertation work on pair rule genes.

When the system is smaller or simpler, the systems level work is usually trivial or obscured. Theoreticians can usually develop computational tools and perform analysis directly. However as we move into understanding more complex and larger scale systems (such as the downstream pair rule genes), and toward a more integrative view of the whole organism (or the whole morphogenetic field), a systems level challenge arises, which is usually manifested in a form of work that is more intensive than theoreticians can carry out alone or are trained for. These are the works that require specific dedication and rigorous approaches from systems engineers, or systems biologists.

The systems engineers are specialized in model production, optimization, simulation, analysis, representation, integration, abstraction, organization, processing and design. The complex and creative problem solving skills involve applications of multiple mathematical, computational and informational

tool sets. Abstraction involves taking out information instead of generating information. Integration involves putting together the system instead of breaking down the system. These are the fundamental strategies and guidelines on the contrary to the other two levels of research phase in the computational systems approach (Fig. 1.1). The model or hypothesis evaluation also requires integration of literature, through information extraction and text mining. It also requires communication with experimentalists, and other interdisciplinary fields, in getting feedbacks such as experimental results for model refinement.

The end product of systems work should be the simplest form of integration and conclusions drawn from both computational and experimental results, on the complex systems operation. For example in this dissertation, a simple regulatory map of pair rule regulation is generated similar to the cartoon diagrams drawn in the early research phase of experimental biology, the difference however is two more levels of work underneath, from theoretical to systems level (Fig. 1.1). We can characterize systems engineering with a quote from Leonardo Da Vinci: "Simplicity is the ultimate sophistication." And elegance is a form of simplicity with sophistication underneath.

To summarize (Fig. 1.1), the core of experimental work involves developing hypotheses, implementing genetic modifications and carrying out quantitative measurements. When the complexity of regulatory processes and interactions rises, quantitative modeling and theoretical analysis are required. The core of theoretical work involves development of mathematical models, computational, visualization and informational tools, and the creation of online databases and repositories for sharing data and models. When the complexity and scale of the regulatory processes rise further, systems level analysis is required. The core of systems level work involves abstraction and integration.

There is also work done at the interface of the 3 levels of computational systems approach (Fig. 1.1). For example there is high-throughput work (measurement and genetic manipulations) done at the interface of the experimental and systems level. There is model development and refinement work done at the interface of the experimental and theoretical level, which involves both bench experiments and numerical programming. There are also computational tools designed with systems level consideration, for example the gene circuit model used in this dissertation has built-in systems level abstraction, which is work done at the interface of both theoretical and systems level. Hence systems work is done by both experimental biologists and theoreticians, and there are also researchers who specialize in both hard-core experiments and computation.

The core identity of systems level scientists and engineers, or systems biologists, are rather new. One reason is because there are no pre-existing training program, and the context of this unique field is continually developing and being defined, depending on the advancement of both experimental and computational tool space and the biological problems to be solved. Only until very recently there are few undergraduate and graduate department of systems biology or systems engineering being established, with specifically designed inter-disciplinary curriculum. Working at the frontier of systems biology also involve higher risk taking and losing depth of skills from the experimental and theoretical level. This dissertation work is fully dedicated to help define the context of the systems level work in computational systems biology.

In the following section I introduce the context of *Drosophila* embryo development, which is the background of the two main problems I am going to solve using the computational systems approach.

1.3 *Drosophila* Embryogenesis and Segmentation

Many animals, from worms and insects to human beings, have segmented body patterns. The fruit fly *Drosophila melanogaster* is the most thoroughly studied example of a segmented animal today. The adult body of fruit fly *Drosophila melanogaster* has fourteen repeating units of segments. There are three segments in the head (mandibular, maxillary, and labial), three in the thorax (T1–T3) and eight in the abdomen (A1–A8) (Lawrence, 1992). Each segment has a different identity specified by the Hox genes (Gilbert and Sarkar, 2000). The *Drosophila* embryo have a roughly ellipsoid shape, with an antero-posterior (A–P)—axis approximately 500 µm, and a dorso-ventral (D–V)—axis about 150 µm.

The life cycle of the fly consists of an embryogenesis stage (∼1 day), a larval stage (∼4 days), a pupal stage (∼4 days), and adulthood (∼60 days) (Campos-Ortega and Hartenstein, 1985). The body segments are determined during the first three hours of embryo development (Gilbert, 2003). This stage is further subdivided by 13 synchronous nuclear divisions (mitoses), into 13 cleavage cycles. Cleavage cycle n is defined as the time between the end of mitosis $n-1$, and the end of mitosis n. No tissue growth is involved during this process (Campos-Ortega and Hartenstein, 1985). Nuclear divisions happen in rapid succession without formation of cell membranes between the nuclei (i.e. the embryo is a syncytium). Each nucleus is surrounded by an island of cytoplasm stabilized by the cytoskeleton. Thus, the embryo may be thought of as a collection of cells not delimited by membranes.

Cleavage cycles 1–9 last only about 10 minutes (min) each. Following the

ninth division, a majority of the nuclei migrate to the periphery of the embryo, leaving behind the yolk cells. The embryo is then a blastoderm, and remains in this state for four more cleavage cycles (10–14A). The part of cycle 14 before the onset of gastrulation is called cleavage cycle 14A. Between cleavage cycles 10 and 13, cell-cycle length increases from 10 to about 15–20 min, while cycle 14A is approximately 50 min long (Foe and Alberts, 1983; Foe, 1989). Cleavage cycles 10–14A (covering approximately $1\frac{1}{2}$ hrs before the onset of gastrulation) are called the syncytial blastoderm stage of development. During the middle of cycle 14A, the cell membrane begins to invaginate; this is called cellularization. During late cycle 14A, the embryo undergoes the midblastula transition (Renzis et al., 2007), when maternal mRNA and proteins are degraded, and zygotic transcription increases many fold. At the completion of cellularization (end of cycle 14A), the embryo undergoes a complex set of tissue movements, called gastrulation, that leads to the formation of the germ layers.

1.4 Segmentation Gene Network

Mutagenesis screens saturating the entire genome of *Drosophila melanogaster* with mutations have led to the isolation of an almost complete set of genes involved in segment determination (Nüsslein-Volhard and Wieschaus, 1980; Nüsslein-Volhard et al., 1984; Jürgens et al., 1984; Wieschaus et al., 1984; Schüpbach and Wieschaus, 1986; Nüsslein-Volhard et al., 1987; Ingham, 1988). Based on their mutant phenotypes, these genes have been subdivided into four hierarchical layers from *maternal coordinate genes* (Nüsslein-Volhard et al., 1987) to *zygotic gap genes, pair-rule genes*, and *segment-polarity genes* (Nüsslein-Volhard and Wieschaus, 1980). Analyses of genetic epistasis have revealed the

hierarchical regulatory layers (Akam, 1987; Ingham, 1988), and defined genes in higher layers regulate genes in lower layers, but not *vice versa*. In addition, there is cross-regulation among genes in the same hierarchical layer. Most of the maternal coordinate and zygotic segmentation genes encode transcription factors and in turn regulate the expression of zygotic segmentation genes through transcriptional control.

Maternal coordinate genes are expressed from the mother's genome. The proteins of the maternal coordinate genes form monotonic gradients from mRNA deposited in the egg by the mother. There are three groups of maternal genes (Schüpbach and Wieschaus, 1986). The anterior group specifies the formation of the head and thorax, the posterior group specifies the abdomen, and the terminal group specifies the terminal regions. The anterior system acts primarily through *bcd*, and is independent of the posterior system and the terminal system in the presumptive germ band of the embryo (Driever and Nüsslein-Volhard, 1988a). *bcd* sets up another maternal gradient in the syncytium, *caudal* (Mlodzik et al., 1985), by repressing its translation (Rivera-Pomar et al., 1996). *cad* is expressed both maternally and zygotically, and embryos lacking both maternal and zygotic gene function show segment deletions like the gap genes (Macdonald and Struhl, 1986). Another gene with both maternal and zygotic activity is the gap gene *hunchback (hb)* (Tautz et al., 1987; Tautz, 1988). The posterior maternal system acts through *hb* by repressing the translation of its uniformly distributed maternal mRNA (Irish et al., 1989; Lehmann and Nüsslein-Volhard, 1991). The terminal system acts through two genes with gap gene-like activity, *tailless (tll)* and *huckebein (hkb)* (Casanova, 1990; Reinitz and Levine, 1990; Duffy and Perrimon, 1994).

The gap genes are expressed in broad overlapping domains, and are among

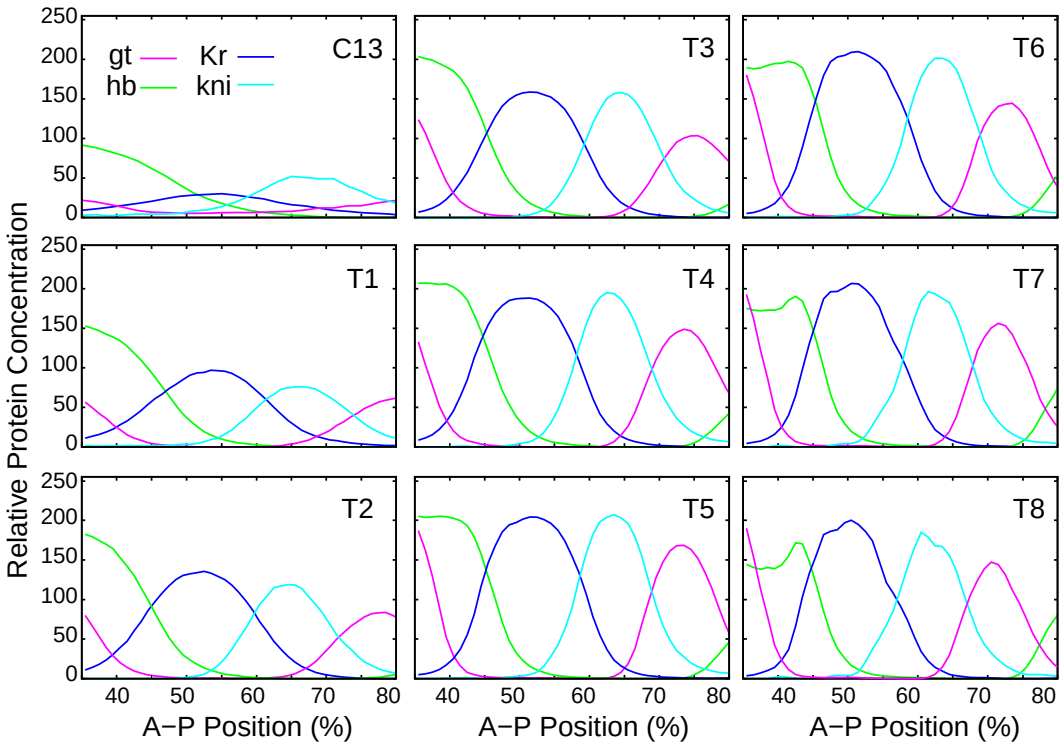

Figure 1.2: The averaged gap gene expression patterns of *hb*, *Kr*, *gt* and *kni* from cycle 13 to the onset of gastrulation. *cad* and *tll* are not included. Source of data is from FlyEx (http://flyex.uchicago.edu/flyex/). The relative protein concentrations (fluorescence intensity observed from immunostaining) are on a relative scale from 0 to 255. The spatial index is in percentage embryo length. Times and gene products are shown in the key.

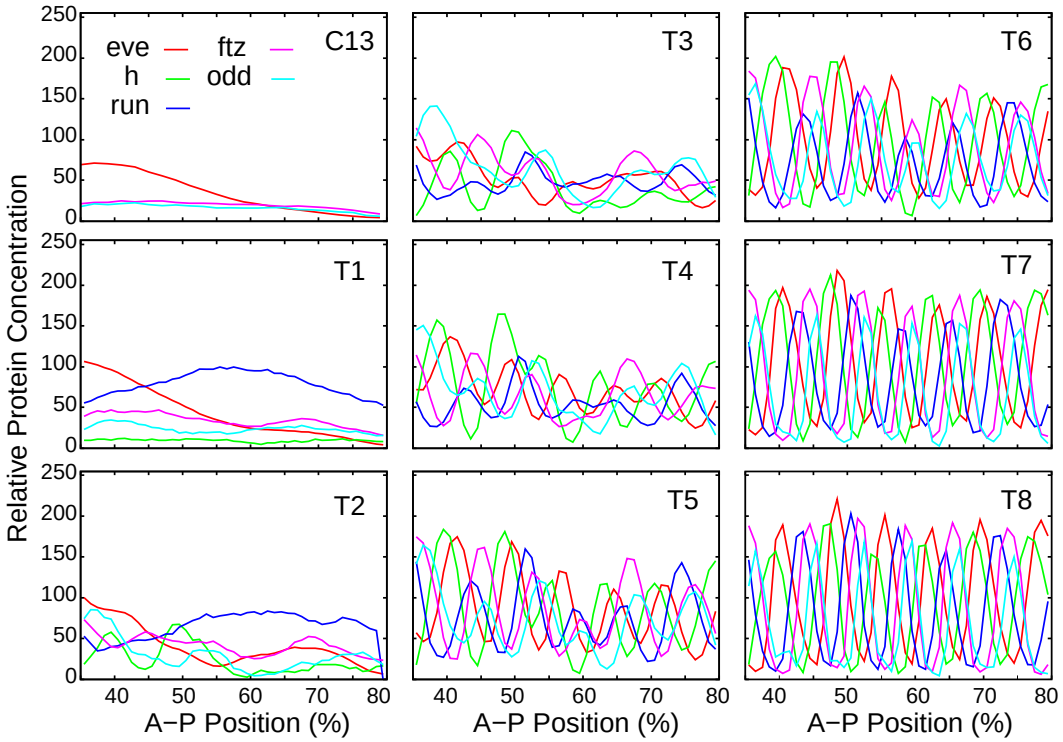

Figure 1.3: The average expression patterns of the five pair-rule genes *eve*, *h*, *run*, *ftz* and *odd* from cycle 13 to the onset of gastrulation. The source of data, time classes, and labeling of axes are the same as in Fig. 1.2.

the first zygotic targets of the maternal transcription factors (Gaul and Jäckle, 1987; Tautz, 1988; Driever and Nüsslein-Volhard, 1989; Hoch et al., 1991; Eldon and Pirrotta, 1991; Kraut and Levine, 1991; Rivera-Pomar et al., 1995). Mutations in gap genes (*hunchback (hb)*, *Krüppel (Kr)*, *knirps (kni)* and *giant (gt)*) lead to deletion of contiguous blocks of segments. Gap gene expression is initiated during cleavage cycles 10–12 (Knipple et al., 1985; Tautz et al., 1987; Rothe et al., 1989; Mohler et al., 1989; Pritchard and Schubiger, 1996). By the late blastoderm stage, the protein products of these genes are present in one or two sharply defined, broad, overlapping domains (Figure 1.2). All gap genes encode transcription factors (Tautz et al., 1987; Tautz, 1988; Bender et al., 1988; Preiss et al., 1985; Nauber et al., 1988; Mohler et al., 1989), which in combination with maternal factors regulate the establishment of the periodic pair-rule expression patterns (Figure 1.3), which are the focus of the second part of this thesis.

The pair rule genes then control the initiation of the expression of segment-polarity genes at the onset of gastrulation, which become expressed in 14 narrow stripes and form the segmental prepattern (Lawrence, 1981; Martinez-Arias and Lawrence, 1985; Ingham and Martinez-Arias, 1992). Two of the segment-polarity genes are *engrailed* (*en*) and *wingless* (*wg*) (Jaynes and Fujioka, 2004; Swantek and Gergen, 2004).

Now we consider the pair-rule genes and maternal *bicoid* gradient in more detail. This thesis will look at two questions at the frontiers of Bcd (Gregor et al., 2005, 2007b,a; Houchmandzadeh et al., 2002, 2005; Driever and Nüsslein-Volhard, 1988b,a) and pair-rule studies (Surkova et al., 2008; Jaynes and Fujioka, 2004; Howard and Ingham, 1986; Goto et al., 1989; Harding et al., 1989; Howard and Struhl, 1990; Warrior and Levine, 1990; Gutjahr et al., 1993;

Klingler and Gergen, 1993; Yu and Pick, 1995), based on previous foundational work on gap genes (Reinitz et al., 1995; Reinitz and Sharp, 1995; Reinitz et al., 1998; Jaeger et al., 2004b,a; Manu et al., 2009, 2008).

1.5 Stochastic Fluctuations of the Morphogen Gradient

Recently considerable attention has been given to the characterization and understanding of intrinsic molecular noise in biological systems (Bar-Even et al., 2006; Blake et al., 2003; Elowitz et al., 2002; Newman et al., 2006; Pedraza and van Oudenaarden, 2005; Raj et al., 2006; Rosenfeld et al., 2005; Volfson et al., 2006). Nearly all of these studies were performed using *in vivo* fluorescent reporters in single cell systems. In multicellular organisms, however, most quantitative gene expression data are obtained from fixed tissues. Examples of such data for the *Drosophila* segmentation system are contained in the FlyEx database, which provides spatiotemporal data on the expression of developmental segmentation genes (Poustelnikova et al., 2004). These data on protein expression levels are at cellular resolution and were obtained by means of immunofluorescence histochemistry and confocal scanning microscopy. At a large spatial scale, expression levels in these embryos form expression domains characteristic for each gene, but smaller fluctuations in expression levels between adjacent nuclei appear random. In this thesis, I investigate the question of whether these fluctuations are a consequence of intrinsic molecular noise or stem from some type of measurement uncertainty. These alternatives are, of course, not mutually exclusive. A complicating factor in separating the above alternatives is that each one involves an unknown chemical mechanism.

Intrinsic noise will have a major contribution from fluctuations in the rate of initiation of transcription, but the chemical mechanisms underlying this process in multicellular organisms are very poorly understood. Measurement uncertainty can stem from chemical causes such as fluctuations in the number of primary and secondary antibody molecules which bind to proteins in the fixed embryo. The chemistry of this process is also very poorly understood. If observations could be made on a process whose fluctuation properties could be reliably predicted by a numerical model, comparison of the predicted fluctuations with those observed will provide critical information for distinguishing whether observed nucleus-to-nucleus variations are a consequence of intrinsic biological noise or merely fluctuations arising from the staining procedure.

An excellent candidate for a process with predictable fluctuation properties is one that involves only diffusion and first order decay. There is good evidence that the formation of the protein gradient of the morphogen Bicoid (Bcd) takes place by means of these two processes. Bcd protein is distributed in an exponential profile along the anterior-posterior (A-P) axis with higher concentrations towards the anterior (Driever and Nüsslein-Volhard, 1988b; Struhl et al., 1989). This gradient forms by translation of maternally deposited mRNA at the anterior pole of the embryo, and the synthesized protein spreads through the syncytial embryo by diffusion accompanied by decay (Houchmandzadeh et al., 2005). The observed exponential profile corresponds to a solution of Fick's equation for a substance undergoing first order decay and diffusing from a point source in one dimension, and hence it is reasonable to suppose that the reaction-diffusion mechanism leading to the formation of the gradient is reasonably well understood. Quantitative observations of this gradient in fixed tissue exhibit small fluctuations between neighboring nuclei, while the overall

exponential profile ensures that such fluctuations can be monitored over a wide range of concentrations which extend to the lower limits of detectability.

The intrinsic fluctuations of the Bcd gradient will be well described by a stochastic Reaction-Diffusion Master Equation (RDME). Such equations typically do not have analytic solutions and are usually solved by running repeated stochastic simulations. A well known simulation algorithm due to Gillespie (Gillespie, 1976, 1977) performs an exact simulation of the Chemical Master Equation for a well mixed system. This method has been extended to spatially distributed systems by Elf and others (Elf and Ehrenberg, 2004; Fange and Elf, 2006). These authors divide the spatially extended system into a series of subvolumes that are small enough to be regarded as well mixed. In each subvolume chemical reactions are simulated by Gillespie's algorithm, while diffusion between subvolumes is treated as a first order reaction. In fact, an exact solution can be found (Lepzelter and Wang, 2008) for the simple Bcd morphogen gradient model. This study appeared after the work reported in chapter 2 was published and did not include a comparison with experimental observations.

In this first part of this thesis, I compare the results of such simulations to data in order to discover whether or not the data is sufficiently accurate as to exhibit the signature of a simple stochastic process. Stochastic processes underlying biological regulation can in general form complex patterns as a result of the reaction network, and for this reason a full consideration of 3 dimensional geometry is often necessary (Elf and Ehrenberg, 2004). In the case considered here fluctuations occur passively in the course of diffusion and the statistical signature that I seek is independent of detailed geometry. For these reasons, I chose to model a 1 dimensional system.

1.6 Pair-Rule Genes

Pair-rule genes are the second major focus of this thesis. Pair-rule genes, including *even-skipped (eve), hairy (h), runt (run), fushi-tarazu (ftz), odd-skipped (odd), sloppy-paired (slp), paired (prd)*, are expressed in overlapping stripes with double segment periodicity. The initial striped patterns of all pair-rule genes, with the exception of *slp* and *prd*, are quite similar, containing seven stripes each 3-4 nuclei wide. They differ primarily with respect to the location of the stripes relative to one another. For example, the pair-rule genes *eve* and *ftz* are expressed in seven roughly complementary stripes overlapping at their edges along the anterior-posterior axis of the embryo trunk. Surkova et al. (2008) has the most thoroughly published study of pair-rule patterns. It also introduced the shifts of pair-rule stripes, which will be covered later in this thesis. Mutations in pair-rule genes affect every other segment. Although the null mutant phenotype of *eve* is more complicated, involving the complete loss of segmental patterns (Frasch et al., 1988), and *slp* may also be considered as a segment-polarity gene (Swantek and Gergen, 2004).

The control of pair rule genes expression are in fact very poorly understood. The earlier research phase of experimental work (Jaynes and Fujioka, 2004; Howard and Ingham, 1986; Goto et al., 1989; Harding et al., 1989; Howard and Struhl, 1990; Warrior and Levine, 1990; Gutjahr et al., 1993; Klingler and Gergen, 1993; Yu and Pick, 1995) has revealed the daunting complexity underlying pair rule stripe formation. For example, even when a gap gene directly controls a pair-rule gene, it affects multiple stripes. In *kni-* mutant embryos (Frasch and Levine, 1987), *eve* stripes 4, 5 and 6 are essentially absent, and it is unclear whether *kni* affects each border the same way. There are also indirect effects involved on other gap genes. In *Kr* mutant embryos (Frasch

and Levine, 1987), *eve* stripes 2-6 are disrupted, presumably stripes 5 and 6 are disrupted because *kni* is absent (Pankratz et al., 1989). In *hb* mutant embryos (Carroll and Vavra, 1989), *Kr* expression expands anteriorly (Jäckle et al., 1986; Gaul et al., 1987), while *h* expression shifts anteriorly and is lost within the new anterior *Kr* domain (Carroll et al., 1988). The combined action from pair rule cross regulation, in addition to gap and maternal genes, further complicates the regulatory understanding. The current experimental work has generated large amount of complex mutant gene expression patterns and other, ectopic, experimental results accumulating in the literature, mostly left without a sound explanation or clear resolution.

All of the systems complexity, resulting in obscurity and frustration in the literature, demands a computational systems approach. In the earlier phase of theoretical work (Bodnar, 1997; Sánchez and Thieffry, 2003), the computational approaches implemented are at a much simplified, Boolean, level. These Boolean models, under much restricted systems assumptions, though capture some qualitative behavior and provide the first leg up into the computational systems analysis of complex network, are still far from realistic dynamical analysis application. Another foundational but more advanced coarse-grained computational modeling approach being developed is called the "gene circuit method", which is used in this thesis and introduced in the next section. This reverse-engineered dynamical neural network model can reproduce more realistic pattern formation dynamics, and has been applied on smaller subsets of upstream gap genes (Jaeger et al., 2004b,a; Manu et al., 2009, 2008), and on *eve* stripe formation study (Reinitz et al., 1995; Reinitz and Sharp, 1995; Reinitz et al., 1998). Based on these foundational work and better resolution gene expression data, I can apply and extend this gene circuit method to ana-

lyze the more complex pair rule gene network, and show that the more robust model also demands more extensive systems level analysis.

Overall, the absence of realistic model and systems level understanding on pair rule genes in the literature signifies the intellectual importance of this thesis to advance into computational systems approach.

1.7 Gene Circuits

In this thesis I use a specific computational systems approach, called the gene circuit method (Mjolsness et al., 1991; Reinitz and Sharp, 1995, 1996), to study the pattern formation of pair-rule genes. The aim is to reverse engineer the pair-rule gene regulatory network from a dynamical systems perspective, in particular to clarify the pair-rule gene cross regulations. More specifically, to understand how gene regulatory interactions control the size, location and timing of the pair-rule stripe formation processes. The quantitative model obtained in this project can help support and elucidate genetic experimental results. Mutant simulations of such models may further help interpret observations from mutant experimental studies. The dynamical model can further serve as a learning and designing tool for predicting and guiding future experiments.

The gene circuit method is a data-driven mathematical modeling approach that aims to extract information about dynamical regulatory interactions between transcription factors from given gene expression patterns. Gene circuits are gene network models based on coarse-grained kinetic equations. Model parameters are not fixed *a priori*, but rather obtained using numerical optimization of model output against a large dataset of gene expression patterns.

Therefore dynamical analysis of such circuits obtained can provide novel insights into the biological regulation underlying the gene expression data. The model demonstrates how intricate balances between synthesis, decay and diffusion among segmentation genes establish the complex pair-rule segmentation patterns, and how balances of linear regulatory inputs from different genes determine the dynamics of synthesis for each gene at different spatial positions of nuclei. The pattern dynamics of segmentation morphogens have been characterized in our databases (Surkova et al., 2008; Myasnikova et al., 2001), and a clear understanding of how such dynamical patterns are regulated by specific gene interactions is the aim of the gene circuit method.

The gene circuit method has been applied on subsets of the gap gene regulatory network (Jaeger et al., 2004b,a; Sharp and Reinitz, 1998; Gursky et al., 2004) and *eve* regulation by gap genes (Reinitz and Sharp, 1995; Reinitz et al., 1995, 1998). These works which develop the gene circuit tools are the foundation for this thesis. And this thesis serves as an extension to complete this method toward applications on more complicated and integrative systems of the morphogen field, and addresses the systems level challenges that arise in achieving the goal.

In the next chapter I will introduce in more detail the theoretical and experimental level of work in the gene circuit method, and demonstrate the systems level challenges, work that is required, when facing more complex systems.

Chapter 2

Master Equation Simulation Analysis of Immunostained Bicoid Morphogen Gradient

This chapter is now published on BMC Systems Biology 1:52 (2007). Here I will start with technical account in materials and methods, followed by detailed analysis in its application.

2.1 Materials and Methods

2.1.1 Stochastic simulations

The Bcd gradient was modeled in one dimension with 101 homogeneous cubic subvolumes indexed by j from 0 to 100. Each subvolume has sides of length $l = 5\mu$m and volume $\Delta = l^3$. These dimensions were chosen in light of those of actual *Drosophila* embryos, which are 500μm long. The subvolume

dimensions are very close to those of blastoderm nuclei. In the first subvolume ($j = 0$), corresponding to the anterior pole of the embryo, I assume a zero-order synthesis reaction of Bcd molecules with constant rate J (molecules/s), representing the translation of a maternally deposited and localized stationary mRNA pool after egg deposition. The jth subvolume contains n_j molecules of Bcd, which are the state variables of the model. I take initial conditions to be $n_j = 0 \ \forall \ j$. Diffusion of Bcd is modeled as a first-order elementary reaction for the exchange of molecules between neighboring subvolumes with rate constant $k = D/l^2$ seconds^{-1}, where D is the effective Fickian diffusion constant. Dispersed degradation (decay) of Bcd is also modeled as a first-order reaction in all subvolumes with rate constant ω (seconds^{-1}).

Thus, for subvolumes $j = 0$ to $j = 100$, the RDME is given by

$$\begin{aligned}\frac{d\,P(\{n_j\},t)}{d\,t} &= (\mathbb{E}_0^{-1} - 1)JP(\{n_j\},t) \\ &+ \sum_{j=0}^{100}[\,(\mathbb{E}_j^{+1} - 1)\,\omega\,n_j\,P(\{n_j\},t)\,] \\ &+ \sum_{j=0}^{100}\sum_{k\in\{j\pm1\}}[\,(\mathbb{E}_j^{+1}\mathbb{E}_k^{-1} - 1)\,(\frac{D}{l^2})\,n_j\,P(\{n_j\},t)\,],\end{aligned} \tag{2.1}$$

where $P(\{n_j\},t)$ is the joint probability of state vector

$$\{n_j\} = [n_0, \ldots, n_j, \ldots, n_{100}].$$

The state operator, $\mathbb{E}$, is defined so that $\mathbb{E}_j^{\pm1} f(..., n_j, ...) = f(..., n_j \pm 1, ...)$. Monte Carlo simulations of the behavior of this equation were obtained using the publicly available software MesoRD 0.2.0 (Hattne et al., 2005). MesoRD can automatically generate a stochastic or deterministic model from its input, and I make use of this feature in the work presented here. In the deterministic limit, mesoRD calculates the mean trajectory $\langle\widehat{n}_j\rangle(t)$. By converting the initial

values of the state variables into concentrations, mesoRD can then integrate the classical Reaction-Diffusion Rate Equation (RDRE) given by

$$\frac{\partial C}{\partial t} = D\frac{\partial^2 C}{\partial x^2} - \omega C, \tag{2.2}$$

where C is the concentration of Bcd. Boundary conditions are given by $\partial_x C|_{x=0} = -J/\Delta$ and $\partial_x C|_{x=500} = 0$. The steady-state solution can be well approximated by $C(x) \approx a\exp(-x/\lambda)$, where $a = (J/\Delta)\lambda$ and $\lambda = \sqrt{(D/\omega)}$. MesoRD solves the deterministic equation by fixing the mesh size at the number of subvolumes chosen for the stochastic system. I used the built-in Euler solver with a stepsize of 0.001 second after verifying that these settings yielded stable and accurate solutions. Further analysis of simulations in comparison with quantitative immunostained data were performed in MATLAB.

2.1.2 Quantitative data

I used Bcd protein expression data from cleavage cycle 13 (Foe and Alberts, 1983) that were downloaded from the FlyEx database (Poustelnikova et al., 2004) `http://urchin.spbcas.ru/flyex`. In FlyEx, confocal scans have been processed into tables containing average fluorescence levels in each nucleus (Janssens et al., 2005); these fluorescence levels are linearly proportional to Bcd concentration (Gregor et al., 2007b), and hence to molecular number. Data were taken from the central 10% strip along the A-P axis with their D-V coordinate suppressed, and normalized to remove the non-specific background (Myasnikova et al., 2005). The gradient is in a steady state at cycle 13 (Surkova et al., 2008). For quantitative analysis and comparison with the model, I pooled data into 5μm 1D intervals to compare with the 5μm subvolumes of the stochastic model. For certain purposes I considered a 17 member subset

of embryos among which the inverse of the spatial exponential coefficient λ varied by less than 1%. This subset contained embryos ab15, cb2, ac1, hz8, ac6, iz4, cb19, ac2, cb31, iz15, ac16, ad18, ad31, hz30, be1, hz33 and as22 from FlyEx.

In the following, I first characterize the statistical properties of random variations in expression level between adjacent nuclei of individual embryos and compare them to the results of stochastic simulations. At the level of single embryos, I do not find a clear signature of stochastic processes in the data, but the need to separate spatially changing mean expression values from their variation limits the amount of statistical information that can be obtained from individual embryos. To address this problem, I consider ensembles of embryos, both over the whole dataset and over a restricted subset with low embryo-to-embryo variation.

In order to interpret these data, I introduce a stochastic model of the immunostaining procedure. I denote all random variables in this article with an upper hat but write a specific value without the hat. Thus, for example, $\widehat{n}_j$ denotes a random variable for the number of Bcd molecules in subvolume j, while n_j denotes a particular value of this variable.

2.2 Single embryo analysis in the logarithmic domain

I find that the Bcd profiles of individual embryos observed by immunostaining (Fig. 2.1A) are exponential, as previously reported (Driever and Nüsslein-Volhard, 1988a; Houchmandzadeh et al., 2002; Surkova et al., 2008). This profile strongly supports the model of an effective Fickian diffusion which gives

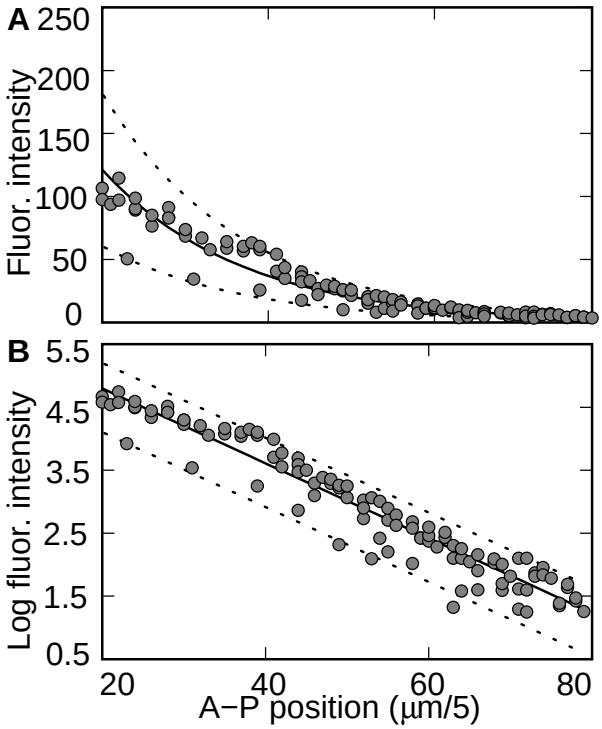

Figure 2.1: (**A**) The spatial index j (μm/5) is the index of 5μm bins. The fluorescence intensity I_j (circles) were fit to an exponential $\mathrm{F}[I_j] = a\,\exp(-j/\lambda)$ (solid line) with two scaling index lines $1.5\mathrm{F}[I_j]$ and $0.5\mathrm{F}[I_j]$ (dashed). The fluorescence intensity were then converted into log scale in panel (**B**).

an exponential decay solution at steady state (Gregor et al., 2005; Houchmandzadeh et al., 2005). Each embryo contains a collection of observations of expression (with variation) I_j, and the observed properties of the exponential gradient will depend on the data through a function F embodying the least squares fitting procedure such that

$$\mathrm{F}\,[\,I_j\,] = a\,\exp(-j/\lambda). \tag{2.3}$$

The residuals of the exponential vary from embryo to embryo in our data. In logarithmic coordinates the size of the residuals is independent of j for the anterior portion of the embryo, and in certain embryos (such as ms18) the size of the residuals is completely independent of j (Fig. 2.1B). For these embryos, the residuals are well described by

$$\ln(I_j) = \ln(a) - j/\lambda + \widehat{W}, \tag{2.4}$$

where $\widehat{W}$ is an unknown random variable independent of j, so that the variance of $\ln(I_j)$ is equal to the variance of $\widehat{W}$.

2.2.1 Intrinsic noise is insufficient

In order to understand whether the observed characteristic variation is a consequence of intrinsic fluctuations in Bcd molecular number, I performed stochastic simulations of an RDME which describes the time evolution of the Bcd gradient and compared them to data. I imagine the observed intensity I_j to be a particular value of the random variable $\widehat{I}_j$. I further suppose that the random variable $\widehat{I}_j$ is determined by a direct linear rescaling of the Bcd molecular number such that

$$\widehat{I}_j = m\,\widehat{n}_j, \tag{2.5}$$

where the factor m represents the proportionality between one Bcd molecule and the corresponding fluorescence intensity, which includes the combined effects of tissue fixation, first and second antibody binding, fluorescence excitation and image processing.

As I do not know the exact *in vivo* system parameters and molecular number within each nucleus, I performed a complete inspection of the behavior of the variance of $m\,\widehat{n}_j$ in the four dimensional parameter space $f(m, J, D, \omega)$, where J is the synthesis rate of Bcd in the anterior compartment, ω is its decay rate, and D is the diffusion coefficient. It was always true that the residuals in logarithmic coordinate increased towards the posterior of the embryo, or in other words at lower levels of Bcd. This behavior strongly contrasts with the position-independent residuals seen in Figure 2.1 and described in equation (2.4).

2.2.2 Measurement rescaling noise dominates

The simulation results suggest that intrinsic noise cannot explain the pattern of variance seen in Figure 2.1. Another possibility is the measurement process itself. In order to analyze this process, I consider a simple model of the measurement of fluorescence intensity, where

$$\widehat{I}_j = \widehat{\alpha}\,\widehat{n}_j + \widehat{\beta}. \tag{2.6}$$

Here $\widehat{\alpha}$ is a spatially uniform random variable which replaces m in equation (2.5), and $\widehat{\beta}$ is a spatially uniform random variable which represents nonspecific background staining. This picture allows us to consider noise that arises from both intrinsic and measurement related sources.

The simplest way to understand the consequences of (2.6) is to imagine

the consequences if only one of $\widehat{\alpha}$, $\widehat{n}_j$, and $\widehat{\beta}$ are allowed to have finite variance while the other two are constrained to deterministic (zero variance) behavior. I have already pointed out that allowing finite variance for $\widehat{n}_j$ with $\widehat{\alpha}$ and $\widehat{\beta}$ deterministic leads to an increase of variance towards the posterior. The same is true if all noise comes from $\widehat{\beta}$, that is if noise from background staining dominates. This will also lead to more noise in the logarithmic domain towards the posterior as $\widehat{\beta}$ provides a larger proportion of the total detected signal. Let us next consider the case where all noise comes from $\widehat{\alpha}$.

In order to understand the role of $\widehat{\alpha}$, note that the spatial pattern of variance observed in Figure 2.1 can be captured by an exponential function multiplied by a normal random variable. This suggests that the simplest picture for (2.6) is given by assuming that there is no background noise $\widehat{\beta}$ and no intrinsic noise for Bcd so that $\widehat{n}_j = \langle \widehat{n}_j \rangle$. Moreover, it suggests that the rescaling noise $\widehat{\alpha}$ from measurement uncertainty is uniform across the embryo (independent of j) and is normally distributed with

$$\widehat{\alpha} = m\,(1 + \sigma_\alpha\,\widehat{N}(0,1)), \tag{2.7}$$

where $\widehat{N}(0,1)$ is a normal independent random variable with mean 0 and variance 1. Then I can model $\widehat{I}_j$ by

$$\widehat{I}_j = \widehat{\alpha}\,\langle \widehat{n}_j \rangle. \tag{2.8}$$

In steady state, $\langle \widehat{n}_j \rangle = a/m\,\exp(-j/\lambda)$. Taking logarithms allows us to write

$$\ln(\widehat{I}_j) = \ln(a) - j/\lambda + \ln(1 + \sigma_\alpha\,\widehat{N}(0,1)).$$

Comparison with equation (2.4) indicates that $\widehat{W} = \ln(1 + \sigma_\alpha\,\widehat{N}(0,1))$.

The reason I do not see intrinsic noise in this individual embryo is most likely low measurement sensitivity, that is to say a low molecule-to-fluorescence

mean rescaling ratio m. When m is small enough, it can mask the variance of $\widehat{n}_j$ because the variance of the rescaled gradient is given by

$$\mathrm{var}(m\,\widehat{n}_j) = m^2 \mathrm{var}(\widehat{n}_j).$$

As $m^2 \to 0$ with $\mathrm{var}(\widehat{n}_j)$ bounded in a reasonable way throughout the embryo, I will get $\mathrm{var}(m\,\widehat{n}_j) \to 0$. Hence the rescaled gradient $m\,\widehat{n}_j$ can be treated as deterministic by letting

$$m\,\widehat{n}_j = \langle m\,\widehat{n}_j \rangle = m\,\langle \widehat{n}_j \rangle.$$

In summary, I suspect the nucleus-to-nucleus variation observed in our data comes chiefly from the experimental rescaling noise $\widehat{\alpha}$, which is normally distributed. If Bcd intrinsic noise is to be observed, then the fluorescence noise intensity should be a function of the mean intensity in logarithm, instead of a constant as observed in embryo ms18. Nevertheless, the necessity of considering data in spatially resolved bins limits the amount of information that can be obtained from a single embryo. More information can be obtained by pooling data from many embryos, and I discuss this point in the next section.

2.3 Statistical analysis of an ensemble of embryos

Statistical analysis of many embryos is required in order to take our analysis further. This analysis will show how physical constraints on the model can be inferred from the ensemble dataset, and independent random variables separated. I consider a set of embryos indexed by i with expression levels I_{ij}, and

then pool data from corresponding bins to obtain the ensemble dataset $\bigcup_i I_{ij}$. Since this dataset includes embryo-to-embryo variability, i.e. the variation of system parameters and experimental conditions over different embryos, the variance of the ensemble profile will be an upper bound for the average variance within each embryo. This allows us to identify physical constraints for system parameters and to determine if the model behaves properly within the permitted range of parameters.

I define independent global random variables $\widehat{I}_j = \widehat{\alpha}\,\widehat{n}_j + \widehat{\beta}$ as described in the last section with normal distributed measurement uncertainty $\widehat{\alpha} = m\,(1 + \sigma_\alpha\,\widehat{N}(0,1))$. I also now assume that background noise is normally distributed with $\widehat{\beta} = \sigma_\beta\,\widehat{N}(0,1)$. I assume such global random variable represent the average variability for each embryo. The statistics of simulated global random variables were then collected from 2000 stochastic simulation runs and the Bcd molecular number random variable $\widehat{n}_j$ were sampled after reaching steady state. In this section I explicitly consider the effects of different choices for the molecule-to-fluorescence rescaling ratio m by comparing simulations to data at differing values of this parameter. Because m is not an explicit input to the model, this comparison is effected by varying the synthesis rate J, which varies the molecular number, and comparing the behavior of the model to fluorescence data which is on a fixed but arbitrary scale.

I seek optimal values of m such that the simulated global random variable $\widehat{I}_j$ is constrained by the variation observed in the immunostained ensemble

data $\bigcup_i I_{ij}$ by the condition

$$\langle \widehat{I}_j \rangle = \langle \bigcup_i I_{ij} \rangle \tag{2.9a}$$

$$\mathrm{var}(\widehat{I}_j) \leq \mathrm{var}(\bigcup_i I_{ij}). \tag{2.9b}$$

Because comparison with mean and variance of the ensemble data is not straightforward, I approximate the above conditions by comparing their exponential fit, F, and the normalized variance η^2, where $\eta^2 = \mathrm{var}(I) \,/\, \langle I \rangle^2$, and $I = \widehat{I}_j$ or I_{ij} for simulation and data respectively. Then (2.9a) and (2.9b) become

$$\langle \widehat{I}_j \rangle = \mathrm{F}[\bigcup_i I_{ij}] \tag{2.10a}$$

$$\eta^2(\widehat{I}_j) \leq \eta^2(\bigcup_i I_{ij}). \tag{2.10b}$$

In (2.10a), $\langle \widehat{I}_j \rangle = m\, a^{'} \exp(-j/\lambda^{'})$ from simulation and $\mathrm{F}[\bigcup_i I_{ij}] = a \exp(-j/\lambda)$ from the ensemble data. Because $\lambda^{'}$ is only determined by D and ω, I first select combinations of D and ω such that $\lambda^{'} = \lambda$. Selecting a synthesis rate J determines a', and also m, because $m = a/a^{'}$. Finally, biologically reasonable values of J are determined by the constraint (2.10b).

I seek to establish which terms of equation (2.6) dominate the observed variance in different parts of the embryo. To do this, I will graphically compare the total observed variance with a set of simulations in which variance arises from different subsets of the random variables in (2.6). I denote these restricted models by placing brackets around the subset of random variables which contribute to the variance. Thus the full model in (2.6) can be denoted by $\widehat{I}_j = [\widehat{\alpha n \beta}]$. A model with no variance contributed by background is denoted by $[\widehat{\alpha n}] = \widehat{\alpha}\,\widehat{n}_j$, while models in which all variance is contributed

only by rescaling, background, or molecular number are denoted respectively by $[\widehat{\alpha}] = \widehat{\alpha}\,\langle\widehat{n}_j\rangle$, $[\widehat{\beta}] = m\,\langle\widehat{n}_j\rangle + \widehat{\beta}$, and $[\widehat{n}] = m\,\widehat{n}_j$. Using this notation, a comparison of the definition of η^2 with (2.6) shows that I can write

$$\begin{aligned}\eta^2(\widehat{I}_j) &= \eta^2([\widehat{\alpha n}]) + \eta^2([\widehat{\beta}]) \\ &= \eta^2([\widehat{n}]) + \sigma_\alpha^2\,\mathrm{var}(\widehat{n}_j\widehat{N}(0,1))\,/\,\langle\widehat{n}_j\rangle^2 + \eta^2([\widehat{\beta}]).\end{aligned} \tag{2.11}$$

The middle term of the above equation simplifies even further when the molecular number is large so that $\widehat{n}_j = \langle\widehat{n}_j\rangle$ and hence $\sigma_\alpha^2\,\mathrm{var}(\widehat{n}_j\widehat{N}(0,1)) = \sigma_\alpha^2$. If the contribution of background noise $\widehat{\beta}$ is also small then it is the case that

$$\eta^2(\widehat{I}_j) = \sigma_\alpha^2 = \eta^2([\widehat{\alpha}]). \tag{2.12}$$

In summary, when Bcd molecular number is large in the anterior region of the embryo, I expect to see a constant level of normalized variance in our fluorescence data, contributed solely by rescaling noise $\widehat{\alpha}$. Thus, $\widehat{\alpha}$ can be identified independently from m and other random variables in our data.

2.3.1 Physical constraints from a high-variance ensemble of embryos

I first show results of the above statistical comparison using all 89 FlyEx cycle 13 embryos. This ensemble contains 9400 nuclei, with about 150 nuclei per bin. In Figure 2.2A I see that the normalized variance of the ensemble data $\eta^2(\bigcup_i I_{ij})$ asymptotically approaches the simulation curve $\eta^2([\widehat{\alpha}]) = \sigma_\alpha^2$ in the anterior region of the embryo. σ_α values that are too high will place the black model curve above the data points on the left, and this constrains σ_α to be less than 0.2.

With regard to the molecular parameters of diffusion, adopting the value of $D = 17.2$ (μm^2/s) given in the literature (Gregor et al., 2005) together

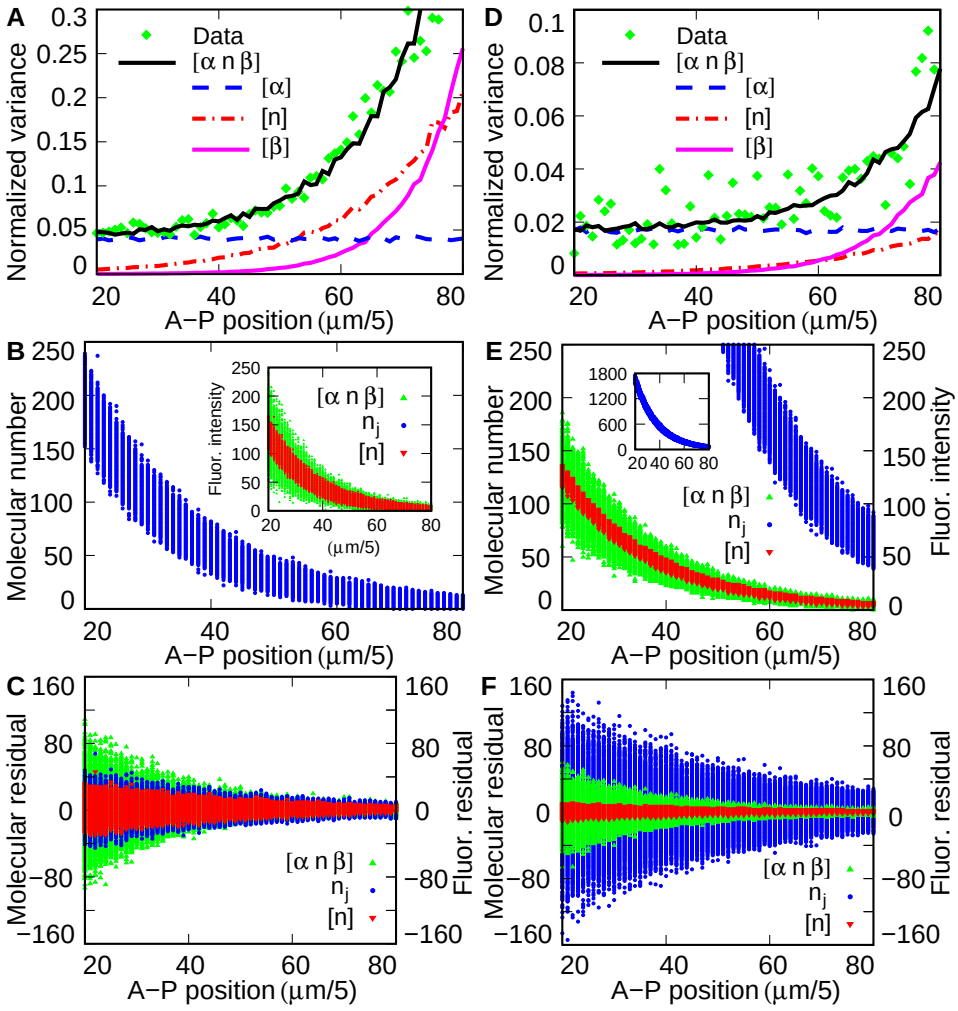

Figure 2.2: (**A**) The normalized variance. In the key, "Data" denotes the members of $\eta^2(\bigcup_i I_{ij})$ from the high-variance ensemble of 89 embryos. Lines denote simulation results as shown in the key. $[\alpha n \beta]$ denotes the full model $\eta^2(\widehat{I}_j) = \eta^2(\widehat{[\alpha n \beta]})$, $[\alpha]$ denotes $\eta^2(\widehat{[\alpha]})$, $[n]$ denotes $\eta^2(\widehat{[n]})$, and $[\beta]$ denotes $\eta^2(\widehat{[\beta]})$. The parameters used in simulation were $\sigma_\alpha = 0.2$, $\sigma_\beta = 1.7$, $J = 30$ (molecules/s), $m = 0.7$, $D = 17.2$ (μm^2/s) and $\omega = 0.0027$ (s^{-1}). (**B**) is a scatterplot of Bcd molecular number $\widehat{n}_j$, while the inset shows simulated fluorescence intensity for models and parameters used in panel A. (**C**) shows the residuals (deviations from mean) of panel B. (**D**), (**E**) and (**F**) show the same information as panel A, B, and C respectively, but from the low-variance ensemble of 17 embryos, with parameters used in simulation $\sigma_\alpha = 0.13$, $\sigma_\beta = 1.0$, $J = 200$ (molecules/s), $m = 0.07$, $D = 17.2$ (μm^2/s) and $\omega = 0.00215$ (s^{-1}). Note that the axes in panel A and D are scaled differently, and the absolute molecule number is shown in the inset to panel E.

with our observed value of $\lambda = 80.65$ (μm) for this ensemble implies that $\omega = 0.0027$ (s^{-1}) in order to satisfy (2.10a). These values, for any J, will cause the mean molecular number gradient, $\langle \widehat{n}_j \rangle$, to be in steady state after about 4000 seconds (cycle 8). A lower bound of $J > 30$ (molecules/s) and an upper bound of $m < 0.7$ is imposed by the experimentally observed magnitude of η^2. Finally, I estimate the constraint for background noise $\widehat{\beta}$ by satisfying (2.10b) in the posterior end of the embryo. Violation of the inequality (2.10b) would cause the black model curve to be above the data on the right hand side of Figure 2.2A, and hence I have an upper bound $\sigma_\beta < 1.7$.

In summary, analysis of our high-variance ensemble of embryos dataset implies that the Bcd synthesis rate is higher than 30 (molecules/s). Figure 2.2B shows a scatterplot of the molecular number associated with this synthesis rate. The panel indicates that most nuclei in the anterior fifth of the embryo contain more than 200 molecules of Bcd after reaching steady state, and that these molecular numbers can fluctuate over a range of more than 80 molecules in this region (Fig. 2.2C). This panel shows that these molecular fluctuations, even at the largest level of normalized variance compatible with data, still do not account for the observed variance in experimental observations. The additional variance comes chiefly from rescaling noise $\widehat{\alpha}$. Background noise $\widehat{\beta}$ only has a significant effect at the posterior end of the embryo, and indeed dominates the normalized variance in that region (Fig. 2.2A). Towards the posterior, $\eta^2([\widehat{\beta}])$ rises faster than $\eta^2(\widehat{n}_j)$, and its sharp rise may in certain cases serve as a marker to distinguish regimes dominated by molecular noise from those dominated by background noise.

2.3.2 Physical constraints from a low-variance ensemble of embryos

In the ensemble of embryos discussed above, a portion of the variance observed is likely to stem from embryo to embryo variation in staining conditions and inherent biological parameters. In order to find a better upper limit for observed molecular fluctuations, it is desirable to analyze a set of embryos whose properties are as uniform as possible. In order to generate such a set, I considered the value of λ_i in the exponential fit $\mathrm{F}\,[\,I_{ij}\,] = a_i \exp(-j/\lambda_i)$ to each embryo. I then grouped embryos according to common values of $1/\lambda_i$, taken to two decimal places. In the largest such group, which contained 17 members, I rescaled the data to a common amplitude by letting

$$I'_{ij} = \frac{\langle a_i \rangle}{a_i} I_{ij}. \tag{2.13}$$

These 17 processed embryos constitute an ensemble $\bigcup_i I'_{ij}$ for statistical analysis as described in the previous section. A trade-off of this treatment is the loss of statistical sample size, with only around 30 nuclei in each bin.

Figure 2.2D shows that this ensemble of 17 embryos has lower normalized variance compared to the 89 embryos ensemble in Figure 2.2A. The fluctuation of normalized variance is also higher because of smaller sample size. Note that rescaling noise is dominant over a larger portion of the embryo than is the case for the full 89 embryo ensemble. I estimate an upper bound for rescaling noise σ_α to be 0.13. At this point it is possible to determine the smallest J compatible with variance as was done for the high variance ensemble. I do not do so, however, because in this ensemble the contribution of $\widehat{\beta}$ is too small to be separated from $\widehat{n}_j$.

I compared this data to simulations performed using the same parameter

values reported in the previous section, except that λ (for the whole ensemble) had a value of 90.91 (μm), leading to ω taking on a value of 0.00215 (s^{-1}). These values cause the deterministic system to relax to steady state after 4000 seconds, as was the case with the high variance ensemble. In the high variance ensemble (Fig. 2.2A), the choice of σ_β was dictated by the necessity of matching the observed variance along the entire A-P axis. In the case of the low variance ensemble this is not required, but measurements from nonexpressing nuclei indicate that σ_β is equal to about 1. It is important to have at least a rough estimate for σ_β so that fluctuations from this source are not spuriously assigned to fluctuations in molecular number. Finally, these constraints require that the lower bound of synthesis rate J be 200 (molecules/s) in order that that $\eta^2(\widehat{I}_j) \simeq \eta^2(\bigcup_i I'_{ij})$. The corresponding upper bound of molecule-to-fluorescence rescaling ratio is $m = 0.07$.

The lower limit of J imposed by this ensemble of low variance embryos in turn implies that there must be more than 300 Bcd molecules per subvolume in the middle of the embryo ($j = 50$) after reaching steady state (Fig. 2.2E). Moreover, it implies that the Bcd molecular gradient does not drop to 0 as the fluorescence intensity reaches the presumed background level, but remains at a level of at least 50 molecules per subvolume at $j = 80$, and 36 molecules per subvolume at the posterior pole ($j = 100$). Note that the variance of fluorescence measurements is similar between the two embryo ensembles (compare the green areas in Fig. 2.2C and Fig. 2.2F), but that the portion of that variance assigned to fluctuations in molecular number is smaller for the ensemble of 17 embryos (compare the red areas in Fig. 2.2C and Fig. 2.2F). The tighter constraints from the smaller ensemble make the lower limits on molecular number higher (compare Fig. 2.2B and Fig. 2.2E), and the lower

limit on the variance of molecular number higher (compare the blue areas in Fig. 2.2C and Fig. 2.2F), although the higher limit of the normalized variance becomes smaller (compare the data points in Fig. 2.2A and Fig. 2.2D). The Bcd molecular number will thus vary by more than 100 molecules in the middle of the embryo . The 13% rescaling noise $\widehat{\alpha}$ is still the main source of the characteristic variation observed in the anterior region of our fluorescence intensity data.

2.3.3 Noise strength

In most applications the most important measure of fluctuation is the normalized variance η^2 (Colman-Lerner et al., 2005; Paulsson, 2004). A different quantity, known as the Fano factor or noise strength (Ozbudak et al., 2002; Paulsson, 2005; Raser and O'Shea, 2004), has been used by some authors as a marker to distinguish different stochastic mechanisms. The Fano factor ν is given by $\nu(\widehat{I}_j) = \mathrm{var}(\widehat{I}_j) \,/\, \langle \widehat{I}_j \rangle$, where $\nu = 1$ in a Poisson process. All stochastic simulations of Bcd intrinsic noise $\widehat{n}_j$ give $\nu = 1$, as shown in Figure 2.3A. By contrast, the full statistical model for either of the two ensembles of embryos examined (green and blue data in Fig. 2.3B) is obviously non-Poisson, not only because $\nu \neq 1$ but also because in the data, ν is a function of the mean. This happens because at larger values of molecular number, the variance of $\widehat{\alpha}$ has a dominant role, even when its value is small. Even if I model our data without rescaling noise using the $[\widehat{n}]$ random variable alone, uncertainty in the value of the rescaling constant m itself leads to ambiguity in the observed value of the Fano factor (red and cyan data in Fig. 2.3B). This is a natural consequence of the dimensions of the Fano factor.

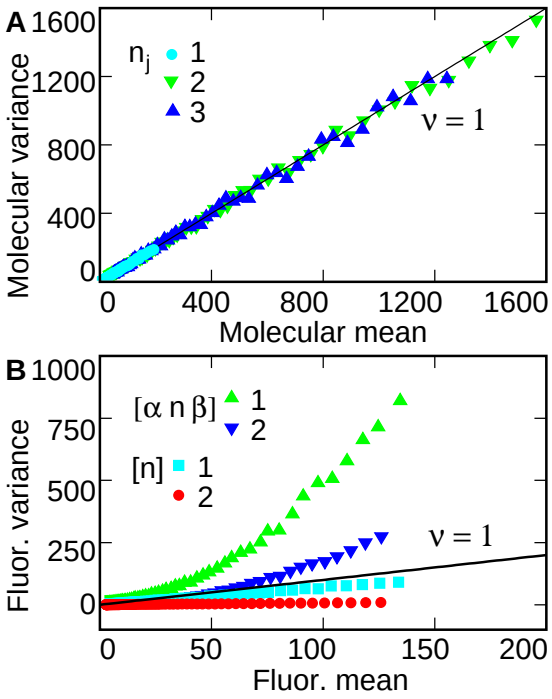

Figure 2.3: (**A**) The noise strength (Fano factor) ν of simulated Bicoid molecular number gradient is defined as molecular variance var($\widehat{n}_j$) divided by molecular mean $\langle\widehat{n}_j\rangle$. The key indicates that parameters were obtained from (1) the high-variance ensemble of 89 embryos, (2) the low-variance ensemble of 17 embryos, and (3) the extreme condition of high diffusion rate $D = 7890$ (μm^2/s), decay rate $\omega = 1.0$ (s^{-1}) and synthesis rate $J = 70000$ (molecules/s). (**B**) As shown in the key, noise strength of simulated fluorescence intensity $\widehat{I}_j = \widehat{[\alpha n \beta]}$ and rescaled gradient $[\widehat{n}]$ were obtained using parameters from (1) the high-variance ensemble of 89 embryos and (2) the low-variance ensemble of 17 embryos.

2.4 Conclusions

I have compared the nucleus to nucleus variation in expression levels of the exponentially distributed Bcd gradient observed in fixed tissue in a steady state with a stochastic model of the diffusion equation. The model is well supported, in the sense that there is a well-supported physical model for the spatial dependence of mean concentrations of Bcd (Gregor et al., 2005; Houchmandzadeh et al., 2005) on the scale of the embryo. The first major result of our analysis is to note that in many individual embryos the nucleus to nucleus variation in the log of concentration is independent of spatial position. This pattern of variation, which amounts to multiplicative noise in concentration space, is completely incompatible with the stochastic behavior of the diffusion equation. Simulations of the diffusion equation over an exhaustively large region of parameter space without exception give rise to solutions in which nucleus to nucleus variation of the *bcd* gradient is a function of position in the embryo, whether this variation is measured directly in Bcd levels or in their logarithms.

The data which I compare the model to is in the form of fluorescence levels, not concentrations. Although there is now good evidence that the specific batch of serum used to obtain this data has a mean response to Bcd (Gregor et al., 2007b) which is linear, there is no quantitative information about the variance of this sensitivity. Previous work on intrinsic molecular noise in yeast and bacteria utilized GFP (Austin et al., 2006; Becskei et al., 2005) *in vivo*, a situation where fluorescence is detected without molecular amplification. In the data reported here, and in most studies with fixed tissue, the signal from bound primary antibodies is amplified by incubation with secondary antibodies conjugated to a fluorescent dye. It is easily imaginable that this amplification

process itself is subject to molecular fluctuations. These fluctuations would then give rise to rescaling noise in the proportionality between fluorescence levels and primary antigen molecular number from nucleus to nucleus. I have shown that such variation can explain the multiplicative noise observed.

When data from fixed embryos are pooled, better statistics are obtained. I analyzed data pooled from the entire dataset ($N = 89$) as well as a smaller pool of data from a set of embryos selected to have nearly identical mean Bcd profiles ($N = 17$). In order to analyze these data, I constructed an explicit statistical model. The model considers three sources of variance: intrinsic noise, rescaling noise, and background noise. By means of this statistical model it is possible to separate, at least roughly, the contributions of different sources of fluctuation. I have discussed mechanisms for the first two of these; the third, background noise, represents small fluctuations in the quantity of nonspecific molecules (background) from nucleus to nucleus. Because mean background has been previously removed from this data (Myasnikova et al., 2005), the background noise has a mean of zero. I have confirmed that the background removal method does not affect our results, and the mean background intensity before removal is independent from the Bcd molecule-to-fluorescence rescaling ratio (data not shown). I also found from non-expressing areas of our data that the background noise (standard deviation) has about 54% positive correlation to the mean background intensity.

The results of this analysis constrained the physical parameters of the stochastic model considerably, with sharper constraints provided by the smaller dataset. The data require that the synthesis rate, J, of Bcd from its pool of anteriorly deposited mRNA be greater than 200 (molecules/s). I chose the subvolumes of the model to have the same volume as a nucleus, and hence the

constraint on J also implies that there are a mean of at least 300 molecules of Bcd per nucleus at the midpoint of the embryo, and mean levels of at least 36 molecules of Bcd per nucleus at the posterior pole. In terms of concentration, our results show that Bcd concentration at the midpoint of the embryo is greater than 4 nM. Recently, a direct *in vivo* measurement of Bcd concentration was performed and yielded a mid embryo Bcd concentration of 8 nM (Gregor et al., 2007a), fully compatible with our results.

Although I am able to extract a clear signature of intrinsic molecular noise from the data by means of the statistical model, I also showed that at least one quantity diagnostic for different stochastic mechanisms, the Fano factor, cannot be read out from the data. Although the Fano factor $\nu = 1$ in the simulations, the full statistical model gives rise to a Fano factor which is a function of the mean, and even if all noise is restricted to be intrinsic, the observed Fano factor depends on the scale for conversion from fluorescence to molecular number.

I believe that our results in general demonstrate that fixed material processed with secondary fluorophores is not well suited to studies of molecular fluctuations. This arises from three issues, which may be separable. Fixation obviously prevents repeated observations on the same cell. While that is clearly a limitation, it need not affect an investigation of a molecule whose mean values are in steady state. The other two issues concern amplification. GFP is intrinsically fluorescent, but antibodies must bind to antigen, a process that is in itself subject to intrinsic molecular fluctuations. In the present study, the level of molecular fluctuation is doubtless increased by the need to bind secondary antibodies conjugated to fluorophore to the already bound primary antibody. It is thus possible that better data from fixed tissue could

be obtained by conjugating dye directly to the primary antibody. This may prove to be a useful measure in situations where constructing a GFP fusion that can functionally substitute for the native gene is difficult or impossible.

More generally, I suggest that it is important to know how precision and robustness of developmental control is achieved at the molecular number level throughout development. Indeed, there is little doubt that stochastic processes are important later in development. Adult *Drosophila* normally have four scutellar bristles. In mutants of the *scute* gene, the number of bristles varies between one and three (Rendel, 1959), strongly suggesting a stochastic process. On a more theoretical level, it has been suggested that fluctuations can augment the operating capabilities of biological regulatory networks (Paulsson et al., 2000). Our results indicate that *in vivo* monitoring of gene expression will be required to obtain high quality data on stochastic gene expression phenomena in eucaryotes. The central technical problem that must be solved to conduct such studies is the complete replacement of the endogenous gene with a fluorescently tagged functional version (Gregor et al., 2007a).

Chapter 3

Gene Circuit Method

3.1 Experimental level Quantitative Data

The experimental level work in the gene circuit method involves obtaining quantitative gene expression data for all segmentation genes at different time points in order to construct and compare with dynamical models at the theoretical level. The raw imaging data must go through a series of advanced data processing techniques. The details are as follows.

Drosophila melanogaster embryos are immunofluorescently stained with segmentation gene antibodies (Kosman et al., 1998). Images of the embryos stained in three different gene products are obtained using three channel laser confocal microscopy.

Image processing techniques (Janssens et al., 2005) are used to obtain relative fluorescence intensities in each nucleus on an 8-bit scale. Embryo images were segmented, meaning that scanned pixel images were converted to tabulated expression data per nucleus. To avoid problems due to the residual curvature (or splaying) of the stripes, subsequent data processing steps were

performed on a strip of nuclei comprising 10% of the embryo in the D-V direction.

The embryos are classified into time classes based on *eve* patterns as embryos are fixed at arbitrary points in their development (Myasnikova et al., 2002). We use data from cleavage cycle 13 and the eight time classes for cycle 14A, each with a duration of about 6.5 minutes, in this project. Time points at half time through each class are used for the comparison with model: C13, $t_0 = 10.550$ min; T1, $t_1 = 24.225$ min; T2, $t_2 = 30.475$ min; T3, $t_3 = 36.725$ min; T4, $t_4 = 42.975$ min; T5, $t_5 = 49.225$ min; T6, $t_6 = 55.475$ min; T7, $t_7 = 61.725$ min; T8, $t_8 = 67.975$ min.

Data registration was performed using the dyadic wavelet transforms (Kozlov et al., 2000; Jaeger et al., 2004a). Different antibodies show different levels of background staining, so this background is removed by approximation of the background by a broad parabola and subsequent renormalization of the data (Myasnikova et al., 2005).

Expression profiles were averaged for each gene and each time class. This was done by grouping the data into 100 regular spatial intervals along the A-P axis, since one nucleus corresponds to about 1% embryo length. Thus, the integrated data used for fitting the model consists of series of 100 averaged concentration values along the embryo's A-P axis for each time class, which corresponds to the concentrations per nucleus that are produced as output from the model.

The pair-rule dataset I used in this thesis for large scale numerical fitting is available on-line at: `http://flyex.ams.sunysb.edu/FlyEx/` (Poustelnikova et al., 2004; Surkova et al., 2008).

3.2 Theoretical level Modeling

The work at theoretical level involves formulating mathematical models and developing computational and visualization tools. In the gene circuit method the model is based on a few simplifying biological assumptions that apply to the *Drosophila* blastoderm. First it is assumed that the expression of zygotic segmentation genes is a function only of their location on the anteroposterior (A-P) axis, independent of the dorsoventral (D-V) axis, so that it is possible to consider a one-dimensional system. Second, it is assumed that the regulatory interactions are constant in time. Each interaction is specified by a single real number for each ordered pair of genes, so for N genes cross regulating each other, there are N^2 such numbers. The number can be positive (activating), negative (repressive) or zero (neutral). Third, the regulatory input of Bicoid on the zygotically regulated genes, and gap genes input on pair-rule genes in this application, is supplied as external input to the equations. Hence, *bicoid* and gap genes in this application are not zygotically regulated by any other segmentation gene. The assumption that pair-rule genes do not regulate gap genes is well supported from single mutant studies, and any exceptions from this rule are limited in scope (Tsai and Gergen, 1994).

The hybrid model is based on discrete reaction-diffusion equations on a row of nuclei that undergo successive interphases and mitoses, the timing of which has been experimentally determined in the *Drosophila* embryo (Foe and Alberts, 1983). The state variables are the concentrations of the segmentation genes in each nucleus (Reinitz and Sharp, 1995) of the *Drosophila* blastoderm. For simplicity, the model is formulated using coarse-grained kinetic equations that do not take into account the fine structure of regulatory elements or the complexity of the transcriptional machinery of each gene (Reinitz and

Sharp, 1995). The mRNA concentrations are omitted for simplicity. The use of Fickian diffusion is a consequence of the fact that all the nuclei are in a common cytoplasm.

The circuit operates according to three rules: interphase, mitosis, and division. The interphase and mitosis rules are described by a set of differential-difference equations for the continuous dynamics of proteins. During interphase the evolution of protein concentrations is determined by three processes: regulated protein synthesis, protein transport, and protein decay (Mjolsness et al., 1991; Reinitz et al., 1995; Reinitz and Sharp, 1995). During mitosis, transcription shuts down and nascent transcripts are destroyed. Therefore, only protein transport and protein decay govern the dynamics in the mitosis rule. The third rule, division, accounts for the cleavage of the blastoderm. It models mitotic division as a discontinuous change in the state of the system. At the end of a mitosis, each nucleus is replaced with its daughter nuclei. The inter-nuclear distance is halved and the daughter nuclei inherit the state of the mother nucleus.

The two continuous rules, interphase and mitosis, use a system of ordinary differential equations (ODEs). Let there be M nuclei in the modeled region during a particular cleavage cycle and N genes represented in the circuit, I denote the concentration of the ath gene product in a nucleus i on the A-P axis of the embryo at time t by $v_i^a(t)$, then the time evolution of state variables $v_i^a(t)$ are given by the solution of the system of $M \times N$ ODEs,

$$\begin{aligned}\frac{dv_i^a}{dt} = R^a g\left(\sum_{b=1}^{N} T^{ab} v_i^b + m^a v_i^{\mathrm{Bcd}} + \sum_{\beta=1}^{N_e} E^{a\beta} v_i^\beta(t) + h^a\right) \\ + D^a(n)\left[(v_{i-1}^a - v_i^a) + (v_{i+1}^a - v_i^a)\right] - \lambda^a v_i^a,\end{aligned} \tag{3.1}$$

where $i = 1, 2, \ldots, n$, and n is the number of nuclei in the embryo during interphase. N is the number of zygotic (pair-rule) genes included in the circuit, N_e is the number of external input (gap) genes in the circuit regulating pair-rule genes, T^{ab} is the regulatory matrix (for pair-rule cross regulation), $E^{a\beta}$ is the external input regulatory matrix (for gap gene regulation on pair-rule genes), v_i^{bcd} is the gradient of maternal gene *bcd* and m^a represents the regulatory effect of *bcd* on gene a. Bicoid, the only time independent maternal input, and gap genes are considered explicitly as external inputs in the model. h^a is a threshold parameter representing the basal transcription level of gene a (in the absence of other transcription factors in the model). The positive values of the regulatory parameters represent activation of a by the product of b, negative values stand for inhibition of a by b and a value of zero means no interaction between genes a and b.

The first term on the right hand side of Eq. (3.1) represents protein synthesis, the second term represents protein transport through Fickian diffusion and the last term represents first-order protein degradation. Protein synthesis rate for a gene a is determined by the maximum synthesis rate R^a and the regulatory input to a, u_a. The rate of protein synthesis is the product of the maximum synthesis rate and the regulation-expression function (Jaeger et al., 2004b,a)

$$g(u^a) = \frac{1}{2}\left[\left(u^a/\sqrt{(u^a)^2 + 1}\right) + 1\right]. \tag{3.2}$$

This function is a sigmoidal function that introduces nonlinearity to the model and represents the response of a promoter to its regulatory inputs, though it can be of any sigmoidal form, monotonically increasing from zero to one.

The diffusion coefficient $D^a(n)$ scales with the inverse square of the distance between nuclei, and hence increases after each nuclear division. The last term in the equation is a linear decay term with a decay parameter λ^a. It is related to the protein half life of the product of gene a by $t^a_{1/2} = \ln 2/\lambda^a$. Several numerical methods for the solution of the gene circuit's equations are evaluated on the criteria of accuracy, stability, and efficiency, and the Bulirsch-Stoer method was chosen from among them (Manu, 2007).

In order to compare with quantitative gene expression data, we calculate the solution of the model at the midpoint of each time class. For the purpose of integrating the equations, the concentration of external input β in nucleus i is determined at arbitrary time t by piecewise linear interpolation.

3.3 Theoretical level Optimization

The optimization method used in this dissertation research is the Parallel Lam Simulated Annealing (PLSA) algorithm (Kirkpatrick et al., 1983; Lam and Delosme, 1988a,b; Chu et al., 1999; Chu, 2001). Simulated Annealing (SA) is a stochastic non-linear optimization method which is able to find the global minimum even for functions with a large number of variables (Kirkpatrick et al., 1983). The Lam annealing schedule is an adaptive exponential annealing schedule devised by Lam and Delosme (1988a,b). The parallel algorithm includes frequent pooling of statistics by all processes and a step which resembles a genetic algorithm approach, in which states reproduce or are annihilated with Boltzmann probability (Chu et al., 1999). When tuned adaptively to a specific problem and a specific number of processors, this algorithm can achieve parallel efficiencies of at least 75%, which means that annealing on

parallel computers will take only a fraction of the time required in serial (Chu, 2001).

The cost function to be minimized is the squared difference between model and data, given by

$$E = \sum \left(v_i^a(t)_{\text{model}} - v_i^a(t)_{\text{data}}\right)^2 + E_{\text{penalty}}, \tag{3.3}$$

where $v_i^a(t)_{\text{data}}$ is the corresponding concentration value in the data. E_{penalty} is a penalty term used for search space control. Summation is performed over the total number of data points N_d, *i. e.* the number of protein measurements across all genes a, nuclei i and time classes t for which we have data. We use the root-mean-square (RMS) score

$$\text{RMS} = \sqrt{\frac{E}{N_d}} \tag{3.4}$$

as a measure for the quality of a gene circuit. The RMS score is independent of N_d and represents the average absolute difference between protein concentrations in data and model output.

The fit thus obtained is the gene circuit for the segmentation gene regulatory network. It is analyzed to further understand the regulatory mechanisms behind segment formation. All the annealing parameters used in this study are the same as in Jaeger et al. (2004b).

3.4 Systems level Analysis

It is in general very difficult to directly reverse engineer a complex gene network. In the foundational work of applying gene circuit method to study gap genes (Jaeger et al., 2004b,a) and *eve* stripe formation mechanism (Reinitz

and Sharp, 1995), the authors were able to obtain optimized regulatory parameter sets that reproduce gene expression patterns of *eve* and the gap genes in silico. However in our earlier attempts of applying gene circuit method to the more complex pair-rule genes on the large part of presumptive germ band (also from Johannes Jaeger and Manu's earlier work), we were unable to obtain any optimized circuit. The shocking complexity of the pair-rule patterns, with 7 sharp stripes for each pair-rule gene, and the challenge of modeling pair-rule gene network, as compared to gap gene network, is clear when comparing the graphs of Fig. 1.3 to Fig. 1.2, and considering that gap genes also participate in the regulation of pair-rule genes in the pair rule circuits. Another challenge associated with rising systems complexity in the gene circuit method is rising computational cost of optimization, demanding both time and expensive computing resources. Different optimization methods, such as steepest descend and differential evolution, have also been tried and was unable to yield feasible circuits.

The setback we faced in fitting the more complex pair-rule genes may be a signal that our theoretical model is wrong, or it may signify an outside-the-box paradigm shift required. Instead of changing our computational model at the theoretical level and hoping for perfect tools, an alternative direction is to shift focus from theoretical level to systems (engineering) level. The challenge we faced in the gene circuit method is likely to be general in the developmental phase of computational biology, and must be resolved in order to move forward into more complex and integrative systems and make best use of the tools we have.

In the following sections I demonstrate another challenge associated with rising systems complexity, the analysis complexity. Here I provide my strate-

gies to overcome such emerging challenges, and make best use of the computational tools we have, in gene circuit method, to reach biological conclusions.

3.4.1 Optimization Modularity

The first task and challenge in systems level analysis of the gene circuit method is to obtain feasible optimized computational circuits for regulatory analysis. In order to obtain optimized circuits for complex pair rule gene network, I apply the engineering concept of modularity. The optimization modularity can be applied at many different levels, including time, space, genetic background, regulatory parameter constraints and the experimental data fed into the optimizer. The optimization modularity can also be applied in two directions, from top down and from bottom up (Fig. 3.1).

The modularity in time can be constructed on subsets of embryonic development, from cycle 13 to the 8 time classes of cycle 14 (see p.44). The modules in time can also be defined on early stripe formation phase or late refinement phase. The spatial modularity can be constructed on subsets of the A-P embryo axis, it can also be defined on each stripe or border, regions corresponding to specific enhancers, or further expansions to include multiple stripes or borders. The modularity on genetic background can be constructed on subsets of the pair-rule genes which we have data, including combinations of *eve*, *h*, *run*, *ftz*, *odd*, *slp* and *prd*. The combinations can include presumed primary pair-rule genes (*eve, h, run*) or secondary pair-rule genes (*ftz, odd*). More genes involved may result in higher level of degeneracy, which is more ways to make stripes. On the other hand, fewer genes involved may result in higher fitting quality, because there are fewer genes and less data to be optimized. The modularity of parameter constraints can be constructed based

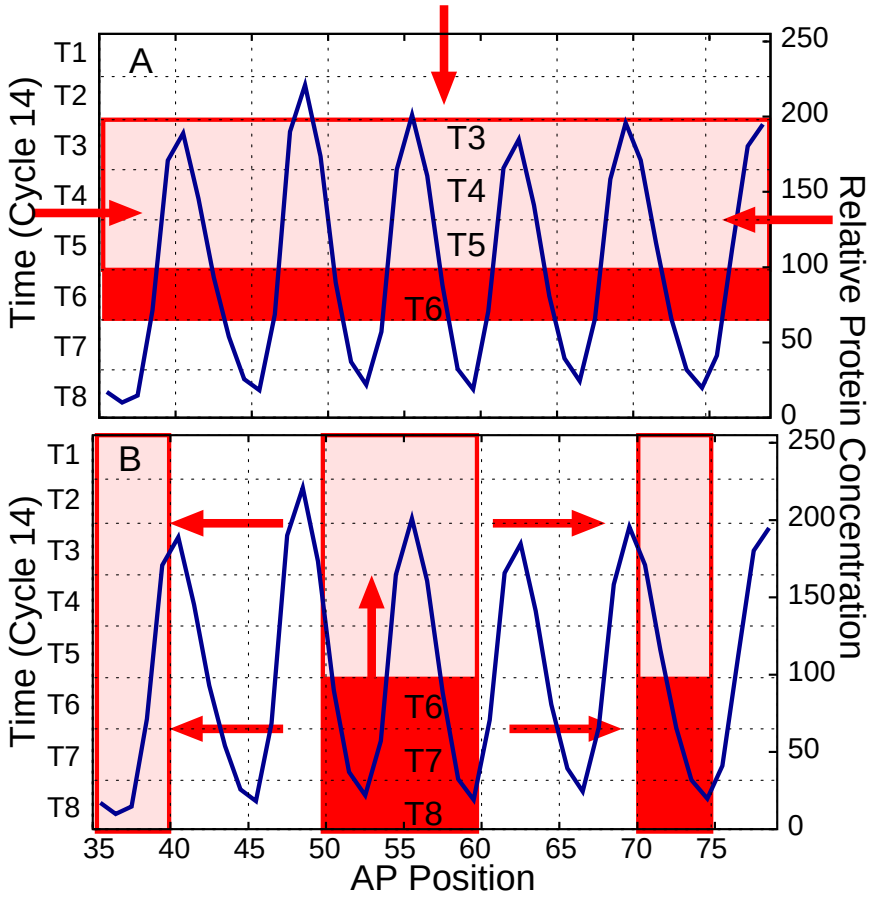

Figure 3.1: Circuit optimization modularity. Consider the y-axis as the projection of both time and relative protein concentration. The x-axis represents space (a-p axis of an embryo). The blue stripe (Eve) represents any pair-rule gene expression on the embryo. (**A**) The top-down optimization modularity on space and time can be done by reducing spatial range of the circuit, while at the same time reducing different combinations of time classes data sets fed into the optimizer in search for a good fit. For example in this thesis two classes of circuits were found optimizing without t6 and t3 to t5 data constraints respectively. Note that the circuits are still continuous in time. (**B**) Bottom up modularity in space and time on the other hand are done by expanding circuitry fits from each stripe and border region, and across different time scales, from early formation phase to late refinement phases, and to finer scales. Modularity can also be applied in genetic background or regulatory parameter constraints of the circuit.

on reports of biological regulation in the literature. For example the external input implementation of gap genes regulation on pair-rule genes in the circuit is a form of parameter constraint that no downstream pair-rule genes can regulate upstream gap genes. The modularity on optimization data constraints, which is experimental data fed into the optimizer, can be constructed on subsets of the 8 time classes of pair-rule gene expression data used to calculate the least squares difference between simulation results and the experimental data. The circuits can be continuous but unconstrained in time, for example in this thesis I present two classes of circuits that are continuous in time but unconstrained in the transient phase (from t3 to t5) and the late refinement phase (t6) respectively, by optimizing without t3 to t5, or without t6 data to compare with.

In the top-down direction, optimization constraints are gradually reduced from its maximal range in search of a good fit. For example circuits found in this thesis, shown in the next section, are found mainly by systematically reducing optimization constraints of temporal experimental data fed into the optimizer. The combinatorial search space for feasible circuits based on modularity can be large, and computational cost is a major bottleneck and limiting resource in this step. This step involves editing and organizing large sets of model optimization input files, and the computation were done in large scale within limited time and computing resources. The results were then examined visually by graphical plotting, and feasible circuits are selected for further analyses.

In the bottom-up direction modules are expanded in space from each stripe or border region, and expanded in time from late refinement phase to early stripe formation and transient phase. Modules have the advantage to relax

or delineate certain nonlinear or context dependent effects, which may be averaged in wider range circuits, and constrained by the linearity of the model equations. Modules can also capture parameter sets that apply better in local spatial and temporal regions in certain combination of genes. Modules can be tested in more genetic backgrounds with plug in regulatory parameter constraints, and hence also have higher evolvability to incorporate future experimental or literature results.

Overall optimization results from top down and bottom up form a spectrum of circuits, or a system of modules, to fully characterize the complex biological system. In general, modules with smaller spatial-temporal range, genetic background and fewer parameter constraints can result in a higher level of degeneracy, more ways to make stripes, but also a higher level of fitting quality (RMS score). On the other hand, circuits on the opposite end of the spectrum with wider ranges tend to have worse fitting quality and higher computational demand (that is, are difficult to optimize), but may show more specificity in stripe forming mechanism.

Circuits optimized from the top down, which is the main result of this thesis, have the advantage of wider range coverage and in general higher specificity in making stripes without regulatory parameter constraints. The modules optimized from bottom up have the advantage of higher fitting quality, computational efficiency, analog to transcriptional enhancers, evolvability, and the ability to handle stripe specific, context dependent or temporal effects of gene regulation. It may require a system of modules, in conjunction with circuitry optimized from top down, to fully characterize a complex biological network and make best use of the computational tools we have. A recent paper (Ashyraliyev et al., 2008) has pointed out that the non-specificity (non-

determinability) of regulatory parameters may be an indication for neutral or irrelevant regulation, in addition to degeneracy. Degeneracy may also be an evolution product (mechanism) optimized for redundancy control, hence are also biologically relevant and important.

3.4.2 Circuits Classification

In this thesis I present two classes of circuits optimized from the top down (Fig. 3.1). These circuits are mainly selected by systematically and combinatorially removing temporal optimization constraints of cycle 14 experimental data fed into the optimizer. In other words, I fit the circuit with all combinations of t1 to t8 data. The spatial range of these circuits were narrowed down from the entire presumptive germ band to 44 nuclei range (35% to 78% EL). The temporal range of these circuits were fixed from cycle 13 to gastrulation (throughout cycle 14A). The genetic background is selected at a combination of 5 pair-rule genes including *eve, h, run, ftz* and *odd*. There are also 6 external input gap genes (*cad, hb, Kr, gt, kni, tll*) and one maternal gene (*bcd*) involved, so there are total 12 segmentation genes in the circuit. I did not find any feasible fit in my preliminary optimization runs by removing *odd* or *ftz* from the circuit, or by removing the presumed primary pair-rule genes *eve, h* and *run*. Adding *slp* or *prd* may improve results in some module setting, but may also increase the degeneracy level.

The class A circuits were obtained by optimization without t6 data. T6 is part of the late refinement phase (t6 to t8) for pair-rule genes, and is a time when the shifting of existing stripes are most prominent (Fig. 3.2 to 3.4). I selected 2 circuits (A1, A2) in this class for detailed dynamic regulatory analysis. The first circuit A1 (Fig. 3.2) has an RMS score 26, and the second circuit

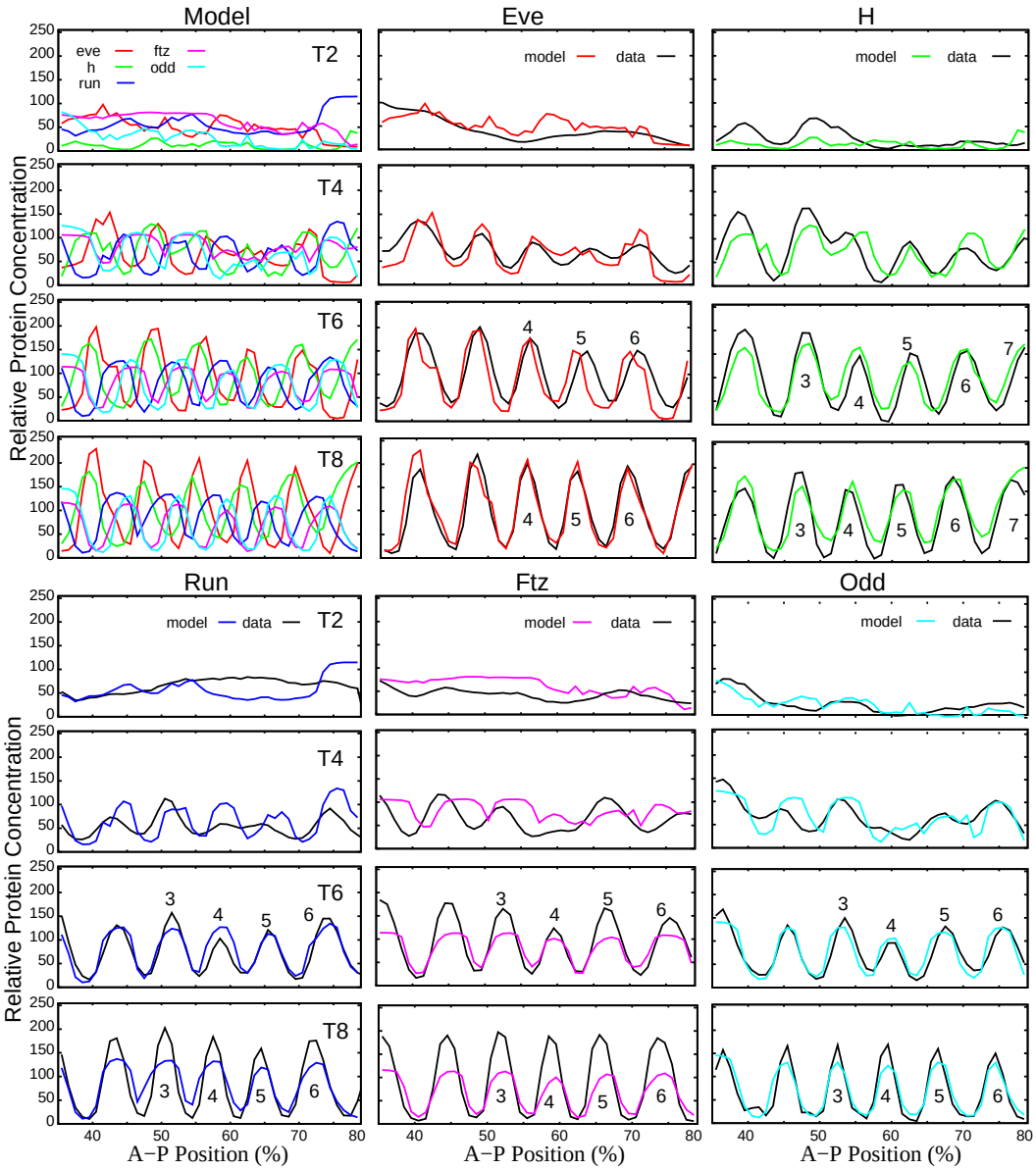

Figure 3.2: Circuit A1 optimized without t6 data. Here I show only even time classes (t2, t4, t6 and t8) results in cycle 14 (displayed on the same row), with model in color and data in black lines as shown in the key. The stripe number of the more prominent shifting stripes in data in the late refinement phase are denoted on the graph.

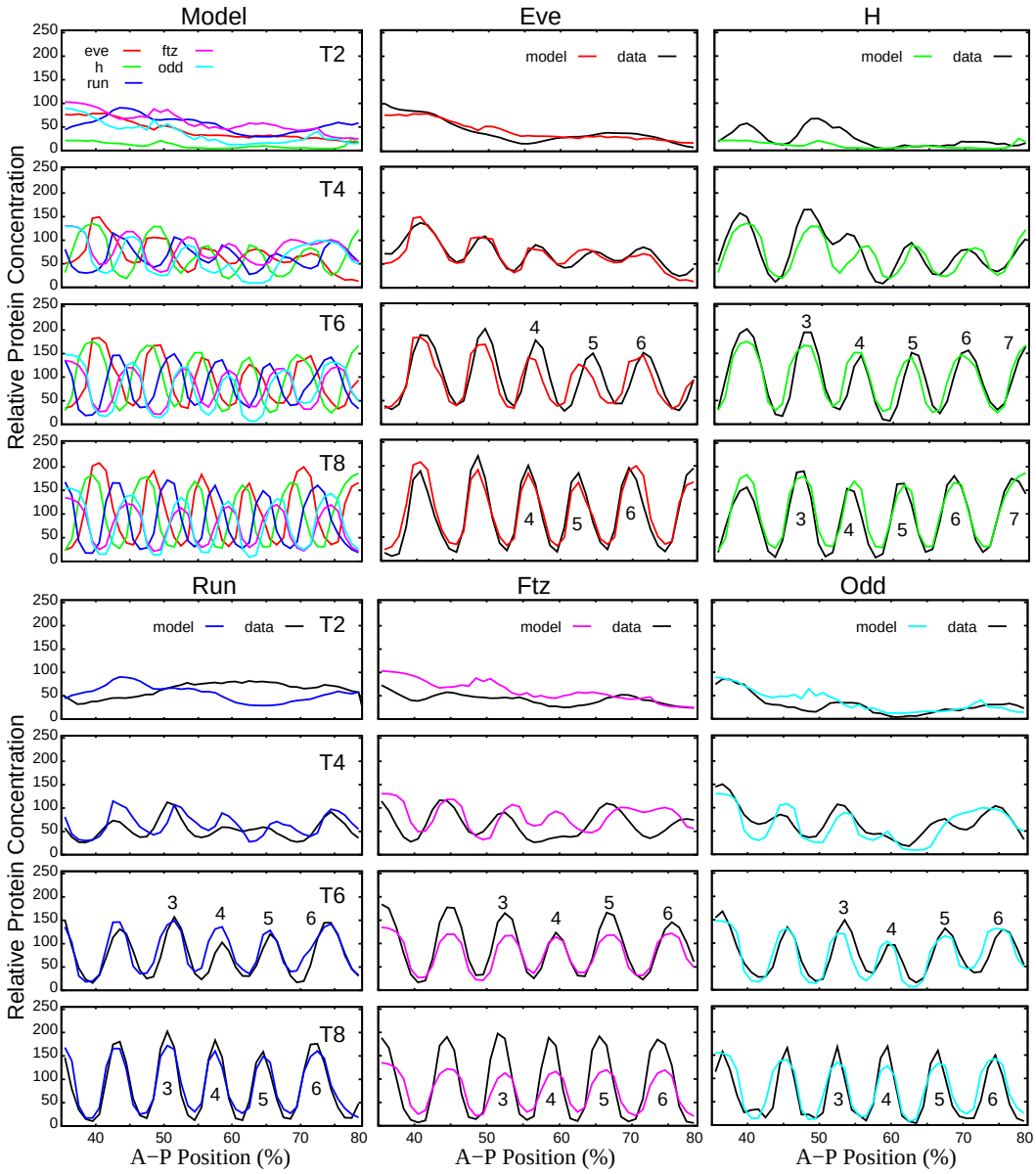

Figure 3.3: Circuit A2 optimized without t6 data. Here I show only even time classes (t2, t4, t6 and t8) results in cycle 14 (displayed on the same row), with model in color and data in black lines as shown in the key. The stripe number of the more prominent shifting stripes in data in the late refinement phase are denoted on the graph.

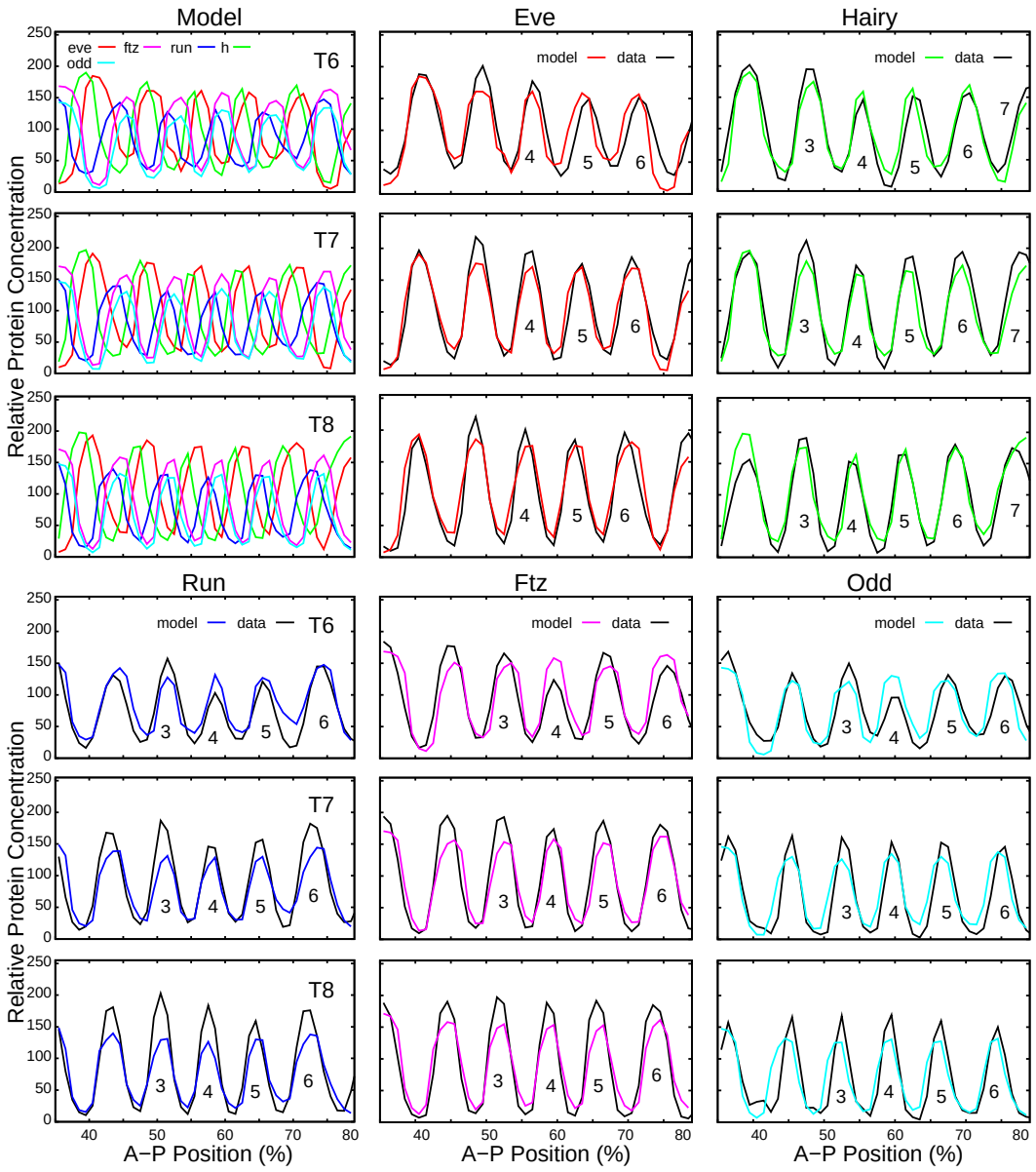

Figure 3.4: Circuit B1 optimized without t3 to t5 data. This circuit fits well to data in the late refinement phase from time classes t6 to t8 in cycle 14 (displayed on the same row), with model in color and data in black lines as shown in the key.The stripe number of the more prominent shifting stripes in data in the late refinement phase are denoted on the graph.

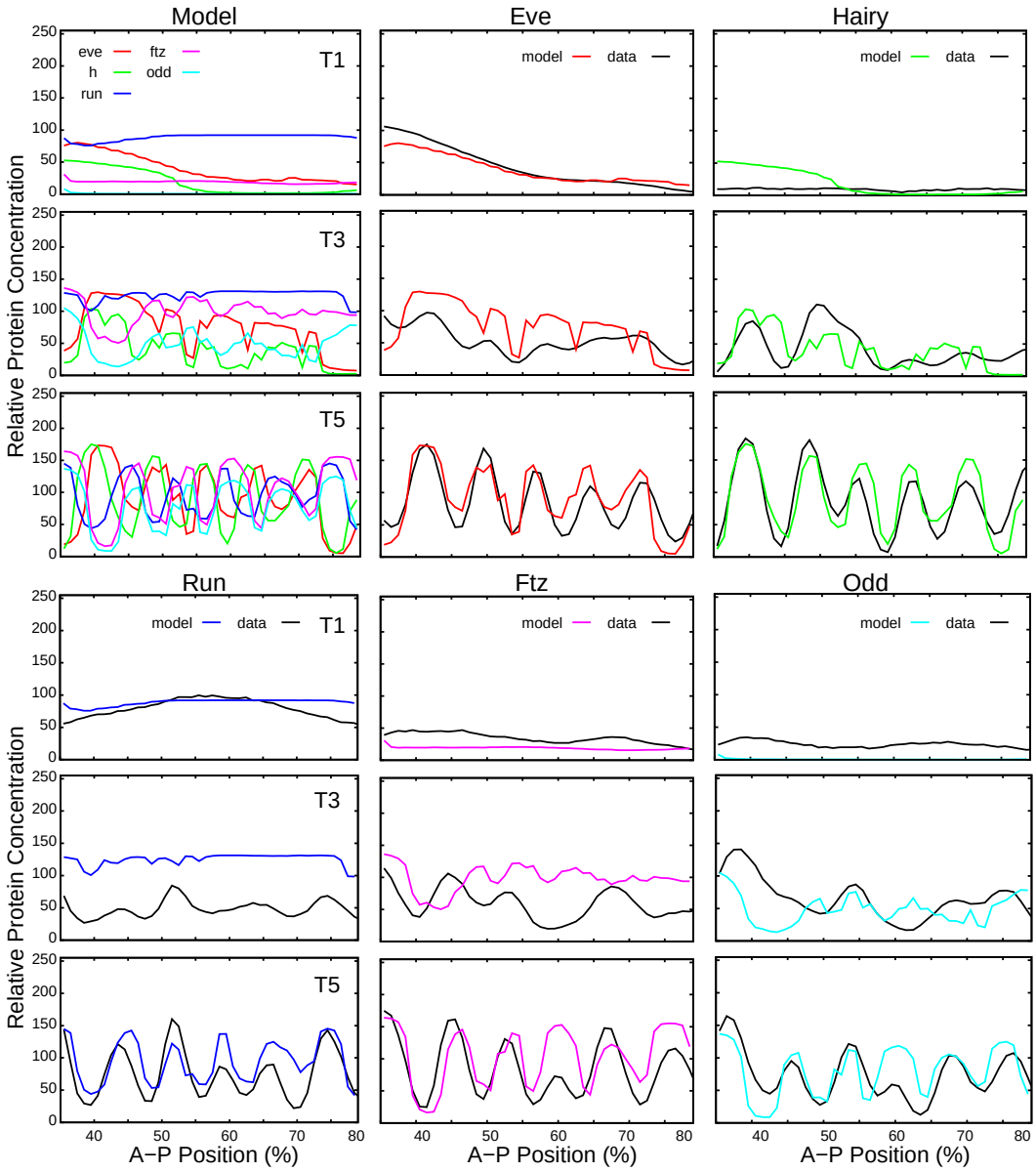

Figure 3.5: The transient patterns of circuit B1 shown in Fig. 3.4. Here I only show time classes t1, t3 and t5 results (displayed on the same row), with model in color and data in black lines as shown in the key.

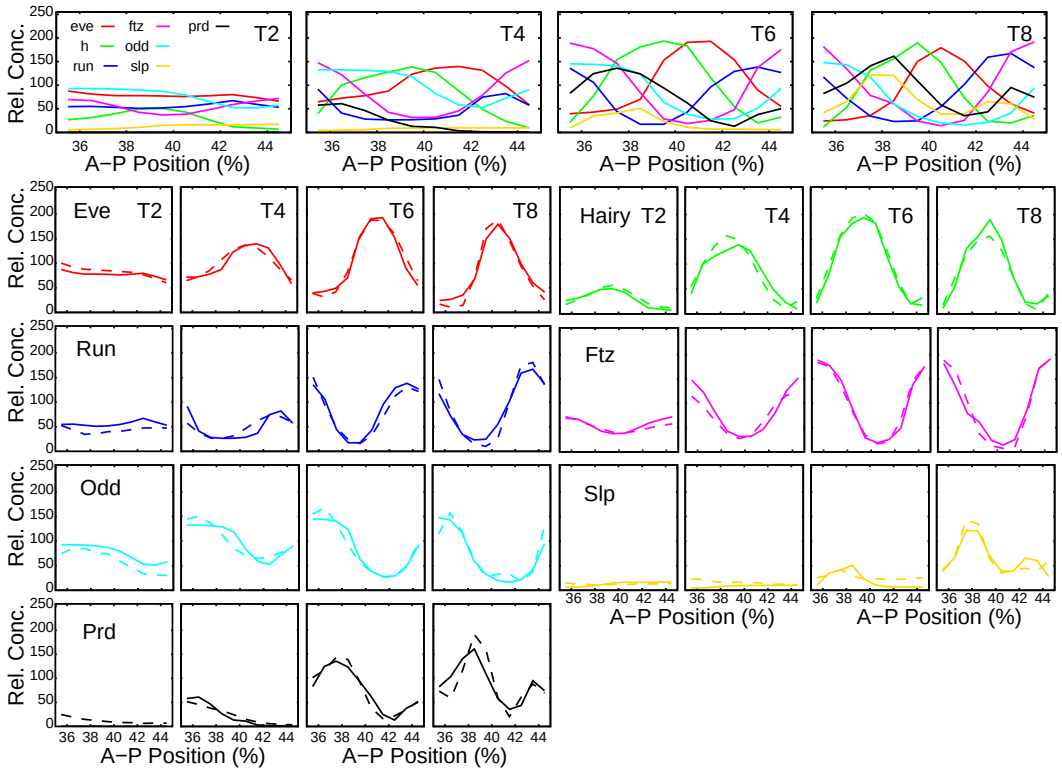

Figure 3.6: A spatially restricted module example including 7 pair-rule genes fitting well to data on a 10% embryo length region. The model results are shown in the first row, comparison with data are shown in the following panels, with model in solid lines and data in dashed lines. Here I only show even time classes (t2, t4, t6 and t8) results as displayed on the same column.

A2 (Fig. 3.3) has an RMS score 23. The class B circuits were selected in the category of optimization without t3 to t5 data. Here I select one circuit (B1) for detailed dynamic regulatory analysis. The circuit B1 (Fig. 3.4) has an RMS score 22. The class B circuits are more representative of the late refinement phase compared to class A circuits because there are no data in the transient phase to compare with during optimization and the late refinement phase has better fitting quality. The class A circuits are, however, more representative of the transient, stripe formation, phase of the pair-rule genes. There is more gap gene regulation involved in the class A circuits, as shown later in the analysis, which is required in the stripe formation phase.

Both of the class A circuits (Fig. 3.2 and 3.3), A1 and A2, have scaling problems regarding *ftz* in the final time classes of cycle 14. The amplitude of *ftz* stripes are about half that of the data. The scaling problems for *run* and *odd* are less severe. In Fig. 3.2 to 3.4, I also show the shifts of pair rule stripes in the late refinement phase. The stripe number of the more prominent shifting stripes in data are denoted on the graph. In both of the class A circuits, the posterior embryo *eve* stripes (4, 5 and 6) do not shift anteriorly as the actual stripes do in t6, instead they are formed in a more anterior position already, since there are no data to compare with during this time in optimization. This may also be a reason that by relieving this shifting constraint in optimization process during t6 allows us to find a closer approximation to the circuit. The transient phase patterns in the class A circuits are not perfect, one complicating factor may be the integrated data used in optimization does not represent well the individual embryo data (Surkova et al., 2008). In this thesis I focus on the regulatory control that contributes to the final phase of striped patterns instead of the detailed dynamic analysis of the transient

phase, which will require higher quality fits and be addressed by the module treatment. The final fitting problem in circuit A1 is minor residual expression in the gap among stripes for *h* and *run* respectively. In the class B circuits (Fig. 3.4 and 3.5), however, there seems to be a trade-off found between the final striped patterns and the transient phase patterns. As shown in circuit B1, the final stripes are well improved compared to class A circuits, but the scaling (amplitude) problem has shifted from the refinement phase to the transient phase, such that *run*, *ftz* and *odd* have minor amplitude problems in the final pattern, but *run*, *ftz* have double amplitude, twice of the data height in time classes t3 and t4.

A module system data set was also collected, though not shown in this thesis, by expanding from the *eve* stripe 2 region from 35% to 45% EL, and also from the 2 borders to further expansions. The time span is set on the formation phase from c13 to t8, and the late refinement phase from t6 to t8, t7 to t8 and t8 alone. The genetic background is established on subsets of *eve* (e), *h* (i), *run* (r), *ftz* (f), *odd* (o), *slp* (s), *prd* (p); including combinations of e, ei, er, ir, eir, eirf, eirfo and eirfosp. The regulatory parameter constraints are constructed on 2 levels of regulatory sets based on most well agreed experimental results collected from the literature. One level includes pair-rule cross regulation and another level only includes *eve* regulation. In Fig. 3.6 I show one example of a module involving 7 pair-rule genes and fitting well on a 10% EL region with full time span from cycle 13 to gastrulation.

3.4.3 Circuits Analysis

After obtaining optimized circuits, we can begin analyzing the circuits for biological insight. In each pair rule gene circuit there are 80 parameters to

	External Regulator gene β, *bcd*						
Target gene a	*bcd*	*cad*	*hb*	*Kr*	*gt*	*kni*	*tll*
eve	–0.091	–0.026	–0.020	–0.047	–0.064	–0.028	–0.620
h	–0.327	–0.039	0.003	0.012	0.013	-0.004	1.249
run	–0.292	–0.067	0.023	0.055	0.049	0.009	0.078
ftz	–0.008	–0.047	0.051	0.066	0.073	0.033	–0.483
odd	0.243	0.037	0.037	0.063	0.109	0.067	0.424

	Regulator gene b				
Target gene a	*eve*	*h*	*run*	*ftz*	*odd*
eve	0.015	0.049	–0.024	0.120	–0.087
h	0.085	–0.068	–0.114	0.054	0.052
run	0.020	–0.074	0.034	–0.127	0.048
ftz	–0.153	0.029	–0.004	0.020	–0.064
odd	–0.060	–0.068	–0.032	0.055	0.037

Parameter	*eve*	*h*	*run*	*ftz*	*odd*
R_a	13.278	13.836	13.672	12.510	13.011
h^a	4.065	3.814	9.541	6.191	–15.988
D^a	0.019	0.059	0.059	0.039	0.049
$t^a_{1/2}$	17.475	12.238	7.599	6.471	7.931

Table 3.1: Parameter values of circuit A1. Parameter values displayed here correspond to m^a (for *bcd*), $E^{a\beta}$ (for external input gap gene regulation), T^{ab} (for pair rule cross regulation), and h^a (for promoter threshold, effect of general transcription factors) in Equation 3.1. The search space during optimization for maximal synthesis rate of promoter R_a (minutes^{-1}) is from 10 to 20, for diffusion operator D^a (minutes^{-1}) is from 0 to 0.2, for protein half life $t^a_{1/2} = \ln 2/\lambda^a$ (minutes) is from 5 to 18.

	External Regulator gene β, *bcd*						
Target gene a	*bcd*	*cad*	*hb*	*Kr*	*gt*	*kni*	*tll*
eve	–0.022	–0.051	–0.041	–0.037	–0.005	–0.054	–0.839
h	–0.154	–0.034	–0.007	–0.005	–0.016	–0.021	0.312
run	–0.204	–0.130	0.002	0.007	0.026	–0.001	–0.192
ftz	0.121	0.034	0.051	0.033	–0.011	0.073	0.322
odd	0.299	–0.036	0.001	0.006	0.062	0.030	–0.524

	Regulator gene b				
Target gene a	*eve*	*h*	*run*	*ftz*	*odd*
eve	–0.013	0.041	0.010	0.138	–0.147
h	0.041	0.006	–0.066	0.066	–0.018
run	–0.037	–0.028	0.018	–0.038	–0.033
ftz	–0.069	–0.005	0.005	–0.128	0.212
odd	–0.182	0.020	0.077	–0.027	0.016

Parameter	*eve*	*h*	*run*	*ftz*	*odd*
R_a	12.717	19.890	13.950	19.029	11.019
h^a	7.663	4.067	18.393	–8.756	0.737
D^a	0.030	0.070	0.041	0.139	0.035
$t^a_{1/2}$	17.766	7.087	10.718	5.016	10.153

Table 3.2: Parameter values of circuit A2. Parameter values displayed here correspond to m^a (for *bcd*), $E^{a\beta}$ (for external input gap gene regulation), T^{ab} (for pair rule cross regulation), and h^a (for promoter threshold, effect of general transcription factors) in Equation 3.1. The search space during optimization for maximal synthesis rate of promoter R_a (minutes^{-1}) is from 10 to 20, for diffusion operator D^a (minutes^{-1}) is from 0 to 0.2, for protein half life $t^a_{1/2} = \ln 2/\lambda^a$ (minutes) is from 5 to 18.

	External Regulator gene β, *bcd*						
Target gene a	*bcd*	*cad*	*hb*	*Kr*	*gt*	*kni*	*tll*
eve	–0.119	–0.057	–0.006	0.005	0.009	0.013	–0.283
h	0.002	0.014	–0.006	–0.023	–0.031	–0.014	–0.059
run	0.152	0.055	0.002	0.023	0.054	0.006	–0.990
ftz	–0.275	–0.204	0.027	0.030	0.037	0.025	–0.278
odd	0.055	–0.079	0.016	0.044	0.058	0.056	0.456

	Regulator gene b				
Target gene a	*eve*	*h*	*run*	*ftz*	*odd*
eve	0.007	0.033	–0.006	0.082	–0.147
h	–0.021	0.106	0.020	0.150	–0.113
run	0.009	–0.112	0.012	–0.121	0.070
ftz	–0.154	–0.024	0.100	–0.011	0.045
odd	–0.063	0.009	0.099	0.013	–0.021

Parameter	*eve*	*h*	*run*	*ftz*	*odd*
R_a	13.948	19.999	11.783	19.999	15.533
h^a	3.427	–12.071	3.922	17.469	–10.552
D^a	0.032	0.060	0.032	0.060	0.042
$t^a_{1/2}$	10.985	7.838	9.258	6.013	6.704

Table 3.3: Parameter values of circuit B1. Parameter values displayed here correspond to m^a (for *bcd*), $E^{a\beta}$ (for external input gap gene regulation), T^{ab} (for pair rule cross regulation), and h^a (for promoter threshold, effect of general transcription factors) in Equation 3.1. The search space during optimization for maximal synthesis rate of promoter R_a (minutes^{-1}) is from 10 to 20, for diffusion operator D^a (minutes^{-1}) is from 0 to 0.2, for protein half life $t^a_{1/2} = \ln 2/\lambda^a$ (minutes) is from 5 to 18.

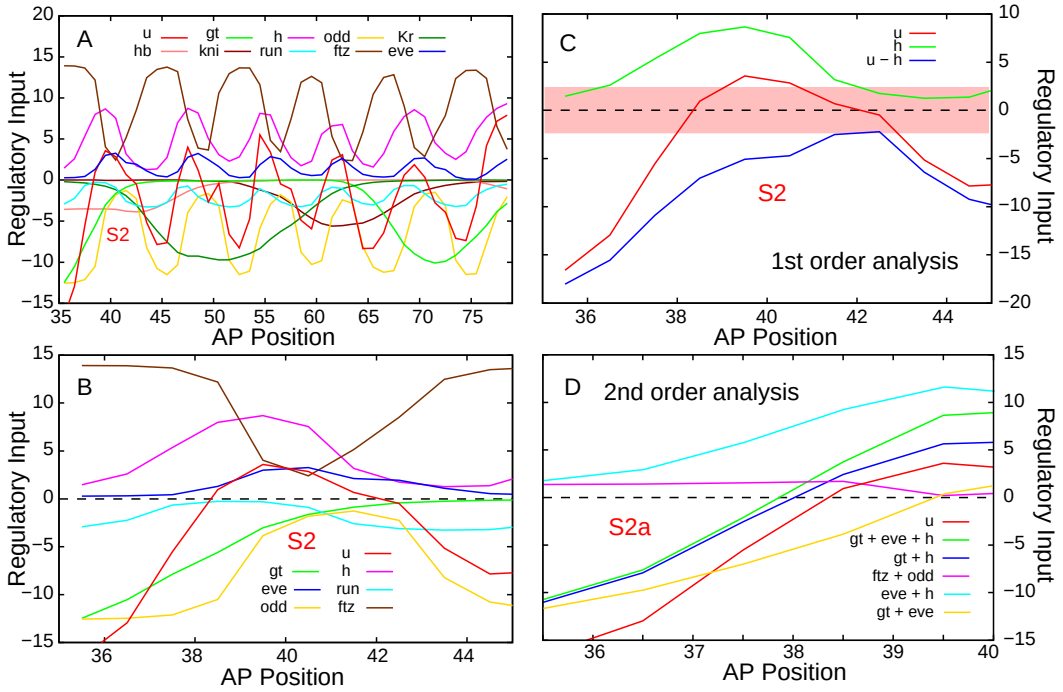

Figure 3.7: (**A**) The regulatory input on *eve* from a subset of genes in circuit A1 at time t7. Key u is the total regulatory input for *eve* ($u^{eve} = \sum_{b=1}^{N} T^{eve \leftarrow b} v_i^b + m^{eve} v_i^{\mathrm{Bcd}} + \sum_{\beta=1}^{N_e} E^{eve \leftarrow \beta} v_i^{\beta}(t) + h^{eve}$). S2 stands for the protein synthesis location for *eve* stripe 2, based on the total regulatory input. (**B**) The *eve* stripe 2 region of panel A with a subset of genes. (**C**) The first order analysis with one gene at a time for h. The pink area is the sigmoidal region of the regulation-expression function $g(u)$ (Eqn. 3.2). Here removing gene h (key $u-h$ refers to $u^{eve} - T^{eve \leftarrow h} v_i^h$) can result in *eve* synthesis to turn off, below the pink region. (**D**) The second order analysis of *eve* stripe 2 anterior border. Regulatory input of different combinations, subsets, of genes are plotted and compared to the total regulatory input u. Here the sum of *ftz* and *odd* regulatory input reduces to a plateau, hence is categorized as a reducible (homeostatic, redundant or non-essential) set to stripe 2 anterior border formation. The combination of *gt* and h input approaches close to the total regulatory input, hence are considered as the essential set for stripe 2 anterior border regulators.

be determined through optimization. In Table 3.1 to 3.3, I first show the parameter values for the 3 major circuits. The regulatory parameters T^{ab}, m^a, $E^{a\beta}$, h^a will be analyzed in detail in the following graphical analysis, statistical pooling (Section 3.4.5), and discussed further in the main text of Chapter 4. In circuit A2 and B1, *h* and *ftz* have the maximal promoter synthesis rate R_a, while in circuit A1, the promoter strength for all pair rule genes are at a similar level. The diffusion coefficient D^a for the pair rule genes are much smaller, by a factor of 10, compared to that of the gap gene circuits in Jaeger et al. (2004b). This observation is also consistent with the early gene circuit method application on the study of *eve* stripe formation (Reinitz and Sharp, 1995), where D^{eve} is close to 0 (see more discussions on the diffusion of pair rule genes in Reinitz and Sharp (1995)). The protein half life $t^a_{1/2} = \ln 2/\lambda^a$ is consistently longer for Eve among the 3 major circuits. This is perhaps a result of the residual expression found in the data between each *eve* stripe. The $t^{eve}_{1/2}$ here is also much longer than the 6 minute estimate in Reinitz and Sharp (1995) using a less resolution gene expression data set.

The major systems level analysis of the gene circuit model is based on graphical analysis of regulatory contributions to specific patterning features in space and time (Reinitz and Sharp, 1995; Jaeger et al., 2004b; Manu et al., 2009, 2008). Graphical analysis allows for studying quantitative regulatory contributions to gene regulation in any nucleus at any point in time during a simulation. It is used to determine whether a given regulatory interaction actually contributes to an expression feature. A boundary can occur where an activator drops below a given concentration threshold, or a repressor exceeds a given concentration threshold. The protein concentrations, obtained by numerically integrating the model, are plotted to identify expression features of

interest, and the time and region of the embryo in which they occur. The combinations of regulatory terms, $T^{ab}v_i^b$, $m^a v_i^{\mathrm{Bcd}}$, and $E^{a\beta}v_i^{\beta}(t)$ (Eq. 3.1), are plotted to identify specific regulatory interactions responsible for the expression feature.

In the analysis of pair rule gene circuits, challenges arise as the systems complexity increases. There are total 12 segmentation genes in the pair rule circuit, hence the combinatorial number for gene regulation is much larger than the gap gene circuits in previous applications (Reinitz and Sharp, 1995; Jaeger et al., 2004b). Furthermore, as I show in Fig. 3.7 (A), it is impossible to directly infer each border regulation from one graph alone, in fact even from one stripe alone (Fig. 3.7 (B)). The analysis must be broken down to one gene at a time, so one can tell the effect of each gene on the total regulatory input, by plotting the residual regulatory input after removing one particular gene and see whether the remaining curve raises above, below, or change significantly near the sigmoidal region of the regulation-expression function (Eq. 3.2, Fig. 3.7 (C) pink area), which can result in change of protein synthesis rate for the controlled gene. I call this level of analysis, with one gene at a time, the first order analysis.

The analysis must also be broken down to one border at a time, so one can distinguish the combinatorial regulatory effect from multiple genes, and from border to border (Fig. 3.7 (D)). I call this level of combinatorial regulatory analysis the second order analysis. The sequence of the analysis, from first order to second order, is very important, because it allows for choosing only the relevant and significant set of genes to examine their combinations, which will be introduced in more detail in the next section of regulatory representational system.

In the first order analysis, the number of graphs I need to generate based on one border at a time can be estimated by taking the product of the total number of input gap and pair rule genes, the number of time classes, the number of stripe borders, the number of pair rule genes in the circuit, and the number of circuits, hence I will need to generate

$$\begin{aligned} &12 \text{ (total segmentation genes)} \times 9 \text{ (time classes)} \times 11 \text{ (borders)} \\ &\times 5 \text{ (pair rule genes)} \times 3 \text{ (circuits)} = 17820 \text{ (graphs)}, \end{aligned} \tag{3.5}$$

which is a lot of graphs. Saving graphs based on one stripe at a time can reduce half of the graphs, but still the analysis must be applied on one border at a time. Fortunately the actual number of genes regulating each border is less than the total number of segmentation genes in the circuit, so I may end up saving less graphs.

Moreover, in the second order analysis I need to look at the combination effects of multiple genes regulating on one border. Suppose there are 8 genes regulating each border, then according to the combination rule, $\sum[\mathrm{C(n,r)}] = \sum[\mathrm{n!/r!(n-r)!}]$, I have to go through

$$\mathrm{C}(8,2) + \mathrm{C}(8,3) + ... + \mathrm{C}(8,7) = 246 \text{ combinations}$$

for each border. If I screen 4 combinations in one graph, then according to Eqn. 3.5 I have to generate another maximal $246/4 \times 17820/12 \approx 91327$ graphs. The combination number can easily explode, consider 13 input genes with $\sum[\mathrm{C}(13,\mathrm{r})] = 8191$. Hence the simple fact of generating, handling, and analyzing large scale of graphs is a serous systems level challenge in circuits analysis, and must be taken on with a systematic approach. Fortunately after the first order analysis, I can narrow down the significant subsets of genes that are contributing to stripe determination from the dynamical perspective, to

lower the combination number required in the second order analysis.

Still, after generating all the first and second order analysis graphs for each border in each circuit, there is a missing piece about how to go from huge numbers of graphs to biological conclusions. The missing step requires organizing circuitry information in a systematic format directly comparable to literature. The graphical (circuitry) complexity and information flow is a systems challenge, and requires a regulatory representational system.

3.4.4 Regulatory Representational System

The regulatory representational system I implemented is a simple symbolic system that can capture and convert the essential graphical information from first and second order analysis into the textual format, similar to some kind of scripting language for dynamic programming of stripe formation. In the linear regime of the gene circuit model, $u = \sum_{b=1}^{N} T^{ab} v_i^b + m^a v_i^{\mathrm{Bcd}} + \sum_{\beta=1}^{N_e} E^{a\beta} v_i^{\beta}(t) + h^a$ in Eqn. 3.1, a stripe forms by relatively increasing activation or reducing repression at the peak level, and relatively increasing repression or decreasing activation at the stripe border position. The complexity lies in how such balances are dynamically programmed or statically maintained among the 12 segmentation genes in the circuits. This is the concept that the regulatory representational system holds, and the complexity that the scripting language encodes.

From the systems analysis perspective, the regulatory representation system controls and directs the information flow. The circuitry information is extracted from the graphical content, which is much harder to handle at large scale, and converted to the logical textual format, which allows for systems level reorganization and compilation to reveal different, systems, levels of bio-

logical correlations. The compilation of textual information can be done across borders, genes, and different circuits, which can not be achieved by simply operating on graphs. The analysis information is stored systematically, which facilitates and enables the comparison with literature.

In Appendix A.1 I give the details of how the simple regulatory representational system is implemented, and include the full circuitry analysis results for the three major circuits after two levels of compilation. In the first order analysis, the regulatory input profile (shape or inclination) of each interaction, can be directly mapped from the graph, in a linearized manner, using simple symbols such as forward slash or backslash. The linear profile of each interaction can encode the relative phasing position and gradient of the regulatory gene expression domain. For direct boundary control by activation or repression, the activator and repressor both require the same spatial gradient of regulatory input to the boundary it controls. The strength of each interaction is recorded at three different levels. The significance of each interaction is evaluated based on the absolute value, intensity, of the regulatory input, or by, relatively, how it affects the total regulatory input after being subtracted from it (Fig. 3.7 (C)).

In the second order analysis, I only look at combinations of significant stripe (or slope) contributing (input) genes from the first order analysis results. This is one of the major reasons for doing first order analysis separately and in the front, so I can exclude irrelevant or insignificant interactions before looking at their combinations. For example in Fig. 3.7 (D) I look at combinations of a subset of significant stripe (slope) contributing genes. I then seek to identify the reducible and irreducible sets of regulatory inputs. The combination of *ftz* and *odd* input reduces to a plateau, hence can be classified as a reducible set,

and may be biologically relevant and significant as a homeostatic or redundant regulatory mechanism. On the other hand the combination of *gt*, *h* and *eve* input approaches to the total regulatory input closely, hence can be classified as the irreducible set, which is essential to the stripe 2 anterior border formation in the circuit.

The final element I examine in the second order analysis is the critical controller of the irreducible set. After isolating the irreducible set, I examine whether removing one particular member (from the first order analysis graphs) can result in total shutdown or inactivation of the protein synthesis rate. Certain genes may be classified as having strong influence (significance) on one border, but its influence is only limited to affecting the shaping or shifting of one border, or stripe. Removal of these genes may only modify (adjust) the protein synthesis rate, without turning it off completely. The subset of critical controllers, however, when removed in the circuit, can result in a total abolishment or disruption of the stripe. For example, *h* is considered as a critical controller for *eve* stripe 2 anterior border in Fig. 3.7 (C), removal of *h* from the total regulatory input results in the total regulatory input to be lower below the sigmoidal region of the regulation-expression function (pink area) (Eqn. 3.2), hence leads to the total shutdown of the protein synthesis rate.

The complication comes in when considering regulatory information from different time classes. One approach I use early in the research, is to include all detailed transient phase regulatory dynamics from all time classes. This can be done by specifying the initial state, final state, and the transition dynamics, which is the state change in time from the initial state to the final state. The transition dynamics can be specified in many different time intervals, and can

be described by specifying the profile of change, and the intensity of change, as compared to the specification of a regulatory state. The principle is to capture both the regulatory state and the regulatory dynamics in a linearized fashion, by specifying time or time intervals, and using simple linearized symbols.

Later in the research phase, I decided to focus on the essential regulators for the final stripe determination. The first and second order analyses were then adopted for all time classes, by selecting the most significant or representative regulatory states among all time classes, or conducting analysis based on the late refinement phase first, and then adjusting for the transient stripe formation phase. For example if there are conflicts between the transient phase and the late refinement phase regulation, the more significant regulatory states are selected, and adopted for the final decision in the regulatory representational system. The detailed transient phase dynamics information are retained only when it is essential to the final stripe determination. Since the full impact of each gene can only be determined by working through all time classes, the final step in first or second order analysis is the adjustment and extension in time. And at a more abstract level, through compromising or in a form of compression, reaching a conclusion about the most representative regulatory status for each gene regulation in time.

3.4.5 Statistical Pooling

Statistical pooling plays an important role in systems level analysis, especially when there are large numbers of circuits, and in the analysis of module systems. When the modules are restricted to one particular border or stripe region, a threshold can be set to directly relate parameter statistics to the threshold of regulatory input in the graphical analysis. The parameter distribution, or

Odd	Class A			Class B		
	(1)	(2)	(3)	(1)	(2)	(3)
Bcd	0/0/1/0/4	1/1/0/0/8	0/2/1/1/11	0/1/0/1/2	1/2/1/0/5	1/0/0/0/5
Cad	1/3/0/1/0	5/1/0/3/1	3/6/1/2/3	3/0/0/0/1	4/3/1/1/0	4/1/0/0/1
Hb	0/0/1/4/0	0/3/0/5/2	0/2/3/9/1	0/0/1/3/0	0/1/2/5/1	0/2/1/3/0
Kr	0/0/2/2/1	0/1/3/5/1	0/1/2/9/3	0/0/0/4/0	0/1/1/6/1	0/1/0/4/1
Gt	0/0/0/3/2	0/0/1/4/5	0/0/1/2/12	0/1/0/0/3	1/0/0/4/4	0/1/0/1/4
Kni	0/0/1/3/1	0/2/2/4/2	0/2/2/10/1	0/1/0/1/2	0/0/1/3/5	0/0/1/3/2
Tll	3/0/0/0/2	3/1/0/0/6	7/0/0/1/7	0/0/0/1/3	1/0/0/0/8	2/0/0/0/4
Eve	5/0/0/0/0	8/2/0/0/0	13/2/0/0/0	3/1/0/0/0	9/0/0/0/0	5/1/0/0/0
H	1/0/2/1/1	0/3/0/4/3	5/1/2/5/2	2/0/2/0/0	1/5/1/2/0	2/4/0/0/0
Run	0/1/0/3/1	3/1/0/3/3	3/3/0/5/4	0/0/0/2/2	0/1/0/3/5	2/2/0/1/1
Ftz	1/1/0/1/2	1/2/0/1/6	1/0/2/6/6	0/1/0/2/1	1/2/1/0/5	0/1/0/1/4
Odd	0/2/0/2/1	5/4/1/0/0	8/4/1/2/0	0/2/0/0/2	0/3/1/4/1	1/2/1/2/0

Table 3.4: Distribution of pair rule circuit parameters involved in regulating *odd*, including m^{odd}, $E^{odd \leftarrow \beta}$, and $T^{odd \leftarrow b}$. Table columns are selected circuits, categorized into three priority sets according to their fitting quality (RMS score), in both class A and class B circuits (see Appendix A.2). Table rows indicate each gene regulating *odd* in the circuit. Parameter values represent types of regulatory interactions as follows: strong repression if $\leq$ –0.005 (red background), weak repression if between –0.005 and –0.001 (red text), no interaction if between –0.001 and 0.001 (green), weak activation if between 0.001 and 0.005 (blue text), and strong activation if $\geq$ 0.005 (blue background). The number format (strong repression/weak repression/no interaction/weak activation/strong activation) shows the numbers of gene circuits in which a parameter falls into each regulatory category. The background color indicates the type of regulatory interaction found in a majority of circuits, the text color indicates a weaker distribution consensus, and blank (no color) cells indicate indeterminable distribution.

consensus, analysis is a form of statistical pooling of regulatory parameters at different threshold levels, for studying the distribution among different circuits and obtaining a qualitative gene network topology, which has been applied in earlier studies of gap genes (Jaeger et al., 2004b), and *eve* stripe formation mechanism with less quantitative data (Reinitz and Sharp, 1995). In this thesis I extend the parameter distribution analysis to more sets of circuits at different fitting quality, and more levels of parameter thresholds to reflect the higher sensitivity in pair rule gene regulation.

Based on the concept of modularity, different optimized circuits may capture biological regulatory mechanisms at different resolutions. For example the realistic regulatory module may be captured at the level of one particular gene, or one particular stripe, but not the others. The statistical pooling of lower fitting quality sets of circuits may still reveal consensus toward realistic regulatory modules at certain sub-circuitry resolutions. Hence I extend the parameter consensus analysis from one set to three sets of circuits from different fitting quality ranges. Three priority sets of circuits were selected from the class A and class B circuits (see Appendix A.2 for circuits and RMS scores list). For class A circuits, the first priority set includes 5 circuits with an average RMS score (Eqn. 3.4) 24.82, the second priority set includes 10 circuits with an average RMS score 25.32, and the third priority set includes 15 circuits with an average RMS score 26.65. For class B circuits, the first priority set includes 4 circuits with an average RMS score 21.83, the second priority set includes 9 circuits with an average RMS score 23.33, and the third priority set includes 6 circuits with an average RMS score 25.31.

The pair rule circuits, with their sharp rise-and-falls of complex stripes, are also more sensitive in response to changes of regulatory parameters, comparing

to the gap gene circuits (Jaeger et al., 2004b). Hence I extend the parameter thresholds from three to five levels at finer scales to reflect such sensitivity. The regulatory parameters T^{ab}, $E^{a\beta}$ and m^a are classified into five types of interactions, delimited by four levels of thresholds. For parameter values $\leq$ –0.005, the interaction is classified as strong repression, for parameter values between –0.005 and –0.001, the interaction is classified as weak repression, for parameter values between -0.001 and 0.001, the interaction is classified as no interaction, likewise for parameter values between 0.001 and 0.005, the interaction is classified as weak activation, and for parameter values $\geq$ 0.005, the interaction is considered as strong activation. The thresholds of 0.001 and 0.005 were chosen empirically. Interactions falling into the 'no interaction' category usually had no detectable effect on pattern formation in the pair rule gene circuits analyzed graphically.

Here I include the parameter distribution analysis results for *odd* regulation (Table 3.4). The analysis for other genes in the circuit (*eve*, *h*, *run* and *ftz*) are included in Appendix A.2. In Table 3.4, background color blue indicates strong distribution toward activation among circuits, text color blue indicates weaker consensus toward activation among circuits. Similarly, background color red indicates strong consensus toward repression, and text color red indicates weaker consensus toward repression. In the tables for other genes (Appendix A.2), background color green indicates strong consensus toward no interaction, and text color green indicates weaker consensus toward no interaction. For the cells without any color, it indicates indeterminable distribution. According to Ashyraliyev et al. (2008), the non-specific distributions are likely to indicate no interaction (irrelevance) as well.

In Table 3.4, there is exceptionally strong parameter consensus toward

gap gene activation on *odd* (mainly from *hb*, *Kr*, *gt* and *kni*), this consensus is strong among all three priority sets of both class A and class B circuits. There is also exceptionally strong consensus toward *eve* repression on *odd*. These results, together with other less compelling regulatory consensus, will be evaluated with other circuitry and literature information to reach final biological conclusions in Chapter 4.

3.4.6 Literature Integration

Literature integration is another part of systems level analysis that gets more complicated and demanding as the system gets more complex. In the systems level analysis of the gene circuit method, it is only necessary to extract information relevant to systems operation, and leaving out information regarding parts, components, and experimental or theoretical details. The systems information may be extracted through text mining, and then stored and organized in a format that is comparable to circuitry information. This process may also require a regulatory representational system, to facilitate integration and compilation.

In the pair rule literature, most papers are about experimental perturbations, mutant or ectopic gene expression patterns, of smaller subsets (or single) pair rule genes. So from each paper, I first extract information about major regulatory conclusions (targets and regulators), then I extract the major experimental observations that supports the conclusion. These conclusions are drawn at the best from experimental biologists already, based on logical reasoning of existing and sometimes limited, experimental evidences, so I do not have to interpret all the experimental data again nor believe in it completely. Rather at systems level I seek higher consensus from other literature, and make

comparison with model circuitry results.

At the second level literature integration, I extract information regarding complex set of experimental observations, such as complex mutant/ectopic gene expression patterns, double mutant gene expression patterns, binding sites and sequence analyses, enhancer studies, etc. All the extracted literature information are then recompiled across literature on a gene by gene bases (targets and regulators). A lot of literature information involve more than one gene pair, and are narrated in a conjugated way, so this process does require a lot of processing and integration to digest complex literature information, sometimes through duplicating and reducing sets.

The literature integration results for all pair rule genes in the circuits are included in Appendix A.3. More details of the experimental observations are discussed in the main text of Chapter 4, and included in Appendix B. The complex subsets of literature experimental results are included in Appendix A.4.

3.4.7 Drawing Biological Conclusions

The final step in systems level analysis is drawing biological conclusions. This step requires generating conclusions by putting together all systems information, from circuit analysis, statistical pooling and literature integration. More specifically, the conclusions are drawn based on critical subsets of both literature and circuitry information (abstraction), on a gene by gene basis first, then extended to multiple genes (integration). The rest of complex literature and circuitry information are reserved as contexts, for further reference and discussion (Appendix A.1 and A.4).

The pair rule gene regulatory conclusions are drawn based on major consensus and contradictions among circuits and literature. The major predictions

made by the gene circuits, in comparison to literature, are summarized in Figure 4.1. In the summary graph of the ensemble regulatory map, which is presented and explained in more detail in Chapter 4 and Appendix B, different consensus levels among circuits and literature are represented in different colors. The systems level understanding of pair rule gene regulation, based on the gene circuits, and the momentum of such understanding can be directly visualized. The literature regulatory conclusions missing from the circuits are included in Fig. 4.7, for a more complete view of current systems level understanding in pair rule genes.

After reaching the systems global conclusions for major predictions, I can then derive and compare the individual subsets of circuits (shown from Fig. 4.2 to Fig. 4.6), through direct reduction of the ensemble regulatory map. This process cannot be reversed during the research phase, and the graphical display can only serve as the final presentation (Appendix A.1). These individual circuits reveal complex subsets (modules) for stripe regulation. It is yet unclear how all the distributions can be biologically interpreted. Different circuits may exhibit different regulatory features that are biologically relevant, and the degeneracy of regulatory control itself may be biologically significant. The class A circuits are also more representative of the early stripe formation phase regulatory module, and the class B circuits are more representative of the late refinement phase regulatory module.

3.4.8 Regulatory Phasing Analysis

The final step of systems level analysis in the gene circuit method, after drawing biological conclusions based on circuitry and literature results, is regulatory phasing analysis. In Jaeger et al. (2004b), the anterior shifts of gap gene do-

mains are found to be rely on asymmetric gap-gap cross-repression and does not require the diffusion of gap proteins. The dynamic shifts of gap gene expression domains are reflected at the level of the rate of change in protein concentration, with protein synthesis dominates anteriorly, whereas protein decay posteriorly. The combination of anterior synthesis and posterior decay leads to an anterior shift of each expression domain. In addition, both the synthesis and decay domains themselves shift anteriorly over time. In Surkova et al. (2008), mild shifts of pair rule gene expression domains during the late refinement phase were also observed, which is more prominent for the posterior embryo stripes (Fig. 3.2 to 3.4). Hence in the phasing analysis I examine whether there exists a similar mechanism in assisting pair rule gene shifts.

I first examine whether there exists a simple phasing rule for assigning pair rule gene cross regulations to facilitate shifts, by assessing whether an anteriorly overlapping stripe tends to be activating, and a posteriorly overlapping stripe tends to be repressing. An anteriorly overlapping pair rule stripe may serve as a pulling force in increasing the protein synthesis rate at the anterior border, while a posteriorly overlapping stripe can serve as a pushing force in reducing the protein synthesis rate at the posterior border.

In addition to the shift constraints for the simple phasing rule, I also examine the stripe formation constraints, in whether the control gene regulatory input, including the gap gene regulatory input, can increase protein synthesis rate at the peak level of each pair rule gene expression domain, and reduce protein synthesis rate at the limit of each border to facilitate formation or maintenance of pair rule stripes. This will require both direct activators and repressors to have the same spatial gradient of regulatory input to its controlled borders. Such that the regulators can directly contribute to the formation or

maintenance of pair rule genes, instead of counter acting to the stripe formation and refinement process.

For example I examine whether an overlapping pair rule stripe tends to be auto-activating in directly shaping the pair rule stripe, and whether a complementary pair rule stripe tends to be repressing in directly setting the borders. The control regulatory input that fits in the simple phasing rule, with similar gradient to its controlled border, has activation input increases toward the peak region of the total regulatory input for the pair rule stripe, and has repression input increases toward the limit of the border of the total regulatory input for the stripe. The control gene regulatory input, on the other hand that do not fit in the simple phasing rule, with opposite gradient to its controlled border, is considered as a regulatory balancer, which may serve a more important role of refinement for pair rule stripes.

The detailed regulatory phasing analysis results are given in Appendix A.5, and the conclusions for regulatory balancers are summarized and presented in Fig. 4.1 to Fig. 4.7, and in the main texts of Chapter 4. In the next chapter I present the main systems analysis results for the pair rule gene network.

Chapter 4

Pair-Rule Gene Regulation

In this chapter I present the main results and major predictions made by the gene circuits, which is summarized in the predictive ensemble regulatory map (Fig. 4.1). The term "prediction" used in the following descriptions of regulatory conclusions refers to circuitry results that are not supported or verified by experimental evidences in the literature, while "findings" refer to circuitry results that are supported by experimental evidences in literature. The term "regulation" or "interaction" used in the following descriptions of regulatory conclusions refers to regulatory actions at the level of transcriptional control, by the act of transcription factors, which is distinguished from the molecular interactions at the post-translational level.

The major predictions and main results are based on the three major circuits A1, A2 and B1. In Fig. 4.2 to Fig. 4.6, I demonstrate the subsets regulatory map for the three major circuits. In the final systems conclusions section (Section 4.6), I show the integrative ensemble regulatory map (Fig. 4.7), which includes literature regulatory information missing from the circuits and provides a more complete view of current systems understanding of the pair rule

genes. In Fig. 4.1 to Fig. 4.7, different colors of interactions represent different levels of consensus and contradictions among circuits and literature. The interactions taken from literature are categorized into two levels (represented in green and yellow). The six levels of regulatory conclusions are defined as the following:

- **First level regulations (black)**

  Interactions with high level consensus among circuits and literature.

- **Second level regulations (blue)**

  Strong predictions made by circuits (critical regulators) but may not be directly supported by literature.

- **Third level regulations (magenta)**

  Interactions found by circuits (essential regulators) but may contradict to literature.

- **Fourth level regulations (cyan)**

  Critical stripe-specific pair rule cross regulations found in the circuits.

- **Fifth level regulations (green)**

  Interactions considered as minor (insignificant), irrelevant (reducible), or indeterminable to biological relevance (such as a plateau input) in circuits analysis, but are asserted by literature.

- **Sixth level regulations (yellow)**

  Interactions asserted by literature, but are totally absent (do not have any input) in the circuits.

The definition for "critical" and "essential" regulators, and definition for interactions that are considered as minor, reducible, or indeterminable in circuits

analysis are given in Section 3.4.4 and Appendix A.1. Other regulatory features that are added on the regulatory maps include:

- **Highest consensus regulators (weighted width)**

  The highest consensus interactions, among all circuits and literature, in the first level regulations (black) are further highlighted with weighted width in Fig. 4.2 to Fig. 4.7.

- **Regulatory balancers (dash-and-dot lines)**

  The regulations that do not fit in the simple phasing rule, in the regulatory phasing analysis, are considered as regulatory balancers and are represented as dash-and-dot lines.

- **Transient regulators (dashed lines)**

  The potential transient phase (time) specific regulations in the early stripe formation phase, usually contradictions between class A and class B circuits, are represented as dashed lines. The class A circuits are more representative of the early stripe formation phase, which demands more gap gene input. The class B circuits are more representative of the late refinement phase, which relies on pair rule gene cross regulations.

In summary, the predictive ensemble regulatory map (Fig. 4.1) includes the first 3 levels of regulations (black, blue, magenta) and the regulatory balancers. The subsets regulatory map (Fig. 4.2 to Fig. 4.6), from reduction of the ensemble regulatory map for the 3 major circuits, includes the first 4 levels of regulations (black, blue, magenta, cyan), regulatory balancers, highest consensus regulators, and transient regulators. The integrative ensemble regulatory map (Fig. 4.7) includes all 6 levels of regulations (black, blue, magenta,

cyan, green, yellow), regulatory balancers, highest consensus regulators, and transient regulators. The details supporting each interaction and regulatory features are given in Appendix B and A.5.

4.1 *even-skipped* regulation

4.1.1 *eve* regulation by gap genes

For gap gene regulations on *eve* (Fig. 4.1), 9 interactions on 9 specific borders are found from the three major circuits (see Appendix B.1.2 for detailed descriptions). All of these interactions are repressive interactions. Five of the interactions are categorized in black as the first level regulations. Four interactions are categorized in blue as the second level regulations. From the parameter distribution analysis (Appendix Table A.13), the major results include that among the four input gap genes in Fig. 4.1 (*hb*, *gt*, *Kr*, *kni*), *gt*, *Kr* and *kni* repression on *eve* are supported by strong parameter consensus in the class A circuits, and *hb* repression on *eve* is supported by significant consensus of both the class A and class B circuits. In the regulatory phasing analysis (Appendix A.5), 2 interactions are considered as regulatory balancers (represented as dash-and-dot lines in Fig. 4.1), with the gradient of each regulatory input opposite to its controlled border, which does not fit in the simple phasing rule.

4.1.2 *eve* regulation by pair-rule genes

For pair-rule cross regulations on *eve* (Fig. 4.1), the three major circuits found 4 interactions on the anterior border and 5 interactions on the posterior bor-

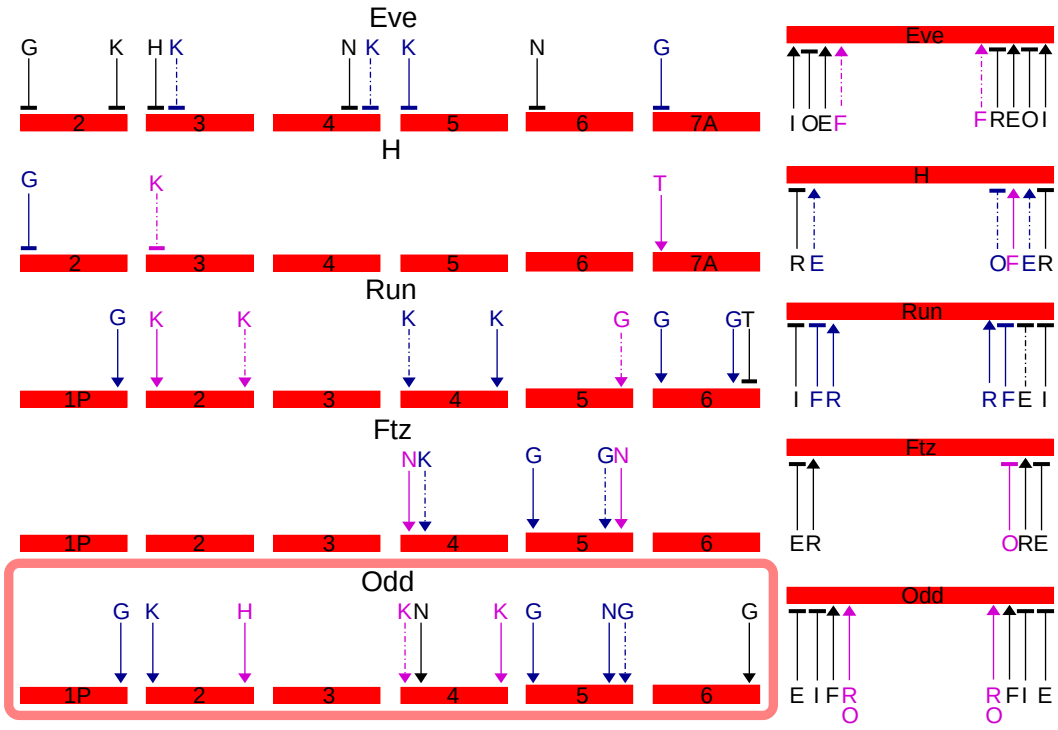

Figure 4.1: Major predictions and findings from systems analysis of *eve*, *h*, *run*, *ftz* and *odd* regulations. Each letter above the arrows represents an input gene in the following pair: B(Bcd), C(Cad), H(Hb), K(Kr), G(Gt), N(Kni), T(Tll), E(Eve), I(H), R(Run), F(Ftz), O(Odd). The number within each red square represents specific stripe number, with "A" stands for anterior border and "P" stands for posterior border. The last panels on the right represent non-stripe-specific regulations on every border for each pair rule gene. The pointed arrows represent activation, blunt arrows represent repression. The color of each interaction represents consensus level among circuits and literature, from the highest level of black, to blue (with no direct literature support, critical regulations), and to magenta (may contradict to literature, essential regulations). Regulatory balancers that do not fit in the simple phasing rule are represented as dash-and-dot lines. Gap gene regulations on *odd* are circled as the primary predictions with full parameter consensus support (Table 3.4). For more information about each interaction and color categorization please see Appendix B and the main text.

der (see Appendix B.1.4 for detailed descriptions). Overall 7 interactions are categorized in black as the first level regulations (3 on the anterior border and 4 on the posterior border), and 2 interactions are categorized in magenta as the third level regulations (1 on each border). Six interactions are activating (3 on the anterior border and 3 on the posterior border) and 3 interactions are repressive (1 on the anterior border and 2 on the posterior border). From the parameter distribution analysis (Appendix Table A.13), the major results include that among the 5 input pair rule genes in Fig. 4.1 (*eve*, *h*, *run*, *ftz*, *odd*), both *h* activation and *odd* repression on *eve* are supported by very strong consensus of both the class A and class B circuits. *ftz* activation on *eve* is supported by stronger consensus of the class B circuits.

In the regulatory phasing analysis (Appendix A.5), 2 interactions (1 on each border) are considered as regulatory balancers. *ftz* is placed in a complementary position to *eve*, with residual expression remaining between the two borders, hence the activator role of *ftz* does not fit in the simple phasing rule. *ftz* activation input increases toward the limit of the two borders of the total regulatory input for *eve*, with opposite gradient to its controlled borders.

4.1.3 Conclusions

In Figure 4.2, I show the complex subsets for *eve* regulation in the three major circuits. Each circuit represents a potential *eve* stripe regulatory module. The class A circuits (A1, A2) are more representative of the stripe formation phase, and the class B circuit (B1) is more representative of the late refinement phase. In Figure 4.2, circuit B1 shows a minimal subset of pair-rule cross regulatory module, which does not require any gap gene input likely in the late refinement and maintenance phase, and primarily depends on *h* activation

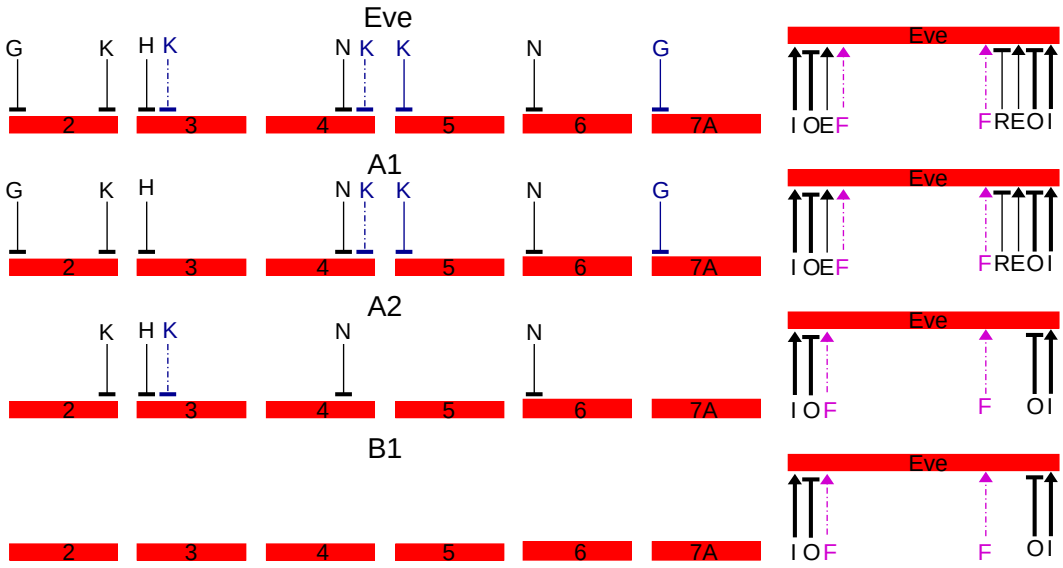

Figure 4.2: Subsets of the ensemble regulatory map for Eve, from circuit A1, A2 and B1. Each letter above the arrows represents an input gene in the following pair: B(Bcd), C(Cad), H(Hb), K(Kr), G(Gt), N(Kni), T(Tll), E(Eve), I(H), R(Run), F(Ftz), O(Odd). Color representations are the same as in Fig. 4.1. The highest consensus interactions among all circuits and literature are highlighted with weighted width in black. Regulatory balancers that do not fit in the simple phasing rule are represented as dash-and-dot lines. For more information about each interaction and color categorization please see Appendix B and the main text.

and *odd* repression. *h* activation and *odd* repression on *eve* also have the most consensus among all circuits and literature, hence are highlighted in weighted width in black.

In the literature (Table A.17 and A.18), *h* activation and *run* repression on *eve* have the most number of literature consensus. Most experimental evidences supporting the first and second level (black and blue) regulations in Fig. 4.1 and contradicting to the third level (magenta) regulations, are based on direct interpretation of perturbation experiments such as mutant and ectopic gene expression. These literature assertions based on experimental observations from diverse sources (Appendix B), together with its complex subsets (Appendix A.4), are put together within the systems context now, and the complex indirect effects will need to be further addressed through modularization and mutant simulations.

In the complex *eve* mutant patterns from literature (Appendix A.4.1), many stripe specific effects were observed for *run* regulation on *eve* from *run* mutant embryos (Frasch and Levine, 1987; Warrior and Levine, 1990; Tsai and Gergen, 1994; Manoukian and Krause, 1993; Hooper et al., 1989). These effects are however not supported by current circuits. In fact, the major circuits have very weak dependence on *run* repression, except in circuit A1 primarily on the posterior border. This may suggest that the stripe-specific *run* mutant effects on *eve* is indirect, through altered effects on other genes. According to Tsai and Gergen (1994), *hs-run* treatment fails to repress a reporter gene containing the *eve* autoregulatory element, which supports that the altered regulation of this element in *run* mutants (Goto et al., 1989) may be indirect.

In the pair-rule cross regulation literature, most perturbation effects, from mutant or ectopic gene expression, are found to be more significant at later

developmental stages. For example in the early literature of Frasch and Levine (1987); Carroll and Vavra (1989), using the strongest available mutant alleles for all the pair-rule genes found only mild perturbation to the establishment of *eve* expression pattern in the early stage. Only relatively mild alterations in the spacing and intensity of expression are detected in cellular blastoderm stage embryos. In the current gene circuits setting, however, there is no parameter constraints for pair-rule cross regulation in the early phase. The mutant effects of pair rule genes, particularly in the early phase, should be tested through mutant simulations. And even though the class B circuits are more representative of the late refinement phase, the specific late refinement phase modules and early stripe formation phase modules should be implemented and investigated separately (see Sections 3.4.1 and 3.4.2 for details on modules). Whether the mutation effects of pair-rule genes in the early stripe formation phase could be compensated or corrected by other pair-rule genes or other regulatory mechanisms remain to be verified.

In the early literature (Frasch and Levine, 1987; Carroll and Vavra, 1989), a general proposition were made that the expression of the primary pair-rule gene *eve* is modulated only by the primary pair-rule genes *h* and *run*, yet remains unaffected by the remaining, secondary and tertiary, pair-rule genes. This proposition is based on earlier observations, such as *eve* pattern is unaffected in *odd* mutant embryos (Mullen and DiNardo, 1995; Coulter and Wieschaus, 1988; Frasch and Levine, 1987). However in later literature, Drean et al. (1998) found in ectopic *hs-odd* embryos, *eve* is the most dramatically affected among the so called primary pair-rule genes at the later stages. In *odd* mutant embryos (Drean et al., 1998), *eve* is also significantly affected especially at later developmental stages. Drean et al. (1998) argues that the above changes

may have been missed in earlier studies due to their subtle nature in certain stage embryos, and the full effect of these actions may also be masked by the redundant actions of other segmentation genes. In my gene circuit results (Fig. 4.1), the earlier hierarchical proposition of pair rule cross regulation is not supported. *odd* is found to be the primary repressor of *eve*, and *ftz* may also serve as an activating balancer. If the presumed secondary or tertiary pair rule genes are not involved in regulating the primary pair rule genes, then restrictive parameter constraints should be placed (imposed) on current gene circuits during optimization, hence to further refine the model and examine, explore, new regulatory possibilities.

4.2 *hairy* regulation

4.2.1 *h* regulation by gap genes

For gap gene regulations on h (Fig. 4.1), the major circuits found only 3 interactions on 3 specific borders (see Appendix B.2.2 for detailed descriptions). Two interactions are repressive and one activating. One interaction is categorized in blue as the second level regulation, and two interactions are categorized in magenta as the third level regulation. From the parameter distribution analysis (Appendix Table A.14), the major results include that among the 3 input gap genes in Fig. 4.1 (gt, Kr, tll), gt repression on h is supported by very strong consensus of both the class A and class B circuits. Kr repression on h, and tll activation on h are supported by stronger consensus of the class A circuits. In the regulatory phasing analysis (Appendix A.5), 1 interaction is considered as a regulatory balancer (represented as dash-and-dot lines in Fig. 4.1), with the gradient of regulatory input opposite to its controlled border, which does not

fit in the simple phasing rule.

4.2.2 *h* regulation by pair-rule genes

For pair-rule cross regulations on *h* (Fig. 4.1), the major circuits found 2 interactions on the anterior border and 4 interactions on the posterior border (see Appendix B.2.4 for detailed descriptions). Overall 2 interactions are categorized in color black as the first level regulation (1 on each border), 3 interactions are categorized in color blue as the second level regulation (1 on the anterior border and 2 on the posterior border), and 1 interaction is categorized in color magenta (on the posterior border). Three interactions are activating (1 on the anterior border and 2 on the posterior border), and 3 interactions are repressive (1 on the anterior border and 2 on the posterior border). From the parameter distribution analysis (Appendix Table A.14), the major results include that among the 4 input pair rule genes in Fig. 4.1 (*eve*, *run*, *ftz*, *odd*), *run* repression on *h* is supported by strong consensus in both class A and class B circuits. *odd* repression on *h*, and *ftz* activation on *h* are both supported by strong consensus in the class B circuits, which is more representative of the late refinement phase. There is also strong consensus for *odd* activation on *h* in the class A circuits, which is more representative of the early stripe formation phase for transient phase (time) specific regulation.

In the regulatory phasing analysis (Appendix A.5), 3 interactions (1 on the anterior border and 2 on the posterior border) are considered as regulatory balancers. *eve* is placed in a posteriorly overlapping position to *h*, hence the activator role of *eve* does not fit in the simple phasing rule. Even though *eve* activation input increases toward the peak of the total regulatory input for *h*, with similar gradient to its controlled borders, it increases in a more

posterior position which does not shift the stripe forward (anteriorly) and violates the shifting constraint of the simple phasing rule. In terms of establishing the *h* stripe, formation constraint in the simple phasing rule, *eve* is certainly capable of being the major activator for *h*. *odd* is positioned in an anteriorly overlapping position to *h*, hence the repressor role of *odd* does not fit in the simple phasing rule. The *odd* repression input increases toward the peak of the total regulatory input for *h*, with opposite gradient to its controlled border, and is more of a plateau on the anterior border in the major circuits.

4.2.3 Conclusions

In Figure 4.3, I show the complex subsets for *h* regulation in the three major circuits. *run* repression on *h* has the most consensus among all circuits and literature, hence are highlighted in weighted width in black. The three major circuits each represents a minimal subset for *h* regulation. In the class A circuits, *run* is the primary repressor and stripe determinant, with activation by constituative promoter expression (bias term h^h in Eqn. 3.1), which represents uniformly distributed maternal transcription factors not explicitly modeled. The repressor role of *run* is consistent with its perfectly complementary phasing position to *h* (Appendix A.5). Even though there are more parameter consensus toward *h* auto-activation in the class B circuits (Appendix Table A.14), which is more representative in the late refinement phase, the contradictions among major circuits is the reason why *h* auto-regulation is not included in the major findings in Fig. 4.1. Three interactions are categorized in cyan as the fourth level regulations, which are the critical stripe specific pair rule cross regulations found in the circuits. *odd* may also have activation effect in the early stripe formation phase, marked as dashed lines in

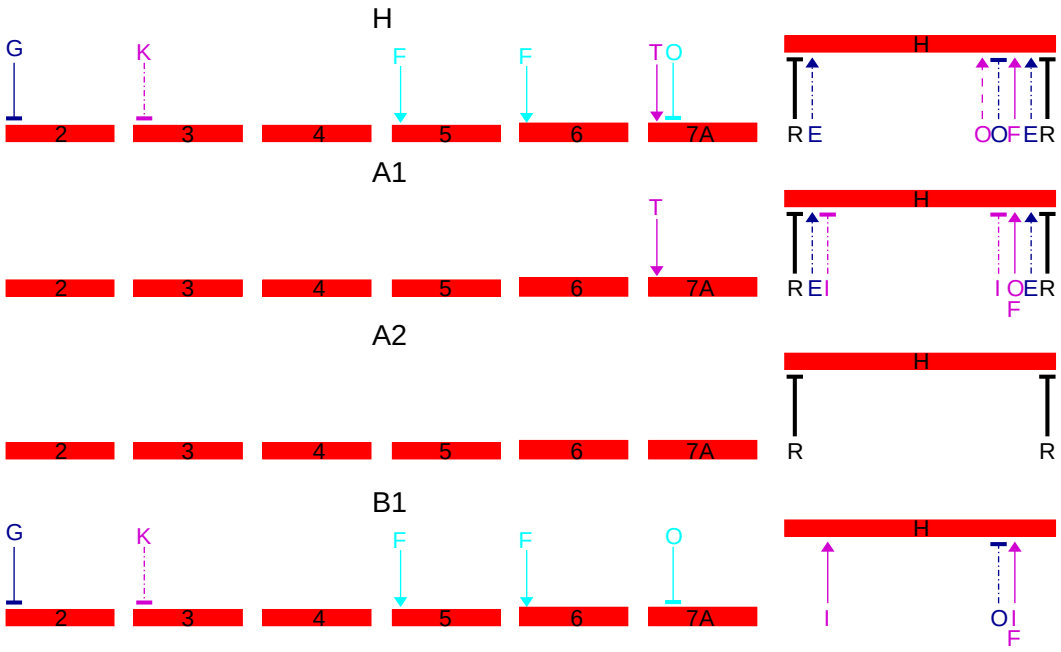

Figure 4.3: Subsets of the ensemble regulatory map for H, from circuit A1, A2 and B1. Each letter above the arrows represents an input gene in the following pair: B(Bcd), C(Cad), H(Hb), K(Kr), G(Gt), N(Kni), T(Tll), E(Eve), I(H), R(Run), F(Ftz), O(Odd). Color representations are the same as in Fig. 4.1, with cyan representing the critical stripe specific pair rule cross regulations found in the circuits. The highest consensus regulations among all circuits and literature are highlighted with weighted width in black. Dashed lines represent potential transient phase (time) specific regulations in the early stripe formation phase. Regulatory balancers that do not fit in the simple phasing rule are represented as dash-and-dot lines. For more information about each interaction and color categorization please see Appendix B and the main text.

Fig. 4.3, which is also supported by activation consensus of the class A circuits (Appendix Table A.14) and essential (non-critical) stripe specific regulations in circuit A1 (Appendix Table A.4).

In the pair rule literature (Appendix A.3), the highest number of regulatory assertions are made for gap gene regulations on *h* (Table A.19 and A.20), even though the major circuits have only found 3 gap gene regulations on *h*. There are also many stripe specific effects reported by literature that are not directly supported by the major circuits. For example *eve* was found important for maintaining *h* stripe 2 (Hooper et al., 1989; Carroll and Vavra, 1989), and *run* was found to be repressing stripe 3/4 and 6/7 (Hooper et al., 1989). In the major circuit A1 (Table A.4), *eve* does have the best phasing position for activation on *h* stripe 2 and stripe 7 anterior border, at a more subtle level. But still the dramatic contradictions between literature and current circuit predictions for gap gene regulations on *h* may imply that many literature assertions are based on interpretations of indirect effects from perturbation experiments. The contradictions between literature and circuits may also imply that there exists strong degeneracy between the pair rule cross regulation module and the gap gene regulation module, such that the early stripe formation module (dominated by gap gene regulations), and the late refinement module for pair rule cross regulations should be implemented and investigated separately, with interactive parameter constraints on the pair rule cross regulations.

4.3 *runt* regulation

4.3.1 *run* regulation by gap genes

For gap gene regulations on *run* (Fig. 4.1), the major circuits found 9 interactions on 9 specific borders (see Appendix B.3.2 for detailed descriptions). Eight interactions are activating and one repressive. One interaction is categorized in black as the first level regulation, 5 interactions are categorized in blue as the second level regulation, and 3 interactions are categorized in magenta as the third level regulation. From the parameter distribution analysis (Appendix Table A.15), the major results include that among the 3 input gap genes in (Fig. 4.1) (*gt*, *Kr*, *tll*), for both class A and class B circuits, *tll* repression on *run* is supported by very strong consensus, *gt* activation on *run* is supported by significant consensus, and *Kr* activation on *run* is supported by mild consensus. In the regulatory phasing analysis (Appendix A.5), 3 interactions are considered as regulatory balancers (represented as dash-and-dot lines in Fig. 4.1), with the gradient of each regulatory input opposite to its controlled border, which does not fit in the simple phasing rule.

4.3.2 *run* regulation by pair-rule genes

For pair-rule cross regulations on *run* (Fig. 4.1), the major circuits found 3 interactions on the anterior border and 4 interactions on the posterior border (see Appendix B.3.4 for detailed descriptions). Overall 3 interactions are categorized in black as the first level regulation (1 on the anterior border and 2 on the posterior border), 4 interactions are categorized in blue as the second level regulation (2 on the anterior border and 2 on the posterior border). Two interactions are activating (1 on each border) and 5 interactions are repressive

(2 on the anterior border and 3 on the posterior border). From the parameter distribution analysis (Appendix Table A.15), the major results include that among the 4 input pair rule genes in Fig. 4.1 (*eve*, *h*, *run*, *ftz*), *h* repression on *run* is supported by very strong consensus of both classes of circuits. *ftz* repression on *run* is supported by stronger consensus in the class B circuits.

In the regulatory phasing analysis (Appendix A.5), 1 interaction (on the posterior border) is considered as a regulatory balancer. *eve* is placed in an anteriorly overlapping position to *run*, hence the repressor role of *eve* does not fit in the simple phasing rule. The *eve* repression input is a plateau on the anterior border of the total regulatory input for *run*, and is increasing toward the peak of the total regulatory input on the posterior border, with opposite gradient to its controlled border. Even though the major circuits do not support *eve* activation on *run*, there is more consensus toward *eve* activation on *run* in the parameter distribution analysis (Appendix Table A.15), and there is also support from the literature (Carroll and Vavra, 1989) for early phase *eve* activation. In this case, an activator role of *eve* in the early phase would fit in the simple phasing rule.

4.3.3 Conclusions

In Figure 4.4, I show the complex subsets for *run* regulation in the three major circuits. *h* repression on *run* has the most consensus among all the major circuits and literature, hence are highlighted in weighted width in black. *gt* activation on *run* also has strong consensus among all the major circuits. Two critical stripe specific pair rule cross regulations were found in the circuits that are categorized in cyan as the fourth level regulations. Even though there is no strong support for *odd* repression on *run* in the three major circuits, except the

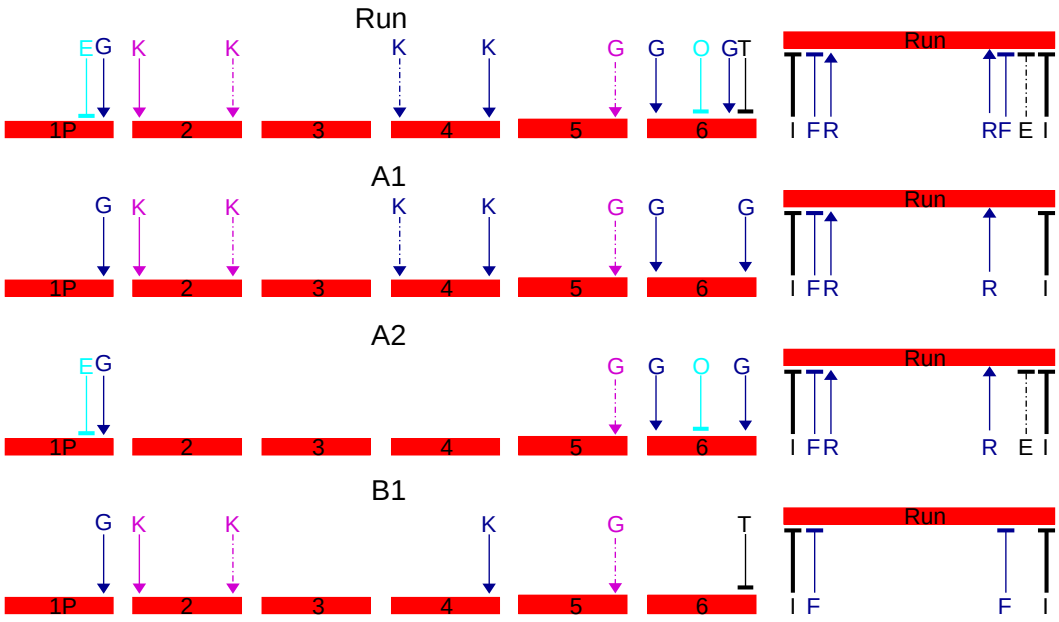

Figure 4.4: Subsets of the ensemble regulatory map for Run, from circuit A1, A2 and B1. Each letter above the arrows represents an input gene in the following pair: B(Bcd), C(Cad), H(Hb), K(Kr), G(Gt), N(Kni), T(Tll), E(Eve), I(H), R(Run), F(Ftz), O(Odd). Color representations are the same as in Fig. 4.1, with cyan representing the critical stripe specific pair rule cross regulations found in the circuits. The highest consensus regulations among all circuits and literature are highlighted with weighted width in black. Regulatory balancers that do not fit in the simple phasing rule are represented as dash-and-dot lines. For more information about each interaction and color categorization please see Appendix B and the main text.

stripe specific effect on stripe 6, there is significant support for *odd* repression on *run* in the parameter distribution analysis (Appendix Table A.15), and in the literature (Drean et al., 1998) for the late refinement phase (Klingler and Gergen, 1993).

In the literature (Table A.21 and A.22), *eve* and *h* repression on *run* have the most number of literature consensus. According to Klingler and Gergen (1993), while the *run* pattern in gap mutations is abnormal from the very beginning, 7 stripes are initially formed in all pair-rule mutations. Mutations in the three primary pair-rule genes (*eve*, *h*, *run*) all lead to patterning defects that are observable during the blastoderm stage. Mutations in all of the secondary pair-rule genes (except *slp*) do not affect the initial 7 stripe patterns of *run* or the other primary pair rule genes. In the primary predictions from the major circuits (Fig. 4.1), all three primary pair-rule genes are involved in regulating *run*, which is expected to have effects on the earlier *run* patterns. The specific effects on the late refinement phase from the repressive input of secondary pair rule gene *ftz*, and the stripe specific input from *odd* (Figure 4.4), remains to be verified. Further mutant simulations and specific modular settings on the early and late refinement phase are required in order to elucidate the roles and involvement of presumed primary and secondary pair rule genes.

4.4 *fushi-tarazu* regulation

4.4.1 *ftz* regulation by gap genes

For gap gene regulations on *ftz* (Fig. 4.1), the major circuits found 5 interactions on 5 specific borders (see Appendix B.4.2 for detailed descriptions), all interactions are activating. Three of the interactions are categorized in blue as

the second level regulation, and the other 2 of the interactions are categorized in magenta as the third level regulation. From the parameter distribution analysis (Appendix Table A.16), the major results include that for all 3 input gap genes in Fig. 4.1 (*Kr*, *gt*, *kni*), the activations on *ftz* are supported by strong consensus of both class A and class B circuits. In the regulatory phasing analysis (Appendix A.5), 2 interactions are considered as regulatory balancers (represented as dash-and-dot lines in Fig. 4.1), with the gradient of each regulatory input opposite to its controlled border, which does not fit in the simple phasing rule.

4.4.2 *ftz* regulation by pair-rule genes

For pair-rule cross regulations on *ftz* (Fig. 4.1), the major circuits predicted 2 interactions on the anterior border and 3 interactions on the posterior border (see Appendix B.4.4 for detailed descriptions). Overall 4 interactions are categorized in black as the first level regulation (2 on each border), 1 interaction (on the posterior border) is categorized in magenta as the third level regulation. Three interactions are repressive (1 on the anterior border and 2 on the posterior border) and 2 interactions are activating (1 on each border). From the parameter distribution analysis (Appendix Table A.16), the major results include that among the 3 input pair rule genes in Fig. 4.1 (*eve*, *run*, *odd*), both *eve* repression and *run* activation on *ftz* are supported by strong consensus of both class A and class B circuits.

In the regulatory phasing analysis (Appendix A.5), *odd* is placed in a posteriorly overlapping position to *ftz* in data, however in the major circuits *odd* is almost overlapping with *ftz*. Hence according to data, it is the repressor role of *odd* that would actually fit in the simple phasing rule.

4.4.3 Conclusions

In Figure 4.5, I show the complex subsets for *ftz* regulation in the three major circuits. Circuit A2 shows a minimal subset which only depends on *odd* activation, however this may be a circuit artifact due to the incorrect overlapping position between *odd* and *ftz* stripes found in the circuit. There is one critical stripe specific pair rule cross regulation found in the circuits, which is categorized in cyan as the fourth level regulation.

In the literature (Table A.23 and A.24), *h* repression on *ftz* has the most number of literature consensus. The more posteriorly overlapping position of *h* to *ftz* also supports the repressor role of *h*, which fits in the simple phasing rule. However, surprisingly, there is no dependence on *h* repression in the 3 major circuits. Even though there is strong parameter consensus in the class B circuits toward *h* repression in the parameter distribution analysis (Table A.16). Placing an interactive parameter constraint for *h* repression on *ftz* in the modular setting may be something to carry out in order to explore and elucidate the regulatory role of *h* on *ftz*.

In summary, according to Yu and Pick (1995), primary pair-rule genes are more involved in the refinement and maintenance rather than establishment phase of the *ftz* stripes. Initial *ftz* pattern was found to form correctly in all three primary pair-rule mutants (Yu and Pick, 1995). In the major circuits, *ftz* has strong dependence on *eve* and *run* cross regulations, however the role of *h* may be obscured by the incorrect overlapping position of *odd* in the major circuits. The early and late mutation effects in the circuits remain to be verified through mutant simulations and modular analysis.

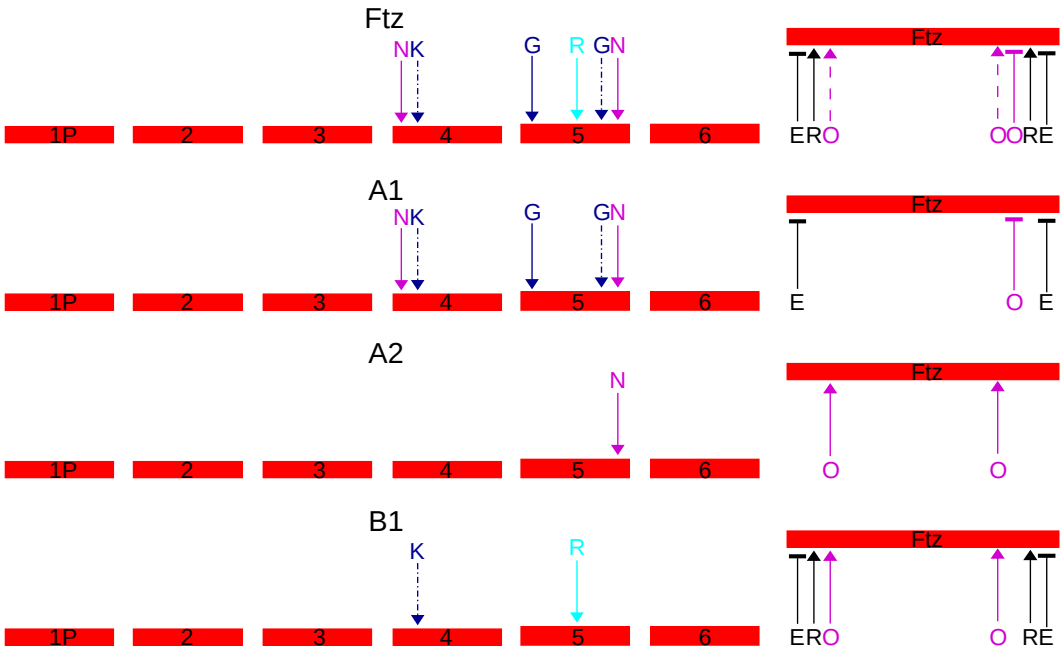

Figure 4.5: Subsets of the ensemble regulatory map for Ftz, from circuit A1, A2 and B1. Each letter above the arrows represents an input gene in the following pair: B(Bcd), C(Cad), H(Hb), K(Kr), G(Gt), N(Kni), T(Tll), E(Eve), I(H), R(Run), F(Ftz), O(Odd). Color representations are the same as in Fig. 4.1, with cyan representing the critical stripe specific pair rule cross regulations found in the circuits. Dashed lines represent potential transient phase (time) specific regulations in the early stripe formation phase. Regulatory balancers that do not fit in the simple phasing rule are represented as dash-and-dot lines. For more information about each interaction and color categorization please see Appendix B and the main text.

4.5 *odd-skipped* regulation

4.5.1 *odd* regulation by gap genes

For gap gene regulations on *odd* (Fig. 4.1), the major circuits predicted 10 interactions on 10 specific borders (see Appendix B.5.2 for detailed descriptions). All predicted interactions are activating. Two interactions are categorized in black as the first level regulation, 5 interactions are categorized in blue as the second level regulation, and 3 interactions are categorized in magenta as the third level regulation. From the parameter distribution analysis (Table 3.4), the major results include that all of the 4 input gap genes in Fig. 4.1 (*hb*, *gt*, *Kr*, *kni*) are supported by strong activation consensus of both the class A and class B circuits. Given that there is surprisingly no literature found for gap gene regulations on *odd*, the predicted gap gene regulations are circled in Fig. 4.1 as the major, featured, predictions. In the regulatory phasing analysis (Appendix A.5), 2 interactions are considered as regulatory balancers (represented as dash-and-dot lines in Fig. 4.1), with the gradient of each regulatory input opposite to its controlled border, which does not fit in the simple phasing rule.

4.5.2 *odd* regulation by pair-rule genes

For pair-rule cross regulations on *odd* (Fig. 4.1), the major circuits found 5 interactions on the anterior border and 5 interactions on the posterior border (see Appendix B.5.4 for detailed descriptions). Overall 6 interactions are categorized in black as the first level regulation (3 on each border), 4 interactions are categorized in magenta (2 on each border). Six interactions are activating (3 on each border) and 4 interactions are repressive (2 on each border). From

the parameter distribution analysis (Table 3.4), the major results include that among the 5 input pair rule genes in Fig. 4.1 (*eve*, *h*, *run*, *ftz*, *odd*), *eve* repression and *ftz* activation on *odd* are both supported by strong consensus of both the class A and class B circuits.

In the regulatory phasing analysis (Appendix A.5), all predicted pair rule cross regulations on *odd* are found to fit in the simple phasing rule. Although *ftz* is placed in an anteriorly overlapping position to *odd* in data, in the major circuits *odd* and *ftz* are almost overlapping. In either case *ftz* remains the main activator on *odd*, and the activator role of *ftz* fits in the simple phasing rule.

4.5.3 Conclusions

In Figure 4.6, I show the complex subsets for *odd* regulation in the 3 major circuits. *eve* repression on *odd* has the most consensus among all circuits and literature, hence are highlighted in weighted width in black. Circuit B1 shows a minimal subset, which is more representative of the late refinement phase, with *run* as the major activator, and *eve* as the only repressor required. There are 7 critical stripe specific pair rule cross regulations found in the major circuits, which are categorized in cyan as the fourth level regulation.

In the literature (Table A.25), *eve* repression on *odd* has the most number of literature consensus. Compared to other pair rule genes, *odd* has the least number of literature references about its regulation, and is categorized as the most downstream of the regulatory hierarchy among the pair rule genes. While there is no literature for gap gene regulations on *odd*, and there is the strongest support from both the parameter consensus (Table 3.4) and the major circuits, *odd* regulations by gap genes are featured as the major predictions in Fig. 4.1.

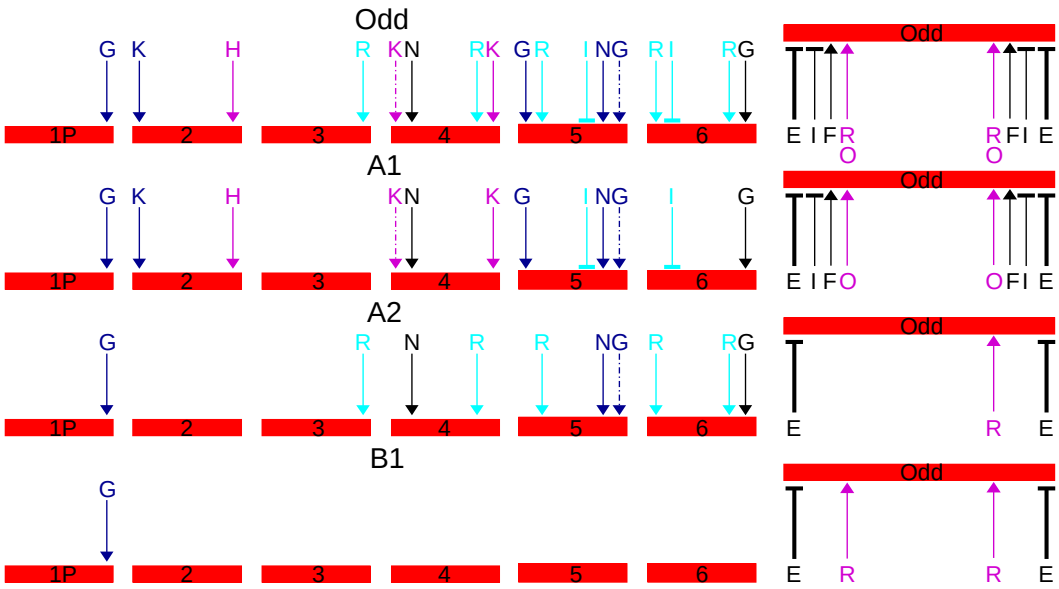

Figure 4.6: Subsets of the ensemble regulatory map for Odd, from circuit A1, A2 and B1. Each letter above the arrows represents an input gene in the following pair: B(Bcd), C(Cad), H(Hb), K(Kr), G(Gt), N(Kni), T(Tll), E(Eve), I(H), R(Run), F(Ftz), O(Odd). Color representations are the same as in Fig. 4.1, with cyan representing the critical stripe specific pair rule cross regulations found in the circuits. The highest consensus regulations among all circuits and literature are highlighted with weighted width in black. Regulatory balancers that do not fit in the simple phasing rule are represented as dash-and-dot lines. For more information about each interaction and color categorization please see Appendix B and the main text.

4.6 Systems Conclusions

In the integrative ensemble regulatory map (Fig. 4.7), I show a more complete view of current systems level understanding of the pair rule genes based on both the gene circuit results and the literature. The fifth level regulations (green) are interactions considered as minor (insignificant), irrelevant (reducible), or indeterminable to biological relevance (such as a plateau input) in the circuits, but are asserted by literature. For gap gene regulations, there are 5 regulations on *eve*, 9 regulations on *h* (on 14 specific borders) that are categorized in green. For pair rule cross regulations, there are 2 regulations on *eve* (on the anterior border), 1 regulation on *h* (on the anterior border), 3 regulations on *run* (2 on the anterior border and 1 on the posterior border), and 5 regulations on *ftz* (3 on the anterior border and 2 on the posterior border) that are categorized in green in Fig. 4.7 as the fifth level regulations.

The sixth level (yellow) regulations are interactions asserted by literature, but are totally absent (do not have any input) in the circuits. For gap gene regulations, there are 3 regulations on *eve*, 14 regulations on *h* (on 15 specific borders), 5 regulations on *run*, and 2 regulations on *ftz* that are categorized in yellow as the sixth level regulations. Overall in the pair rule literature, gap gene regulations on *h* has the most number of regulatory assertions, while in the current gene circuits there are only 3 interactions found (Fig. 4.7).

There is also no direct support for most stripe specific pair rule cross regulations found in the circuits (Fig. 4.2 to Fig. 4.7), hence only the critical subset of such stripe specific regulations are shown (see Appendix B and Appendix A.1 for more details). These findings and contradictions demand further investigations to continually refine and improve our understanding of the pair rule network. Through modularization and interactive parameter constraints, we

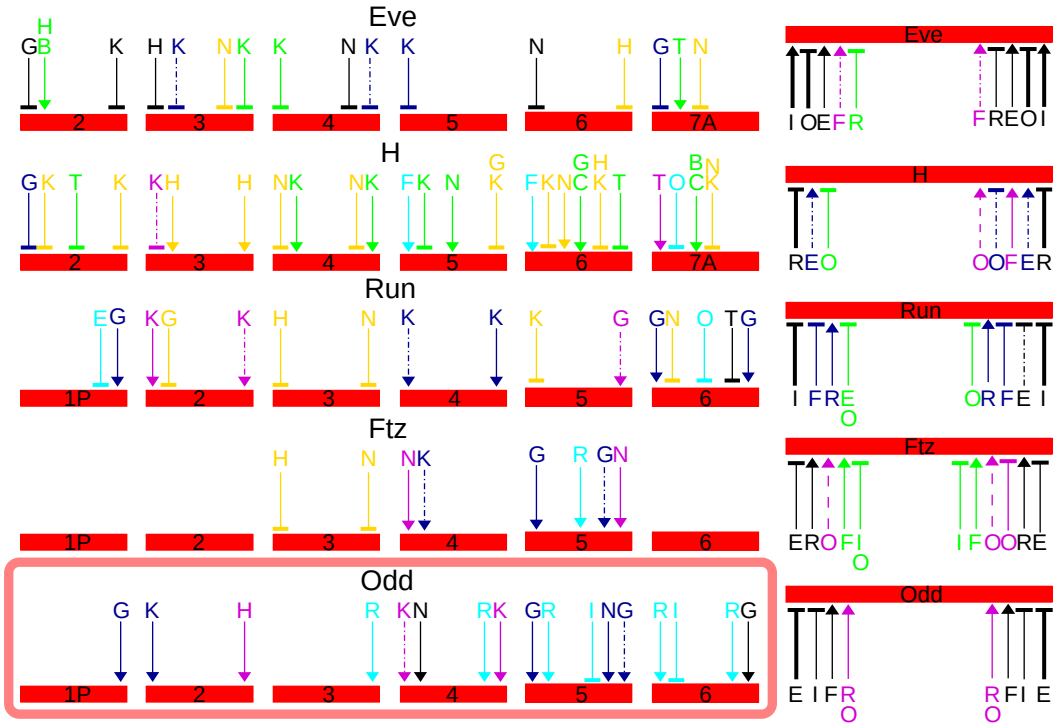

Figure 4.7: Summary systems level analysis results for *eve*, *h*, *run*, *ftz* and *odd* regulation. Each letter above the arrows represents an input gene in the following pair: B(Bcd), C(Cad), H(Hb), K(Kr), G(Gt), N(Kni), T(Tll), E(Eve), I(H), R(Run), F(Ftz), O(Odd). Color representations are the same as in Fig. 4.1 and Fig. 4.2 to Fig. 4.6, with green representing the fifth level regulations, which are regulations considered as minor (insignificant), irrelevant (reducible) or indeterminable (plateau) during circuits analysis, but are asserted by literature. Yellow represents the sixth level regulations, which are regulations totally absent in the circuits but are supported by literature. For more information about each interaction and color categorization please see Appendix B and the main text.

can continually evolve the model and resolve conflicts with experimental observations using the computational systems approach.

Other systems level features include that in the predicted non-stripe-specific pair rule cross regulations, there are pairings of activating and repressive regulations that fit in the simple phasing rule (non regulatory balancers) for every pair rule gene except *h*. For *h* regulation in circuit A1 (Fig. 4.3), *eve* plays a unique and more subtle role as a regulatory balancer that only violates the shifting constraint in the simple phasing rule. Hence *eve* is certainly capable of serving as the major, stripe determining, activator for *h*, but there is no activating, pulling, driving force for *h* shifts found in the major circuits, especially on the anterior border. In circuit A2 and B1 (Fig. 4.3), *h* stripes form primarily through constituative promoter activation (bias term h^h in Eqn. 3.1) and *run* repression, or through constituative promoter repression and *h* autoactivation, which is controversial with contradictions among the major circuits and literature. On the other hand, in the literature, gap genes are considered as the major, stripe determining, activators for *h*, with an exception of *h* stripe 2, which is reported to be formed, or maintained, by *eve* (Hooper et al., 1989; Carroll and Vavra, 1989).

Interestingly for the predicted gap gene regulations, all regulations are repressive on *eve*, while on the other end of the spectrum, all regulations are activating on *odd*, and also on *run* and *ftz*, except for *tll* repression on *run* stripe 6 posterior border. It is unclear about the distribution why gap genes tend to set *eve* stripes through repression, and on the other hand, in the complex system, setting *run*, *ftz*, and *odd* stripes through activation. The effect of promoter threshold (h^a in Equation. 3.1) does not have a strong and direct correlation to such distribution (see Table 3.1 to Table 3.3), for example

h^{run} is much higher than h^{eve} in circuit A1 and A2, and is at a similar positive level in circuit B1. h^{odd} has a strong negative value in circuit A1 and B1, but in circuit B1 there is only one gap gene input on *odd*, and in circuit A2 the h^{odd} is positive. *eve*, *run* and *odd* also have the largest number of predicted gap gene regulations, while *h* and *ftz* have the least. In this regard *eve*, *run* and *odd* seem to be more primarily connected to the upstream gap gene signals.

Since *h* and *ftz* have the fewest number of predicted gap gene regulations, the role of *odd* becomes more controversial. The contradicting regulatory results of *odd* regulation on *h* and *ftz*, between the class A and class B circuits, suggests potential early phase activation from *odd*, or it could simply mean that *odd* regulation on *h* and *ftz* is irrelevant or indeterminable. It is unclear whether the conflicting role of *odd* is related to the absence, or obscured, gap gene regulations on *h* and *ftz* in the circuits.

Overall from the perspectives of par rule cross regulations in the model, there is no strong indication for which pair rule gene is primary or secondary. There is a potential for all pair rule genes to be involved in the cross regulations on *eve*, *h*, *run* and *odd*, except for *ftz* (Fig. 4.7), since *h* regulation on *ftz* and *ftz* auto-regulation are absent in the circuits.

In the regulatory phasing analysis (Appendix A.5), according to the simple phasing rule, the complementary pair rule genes (with complementary patterns) should be mutually repressive in order to directly set the borders. Among the 3 complementary sets of pair rule genes, including *eve*/*ftz*, *eve*/*odd*, and *h*/*run*, only *ftz* regulation on *eve* is activating in the circuits, which violates the simple phasing rule, all the other regulations with complementary patterns are repressive. The complementary sets can also form a reducible (homeostatic) set when regulating other pair rule genes at the same time with

the same (activating or repressive) function, which is suitable for degeneracy (redundancy) control mechanism. For example *eve* and *ftz* were in a reducible set when both activating *h*, and both repressing *ftz*, in circuit A2 (see Appendix A.1 for details on reducible sets, including gap gene reducible sets).

Bibliography

Akam, M. (1987). The molecular basis for metameric pattern in the *Drosophila* embryo. *Development*, 101:1–22.

Arnosti, D. N., Barolo, S., Levine, M., and Small, S. (1996). The eve stripe 2 enhancer employs multiple modes of transcriptional synergy. *Development*, 122:205–214.

Ashyraliyev, M., Jaeger, J., and Blom, J. G. (2008). Parameter estimation and determinability analysis applied to *Drosophila* gap gene circuits. *BMC Systems Biology*, 2:83.

Austin, D. W., Allen, M. S., McCollum, J. M., Dar, R. D., Wilgus, J. R., Sayler, G. S., Samatova, N. F., Cox, C. D., and Simpson, M. L. (2006). Gene network shaping of inherent noise spectra. *Nature*, 439:608–611.

Bar-Even, A., Paulsson, J., Maheshri, N., Carmi, M., O'Shea, E., Pilpel, Y., and Barkai, N. (2006). Noise in protein expression scales with natural protein abundance. *Nature Genetics*, 38:636–643.

Becskei, A., Kaufmann, B. B., and van Oudenaarden, A. (2005). Contributions of low molecule number and chromosomal positioning to stochastic gene expression. *Nature Genetics*, 37:937–944.

Bender, M., Horikami, S., Cribbs, D., and Kaufman, T. C. (1988). Identification and expression of the gap segmentation gene *hunchback* in *drosophila melanogaster*. *Developmental Genetics*, 9:715–732.

Blake, W. J., Kaern, M., Cantor, C. R., and Collins, J. J. (2003). Noise in eukaryotic gene expression. *Nature*, 422:633–637.

Bodnar, J. W. (1997). Programming the *Drosophila* embryo. *The Journal of Theoretical Biology*, 188:391–445.

Campos-Ortega, J. A. and Hartenstein, V. (1985). *The Embryonic Development of* Drosophila melanogaster. Springer, Heidelberg, Germany.

Carroll, S. B. (1990). Zebra patterns in fly embryos: activation of stripes or repression of interstripes? *Cell*, 60:9–16.

Carroll, S. B., Laughon, A., and S., T. B. (1988). Expression, function and regulation of the *hairy* segmentation protein in the *Drosophila* embryo. *Genes and Development*, 2:883–890.

Carroll, S. B. and Scott, M. P. (1986). Zygotically active genes that affect the spatial expression of the *fushi tarazu* segmentation gene during early *Drosophila* embryogenesis. *Cell*, 45:113–126.

Carroll, S. B. and Vavra, S. H. (1989). The zygotic control of *Drosophila* pair-rule gene expression: II. spatial repression by gap and pair-rule gene products. *Development*, 107:673–683.

Casanova, J. (1990). Pattern formation under the control of the terminal system in the *Drosophila* embryo. *Development*, 110:621–628.

Chu, K.-W. (2001). *Optimal Parallelization of Simulated Annealing by State Mixing*. PhD Thesis, Department of Applied Mathematics and Statistics, Stony Brook University.

Chu, K. W., Deng, Y., and Reinitz, J. (1999). Parallel simulated annealing by mixing of states. *The Journal of Computational Physics*, 148:646–662.

Colman-Lerner, A., Gordon, A., Serra, E., Chin, T., Resnekov, O., Endy, D., Pesce, C. G., and Brent, R. (2005). Regulated cell-to-cell variation in a cell-fate decision system. *Nature*, 437:699–706.

Coulter, D. E. and Wieschaus, E. (1988). Gene activities and segmental patterning in *Drosophila*: analysis of *odd-skipped* and pair-rule double mutants. *Genes and Development*, 2:1812–1823.

Csete, M. E. and Doyle, J. C. (2002). Reverse engineering of biological complexity. *Science*, 295:1664–1669.

Dearolf, C. R., Topol, J., and Parker, C. S. (1989a). The *caudal* gene product is a direct activator of *fushi tarazu* transcription during *Drosophila* embryogenesis. *Nature*, 341:340–343.

Dearolf, C. R., Topol, J., and Parker, C. S. (1989b). Transcriptional control of *drosophila fushi tarazu* zebra stripe expression. *Genes and Development*, 3:384–398.

Dearolf, C. R., Topol, J., and Parker, C. S. (1990). Transcriptional regulation of the *Drosophila* segmentation gene *fushi tarazu* (*ftz*). *BioEssays*, 12(3):109–113.

Drean, B. S.-L., Nasiadka, A., Dong, J., and Krause, H. M. (1998). Dynamic changes in the functions of Odd-skipped during early *Drosophila* embryogenesis. *Development*, 125:4851–4861.

Driever, W. and Nüsslein-Volhard, C. (1988a). The Bicoid protein determines position in the *Drosophila* embryo in a concentration-dependent manner. *Cell*, 54:95–104.

Driever, W. and Nüsslein-Volhard, C. (1988b). A gradient of Bicoid protein in *Drosophila* embryos. *Cell*, 54:83–93.

Driever, W. and Nüsslein-Volhard, C. (1989). The Bicoid protein is a positive regulator of *hunchback* transcription in the early *Drosophila* embryo. *Nature*, 337:138–143.

Driever, W., Thoma, G., and Nüsslein-Volhard, C. (1989). Determination of spatial domains of zygotic gene expression in the *Drosophila* embryo by the affinity of binding sites for the Bicoid morphogen. *Nature*, 340:363–367.

Duffy, J. B. and Perrimon, N. (1994). The torso pathway in *Drosophila*: Lessons on receptor Tyrosine Kinase signaling and pattern formation. *Developmental Biology*, 166:380–395.

Eldon, E. D. and Pirrotta, V. (1991). Interactions of the *Drosophila* gap gene *giant* with maternal and zygotic pattern-forming genes. *Development*, 111:367–378.

Elf, J. and Ehrenberg, M. (2004). Spontaneous separation of bi-stable biochemical systems into spatial domains of opposite phases. *Syst. Biol.*, 2:230–236.

Elowitz, M. B., Levine, A. J., Siggia, E. D., and Swain, P. S. (2002). Stochastic gene expression in a single cell. *Science*, 297:1183–1186.

Fange, D. and Elf, J. (2006). Noise-induced min phenotypes in *e. coli*. *PLoS Computational Biology*, 2:0637–0648.

Foe, V. E. (1989). Mitotic domains reveal early commitment of cells in *Drosophila* embryos. *Development*, 107:1–25.

Foe, V. E. and Alberts, B. M. (1983). Studies of nuclear and cytoplasmic behaviour during the five mitotic cycles that precede gastrulation in *Drosophila* embryogenesis. *The Journal of Cell Science*, 61:31–70.

Frasch, M. and Levine, M. (1987). Complementary patterns of *even-skipped* and *fushi-tarazu* expression involve their differential regulation by a common set of segmentation genes in *Drosophila*. *Genes and Development*, 1:981–995.

Frasch, M., Warrior, R., Tugwood, J., and Levine, M. (1988). Molecular analysis of *even-skipped* mutants in *Drosophila* development. *Genes and Development*, 2:1824–1838.

Frohnhöfer, H. G. and Nüsslein-Volhard, C. (1986). Organization of anterior pattern in the *Drosophila* embryo by the maternal gene *bicoid*. *Nature*, 324:120–125.

Frohnhöfer, H. G. and Nüsslein-Volhard, C. (1987). Maternal genes required for the anterior localization of *bicoid* activity in the embryo of *Drosophila*. *Genes and Development*, 1:880–890.

Fujioka, M., Emi-Sarker, Y., Yusibova, G. L., Goto, T., and Jaynes, J. B. (1999). Analysis of an *even-skipped* rescue transgene reveals both compos-

ite and discrete neuronal and early blastoderm enhancers, and multi-stripe positioning by gap gene repressor gradients. *Development*, 126:2527–2538.

Fujioka, M., Jaynes, J. B., and Goto, T. (1995). Early *even-skipped* stripes act as morphogenetic gradients at the single cell level to establish *engrailed* expression. *Development*, 121:4371–4382.

Fujioka, M., Miskiewicz, P., Raj, L., Gulledge, A. A., Weir, M., and Goto, T. (1996). *Drosophila* Paired regulates late *even-skipped* expression through a composite binding site for the paired domain and the homeodomain. *Development*, 122:2697–2707.

Gaul, U. and Jäckle, H. (1987). Pole region-dependent repression of the *Drosophila* gap gene *Krüppel* by maternal gene products. *Cell*, 51:549–555.

Gaul, U., Seifert, E., Schuh, R., and Jäckle, H. (1987). Analysis of *Krüppel* protein distribution during early *Drosophila* development reveals posttranscriptional regulation. *Cell*, 50:639–647.

Gilbert, S. F. (2003). *Developmental Biology*. Sinauer Associates, Sunderland, MA, seventh edition.

Gilbert, S. F. and Sarkar, S. (2000). Embracing complexity: Organicism for the 21st century. *Developmental Dynamics*, 219:1–9.

Gillespie, D. T. (1976). A general method for numerically simulating the stochastic time evolution of coupled chemical reactions. *The Journal of Computational Physics*, 22:403–434.

Gillespie, D. T. (1977). Exact stochastic simulation of coupled chemical reactions. *The Journal of Physical Chemistry*, 81:2340–2361.

Goto, T., MacDonald, P., and Maniatis, T. (1989). Early and late periodic patterns of *even-skipped* expression are controlled by distinct regulatory elements that respond to different spatial cues. *Cell*, 57:413–422.

Gregor, T., Bialek, W., de Ruyter van Steveninck, R. R., Tank, D. W., and Wieschaus, E. F. (2005). Diffusion and scaling during early embryonic pattern formation. *Proceedings of the National Academy of Sciences USA*, 102(51):18403–18407.

Gregor, T., Tank, D. W., Wieschaus, E. F., and Bialek, W. (2007a). Probing the limits to positional information. *Cell*, 130:153–164.

Gregor, T., Wieschaus, E. F., McGregor, A. P., Bialek, W., and Tank, D. W. (2007b). Stability and nuclear dynamics of the Bicoid morphogen gradient. *Cell*, 130:141–152.

Gursky, V. V., Jaeger, J., Kozlov, K. N., Reinitz, J., and Samsonova, A. M. (2004). Pattern formation and nuclear divisions are uncoupled in *Drosophila* segmentation: comparison of spatially discrete and continuous models. *Physica D*, 197:286–302.

Gutjahr, T., Frei, E., and Noll, M. (1993). Complex regulation of early *paired* expression: Initial activation by gap genes and pattern modulation by pair-rule genes. *Development*, 117:609–623.

Häder, T., Rosée, A. L., Ziebold, U., Busch, M., Taubert, H., Jäckle, H., and Rivera-Pomar, R. (1998). Activation of posterior pair-rule stripe expression in response to maternal *caudal* and zygotic *knirps* activities. *Mechanisms of Development*, 71:177–186.

Harding, K., Hoey, T., Warrior, R., and Levine, M. (1989). Autoregulatory and gap gene response elements of the *even-skipped* promoter of *Drosophila*. *The EMBO Journal*, 8:1205–1212.

Harding, K., Rushlow, C., Doyle, H. J., Hoey, T., and Levine, M. (1986). Cross-regulatory interactions among pair-rule genes in *Drosophila*. *Science*, 233:953–959.

Hartmann, C., Taubert, H., Jäckle, H., and Pankratz, M. J. (1994). A two-step mode of stripe formation in the *Drosophila* blastoderm requires interactions among primary pair rule genes. *Mechanisms of Development*, 45:3–13.

Hattne, J., Fange, D., and Elf, J. (2005). Stochastic reaction-diffusion simulation with Mesord. *Bioinformatics*, 21:2923–2924.

Hiromi, Y. and Gehring, W. J. (1987). Regulation and function of the *Drosophila* segmentation gene *fushi tarazu*. *Cell*, 50:963–974.

Hiromi, Y., Kuroiwa, A., and Gehring, W. J. (1985). Control elements of the *Drosophila* segmentation gene fushi tarazu. *Cell*, 43:603–613.

Hoch, M., Seifert, E., and Jäckle, H. (1991). Gene expression mediated by cis-acting sequences of the *Krüppel* gene in response to the *Drosophila* morphogens Bicoid and Hunchback. *The EMBO Journal*, 10:2267–2278.

Hooper, K. L., Parkhurst, S. M., and Ish-Horowicz, D. (1989). Spatial control of *hairy* protein expression during embryogenesis. *Development*, 107:489–504.

Houchmandzadeh, B., Wieschaus, E., and Leibler, S. (2002). Establishment

of developmental precision and proportions in the early *Drosophila* embryo. *Nature*, 415:798–802.

Houchmandzadeh, B., Wieschaus, E., and Leibler, S. (2005). Precise domain specification in the developing *Drosophila* embryo. *Physical Review E*, 72. Art. No. 061920 Part 1.

Howard, K., Ingham, P., and Rushlow, C. (1988). Region-specific alleles of the *Drosophila* segmentation gene *hairy*. *Genes and Development*, 2:1037–1046.

Howard, K. and Ingham, P. W. (1986). Regulatory interactions between the segmentation genes *fushi tarazu, hairy*, and *engrailed* in the *Drosophila* blastoderm. *Cell*, 44:949–957.

Howard, K. and Struhl, G. (1990). Decoding positional information: Regulation of the pair-rule gene *hairy*. *Development*, 110:1223–1231.

Hülskamp, M., Lukowitz, W., Beermann, A., Glaser, G., and Tautz, D. (1994). Differential regulation of target genes by different alleles of the segmentation gene *hunchback* in *Drosophila*. *Genetics*, 138:125–134.

Ingham, P. W. (1988). The molecular genetics of embryonic pattern formation in *Drosophila*. *Nature*, 335:25–34.

Ingham, P. W., Baker, N. E., and Martinez-Arias, A. (1988). Regulation of segment polarity genes in the *Drosophila* blastoderm by *fushi tarazu* and *even skipped*. *Nature*, 331:73–75.

Ingham, P. W. and Gergen, J. P. (1988). Interactions between the pair-rule genes *runt*, *hairy*, *even-skipped*, and *fushi-tarazu* and the establishment of pe-

riodic pattern in the *Drosophila* embryo. *Development*, 104 Supplement:51–60.

Ingham, P. W., Ish-Horowicz, D., and Howard, K. R. (1986). Correlative changes in homeotic and segmentation gene expression in *Krüppel* mutant embryos of *Drosophila*. *The EMBO Journal*, 5:1659–1665.

Ingham, P. W. and Martinez-Arias, A. (1992). Boundaries and fields in early embryos. *Cell*, 68:221–235.

Irish, V., Lehmann, R., and Akam, M. (1989). The *Drosophila* posterior-group gene *nanos* functions by repressing *hunchback* activity. *Nature*, 338:646–648.

Ish-Horowicz, D. and Pinchin, S. M. (1987). Pattern abnormalities induced by ectopic expression of the *Drosophila* gene *hairy* are associated with repression of *ftz* transcription. *Cell*, 51:405–415.

Ish-Horowicz, D., Pinchin, S. M., Ingham, P. W., and Gyurkovics, H. G. (1989). Autocatalytic *ftz* activation and metameric instability induced by ectopic *ftz* expression. *Cell*, 57:223–232.

Jäckle, H., Tautz, D., Schuh, R., Seifert, E., and Lehmann, R. (1986). Cross-regulatory interactions among the gap genes of *Drosophila*. *Nature*, 324:668–670.

Jaeger, J., Blagov, M., Kosman, D., Kozlov, K. N., Manu, Myasnikova, E., Surkova, S., Vanario-Alonso, C. E., Samsonova, M., Sharp, D. H., and Reinitz, J. (2004a). Dynamical analysis of regulatory interactions in the gap gene system of *Drosophila melanogaster*. *Genetics*, 167:1721–1737.

Jaeger, J., Surkova, S., Blagov, M., Janssens, H., Kosman, D., Kozlov, K. N., Manu, Myasnikova, E., Vanario-Alonso, C. E., Samsonova, M., Sharp, D. H., and Reinitz, J. (2004b). Dynamic control of positional information in the early *Drosophila* embryo. *Nature*, 430:368–371.

Janssens, H., Kosman, D., Vanario-Alonso, C. E., Jaeger, J., Samsonova, M., and Reinitz, J. (2005). A high-throughput method for quantifying gene expression data from early *Drosophila* embryos. *Development, Genes and Evolution*, 215:374–381.

Jaynes, J. B. and Fujioka, M. (2004). Drawing lines in the sand: *even-skipped* et al. and parasegment boundaries. *Developmental Biology*, 269:609–622.

Jiménez, G., M.Pinchin, S., and Ish-Horowicz, D. (1996). *In vivo* interactions of the *Drosophila* Hairy and Runt transcriptional repressors with target promoters. *EMBO J.*, 15:7088–7098.

Jürgens, G., Wieschaus, E., Nüsslein-Volhard, C., and Kluding, H. (1984). Mutations affecting the pattern of the larval cuticle in *Drosophila melanogaster*. II. Zygotic loci on the third chromosome. *Roux's Archives of Developmental Biology*, 193:283–295.

Kania, M. A., Bonner, A. S., Duffy, J. P., and Gergen, J. P. (1990). The *Drosophila* segmentation gene *runt* encodes a novel nuclear regulatory protein that is also expressed in the developing nervous system. *Genes and Development*, 4:1701–1713.

Kauffman, S. A. and Goodwin, B. C. (1990). Spatial harmonics and pattern specification in early *Drosophila* development. II: The four color wheels model. *The Journal of Theoretical Biology*, 144:321–345.

Kirkpatrick, S., Gelatt, C. D., and Vecchi, M. P. (1983). Optimization by simulated annealing. *Science*, 220:671–680.

Kitano, H. (2002). Computational systems biology. *Nature*, 420:206–210.

Klingler, M. and Gergen, J. P. (1993). Regulation of *runt* transcription by *Drosophila* segmentation genes. *Mechanisms of Development*, 43:3–19.

Knipple, D. C., Seifert, E., Rosenberg, U. B., Preiss, A., and Jäckle, H. (1985). Spatial and temporal patterns of *Krüppel* gene expression in early *Drosophila* embryos. *Nature*, 317:40–44.

Kobayashi, M., Goldstein, R. E., Fujioka, M., Paroush, Z., , and Jaynes, J. B. (2001). Groucho augments the repression of multiple even skipped target genes in establishing parasegment boundaries. volume 128, pages 1805–1815.

Kosman, D. and Small, S. (1997). Concentration-dependent patterning by an ectopic expression domain of the *Drosophila* gap gene *knirps*. *Development*, 124:1343–1354.

Kosman, D., Small, S., and Reinitz, J. (1998). Rapid preparation of a panel of polyclonal antibodies to *Drosophila* segmentation proteins. *Development, Genes and Evolution*, 208:290–294.

Kozlov, K., Myasnikova, E., Samsonova, M., Reinitz, J., and Kosman, D. (2000). Method for spatial registration of the expression patterns of *Drosophila* segmentation genes using wavelets. *Computational Technologies*, 5:112–119.

Kraut, R. and Levine, M. (1991). Spatial regulation of the gap gene *giant* during *Drosophila* development. *Development*, 111:601–609.

Lam, J. and Delosme, J.-M. (1988a). An efficient simulated annealing schedule: Derivation. Technical Report 8816, Yale Electrical Engineering Department, New Haven, CT.

Lam, J. and Delosme, J.-M. (1988b). An efficient simulated annealing schedule: Implementation and evaluation. Technical Report 8817, Yale Electrical Engineering Department, New Haven, CT.

Langeland, J. A., Attai, S. F., Vorwerk, K., and Carroll, S. B. (1994). Positioning adjacent pair-rule stripes in the posterior *Drosophila* embryo. *Development*, 120:2945–2955.

Langeland, J. A. and Carroll, S. B. (1993). Conservation of regulatory elements controlling *hairy* pair-rule stripe formation. *Development*, 117:585–596.

Lardelli, M. and Ish-Horowicz, D. (1993). *Drosophila hairy* pair-rule gene regulates embryonic patterning outside its apparent stripe domains. *Genes and Development*, 2:1021–1036.

Lawrence, P. A. (1981). The cellular basis of segmentation in insects. *Cell*, 26:3–10.

Lawrence, P. A. (1992). *The Making of a Fly*. Blackwell Scientific Publications, Oxford, UK.

Lawrence, P. A. and Johnston, P. (1989). Pattern formation in the *Drosophila* embryo: allocation of cells to parasegments by *even-skipped* and *fushi-tarazu*. *Development*, 105:761–767.

Lehmann, R. and Nüsslein-Volhard, C. (1991). The maternal gene *nanos*

has a central role in posterior pattern formation of the *Drosophila* embryo. *Development*, 112:679–691.

Lepzelter, D. and Wang, J. (2008). Exact probabilistic solution of spatial-dependent stochastics and associated spatial potential landscape for the bicoid protein. *Physical Review E*, 77. Art. No. 041917.

Macdonald, P. M. and Struhl, G. (1986). A molecular gradient in early *Drosophila* embryos and its role in specifying the body pattern. *Nature*, 324:537–545.

Mahoney, P. A. and Lengyel, J. A. (1987). The zygotic segmentation mutant *tailless* alters the blastoderm fate map of the *Drosophila* embryo. *Developmental Biology*, 122:464–470.

Manoukian, A. S. and Krause, H. M. (1992). Concentration-dependent activities of the *even-skipped* protein in *Drosophila* embryos. *Genes and Development*, 6:1740–1751.

Manoukian, A. S. and Krause, H. M. (1993). Control of segmental asymmetry in *Drosophila* embryos. *Development*, 118:785–796.

Manu (2007). *Canalization of Gap Gene Expression During Early Development in Drosophila melanogaster*. PhD Thesis, Department of Applied Mathematics and Statistics, Stony Brook University.

Manu, Surkova, S., Spirov, A. V., Gursky, V., Janssens, H., Kim, A., Radulescu, O., Vanario-Alonso, C. E., Sharp, D. H., Samsonova, M., and Reinitz, J. (2008). Canalization of gene expression and domain shifts in the *Drosophila* blastoderm by dynamical attractors. *PLoS Computational Biology*, 5:e1000303. doi:10.1371/journal.pcbi.1000303.

Manu, Surkova, S., Spirov, A. V., Gursky, V., Janssens, H., Kim, A., Radulescu, O., Vanario-Alonso, C. E., Sharp, D. H., Samsonova, M., and Reinitz, J. (2009). Canalization of gene expression in the *Drosophila* blastoderm by gap gene cross regulation. doi:10.371/journal.pbio.1000049.

Martinez-Arias, A. and Lawrence, P. (1985). Parasegments and compartments in the *Drosophila* embryo. *Nature*, 313:639–642.

Mjolsness, E., Sharp, D. H., and Reinitz, J. (1991). A connectionist model of development. *The Journal of Theoretical Biology*, 152:429–453.

Mlodzik, M., Fjose, A., and Gehring, W. J. (1985). Isolation of *caudal*, a *Drosophila* homeo box- containing gene with maternal expression, whose transcripts form a concentration gradient at pre-blastoderm stage. *The EMBO Journal*, 4:2961–2969.

Mlodzik, M. and Gehring, W. J. (1987). Expression of the *caudal* gene in the germ line of *Drosophila*: formation of an RNA and protein gradient during early embryogenesis. *Cell*, 48:465–478.

Mohler, J., Eldon, E. D., and Pirrotta, V. (1989). A novel spatial transcription pattern associated with the segmentation gene, *giant*, of *Drosophila*. *The EMBO Journal*, 8:1539–1548.

Mullen, J. R. and DiNardo, S. (1995). Establishing parasegments in *Drosophila* embryos: Roles of the *odd-skipped* and *naked* genes. *Developmental Biology*, 169:295–308.

Myasnikova, E., Samsonova, A., Kozlov, K., Samsonova, M., and Reinitz, J. (2001). Registration of the expression patterns of *Drosophila* segmentation genes by two independent methods. *Bioinformatics*, 17:3–12.

Myasnikova, E., Samsonova, A., Samsonova, M., and Reinitz, J. (2002). Support vector regression applied to the determination of the developmental age of a *Drosophila* embryo from its segmentation gene expression patterns. *Bioinformatics*, 18 (Supplement):S87–S95.

Myasnikova, E., Samsonova, M., Kosman, D., and Reinitz, J. (2005). Removal of background signal from *in situ* data on the expression of segmentation genes in *Drosophila*. *Development, Genes and Evolution*, 215:320–326.

Nasiadka, A. and Krause, H. M. (1999). Kinetic analysis of segmentation gene interactions in *drosophila* embryos. *Development*, 126:1515–1526.

Nauber, U., Pankratz, M. J., Kienlin, A., Seifert, E., Klemm, U., and Jäckle, H. (1988). Abdominal segmentation of the *Drosophila* embryo requires a hormone receptor-like protein encoded by the gap gene *knirps*. *Nature*, 336:489–492.

Newman, J. R. S., Ghaemmaghami, S., Ihmels, J., Breslow, D. K., Noble, M., DeRisi, J. L., and Weissman, J. S. (2006). Single-cell proteomic analysis of *s. cerevisiae* reveals the architecture of biological noise. *Nature*, 441:840–846.

Nüsslein-Volhard, C., Frohnhofer, H. G., and Lehmann, R. (1987). Determination of anteroposterior polarity in *Drosophila*. *Science*, 238:1675–1687.

Nüsslein-Volhard, C., Kluding, H., and Jurgens, G. (1985). Genes affecting the segmental subdivision of the *Drosophila* embryo. *Cold Spring Harbor Symposiums on Quantitative Biology*, 50:145–154.

Nüsslein-Volhard, C. and Wieschaus, E. (1980). Mutations affecting segment number and polarity in *Drosophila*. *Nature*, 287:795–801.

Nüsslein-Volhard, C., Wieschaus, E., and Kluding, H. (1984). Mutations affecting the pattern of the larval cuticle in *Drosophila melanogaster*. I. Zygotic loci on the second chromosome. *Roux's Archives of Developmental Biology*, 193:267–282.

Ozbudak, E. M., Thattai, M., Kurtser, I., Grossman, A. D., and van Oudenaarden, A. (2002). Regulation of noise in the expression of a single gene. *Nature Genetics*, 31:69–73.

Pankratz, M. J., Hoch, M., Seifert, E., and Jäckle, H. (1989). *Krüppel* requirement for *knirps* enhancement reflects overlapping gap gene activities in the *Drosophila* embryo. *Nature*, 341:337–340.

Pankratz, M. J., Seifert, E., Gerwin, N., Billi, B., Nauber, U., and Jäckle, H. (1990). Gradients of *Krüppel* and *knirps* gene products direct pair-rule gene stripe patterning in the posterior region of the *Drosophila* embryo. *Cell*, 61:309–317.

Parkhurst, S. M. and Ish-Horowicz, D. (1991). Mis-regulating segmentation gene expression in *Drosophila*. *Development*, 111:1121–1135.

Paulsson, J. (2004). Summing up the noise in gene networks. *Nature*, 427:415–418.

Paulsson, J. (2005). Models of stochastic gene expression. *Physics of Life Reviews*, 2:157–175.

Paulsson, J., Berg, O. G., and Ehrenberg, M. (2000). Stochastic focusing: Fluctuation-enhanced sensitivity of intracellular regulation. *PNAS*, 97:7148–7153.

Pedraza, J. M. and van Oudenaarden, A. (2005). Noise propagation in gene networks. *Science*, 307:1965–1969.

Pick, L., Schier, A., Affolter, M., Schmidt-Glenewinkel, T., and Gehring, W. J. (1990). Analysis of the *ftz* upstream element: germ layer-specific enhancers are independently autoregulated. *Genes Dev.*, 4:1224–1239.

Poustelnikova, E., Pisarev, A., Blagov, M., Samsonova, M., and Reinitz, J. (2004). A database for management of gene expression data in situ. *Bioinformatics*, 20:2212–2221.

Preiss, A., Rosenberg, U. B., Kienlin, A., Seifert, E., and Jäckle, H. (1985). Molecular genetics of *Krüppel*, a gene required for segmentation of the *Drosophila* embryo. *Nature*, 313:27–32.

Pritchard, D. K. and Schubiger, G. (1996). Activation of transcription in *Drosophila* embryos is a gradual process mediated by the nucleocytoplasmic ratio. *Genes and Development*, 10:1131–1142.

Raj, A., Peskin, C. S., Tranchina, D., Vargas, D. Y., and Tyagi, S. (2006). Stochastic mRNA synthesis in mammalian cells. *PLoS Biology*, 4:0001–0013.

Raser, J. M. and O'Shea, E. K. (2004). Control of stochasticity in eukaryotic gene expression. *Science*, 304:1811–1814.

Read, D., Levine, M., and Manley, J. L. (1992). Ectopic expression of the *drosophila tramtrack* gene results in multiple embryonic defects, including repression of *even-skipped and fushi tarazu*. *Mechanisms of Development*, 38:183–195.

Reinitz, J., Kosman, D., Vanario-Alonso, C. E., and Sharp, D. H. (1998). Stripe forming architecture of the gap gene system. *Developmental Genetics*, 23:11–27.

Reinitz, J. and Levine, M. (1990). Control of the initiation of homeotic gene expression by the gap genes *giant* and *tailless* in *Drosophila*. *Developmental Biology*, 140:57–72.

Reinitz, J., Mjolsness, E., and Sharp, D. H. (1995). Cooperative control of positional information in *Drosophila* by *bicoid* and maternal *hunchback*. *The Journal of Experimental Zoology*, 271:47–56.

Reinitz, J. and Sharp, D. H. (1995). Mechanism of *eve* stripe formation. *Mechanisms of Development*, 49:133–158.

Reinitz, J. and Sharp, D. H. (1996). Gene Circuits and Their Uses. In Collado, J., Magasanik, B., and Smith, T., editors, *Integrative Approaches to Molecular Biology*, chapter 13, pages 253–272. MIT Press, Cambridge, Massachusetts, USA.

Rendel, J. M. (1959). The canalization of the *scute* phenotype of *Drosophila*. *Evolution*, 13(4):425–439.

Renzis, S., Elemento, O., and Wieschaus, S. T. E. (2007). Unmasking activation of the zygotic genome using chromosomal deletions in the *Drosophila* embryo. *PLoS Biology*, 5:e117.

Riddihough, G. and Ish-Horowicz, D. (1991). Individual stripe regulatory elements in the *Drosophila hairy* promoter respond to maternal, gap, and pair-rule genes. *Genes and Development*, 5:840–854.

Rivera-Pomar, R., Lu, X., Perrimon, N., Taubert, H., and Jäckle, H. (1995). Activation of posterior gap gene expression in the *Drosophila* blastoderm. *Nature*, 376:253–256.

Rivera-Pomar, R., Niessing, D., Schmidt-Ott, U., Gehring, W. J., and Jäckle, H. (1996). RNA binding and translational suppression by Bicoid. *Nature*, 379:746–749.

Rosée, A. L., T.homas, Häder, Taubert, H., Rivera-Pomar, R., and Jäckle, H. (1997). Mechanism and Bicoid-dependent control of *hairy* stripe 7 expression in the posterior region of the *Drosophila* embryo. *EMBO J.*, 16:4403–4411.

Rosenfeld, N., Young, J. W., Alon, U., Swain, P. S., and Elowitz, M. B. (2005). Gene regulation at the single-cell level. *Science*, 307:1962–1965.

Rothe, M., Nauber, U., and Jäckle, H. (1989). Three hormone receptor-like *Drosophila* genes encode an identical DNA-binding finger. *The EMBO Journal*, 8:3087–3094.

Rushlow, C. A., Hogan, A., Pinchin, S. M., Howe, K. H., Lardelli, M., and Ish-Horowicz, D. (1989). The *Drosophila hairy* protein acts in both segmentation and bristle patterning and shows homology to N-myc. *The EMBO Journal*, 8:3095–3103.

Sánchez, L. and Thieffry, D. (2003). Segmenting the fly embryo: a logical analysis of the *pair-rule* cross-regulatory module. *The Journal of Theoretical Biology*, 224:517–537.

Schier, A. F. and Gehring, W. J. (1992). Direct homeodomain–dna interaction in the autoregulation of the *fushi tarazu* gene. *Nature*, 356:804–807.

Schüpbach, T. and Wieschaus, E. (1986). Maternal effect mutations altering the anterior-posterior pattern of the *Drosophila* embryo. *Roux Archives of Developmental Biology*, 195:302–317.

Sharp, D. H. and Reinitz, J. (1998). Prediction of mutant expression patterns using gene circuits. *Biosystems*, 47:79–90.

Small, S., Arnosti, D. N., and Levine, M. (1993). Spacing ensures autonomous expression of different stripe enhancers in the *even-skipped* promoter. *Development*, 119:767–772.

Small, S., Blair, A., and Levine, M. (1992). Regulation of *even-skipped* stripe 2 in the *Drosophila* embryo. *The EMBO Journal*, 11:4047–4057.

Small, S., Blair, A., and Levine, M. (1996). Regulation of two pair-rule stripes by a single enhancer in the *Drosophila* embryo. *Developmental Biology*, 175:314–324.

Small, S., Kraut, R., Hoey, T., Warrior, R., and Levine, M. (1991). Transcriptional regulation of a pair-rule stripe in *Drosophila*. *Genes and Development*, 5:827–839.

Stanojevic, D., Hoey, T., and Levine, M. (1989). Sequence-specific DNA-binding activities of the gap proteins encoded by *hunchback* and *Krüppel* in *Drosophila*. *Nature*, 341:331–335.

Stanojevic, D., Small, S., and Levine, M. (1991). Regulation of a segmentation stripe by overlapping activators and repressors in the *Drosophila* embryo. *Science*, 254:1385–1387.

Struhl, G., Struhl, K., and Macdonald, P. M. (1989). The gradient morphogen Bicoid is a concentration-dependent transcriptional activator. *Cell*, 57:1259–1273.

Surkova, S., Kosman, D., Kozlov, K., Manu, Myasnikova, E., Samsonova, A., Spirov, A., Vanario-Alonso, C. E., Samsonova, M., and Reinitz, J. (2008). Characterization of the *Drosophila* segment determination morphome. *Developmental Biology*, 313(2):844–862.

Swantek, D. and Gergen, J. P. (2004). Ftz modulates Runt-dependent activation and repression of segment-polarity gene transcription. *Development*, 131:2281–2290.

Tautz, D. (1988). Regulation of the *Drosophila* segmentation gene *hunchback* by two maternal morphogenetic centres. *Nature*, 332:281–284.

Tautz, D., Lehmann, R., Schnürch, H., Schuh, R., Seifert, E., Kienlin, A., Jones, K., and Jäckle, H. (1987). Finger protein of novel structure encoded by *hunchback*, a second member of the gap class of *Drosophila* segmentation genes. *Nature*, 327:383–389.

Tsai, C. and Gergen, J. P. (1994). Gap gene properties of the pair-rule gene *runt* during *Drosophila* segmentation. *Development*, 120:1671–1683.

Tsai, C. and Gergen, J. P. (1995). Pair-rule expression of the *Drosophila fushi tarazu* gene: A nuclear receptor response element mediates the opposing regulatory effects of *runt* and *hairy*. *Development*, 121:453.

Vavra, S. H. and Carroll, S. B. (1989). The zygotic control of *Drosophila* pair-rule gene expression: I. A search for new pair-rule regulatory loci. *Development*, 107:663–672.

Volfson, D., Marciniak, J., Blake, W. J., Ostroff, N., Tsimring, L. S., and Hasty, J. (2006). Origins of extrinsic variability in eukaryotic gene expression. *Nature*, 439:861–864.

Warrior, R. and Levine, M. (1990). Dose-dependent regulation of pair-rule stripes by gap proteins and the initiation of segment polarity. *Development*, 110:759–767.

Wieschaus, E., Nüsslein-Volhard, C., and Jürgens, G. (1984). Mutations affecting the pattern of the larval cuticle in *Drosophila melanogaster*. III. Zygotic loci on the X-chromosome and fourth chromosome. *Roux's Archives of Developmental Biology*, 1983:296–307.

Yu, Y. and Pick, L. (1995). Non-periodic cues generate seven *ftz* stripes in the *Drosophila* embryo. *Mechanisms of Development*, 50:163–175.

Appendix A

Systems Level Analysis

A.1 Regulatory Representational System

In the first order analysis, after generating all the graphs with one gene and one border at a time (Fig. 3.7 (C)), I use the following format

gene name (regulatory input profile, significance)

to first write down the name of the gene involved in regulating one particular border, then I note down the profile of the interaction by a linear mapping of the shape (or inclination) of the regulatory input using a forward slash (/) or backslash (\) symbol, or more complicated (/\, \/), and without any symbol (which means a uniform, plateau, input). For example, *h* is involved in regulating *eve* stripe 2 anterior border in circuit A1 at time t7 (Fig. 3.7 (C)), so I wrote down h(/,+) in the part of pair-rule gene activation input, where the forward slash "/" is a direct linear mapping of the *h* input in the graph, which means the *h* activating input on *eve* is increasing, with a positive gradient or slope, toward the peak of the total regulatory input for *h* stripe 2 anterior border, hence the *h* stripe is likely anteriorly overlapping with *eve* stripe 2 at t7, and the peak

of h stripe is positioned relatively posterior on the anterior border of *eve* stripe 2. The "+" sign indicates the activation input from h is very strong, in this case it can turn off protein synthesis when removed from the total regulatory input (Fig. 3.7 (C)). There are three levels of significance (strength or intensity) of each interaction, denoted from "+" (high), to no symbol (medium), to "-" (low). The significance is either determined by its absolute value (intensity) of regulatory input, or by relatively how it impacts the total regulatory input after being excluded from it (significance) (Fig. 3.7 (C)).

Based on the above rule, the full first order analysis on *eve* stripe 2 anterior border in circuit A1 at time t7 can be written down as

s2 anterior:
gap activation:
    repression: bcd, hb, gt(/,+)
pr activation: eve(/), h(/,+), ftz(\,+)
    repression: run(/,-), odd(/,+)

where the backslash means within the context of activation, the activation is decreasing toward the peak of *eve* stripe 2; and on the other hand within the context of repression, the repression is increasing toward the peak of *eve* stripe 2. Without a forward slash or backslash means the regulatory input is a plateau, and hence is not contributing to the stripe formation, or maintenance, in the linear regime of the dynamical model. The strength of the regulation is medium when there is no sign of "+" or "-" specified.

In the second order analysis, I only look at combinations of significant stripe (or slope) contributing input from the first order analysis, which means inputs with a forward slash "/" or backslash "\" sign specified, and with intensity level equal or higher than medium (without a "-" sign). This is one of the major reason for doing first order analysis first, so I can exclude irrelevant or insignificant interactions before looking at their combinations.

For example in the second order analysis of circuit A1 on the *eve* stripe 2 anterior border (Fig. 3.7 (D)), I look at combinations of slope contributing inputs from *gt, eve, h, ftz* and *odd*. The second order analysis of this five genes requires going through $\sum[\mathrm{C}(5,\mathrm{r})] - 6 = 25$ combinations of regulations. In Fig. 3.7 (D) I show a subset of such combinations. The combination of *ftz* and *odd* input reduces to a plateau, hence can be classified as a reducible set, which may be biologically relevant or significant for homeostatic and degeneracy (redundancy) control. On the other hand the combination of *gt*, *h* and *eve* input approaches the total regulatory input closely, hence can be classified as an irreducible set, which is essential to the stripe 2 anterior border determination in the circuit.

The final element I determine in the second order analysis is the critical controller of the irreducible set. After isolating the irreducible set, I examine whether removing one particular member (from first order analysis graphs) can result in total shutdown or inactivation of the protein synthesis rate. For example *h* is considered as a critical controller for *eve* stripe 2 anterior border (Fig. 3.7 (C)), removal of *h* from the total regulatory input causes the total regulatory input to be lower below the sigmoidal region of the regulation-expression function (pink area) (Eqn. 3.2), which leads to a total shutdown of the protein synthesis rate.

Based on the above rules, the second order analysis for *eve* stripe 2 anterior border in circuit A1 at t7 can be writen as

s2 anterior:
gap activation:
    repression: bcd, hb, gt(/,+,ir)
pr activation: eve(/,ir), h(/,+,ir*), ftz(\,+,re)
    repression: run(/,-), odd(/,+,re)

where the red color indicates information added from the second order analysis. The note "re" stands for reducible set, "ir" stands for irreducible set, and "*" indicates a critical controller.

The complication comes in when adding information from different time classes. In the early research phase, I use the following format to add first order analysis information from all time classes including the transient phase

(initial state; transition dynamics; final state).

If no specific time is specified, the initial state starts from cycle 13, and the final state refers to cycle 14 t8. Usually the time is specified with ":" in initial or final state, and separated with "|" in transition dynamics (state change in time) specification. The transition dynamics is described by

time interval | <profile of change> intensity of change

The profile (shape or inclination) of change for the stripe (or slope) contributing regulatory input is specified in angle brackets "< >" such that for "<-/+>" within the context of activation means the slope of the regulatory input is increasing in time, on the other hand "<+/->" or "</->" means the slope is decreasing in time, on both end or on one end of the border respectively. If the profile of change is not specified, it means the change is uniform. The intensity of change is specified at three levels, from "+" (strong), to no sign (medium), and to "-" (low).

For example the full time class first order analysis of stripe 2 anterior border in circuit A1 can be written down as:

s2 anterior:
gap activation:
repression: bcd, cad(-; c13--), hb(-; c13-t3+; ; t6-t8--;), gt(-; c13-t5|<+/+>+; /,+)
pr activation: eve(-; t3-t6|<-/+>; /), h(t3-t6|</+>+; /,+)
ftz(; c13-t3++; +; t4-t7|<+\->+; \,+)
repression: odd(c13-t4|<+/+>+; +; t5-t8|</->; /,+)

where "++" means strongly increase uniformly, "+" means moderately increase uniformly. "c13-t5|<+/+>+" within the context of repression means that from

cycle 13 to cycle 14 t5, the repressive regulatory input is increasing strongly with a slope toward the anterior border of stripe 2 and increasing from both sides of the border. "t3-t6|<-/+>" within the context of activation means from cycle 14 t3 to t6, the activation input is increasing moderately with a slope toward the peak of stripe 2 and the slope is increasing.

Later in the research phase, I decided to focus on the essential regulators for the final stripe determination. The first and second order analysis are then adopted for all time classes, by selecting the most significant or representative regulatory states among all time classes, or conduct analysis on late refinement phase first, then adjust for the transient phase analysis. Detailed transient phase dynamics information are retained when it is essential to the final stripe determination. If there are conflicts between the transient phase and the late refinement phase regulation, the more significant regulatory states are adopted for the final decision, or at a more abstract level, compressed or compromised into the final representation.

In the following I include the early research phase, full time classes first order analysis of *eve* regulation in circuit A1.

s2 anterior:
gap activation:
    repression: bcd, cad(-; c13--), hb(-; c13-t3+; ; t6-t8--;), gt(-; c13-t5|<+/+>+; /,+)
pr activation: eve(-; t3-t6|<-/+>; /), h(t3-t6|</+>+; /,+), ftz(; c13-t3++; +; t4-t7|<+\->+; \,+)
    repression: odd(c13-t4|<+/+>+; +; t5-t8|</->; /,+)
bias: activation
s2 posterior:
gap activation:
    repression: bcd, cad(; c13--), hb(-; c13-t3+; ; t6-t8--;), gt(-; c13-t5|<+/>-; /,-)
                kr(c13-t4|<\+>; \,+)
pr activation: eve(-; t3-t6|<+\->; \), h(t3-t6|<+\>+; \,+), ftz(-; c13-t2++; +; t3-t7|<-/+>+; /,+)
    repression: run(t1-t6|<\+>; \), odd(t2-t3+; ; t4-t8|<-\+>+; \,+)
bias: activation
s3 anterior:
gap activation:
    repression: bcd, cad(; c13-t5--), hb(-; c13-t3+; /), kr(c13-t6|<+\+>+; +)
pr activation: eve(t4|</+>; /), h(t3<+/+>+; /,+), ftz(-; c13-t4++; +; t5-t8|<\->+; \,+)

repression: run(t1-t6|<+/>; /\), odd(t2-t4++; +; t5</->; /,+)

bias: activation

s3 posterior:

gap activation:

repression: bcd, cad(; c13-t5--), kr(-; c13-t5++; +)

pr activation: eve(t3|<+\>; \), h(t3-t6|<+\+>+; \,+), ftz(; c13-t2++; +; t3-t7|<-/+>+; /,+)

repression: run(t1-t7|<+\+>;), odd(t2-t3|<+/\+>; /\; t4-t8|<-\+>+; \,+)

bias: activation

s4 anterior:

gap activation:

repression: bcd(-), cad(; c13-t5--; -), kr(c13-t6|<+/+>+; +; t7<-/->-; /,+)

kni(c13<\+>-; \,-), tll(t6:/)

pr activation: eve(t4|</+>-; /), h(t3<+/+>+; /,+), ftz(; c13-t4++; +; t5-t8|<\->+; \,+)

repression: run(t1-t6|<+/>-; /,-), odd(t2-t4++; +; t5</->+; /,+)

bias: activation

s4 posterior:

gap activation:

repression: bcd(-), cad(; c13-t5--; -), kr(-; c13-t5|<+/+>+; t6-t8|<-/->-; /,+)

kni(c13<\+>; \), tll(t8:\)

pr activation: eve(t3|<+\>-; \), h(t3-t6|<+\+>+; \,+)

ftz(; c13-t2++; +; t3-t4|<\->+; t5-t7|<-/+>+; /,+)

repression: run(t1-t7|<\+>; \), odd(t2-t4|<+/>; /,+; t5-t8|<-\+>+; \,+)

bias: activation

s5 anterior:

gap activation:

repression: bcd(-), cad(; c13-t5--;), kr(c13-t6|<+/+>+; /; t7<-/->-; /,-)

kni(c13-t4++; +), tll(t6:/)

pr activation: eve(t5|</+>-; /), h(t3<+/+>+; +), ftz(; c13-t4++; +; t5-t8|<\->+; \,+)

repression: run(t4-t6: /), odd(t2-t4|<+\+>; ; t5-t8<+/->+; /,+)

bias: activation

s5 posterior:

gap activation:

repression: bcd(-), cad(; c13-t5--;), kr(t1: ; t1-t6--), kni(c13-t3++; +), gt(t4|<\+>; \)

pr activation: eve(t5|<+\>-; \), h(t3-t6|<+\+>+; \,+), ftz(; c13-t4++; +; t5-t8|<-/+>+; /,+)

repression: run(t4-t7|<\+>; \), odd(t2-t4|<+/+>; ; t5-t8|<-\+>+; \,+)

bias: activation

s6 anterior:

gap activation:

repression: cad(; c13--;), gt(t2<+\+>+; \,+), kni(c13-t3|<+/>; /)

pr activation: eve(t5|</+>-; /), h(t3<+/+>+; /,+), ftz(; c13-t4++; +; t5-t8|<\->+; \,+)

repression: run(; c13</->-; /,-), odd(t3-t4|<+\+>; ; t5-t8<+/->+; /,+)

bias: activation

s6 posterior:

gap activation:

repression: cad(; c13--;), gt(t1-t5<+\+>+; +), kni(/,-)

pr activation: eve(t5|<+\>-; \), h(t3-t6|<+\+>+; \,+), ftz(; c13-t4++; +; t5-t8|<-/>+; /,+)

repression: run(; c13--; t5-t8:\), odd(t3-t8|<\+>+; \,+)

bias: activation

s7 anterior:

gap activation:

repression: cad, gt(c13-t5|<+/+>+; t6-t8--; /,+), tll(-; c13-t3|<+\+>+; \,+; t6--;)

pr activation: eve(t7-t8|</+>-; /,-), ftz(t2-t4|<+\+>+; +; t6-t8|<\->+; \,+)

repression: run(t4: ; t4-t7-; -), odd(t3-t5|<+/>+; /,+)

bias: activation

These detailed transient phase dynamics were combined or adopted into the final version of second order analysis after adjustment in time, as shown in the following.

s2 anterior:

gap activation:

repression: bcd, hb, gt(/,+,ir)

pr activation: eve(/,ir), h(/,+,ir*), ftz(\,+,re)

repression: run(/,-), odd(/,+,re)

s2 posterior:

gap activation:

repression: bcd, hb, gt(/,-), kr(\,+,ir*)

pr activation: eve(\,ir), h(\,+,ir*), ftz(/,+,ir)

repression: run(\,ir), odd(/\,+,ir*)

s3 anterior:

gap activation:

repression: bcd(-), hb(/,-), kr(+)

pr activation: eve(/,-), h(/,+,ir*), ftz(\,+,ir)

repression: run(/,-), odd(/,+,ir*)

s3 posterior:

gap activation:

repression: bcd(-), kr(+)

pr activation: eve(\,ir), h(\,+,ir*), ftz(/,+,ir)

repression: run(\,ir), odd(/\,+,ir*)

s4 anterior:

gap activation:

repression: bcd(-), cad(-), kr(+), kni(\,-), tll(t6:/)

pr activation: eve(/,-), h(/,+,ir*), ftz(\,+,ir)

repression: run(/,-), odd(/,+,ir*)

s4 posterior:

gap activation:

repression: bcd(-), cad(-), kr(/,+,ir*), kni(\,ir*), tll(t8:\)

pr activation: eve(\,ir), h(\,+,ir*), ftz(/,+,ir)

repression: run(\,ir), odd(/\,+,ir*)

s5 anterior:

gap activation:

repression: cad(-), kr(/,ir*), kni(+), tll(/,-)

pr activation: eve(/,-), h(/,+,ir*), ftz(\,+,ir)

repression: run(/,-), odd(/,+,ir*)

s5 posterior:

gap activation:

repression: cad(-), kni(+), gt(\)

pr activation: eve(\,ir), h(\,+,ir*), ftz(/,+,ir)

repression: run(\,ir), odd(\,+,ir*)

s6 anterior:

gap activation:

repression: cad(-), gt(\,+,re), kni(/,ir*)

pr activation: eve(/,-), h(/,+,re), ftz(\,+,re)

repression: run(/,-), odd(/,+,re)

s6 posterior:

gap activation:

repression: cad(-), gt(+), kni(/,-)

pr activation: eve(\,ir), h(\,+,ir*), ftz(/,+,ir)

repression: run(\,ir), odd(\,+,ir*)

s7 anterior:

gap activation:

repression: cad(-), gt(/,+,ir*), tll

pr activation: eve(/,-), h(/,+,ir*), ftz(\,+,ir)

repression: run(/,-), odd(/,+,ir*)

We can then compile the above circuitry information across borders to obtain a more compact form in the following.

gap activation:

repression: bcd(s2, s3-4-), cad(s4-7a-), hb(s2, s3a:/,-)

gt[ir:s2a,s7a*][re:s6a](s2a:/,+; s2p:/,-; s5p\, s6a:\,+; s6p+, s7a:/,+)

kr[ir:s2p*,s4p*,s5a*](s2p:\,+; s3+, s4a+, s4p:/,+; s5a:/)

kni[ir:s4p*,s6a*](s4a:\,-; s4p\, s5+, s6a/,s6p:/,-), tll(s5a:/,-; s7a)

bias: activation

anterior:

pr activation: eve[ir:s2a](/,-)[s2a/], hairy[ir:(!s6a)*][re:s6a](/,+)

ftz[ir:s3a,s4a,s5a,s7a][re:s2a,s6a](\,+)

repression: run(/,-), odd[ir:s3a*,s4a*,s5a*,s7a*][re:s2a,s6a](/,+)

posterior:

pr activation: eve[ir:all](\), hairy[ir:all*](\,+), ftz[ir:all](/,+)

repression: run[ir:all](\), odd[ir:all*](/\,+)[s5p,s6p:\,+]

where "s3a" means stripe 3 anterior border, and "s5p" means stripe 5 posterior border, and so forth. The reducible sets, irreducible sets and critical controllers (results from second order analysis) are collected in brackets ahead of the first order analysis results in parentheses. The "!" mark are used as a "negation" (exclusion) set.

The same compilation can be done for the final analysis results of circuit A2 and circuit B1, as included in the following.

Circuit A2:

gap activation:

repression: hb[ir:s3a*](s2+, s3a/), kr[ir:s2p,s3a](s2p\, s3a\, s3p-4a+, s4p:/)

tll(s2p:/,-; s6p:\,-; s7a), cad(s3-5-, s6-7a)

kni[ir:s4p*,s6a*](s4a:\,-; s4p:\,+; s5+, s6a:/,+; s6p:/,-)

bias: activation(+)

anterior:

pr activation: ftz[ir:all](\,+), h[ir:all*](/,+)

repression: eve(\,-), odd[ir:all*](/,+)

posterior

pr activation: ftz[ir:all](/,+), h[ir:all*](\,+), run(/,-)

repression: eve(/,-), odd[ir:all*](\,+)

Circuit B1:

gap activation: kni(s5-, s6a:\,-), gt(s6p-), tll(s7a-)

repression: bcd(s2-s3, s4-s5-), cad(s2p:\,-; s3a-, s3p-7a)

bias: activation

anterior:

pr activation: ftz[ir:all](\,+), hairy[ir:all*](/,+)

repression: odd[ir:all*](/,+)

posterior:

pr activation: ftz[ir:all](/,+), hairy[ir:all*](\)

repression: odd[ir:all*](\,+)

The above circuitry information can then be further compiled across different genes and circuits to reveal different, systems, level correlations, which can not be achieved by operating on graphs.

The final compilation for *eve*, *h*, *run*, *ftz* and *odd* regulation across circuit A1, A2 and B1 are included in the following table, where "A" stands for activation and "R" stands for "repression".

Input	Circuit	Eve Regulation by Gap Genes
Bcd	A1	R(s2, s3-4-)
	A2	
	B1	R(s2-s3, s4-s5-)
Cad	A1	R(s4-7a-)
	A2	R(s3-5-, s6-7a)
	B1	R(s2p:\,-; s3a-, s3p-7a)
Hb	A1	R(s2, s3a:/,-)
	A2	R[ir:s3a*](s2+, s3a/)
	B1	
Kr	A1	R[ir:s2p*,s4p*,s5a*](s2p:\,+; s3+, s4a+, s4p:/,+; s5a:/)
	A2	R[ir:s2p,s3a](s2p\, s3a\, s3p-4a+, s4p:/)
	B1	
Gt	A1	R[ir:s2a,s7a*][re:s6a](s2a:/,+; s2p:/,-; s5p\, s6a:\,+; s6p+, s7a:/,+)
	A2	
	B1	A(s6p-)
Kni	A1	R[ir:s4p*,s6a*](s4a:\,-; s4p\, s5+, s6a/,s6p:/,-)
	A2	R[ir:s4p*,s6a*](s4a:\,-; s4p:\,+; s5+, s6a:/,+; s6p:/,-)
	B1	A(s5-, s6a:\,-)
Tll	A1	R(s5a:/,-; s7a)
	A2	R(s2p:/,-; s6p:\,-; s7a)
	B1	A(s7a-)

Table A.1: Circuits analysis results compilation for *eve* regulation by gap genes across circuits A1, A2 and B1, where "A" stands for activation and "R" stands for "repression".

Input	Circuit	Eve Regulation by Pair Rule Genes	
		(anterior border)	(posterior border)
Eve	A1	A[ir:s2a](/,-)[s2a/]	A[ir:all](\)
	A2	R(\,-)	R(/,-)
	B1		
Hairy	A1	A[ir:(!s6a)*][re:s6a](/,+)	A[ir:all*](\,+)
	A2	A[ir:all*](/,+)	A[ir:all*](\,+)
	B1	A[ir:all*](/,+)	A[ir:all*](\)
Runt	A1	R(/,-)	R[ir:all](\)
	A2		A(/,-)
	B1		
Ftz	A1	A[ir:s3a,s4a,s5a,s7a][re:s2a,s6a](\,+)	A[ir:all](/,+)
	A2	A[ir:all](\,+)	A[ir:all](/,+)
	B1	A[ir:all](\,+)	A[ir:all](/,+)
Odd	A1	R[ir:s3a*,s4a*,s5a*,s7a*][re:s2a,s6a](/,+)	R[ir:all*](/\,+)[s5p,s6p:\,+]
	A2	R[ir:all*](/,+)	R[ir:all*](\,+)
	B1	R[ir:all*](/,+)	R[ir:all*](\,+)

Table A.2: Circuits analysis results compilation for *eve* regulation by pair rule genes across circuits A1, A2 and B1, where "A" stands for activation and "R" stands for "repression".

Input	Circuit	H Regulation by Gap Genes
Bcd	A1	R(s2a:/,+; s2p+,s3-4+,s5,s6-7a-)
	A2	R(s2a-s3a, s3p-)
	B1	
Cad	A1	R(s3-,s4-7a)
	A2	R(s6a-7a-)
	B1	A(s6-7a-)
Hb	A1	
	A2	
	B1	
Kr	A1	A(s3-4)
	A2	
	B1	R[ir:s3a](s3a\, s3p-4, s5a:/,-)
Gt	A1	A(s2a:\,-; s6a:/,-; s6p-,s7a:\,-)
	A2	R(s2a:/,-; s6p-)
	B1	R[ir:s2a*](s2a/, s2p:/,-; s6a:\,-; s6p, s7a)
Kni	A1	
	A2	R(s5a\, s5p, s6a:/,-)
	B1	R(s5)
Tll	A1	A[ir:s7a*](s2a-,s2p\,s4a,s5a+,s6a,s6p-,s7a:/,+)
	A2	
	B1	

Table A.3: Circuits analysis results compilation for h regulation by gap genes across circuits A1, A2 and B1, where "A" stands for activation and "R" stands for "repression".

Input	Circuit	H Regulation by Pair Rule Genes	
		(anterior border)	(posterior border)
Eve	A1	A[ir:all*](\/,+)[s2a,s7a:/,+]	A[ir:all*](\,+)
	A2	A[re:all](/)	A[re:all](\,+)
	B1	R(/,-)	R[s4p\][s6p:\,-]
Hairy	A1	R[ir:all](\,+)	R[ir:all](/,+)
	A2		
	B1	A[ir:all*](/,+)	A[ir:all*](\,+)
Runt	A1	R[ir:all*](/,+)	R[ir:all*](\,+)
	A2	R[ir:all*](/,+)	R[ir:all*](\,+)
	B1	A(\,-)[s3a\]	
Ftz	A1	A[ir:s2a](+)[s2a:\,+]	A[ir:!s2p](\/)[s2p:]
	A2	A[re:all](\,+)	A[re:all](/)
	B1	A[ir:s5a*,s6a*](+)[s5a,s6a:/,+]	A[ir:all*](\,+)
Odd	A1	A[ir:s2a,s7a](+)[s2a,s7a:\,+]	A[ir:!s2p](\/)[s2p:\/,-][s4p\]
	A2	R(/,-)	
	B1	R[ir:s7a*](+)[s7a:/,+]	R[ir:!s2p](/)[s2p:/,-]

Table A.4: Circuits analysis results compilation for h regulation by gap genes across circuits A1, A2 and B1, where "A" stands for activation and "R" stands for "repression".

Input	Circuit	Run Regulation by Gap Genes
Bcd	A1	R(s2a:/,+; s2p+,s3-4+,s5,s6-7a-)
	A2	R(s1p-s2a+, s2p-s3a, s3p-s4p-)
	B1	A(s1p+, s2-3, s4-)
Cad	A1	R(s3-,s4-7a)
	A2	R(s2a-, s2p-s3a, s3p-s6p+)
	B1	A(s2p-, s3-6)
Hb	A1	
	A2	
	B1	
Kr	A1	A(s3-4)
	A2	
	B1	A[ir:s2p,s4p](s2a:/,-; s2p/, s3-s4a, s4p\)
Gt	A1	A(s2a:\,-; s6a:/,-; s6p-,s7a:\,-)
	A2	A[ir:s1p*,s6*](s1p\, s5p:/,-; s6a:/,+; s6p\,+)
	B1	A[ir:s1p*,s5p](s1p:\,+; s5p/, s6a:/,+; s6p:\,+)
Kni	A1	
	A2	
	B1	
Tll	A1	A[ir:s7a*](s2a-,s2p\,s4a,s5a+,s6a,s6p-,s7a:/,+)
	A2	
	B1	R[ir:s6p](s2a:/,-; s3p-, s4p\,-, s5p\,-, s6p\)

Table A.5: Circuits analysis results compilation for *run* regulation by gap genes across circuits A1, A2 and B1, where "A" stands for activation and "R" stands for "repression".

Input	Circuit	Run Regulation by Pair Rule Genes	
		(anterior border)	(posterior border)
Eve	A1	A[ir:all*](\/,+)[s2a,s7a:/,+]	A[ir:all*](\,+)
	A2	R(+)	R[ir:all][*:s1p](/)[s1p\]
	B1	A(-)	
Hairy	A1	R[ir:all](\,+)	R[ir:all](/,+)
	A2	R[ir:all][*:!s4p](\,+)[s4p,s5p,s6p:\]	R[ir:s2a*](+)[s2a:/,+]
	B1	R[ir:all*](\,+)	R[ir:all*](/,+)
Runt	A1	R[ir:all*](/,+)	R[ir:all*](\,+)
	A2	A[ir:all][*:!(s1p,s3p)](\)	A[ir:all][*:!s3a](/)
	B1	A(-)[s1p:\,-]	
Ftz	A1	A[ir:s2a](+)[s2a:\,+]	A[ir:!s2p](\/)[s2p:]
	A2	R[ir:!s2a][*:s6a](/)[s2a:/,-]	R[ir:s1p](+)[s1p/]
	B1	R[ir:all)[*:!s2a](/,+)[s2a:/]	R[ir:!s1p][*:!(s1p,s6p)](\,+)[s1p:+]
Odd	A1	A[ir:s2a,s7a](+)[s2a,s7a:\,+]	A[ir:!s2p](\/)[s2p:\/,-][s4p\]
	A2	R[ir:s6a*](/,-)[s2a:-][s6a/]	R[ir:s1p](+)[s1p/]
	B1	A(\,-)	A(+)

Table A.6: Circuits analysis results compilation for *run* regulation by pair rule genes across circuits A1, A2 and B1, where "A" stands for activation and "R" stands for "repression".

Input	Circuit	Ftz Regulation by Gap Genes
Bcd	A1	
	A2	A(s1p-s2a, s2p-)
	B1	R(s1p-s2p+, s3, s4a-s5a-)
Cad	A1	R(s2p-s3p-, s4-6)
	A2	A(s6-)
	B1	R[ir:s2a](s1p-, s2a\, s2p-s6+)
Hb	A1	A[re:s2p](s1p-s2a+, s2p\)
	A2	A[re:s2p](s1p-s2a+, s2p\)
	B1	A(s1p-s2a, s2p:\,-)
Kr	A1	A[ir:s4a*][re:s4p](s2a:/,+; s2p-s3p+, s4a:\,+; s4p\)
	A2	A[re:s4a](s2a:/,-; s2p-s3p, s4a\)
	B1	A[ir:s4a](s2a:/,-; s2p-s3p, s4a\)
Gt	A1	A[ir:s5][re:s6p](s1p:\,+; s5a/, s5p:/,+; s6a+; s6p:\,+)
	A2	
	B1	A[ir:s1p][re:s5p](s1p\, s5p/, s6a, s6p\,-)
Kni	A1	A[ir:s4a*,s5a,s5p](s4a/, s4p+, s5a\, s5p\)
	A2	A[ir:s5p][re:s4a](s4a:/,+; s4p-5a+, s5p:\,+, s6a:\,-)
	B1	A(s4a:/,-; s4p-s5a, s5p:\,-)
Tll	A1	R(s4p:/,-; s6p-)
	A2	
	B1	

Table A.7: Circuits analysis results compilation for *ftz* regulation by gap genes across circuits A1, A2 and B1, where "A" stands for activation and "R" stands for "repression".

Input	Circuit	Ftz Regulation by Pair Rule Genes	
		(anterior border)	(posterior border)
Eve	A1	R[ir:all*](/,+)	R[ir:all*](\,+)
	A2	R[re:all](/,+)	R[re:all](\,+)
	B1	R[ir:all*](/,+)	R[ir:all*](\,+)
Hairy	A1	A(\,-)	A[ir:s3p,s5p][re:s2p,s4p,s6p](/)
	A2		
	B1	R(/,-)	R[re:s5p](\,-)[s1p,s5p:\]
Runt	A1		
	A2		
	B1	A[ir:all][*:s5a](/,+)	A[ir:all][*:s5p](\)[s5p,s6p:\,+]
Ftz	A1	A(/,-)	A(\,-)
	A2	R[re:all](\,+)	R[re:all](/,+)
	B1		
Odd	A1	R[ir:s4a,s5a](\)[s2a,s3a,s6a:\,-]	R[ir:!s1p](/)
	A2	A[ir:all*](/,+)	A[ir:all*](\,+)
	B1	A[ir:s4a,s5a](/,-)[s4a,s5a:/]	A[ir:all](\)

Table A.8: Circuits analysis results compilation for *ftz* regulation by pair rule genes across circuits A1, A2 and B1, where "A" stands for activation and "R" stands for "repression".

Input	Circuit	Odd Regulation by Gap Genes
Bcd	A1	A(s1p+, s2-3, s4-)
	A2	A(s1p-2+, s3-4, s5-)
	B1	A(s1p-s2-)
Cad	A1	A(s3a-s5p-, s6)
	A2	R(s4a-s6-)
	B1	R(s2a-s5, s6+)
Hb	A1	A[ir:s2p](s1p, s2a+, s2p\)
	A2	
	B1	A(s1p-, s2a, s2p:\,-)
Kr	A1	A[ir:s2a*,s4a,s4p](s2a:/,+; s2p-s3p+, s4a:\,+; s4p\)
	A2	
	B1	A(s2:/,+; s3+, s4a:\,+, s4p\)
Gt	A1	A[ir:s1p,s5a,s5p*,s6p*](s1p:\,+; s5a/, s5p:/,+; s6a+, s6p:\,+)
	A2	A[ir:s1p,s5p,s6p*](s1p\, s5p:/,+; s6a+, s6p:\,+)
	B1	A[ir:s1p][re:s5p](s1p:\,+; s5a:/,-; s5p:/,+; s6a+, s6p:\,+)
Kni	A1	A[ir:s4a*,s5p*](s3p:/,-; s4a:/,+; s4p-,s5a:\,+, s5p:\,+)
	A2	A[ir:s4a,s5p](s4a/, s4p-s5a, s5p\)
	B1	A[re:s5p](s3p:/,-; s4:/,+; s5a+, s5p:\,+; s6a:\,-)
Tll	A1	R(s6p-)
	A2	R(s6p:\,-)
	B1	A(s3p:/,-; s4p-, s6p/)

Table A.9: Circuits analysis results compilation for *odd* regulation by gap genes across circuits A1, A2 and B1, where "A" stands for activation and "R" stands for "repression".

Input	Circuit	Odd Regulation by Pair Rule Genes	
		(anterior border)	(posterior border)
Eve	A1	R[ir:all][*:s2a,s6a](/,+)[s5a/]	R[ir:all][*:s1p,s2p,s5p](\,+)[s6p\]
	A2	R[ir:all*](/,+)	R[ir:all*](\,+)
	B1	R[ir:all*](/,+)	R[ir:all][*:!s6p](\,+)[s6p\]
Hairy	A1	R[ir:all][*:s6a](/)[s6a:/,+]	R[ir:all][*:s5p](\,+)
	A2		A(/,-)
	B1		A(/,-)
Runt	A1	R(\)[s6a:\,-]	R(/,-)
	A2	A[ir:s5a*,s6a*](+)[s5a,s6a:/,+]	A[ir:!s1p][*:s3p,s4p,s6p](\)[s6p:\,+]
	B1	A[ir:all*](/,+)	A[ir:all][*:!s1p](\,+)
Ftz	A1	A[ir:all*](/)	A[ir:all][*:!s1p](\)
	A2	R(\,-)	R(/,-)
	B1	A(/,-)	A(\,-)
Odd	A1	A[ir:all](/)	A[ir:all](\)
	A2		
	B1	R(\,-)	R(/,-)

Table A.10: Circuits analysis results compilation for *odd* regulation by pair rule genes across circuits A1, A2 and B1, where "A" stands for activation and "R" stands for "repression".

A.2 Statistical Pooling

In this section I include tables for the RMS scores of the 3 priority sets of both class A and class B circuits. I also include the parameter distribution analysis tables for *eve*, *h*, *run*, and *ftz* regulation. The consensus analysis table for *odd* regulation is included in the main text.

Class A					
(1)		(2)		(3)	
Circuit	RMS	Circuit	RMS	Circuit	RMS
A1	26.35	A6	25.23	A16	26.84
A2	23.47	A7	24.49	A17	25.5
A3	22.68	A8	24.12	A18	25.54
A4	26.29	A9	24.62	A19	28.21
A5	25.33	A10	26.7	A20	27.31
		A11	25.32	A21	26.08
		A12	24.91	A22	27.12
		A13	25.44	A23	26.46
		A14	25.75	A24	26.64
		A15	26.62	A25	27.3
				A26	26.85
				A27	26.52
				A28	28.12
				A29	25.4
				A30	25.84
Avg	24.82	Avg	25.32	Avg	26.65

Table A.11: RMS scores list for the 3 priority sets of the class A circuits. The RMS scores are rounded at the second decimal place. Full parameter sets of these circuits, except for the 3 major circuits (A1, A2 and B1), are not included in this thesis.

Class B					
(1)		(2)		(3)	
Circuit	RMS	Circuit	RMS	Circuit	RMS
B1	22.37	B5	24.12	B14	25.02
B2	22.22	B6	23.89	B15	23.72
B3	21.08	B7	23.92	B16	24.95
B4	21.65	B8	25.23	B17	25.54
		B9	22.92	B18	26.31
		B10	24.96	B19	26.29
		B11	22.73		
		B12	21.27		
		B13	20.96		
Avg	21.83	Avg	23.33	Avg	25.31

Table A.12: RMS scores list for the 3 priority sets of the class B circuits. The RMS scores are rounded at the second decimal place. Full parameter sets of these circuits, except for the 3 major circuits (A1, A2 and B1), are not included in this thesis.

Eve	Class A			Class B		
	(1)	(2)	(3)	(1)	(2)	(3)
Bcd	3/1/0/1/0	6/2/1/1/0	14/1/0/0/0	2/0/0/1/1	6/1/0/1/1	2/1/1/1/1
Cad	3/1/0/1/0	6/2/2/0/0	9/6/0/0/0	3/0/0/0/1	6/3/0/0/0	3/2/0/1/0
Hb	0/5/0/0/0	1/3/6/0/0	0/10/4/1/0	1/1/1/1/0	1/8/0/0/0	2/2/1/1/0
Kr	0/4/1/0/0	1/8/0/1/0	0/12/3/0/0	1/0/3/0/0	1/5/2/1/0	1/0/3/2/0
Gt	2/1/1/1/0	2/6/1/1/0	1/10/4/0/0	0/2/1/1/0	3/3/1/2/0	1/2/1/2/0
Kni	1/4/0/0/0	2/6/1/1/0	3/11/1/0/0	0/2/1/1/0	2/5/1/1/0	1/2/1/2/0
Tll	4/1/0/0/0	10/0/0/0/0	15/0/0/0/0	4/0/0/0/0	8/0/0/0/1	6/0/0/0/0
Eve	1/1/0/3/0	1/5/2/2/0	5/3/1/6/0	0/1/1/1/1	1/5/2/0/1	0/3/2/1/0
H	0/0/0/3/2	0/1/0/3/6	0/2/4/3/6	0/0/0/1/3	0/0/0/1/8	0/0/0/1/5
Run	0/1/0/4/0	3/4/0/1/2	2/10/1/1/1	0/1/1/1/1	2/1/0/3/3	2/3/0/0/1
Ftz	2/0/1/0/2	4/0/0/1/5	1/3/0/3/8	1/0/0/2/1	2/1/1/1/4	2/0/0/1/3
Odd	3/0/0/0/2	5/2/1/0/2	8/4/0/1/2	3/0/0/0/1	7/1/0/0/1	4/0/0/0/2

Table A.13: Distribution of pair rule circuit parameters involved in regulating *eve*, including m^{eve}, $E^{eve \leftarrow \beta}$, and $T^{eve \leftarrow b}$. Table columns are selected circuits, categorized into three priority sets according to their fitting quality (RMS score), in both class A and class B circuits (see Appendix A.2). Table rows indicate each gene regulating *eve* in the circuit. Parameter values represent types of regulatory interactions as follows: strong repression if $\leq$ –0.005 (red background), weak repression if between –0.005 and –0.001 (red text), no interaction if between –0.001 and 0.001 (green), weak activation if between 0.001 and 0.005 (blue text), and strong activation if $\geq$ 0.005 (blue background). The number format (strong repression/weak repression/no interaction/weak activation/strong activation) shows the numbers of gene circuits in which a parameter falls into each regulatory category. The background color indicates the type of regulatory interaction found in a majority of circuits, the text color indicates a weaker distribution consensus, and blank (no color) cells indicate indeterminable distribution.

H	Class A			Class B		
	(1)	(2)	(3)	(1)	(2)	(3)
Bcd	4/0/0/1/0	7/2/0/0/1	7/4/1/0/3	2/0/1/0/1	4/1/0/0/4	4/0/1/0/1
Cad	1/3/1/0/0	5/1/0/4/0	4/4/2/2/3	1/1/0/1/1	3/2/1/1/2	0/1/0/5/0
Hb	0/2/2/1/0	1/3/4/2/0	1/8/4/2/0	0/0/3/1/0	0/2/2/5/0	0/1/2/3/0
Kr	0/1/2/2/0	0/4/3/3/0	0/3/7/5/0	0/2/1/1/0	0/2/5/2/0	1/2/0/3/0
Gt	0/3/1/1/0	1/6/1/2/0	1/8/4/2/0	0/3/0/1/0	0/5/4/0/0	2/1/0/3/0
Kni	0/3/2/0/0	0/4/5/1/0	0/4/7/4/0	0/4/0/0/0	0/3/4/2/0	0/3/1/2/0
Tll	1/0/0/0/4	3/0/0/1/6	4/0/1/1/9	3/0/0/1/0	1/0/1/0/7	2/0/0/0/4
Eve	1/1/1/1/1	1/1/0/6/2	1/2/1/3/8	1/1/1/1/0	4/2/1/2/0	0/1/0/3/2
H	1/0/2/1/1	2/3/1/3/1	1/7/1/4/2	0/0/1/1/2	0/1/0/2/6	1/1/2/1/1
Run	4/1/0/0/0	8/1/0/1/0	11/1/1/1/1	2/1/0/1/0	3/2/1/3/0	4/1/1/0/0
Ftz	1/0/0/1/3	4/2/1/0/3	4/1/1/5/4	1/0/0/0/3	0/0/1/1/7	2/0/0/1/3
Odd	0/1/1/0/3	0/1/1/0/8	1/0/0/2/12	3/0/0/0/1	6/1/1/0/1	0/2/1/0/3

Table A.14: Distribution of pair rule circuit parameters involved in regulating h, including m^h, $E^{h \leftarrow \beta}$, and $T^{h \leftarrow b}$. Table columns are selected circuits, categorized into three priority sets according to their fitting quality (RMS score), in both class A and class B circuits (see Appendix A.2). Table rows indicate each gene regulating h in the circuit. Parameter values represent types of regulatory interactions as follows: strong repression if $\leq$ –0.005 (red background), weak repression if between –0.005 and –0.001 (red text), no interaction if between –0.001 and 0.001 (green), weak activation if between 0.001 and 0.005 (blue text), and strong activation if $\geq$ 0.005 (blue background). The number format (strong repression/weak repression/no interaction/weak activation/strong activation) shows the numbers of gene circuits in which a parameter falls into each regulatory category. The background color indicates the type of regulatory interaction found in a majority of circuits, the text color indicates a weaker distribution consensus, and blank (no color) cells indicate indeterminable distribution.

Run	Class A			Class B		
	(1)	(2)	(3)	(1)	(2)	(3)
Bcd	5/0/0/0/0	6/3/0/0/1	13/0/0/0/2	0/1/0/0/3	3/1/1/2/2	4/0/0/1/1
Cad	5/0/0/0/0	5/1/1/3/0	8/5/0/1/1	0/0/0/2/2	3/3/1/2/0	0/1/2/2/1
Hb	0/1/2/2/0	0/5/2/3/0	1/4/5/4/1	1/1/1/1/0	0/6/2/1/0	0/0/1/4/1
Kr	0/2/1/1/1	0/3/4/3/0	0/1/2/10/2	0/0/1/3/0	0/2/5/2/0	0/0/3/2/1
Gt	0/0/2/3/0	0/1/3/4/2	0/1/1/5/8	0/0/0/3/1	0/2/3/4/0	0/0/1/3/2
Kni	0/2/2/1/0	1/5/3/1/0	1/4/7/3/0	0/1/3/0/0	0/6/0/3/0	0/1/4/1/0
Tll	4/0/0/0/1	7/2/0/0/1	10/1/0/3/1	4/0/0/0/0	8/0/1/0/0	5/0/0/0/1
Eve	0/2/0/2/1	0/2/2/3/3	2/1/2/6/4	0/0/1/0/3	0/0/3/6/0	0/2/3/1/0
H	3/2/0/0/0	7/3/0/0/0	12/1/0/2/0	4/0/0/0/0	7/2/0/0/0	6/0/0/0/0
Run	0/0/2/2/1	2/3/3/2/0	5/5/2/3/0	0/2/1/1/0	0/5/2/2/0	1/3/0/2/0
Ftz	3/1/0/0/1	2/1/1/1/5	4/2/0/5/4	2/0/1/1/0	4/1/2/1/1	2/1/1/1/1
Odd	1/2/1/1/0	6/2/0/0/2	10/1/1/1/2	0/0/1/1/2	1/3/3/1/1	3/1/1/1/0

Table A.15: Distribution of pair rule circuit parameters involved in regulating *run*, including m^{run}, $E^{run \leftarrow \beta}$, and $T^{run \leftarrow b}$. Table columns are selected circuits, categorized into three priority sets according to their fitting quality (RMS score), in both class A and class B circuits (see Appendix A.2). Table rows indicate each gene regulating *run* in the circuit. Parameter values represent types of regulatory interactions as follows: strong repression if $\leq$ –0.005 (red background), weak repression if between –0.005 and –0.001 (red text), no interaction if between –0.001 and 0.001 (green), weak activation if between 0.001 and 0.005 (blue text), and strong activation if $\geq$ 0.005 (blue background). The number format (strong repression/weak repression/no interaction/weak activation/strong activation) shows the numbers of gene circuits in which a parameter falls into each regulatory category. The background color indicates the type of regulatory interaction found in a majority of circuits, the text color indicates a weaker distribution consensus, and blank (no color) cells indicate indeterminable distribution.

Ftz	Class A			Class B		
	(1)	(2)	(3)	(1)	(2)	(3)
Bcd	2/0/1/0/2	6/0/0/2/2	5/0/2/3/5	2/0/0/1/1	8/0/1/0/0	2/0/0/0/4
Cad	2/1/0/2/0	6/3/0/1/0	8/4/1/1/1	4/0/0/0/0	8/1/0/0/0	5/1/0/0/0
Hb	0/0/2/1/2	0/1/3/4/2	0/0/1/12/2	0/1/1/2/0	0/1/1/6/1	0/2/3/1/0
Kr	0/0/1/3/1	0/0/1/6/3	0/0/3/8/4	0/0/2/1/1	0/1/0/7/1	0/1/2/3/0
Gt	0/2/0/1/2	0/0/2/2/6	0/0/2/7/6	0/0/0/2/2	0/0/2/5/2	0/1/0/3/2
Kni	0/0/0/3/2	0/0/1/9/0	0/0/1/12/2	0/0/1/3/0	0/0/1/5/3	0/0/1/5/0
Tll	2/1/0/0/2	5/0/0/0/5	9/0/0/1/5	3/0/0/0/1	7/0/0/1/1	5/0/0/0/1
Eve	4/0/1/0/0	6/4/0/0/0	13/2/0/0/0	3/1/0/0/0	7/2/0/0/0	6/0/0/0/0
H	1/0/2/2/0	2/4/2/2/0	3/3/2/6/1	3/1/0/0/0	6/1/1/1/0	3/2/0/0/1
Run	0/0/2/1/2	0/0/2/3/5	0/1/0/7/7	0/0/0/0/4	0/1/2/2/4	0/1/0/2/3
Ftz	2/1/0/2/0	2/4/0/2/2	5/4/2/3/1	1/2/0/0/1	3/4/1/1/0	1/3/1/1/0
Odd	3/0/0/0/2	3/0/1/2/4	3/2/1/2/7	0/1/0/1/2	0/0/1/1/7	1/1/0/1/3

Table A.16: Distribution of pair rule circuit parameters involved in regulating *ftz*, including m^{ftz}, $E^{ftz \leftarrow \beta}$, and $T^{ftz \leftarrow b}$. Table columns are selected circuits, categorized into three priority sets according to their fitting quality (RMS score), in both class A and class B circuits (see Appendix A.2). Table rows indicate each gene regulating *ftz* in the circuit. Parameter values represent types of regulatory interactions as follows: strong repression if ≤ -0.005 (red background), weak repression if between -0.005 and -0.001 (red text), no interaction if between -0.001 and 0.001 (green), weak activation if between 0.001 and 0.005 (blue text), and strong activation if $\geq$ 0.005 (blue background). The number format (strong repression/weak repression/no interaction/weak activation/strong activation) shows the numbers of gene circuits in which a parameter falls into each regulatory category. The background color indicates the type of regulatory interaction found in a majority of circuits, the text color indicates a weaker distribution consensus, and blank (no color) cells indicate indeterminable distribution.

A.3 Literature Integration

The first column specifies pair rule interaction, where normal arrows (→) represent activation, blunt arrows (-|) represent repression. The second column specifies the specific, spatial or temporal, context of the interaction. The bibliographical references are given in the last column, followed by lines of experimental evidence supporting each interaction.

A.3.1 *eve* literature integration

Gene	Specifics	Reference
bcd →*eve*	stripe 2	Small et al. (1991, 1992, 1993)
		exp.: *eve* stripe 2 enhancer (Small et al., 1991)
bcd -| *eve*	anterior stripes	Vavra and Carroll (1989)
	stripe 3 anterior	Small et al. (1996)
		exp.: stripe 3 enhancer study (Small et al., 1996)
		mutant exp.: anterior expansion and shift of the stripe 3 pattern were observed, while stripe 7 staining seems reduced.
cad		No literature conclusions found.
hb →*eve*	stripe 2	Small et al. (1991, 1992); Goto et al. (1989)
		exp.: *eve* stripe 2 enhancer (Small et al., 1991)
hb →*eve*	stripe 3	Small et al. (1993)
hb -| *eve*	stripe 3 anterior	Klingler and Gergen (1993); Small et al. (1996); Kosman and Small (1997)
		exp.: *eve* stripe 3 enhancer (Small et al., 1996)

Continued on next page

Continued from previous page

Gene	Specifics	Reference
hb -| *eve*	stripe 3 anterior, stripe 7 posterior	Small et al. (1996) exp.: *eve* stripe 3 enhancer (Small et al., 1996) mutant exp.: expand the initial limits of the stripe 3 pattern, the posterior border of stripe 7 is also expanded.
hb -| *eve*	stripe 6 posterior	Fujioka et al. (1999)
Kr -| *eve*	stripe 2, 3 posterior	Small et al. (1991, 1992, 1993) exp.: *eve* stripe 2 enhancer (Small et al., 1991) mutant exp.: *eve* stripes 2 and 3 are fused, replaced by a composite band of expression (Goto et al., 1989).
gt -| *eve*	stripe 2 anterior	Small et al. (1991, 1992, 1993) exp.: *eve* stripe 2 enhancer (Small et al., 1991) mutant exp.: (Small et al., 1996) severe anterior expansion of the stripe 2 pattern, but have no effect on stripe 3 expression.
kni -| *eve*	stripe 3 posterior	Carroll and Scott (1986); Klingler and Gergen (1993); Small et al. (1996); Kosman and Small (1997) exp.: *eve* stripe 3 enhancer (Small et al., 1996) mutant exp.: posterior expansion of endogeous *eve* and the reporter gene expression driven by the stripe 3 enhancer.
kni -| *eve*	stripe 4 posterior, stripe 5 anterior	Reinitz and Sharp (1995)
kni -| *eve*	stripe 6, 7 anterior	Small et al. (1996)

Continued on next page

Continued from previous page

Gene	Specifics	Reference
		exp.: *eve* stripe 3 enhancer (Small et al., 1996)
tll →*eve*	stripe 7	Small et al. (1996) exp.: *eve* stripe 3 enhancer (Small et al., 1996) mutant exp.: stripe 7 expression is abolished in embryos that lack *tll*+ function.

Table A.17: Literature integration for gap genes regulating *eve*.

Gene	Specifics	Reference
eve →*eve*	late phase	Goto et al. (1989); Ingham and Gergen (1988); Frasch and Levine (1987) mutant exp.: *eve* promoter was found to contain Eve-binding sites that when mutated dramatically affect expression of gene *eve* (Frasch et al., 1988; Goto et al., 1989).
h →*eve*	late phase	Frasch and Levine (1987); Kosman and Small (1997); Warrior and Levine (1990); Carroll and Scott (1986); Ingham and Gergen (1988) mutant exp.: *eve* expression is lost prematurely (Frasch and Levine, 1987; Ingham and Gergen, 1988). ectopic exp.: brief expression of *h* in all nuclei led to a broadening of the *eve* stripes and in some cases to partial fusions between stripes (Warrior and Levine, 1990).
run -| *eve*	late phase	Carroll and Vavra (1989); Manoukian and Krause (1993); Jaynes and Fujioka (2004); Jiménez et al. (1996); Ingham and Gergen (1988) mutant exp.: *eve* stripes expanded (Manoukian and Krause, 1993; Frasch and Levine, 1987; Ingham and Gergen, 1988; Warrior and Levine, 1990).

Continued on next page

Continued from previous page

Gene	**Specifics**	**Reference**
run -| *eve*	posterior borders	Warrior and Levine (1990); Frasch and Levine (1987); Fujioka et al. (1996) ectopic exp.: *eve* is rapidly repressed in *hs-runt* embryos (Manoukian and Krause, 1993; Tsai and Gergen, 1994; Hooper et al., 1989).
ftz	(no effect)	(Frasch et al., 1988; Frasch and Levine, 1987) mutant exp.: *eve* gene expression was found to be appearing normal (Frasch et al., 1988; Frasch and Levine, 1987).
odd -| *eve*	late phase	Jaynes and Fujioka (2004); Drean et al. (1998) mutant exp.: the entire 7-stripe pattern appears to expand, both anteriorly and posteriorly (Drean et al., 1998). ectopic exp.: all 7 *eve* stripes are strongly repressed.

Table A.18: Literature integration for pair rule genes regulating *eve*.

A.3.2 *h* literature integration

Gene	Specifics	Reference
bcd →*h*	stripe 1	(Howard and Struhl, 1990; Riddihough and Ish-Horowicz, 1991)
		mutant exp.: mutations that abolish or reduce *bcd* concentrations cause loss of *h* stripe 1 (Riddihough and Ish-Horowicz, 1991).
	stripe 7	(Rosée et al., 1997)
bcd -| *h*	stripe 4	(Howard and Struhl, 1990; Riddihough and Ish-Horowicz, 1991)
cad →*h*	stripe 6, 7	(Rosée et al., 1997)
		mutant exp.: in the absence of *cad*, *h*7-*lac*Z expression is strongly affected.
hb →*h*	stripe 3	(Hartmann et al., 1994)
		mutant exp.: *h* stripe 3 is missing.
		mutant exp.: *h* stripe 4 were found to be shifted anteriorly (Klingler and Gergen, 1993).
hb -| *h*		(Carroll and Vavra, 1989)
	stripe 3	(Howard and Struhl, 1990; Riddihough and Ish-Horowicz, 1991)
	stripe 6 posterior	(Langeland et al., 1994)
		mutant exp.: stripe 6 expands posteriorly when *hb* is removed (Langeland et al., 1994).
Kr -| *h*		(Carroll and Vavra, 1989)
		mutant exp.: only four broad *h* stripes are seen roughly in the positions of stripe 1, a fused stripe 2/3/4, a fused stripe 5/6, and stripe 7 (Carroll and Vavra, 1989; Hooper et al., 1989).

Continued on next page

Continued from previous page

Gene	Specifics	Reference
	stripe 2, 6	(Riddihough and Ish-Horowicz, 1991)
	stripe 5	(Langeland and Carroll, 1993)
	stripe 5 anterior, stripe 6 anterior	(Langeland et al., 1994)
		mutant exp.: *h* stripes 5 and 6 each display significant anterior expansion when *Kr* is removed (Langeland et al., 1994).
	stripe 7	(Rosée et al., 1997)
Kr →*h*	stripe 4	(Howard and Struhl, 1990; Riddihough and Ish-Horowicz, 1991)
gt -| *h*	stripe 5 posterior	(Riddihough and Ish-Horowicz, 1991; Langeland and Carroll, 1993; Langeland et al., 1994)
		mutant exp.: expand stripe 5' posteriorly, but abolish stripe 6' (Riddihough and Ish-Horowicz, 1991).
gt →*h*	stripe 6	(Riddihough and Ish-Horowicz, 1991)
kni →*h*	stripe 6	(Riddihough and Ish-Horowicz, 1991; Langeland et al., 1994)
		mutant exp.: reduce stripe 5', abolish stripe 6', and expand stripe 7' (Riddihough and Ish-Horowicz, 1991).
		mutant exp.: stripe 3'-4' is broadened in *kni*– embryos, where the *Kr* domain is expanded (Gaul et al., 1987; Jäckle et al., 1986).
	stripe 5	(Riddihough and Ish-Horowicz, 1991; Langeland and Carroll, 1993; Langeland et al., 1994)
kni -| *h*	stripe 4	(Riddihough and Ish-Horowicz, 1991; Hartmann et al., 1994)
	stripe 7 anterior	(Howard and Struhl, 1990; Riddihough and Ish-Horowicz, 1991; Rosée et al., 1997)

Continued on next page

Continued from previous page

Gene	Specifics	Reference
tll -| *h*	stripe 1	(Howard and Struhl, 1990; Riddihough and Ish-Horowicz, 1991)
		mutant exp.: stripe 1 expanded anteriorally and stripe 6' expanded posteriorly (Riddihough and Ish-Horowicz, 1991).
	stripe 2, 6	(Riddihough and Ish-Horowicz, 1991)
	stripe 7 posterior border	(Rosée et al., 1997)
		mutant exp.: stripe 7' is completely abolished and the *h*7-*lac*Z expression is also absent (Rosée et al., 1997).

Table A.19: Literature integration for gap genes regulating *h*.

Gene	Specifics	Reference
eve →*h*	stripe 2, maintenance	(Hooper et al., 1989; Carroll and Vavra, 1989)
		mutant exp.: the strongest effect on *h* involves the second stripe which is greatly reduced while the other stripes are generally narrower and irregularly spaced (Carroll and Vavra, 1989).
		ectopic exp.: in *hs-eve* embryos (Manoukian and Krause, 1992), there was no effect on *h* expression.
	early formation	(Ingham and Gergen, 1988)
h	(no effect)	(Hooper et al., 1989; Parkhurst and Ish-Horowicz, 1991; Jiménez et al., 1996; Riddihough and Ish-Horowicz, 1991)
		mutant exp.: normal *h* patterning occurs in the absence of active *h* protein.
run -| *h*		(Carroll and Vavra, 1989; Warrior and Levine, 1990; Manoukian and Krause, 1993; Jiménez et al., 1996)

Continued on next page

Continued from previous page

Gene	**Specifics**	**Reference**
		mutant exp.: *h* pattern was found more severely disrupted than *eve*, stripe 5 of *h* is weaker than normal, as is stripe 2. stripes 3 and 4, as well as stripes 6 and 7 are fused (Warrior and Levine, 1990).
		mutant exp.: *h* pattern was also found expanded (Ingham and Gergen, 1988; Hartmann et al., 1994; Carroll and Vavra, 1989; Manoukian and Krause, 1993; Warrior and Levine, 1990).
		ectopic exp.: when heat shocked for 30-45 minutes all *h* expression are repressed (Manoukian and Krause, 1993).
	late phase	(Jaynes and Fujioka, 2004)
	stripe 1	(Manoukian and Krause, 1993; Tsai and Gergen, 1994)
	stripe 3/4, 6/7	(Hooper et al., 1989)
run	independent	(Hooper et al., 1989)
ftz	no influence	(Howard and Ingham, 1986)
odd -| *h*		(Drean et al., 1998)
		mutant exp.: the entire 7-stripe pattern of *h* appears to expand, both anteriorly and posteriorly (Drean et al., 1998).
		ectopic exp.: the earliest observed effects of ectopic Odd are on the anterior-most stripes.

Table A.20: Literature integration for pair rule genes regulating *h*.

A.3.3 *run* literature integration

Gene	Specifics	Reference
bcd -| *run*	anterior early broad field	(Klingler and Gergen, 1993; Tsai and Gergen, 1994) mutant exp.: *run* is de-repressed over a large anterior region, about 30% of the embryo (Klingler and Gergen, 1993).
cad		No literature conclusions found.
hb -| *run*	stripe 3 anterior	(Klingler and Gergen, 1993; Small et al., 1996)
Kr -| *run*	stripe 2 posterior, stripe 5 anterior	(Klingler and Gergen, 1993) mutant exp.: stripes 2 to 5 are replaced by one large domain (Klingler and Gergen, 1993).
gt -| *run*	stripe 2 anterior, stripe 5 posterior	(Klingler and Gergen, 1993)
kni -| *run*	stripe 3 posterior	(Carroll and Scott, 1986; Klingler and Gergen, 1993; Small et al., 1996; Kosman and Small, 1997) mutant exp.: stripes 3 to 6 are affected (Klingler and Gergen, 1993). At early stages stripe 3 is fused to the de-repression domain. ectopic exp.: *eve stripe 2-kni* constructs caused disruptions of *run* stripes 2 and 3, but had no effect on stripe 1 (Kosman and Small, 1997).
	stripe 6 anterior	(Klingler and Gergen, 1993)
tll -| *run*	stripe 6 posterior	(Klingler and Gergen, 1993)

Continued on next page

Continued from previous page

Gene	Specifics	Reference
		mutant exp.: stripe 7 is not formed at all (Klingler and Gergen, 1993). Stripe 6 appears belatedly (in wild type, stripe 6 appears very early), and this stripe as well as stripe 5 are shifted posteriorly.
tll →*run*	stripe 7 anterior	(Klingler and Gergen, 1993)

Table A.21: Literature integration for gap genes regulating *run*.

Gene	Specifics	Reference
eve -| *run*		(Manoukian and Krause, 1992, 1993; Jaynes and Fujioka, 2004; Ingham and Gergen, 1988; Fujioka et al., 1996; Klingler and Gergen, 1993) mutant exp.: late *run* expression expands throughout the *eve* domain (Jaynes and Fujioka, 2004; Fujioka et al., 1995). ectopic exp.: *eve* expression at high level was found to be repressing *run* (Manoukian and Krause, 1992).
eve →*run*	early phase	(Carroll and Vavra, 1989)
h -| *run*		(Jaynes and Fujioka, 2004; Howard and Ingham, 1986; Carroll and Scott, 1986; Ish-Horowicz and Pinchin, 1987; Ingham and Gergen, 1988; Carroll and Vavra, 1989; Klingler and Gergen, 1993; Jiménez et al., 1996) mutant exp.: *run* expression expands and is ectopically expressed (Jaynes and Fujioka, 2004; Ingham and Gergen, 1988; Carroll and Vavra, 1989).
run		No literature conclusions found.
ftz -| *run*	late phase	(Klingler and Gergen, 1993)
odd -| *run*		(Drean et al., 1998)

Continued on next page

Continued from previous page

Gene	Specifics	Reference
	late phase	(Klingler and Gergen, 1993) ectopic exp.: all seven stripes of *run* are moderately repressed by ectopic Odd (Drean et al., 1998). mutant exp. slight broadening and strengthening of *run* stripes (Drean et al., 1998).

Table A.22: Literature integration for pair rule genes regulating *run*.

A.3.4 *ftz* literature integration

Gene	Specifics	Reference
bcd -| *ftz*	anterior pole	(Yu and Pick, 1995; Vavra and Carroll, 1989) mutant exp.: *ftz* differs in forming a separate stripe at the anterior pole, apparently a duplicated stripe 7 (Klingler and Gergen, 1993).
cad →*ftz*		(Dearolf et al., 1989a) mutant exp.: posterior *ftz* expression is drastically reduced. Caudal binding site was also found required for posterior expression in *ftz*-*lac*Z fusion constructs.
hb -| *ftz*	stripe 3 anterior	(Hülskamp et al., 1994) mutant exp.: *ftz* stripes 2 and 3 are fused
Kr		No literature conclusions found. mutant exp.: *ftz* pattern was found to be strongly disrupted (Carroll and Scott, 1986; Ingham et al., 1986).
gt		No literature conclusions found. mutant exp.: *ftz* expression pattern is found strongly altered (Carroll and Scott, 1986; Frasch and Levine, 1987). mutant exp.: *ftz* stripes 1 and 2 fused early, but resolve perfectly later on. Only stripes 5 and 6 are fused (Klingler and Gergen, 1993).
kni -| *ftz*	stripe 3 posterior	(Frasch and Levine, 1987) (Carroll and Scott, 1986; Klingler and Gergen, 1993; Small et al., 1996; Kosman and Small, 1997) mutant exp.: *ftz* stripe 3 fused to broad expression domain, while stripe 7 remain normal (Klingler and Gergen, 1993).

Continued on next page

Continued from previous page

Gene	Specifics	Reference
		ectopic exp.: different levels of ectopic *kni* caused disruptions of *ftz* stripes 2 and 3, but had no effect on the expression of *ftz* stripe 1 (Kosman and Small, 1997).
tll		No literature conclusions found.

Table A.23: Literature integration for gap genes regulating *ftz*.

Gene	Specifics	Reference
eve -| *ftz*		(Frasch et al., 1988; Tsai and Gergen, 1995; Manoukian and Krause, 1993; Parkhurst and Ish-Horowicz, 1991; Ingham and Gergen, 1988; Jiménez et al., 1996) ectopic exp.: ectopic *eve* expression was found to repress gene *ftz* (Manoukian and Krause, 1992, 1993).
	intermediate to higher level	(Fujioka et al., 1995; Jaynes and Fujioka, 2004; Manoukian and Krause, 1992)
	anterior border	(Ish-Horowicz et al., 1989)
eve →*ftz*	stripe 1, earlier phase	(Yu and Pick, 1995; Carroll and Scott, 1986; Carroll and Vavra, 1989; Frasch and Levine, 1987; Frasch et al., 1988; Lawrence and Johnston, 1989) mutant exp.: *ftz* expression is lost from the region where the first stripe would normally form and there are shifts in the regularity of stripe width and spacing (Carroll and Vavra, 1989).
h -| *ftz*	late phase	(Carroll and Vavra, 1989; Jaynes and Fujioka, 2004; Howard and Ingham, 1986; Howard et al., 1988; Carroll and Scott, 1986; Carroll et al., 1988; Carroll, 1990; Ish-Horowicz and Pinchin, 1987; Ingham and Gergen, 1988; Yu and Pick, 1995; Dearolf et al., 1990; Tsai and Gergen, 1995; Manoukian and Krause, 1993; Frasch and Levine, 1987; Frasch et al., 1988; Lardelli and Ish-Horowicz, 1993) mutant exp.: *ftz* stripes expand, and fail to narrow properly (Ingham and Gergen, 1988). ectopic exp.: *h* expression suppresses *ftz* expression (Howard and Ingham, 1986; Carroll and Scott, 1986; Ingham and Gergen, 1988; Carroll and Vavra, 1989; Lardelli and Ish-Horowicz, 1993).

Continued on next page

Continued from previous page

Gene	Specifics	Reference
run →*ftz*		(Tsai and Gergen, 1995; Manoukian and Krause, 1993; Yu and Pick, 1995; Ingham et al., 1988; Frasch and Levine, 1987; Swantek and Gergen, 2004) mutant exp.: there is a premature narrowing, and loss, of the *ftz* expression stripes (Frasch and Levine, 1987). ectopic exp.: short heat-shock treatment during the early blastoderm stage leads to stable, broadened *ftz* stripes.
ftz →*ftz*	late phase	(Pick et al., 1990; Ish-Horowicz et al., 1989; Tsai and Gergen, 1995) exp.: *ftz* protein was found to directly bind and regulate expression of its own gene.
odd -| *ftz*	posterior edge	(Jaynes and Fujioka, 2004; Manoukian and Krause, 1993) (Mullen and DiNardo, 1995)) mutant exp.: *ftz* stripes fail to narrow properly (Mullen and DiNardo, 1995).
odd →*ftz*	before/beginning cellularization)	(Drean et al., 1998; Manoukian and Krause, 1992) ectopic exp.: activation of *ftz* occurs when ectopic Odd is expressed prior to the completion of cellularization and is most pronounced at the beginning of cellularization (Drean et al., 1998).
odd -| *ftz*	late	(Drean et al., 1998; Manoukian and Krause, 1992)

Table A.24: Literature integration for pair rule genes regulating *ftz*.

A.3.5 *odd* literature integration

No literature for gap gene regulations on *odd* were found.

Gene	Specifics	Reference
eve -| *odd*		(Jaynes and Fujioka, 2004; Fujioka et al., 1995; Manoukian and Krause, 1992; Kobayashi et al., 2001) mutant exp.: *odd* expression remains from the anterior-most cells of each Ftz-stripe (Jaynes and Fujioka, 2004). ectopic exp.: *odd* is rapidly repressed (Manoukian and Krause, 1992)
h -| *odd*		(Jiménez et al., 1996) mutant exp.: broadening of *odd* expression observed.
run -| *odd*		(Jaynes and Fujioka, 2004) null mutant exp.: primary *odd* stripes disappear essentially completely.
ftz →*odd*		(Jaynes and Fujioka, 2004; Nasiadka and Krause, 1999) mutant exp.: *ftz* required to maintain *odd* expression. ectopic exp.: *odd* is rapidly activated.
odd		No literature conclusions found.

Table A.25: Literature integration for pair rule genes regulating *odd*.

A.4 Complex Mutant Patterns

A.4.1 *eve* complex mutant patterns

bcd In Klingler and Gergen (1993), *eve* pattern in *bcd*– embryos initially form a very large anterior domain which later shrinks.

cad No complex patterns found.

hb Mutations in *hb* were found to expand the initial limits of the stripe 3 pattern. Although the anterior shift and expansion is not quite as severe as that observed for *bcd* mutants, suggesting that *bcd* might influence the anterior stripe 3 border beyond its regulation of *hb* (Small et al., 1996).

Controversial experimental observations found in Frasch and Levine (1987), *hb* mutant embryos have *eve* stripes 2, 3, 4, and 7 deleted. However in Klingler and Gergen (1993) found *eve* stripe 4 position was unaffected, and stripe 7 was also unaffected.

Kr In Frasch and Levine (1987), *Kr* mutant embryos after cellularization show two broad bands of *eve* expression in place of *eve* stripes 2-6. The first and seventh *eve* stripes appear normal. And abnormal *eve* patterns were also detected before cellularization. In Klingler and Gergen (1993) and Carroll and Vavra (1989), *eve* expression in *Kr* mutant embryos were described as two broad domains of expression expanded from the middle of the embryo.

gt In Frasch and Levine (1987), in *gt* mutant embryos, an abnormal *eve* expression pattern is first detected in after cellularization, the first and second *eve* stripes fail to resolve, as does the broad band of staining that normally

yields the fifth and sixth stripes, moreover the seventh stripe is strongly reduced, and never reaches wild-type levels of expression. Hence *gt* may also affect *eve* stripe 7 formation.

kni Controversial results were found in Frasch and Levine (1987), suggest that *kni* may even activate *eve*. *kni* mutant embryos after cellularization were described as having the fourth, fifth and sixth *eve* stripes essentially absent, whereas stripes 1, 2, and 3 appear normal. the seventh stripe is shifted toward a more anterior position.

tll Further complicating experimental observation were found in Frasch and Levine (1987), *tll* mutant shows only 6, not 7 transverse stripes of *eve* staining. There is a progressive expansion of the six remaining stripes along the A-P axis which results in strongly altered positions, and widths, for the fifth and sixth *eve* stripes. Correspondingly there are abnormally large gaps of unstained cells separating the fourth and fifth stripes, as well as the fifth and sixth stripes.

eve No complex patterns found.

hairy In Warrior and Levine (1990), the expanded *eve* stripes retained their polarity and on refinement the anterior margin was found to be more sharply defined than the posterior margin. The posterior cells in each *eve* stripe that normally showed a rapid decay of *eve* expression were still stained strongly. In *h* mutant embryos (Frasch and Levine, 1987; Ingham and Gergen, 1988), an abnormal *eve* pattern is detected after cellularization. At this time the second and fifth *eve* stripes show reduced levels of staining, whereas the remaining stripes appear normal. This stripe specific effect was not found in our 3 major

circuits.

runt The stripe specific effect of *run* regulation on *eve* is not found in my circuits. However there are extensive observations of stripe specific effects of *run* mutants in the literature. According to Frasch and Levine (1987), in *run* mutant embryos, an abnormal pattern of *eve* expression is first detected after cellularization, when the fifth expression stripe is narrower and weaker than in wild type. Just prior to gastrulation, each of the *eve* stripes, except 5, broadens and encompasses an average of five cells. In addition, irregularities in the spacing of adjacent stripes can be observed, and both the anterior and posterior margins of each expression stripe sharpen after cellularization. See also Warrior and Levine (1990), stripes 6 and 7 of *eve* are partially fused, while stripes 3 and 4 are clearly separate. The *eve* stripes do not show the bell-shaped concentration distributions seen in wild-type cellular blastoderms or the polarized stripes seen in gastrulating wild-type embryos.

In ectopic experiments, all stripes were not equally affected in *hs-runt* embryos (Manoukian and Krause, 1993; Tsai and Gergen, 1994; Hooper et al., 1989), stripe 2 was the most efficiently repressed while stripes 3 and 7 were relatively resistant to repression. According to Tsai and Gergen (1994), the most dramatic alteration is the elimination of stripe 2. The intensity of *eve* stripes 4 and 7 is also consistently reduced and stripes 5 and 6 are not well resolved. These stripe-specific effects of *hs-runt* on *eve* and hairy are most apparent at the mid-blastoderm stage when the pair-rule patterns are normally well formed, but similar effects are also observed on both younger and older blastoderm stage embryos. Finally, it is notable that *hs-runt* treatment fails to repress a reporter gene containing the *eve* autoregulatory element. This sug-

gests that the altered regulation of this element in *run* mutants (Goto et al., 1989) may be indirect and due to effects on the expression of other genes.

ftz No complex patterns found.

odd No complex patterns found.

double mutants In *run–/slp–* double mutant embryos, late *eve* patterns were found to be expanding anteriorly (Jaynes and Fujioka, 2004). In *run–/h–* embryos, *eve* patterns were not strongly disrupted in these mutants until gastrulation (Carroll and Vavra, 1989; Frasch and Levine, 1987), and is identical to the *eve* pattern in *run–* embryos (Warrior and Levine, 1990).

A.4.2 *h* complex mutant patterns

bcd The stripe 1 element includes an excellent match to the consensus *bcd*-binding site (Rushlow et al., 1989), suggesting that *bcd* might be acting directly. The DNA sequences upstream of the *h* promoter includes a strong homology to the consensus *bcd* binding-site defined for *hb* activation (Driever et al., 1989). It maps within a region that is implicated in controlling *h* stripe 1 expression (Hooper et al., 1989). In *bicoid nanos* embryos (embryos derived from *bcd nos* mothers), stripe 1 is missing (the *nos* mutation does not affect stripe 1) (Riddihough and Ish-Horowicz, 1991).

In *bicoid nanos* embryos (embryos derived from *bcd nos* mothers), stripe 1 is missing (the *nos* mutation does not affect stripe 1) (Riddihough and Ish-Horowicz, 1991). Displaced stripe 7' depends on the terminal and posterior genes. It is present and duplicated in *bcd nos* embryos that retain only the terminal coordinate system. In *bcd* mutant embryos (Klingler and Gergen, 1993), *h* initially form a very large anterior domain which later shrinks. According to Hooper et al. (1989), only 4 *h* stripes are retained. As posterior structures arise normally, the posterior 3 stripes probably reflect normal stripes 5 to 7 that are shifted somewhat anteriorly. However, the anterior-most stripe is stronger than would be expected for stripe 4. More likely, it represents a duplicated stripe 7 (displaced stripe 7') corresponding to the duplicated posterior structures that develop at the anterior of *bcd* embryos (Frohnhöfer and Nüsslein-Volhard, 1986). In embryos lacking *bcd* as the key component of the anterior organizer system (Rosée et al., 1997), the *h*7-*lac*Z expression domain is duplicated. The normal posterior expression domain appears irregular and is shifted anteriorly.

cad A large number of Caudal-binding sites were found to be present in both the *eve* stripe 3,7-element, and in the *h* stripe 6-element (Häder et al., 1998). *cad* may serve as a general activator of posterior genes which acts in concert with the Jak/Stat system to mediate activation through the *eve* stripe 3,7-element, and in combination with Knirps (Pankratz et al., 1990; Langeland et al., 1994) to activate *h* stripe 6 expression (Häder et al., 1998).

cad is expressed both maternally and zygotically (Macdonald and Struhl, 1986; Mlodzik and Gehring, 1987). In the absence of zygotic *cad* activity, *h*7-*lac*Z expression appears normal. In the absence of maternal *cad* activity, and in the absence of both maternal and zygotic *cad* activities, *h*7-*lac*Z expression is decreased. In embryos lacking *bcd* and zygotic *cad* activities, *h*7-*lac*Z expression is decreased. Embryos which lack *bcd* and both maternal and zygotic *cad* activities show weak *h*7-*lac*Z expression.

hb According to Carroll and Vavra (1989), in *hb* mutant *Kr* expression expands anteriorly (Jäckle et al., 1986; Gaul et al., 1987), while *h* expression shifts anterior to and is lost within the new anterior *Kr* domain (Carroll et al., 1988).

According to Hooper et al. (1989), in embryos homozygous for *hb* mutant, displaced *h* stripe 0' is retained, displaced stripe 1' is narrower, stripe 2 is lacking, and a broad stripe covers the stripe 3-4' region. The posterior 3 stripes are broader than wild-type, but spaced normally. The anterior *h* stripes are not maintained so that only the 3 posterior stripes remain by the onset of germ band extension.

In *hb* mutant embryo (Klingler and Gergen, 1993), *h* stripe 4 were found to be shifted anteriorly, and stripe 7 is unaffected. *hairy* stripe 2 (or maybe an

anteriorly shifted stripe 3) which is present early but then is lost later on in *hb* mutant embryo. Displaced stripe 3'-4' expression is unaffected in *hb* mutant embryo (Riddihough and Ish-Horowicz, 1991). Stripe 6 expands posteriorly when *hb* is removed (Langeland et al., 1994). Several putative *hb*-binding sites were also found in the stripe 6 regulatory sequence. Stripe 6 is also flanked by the posterior domain of *hb*. The spatial limit of *h*7-*lac*Z expression is not altered in *hb* mutant embryos (Rosée et al., 1997).

Kr In *Kr* mutant embryos (Carroll and Vavra, 1989; Hooper et al., 1989), only four broad *h* stripes are seen roughly in the positions of stripe 1, a fused stripe 2/3/4, a fused stripe 5/6, and stripe 7. According to Warrior and Levine (1990), in *Kr* heterozygous mutant embryos, *h* stripe 2 is expanded posteriorly while the distance between stripes 2 and 3 is reduced. The first *h* stripe shows a higher level of expression. In *Kr* homozygous mutant embryo, *h* stripes 1 and 7 appear normal and are in the same positions relative to each other as in wild-type. Stripes 2 and 3 are fused. Stripes 4-6 are also fused, but the composite stripe is narrower so that, *h* and *eve* stripes reverse their relative positions in this region of the embryo.

According to Langeland et al. (1994), *h* stripes 5 and 6 each display significant anterior expansion when *Kr* is removed. Several binding sites for the *Kr* repressor were identified in both the stripe 5 and 6 regulatory sequences. In ectopic *hs-Kr* expression (Langeland et al., 1994), all *h* stripes are extinguished except stripes 3 and 4, which normally fall within the wild-type *Kr* domain. Since stripes 3 and 4 are neither repressed nor ectopically activated, *Kr* protein does not appear to be sufficient to activate the stripes within its normal domain.

In *Kr* mutant embryos (Klingler and Gergen, 1993), *h* forms two broad domains of expression. According to Riddihough and Ish-Horowicz (1991), *Kr* mutations abolish displaced stripe 3'-4' and stripe 5', and expand stripe 6' anteriorly. *h* stripes 3 and 4 lie in the middle of the *Kr* domain, suggesting that they are activated by *Kr*. Displaced stripe 3'-4' expression is much thinner but not abolished in *Kr* mutant embryos, suggesting that *Kr* is not the sole activator of this domain. Displaced stripe 5' construct is affected by *Kr*, which behave as activators. According to Carroll and Vavra (1989), in *hb* mutant *Kr* expression expands anteriorly (Jäckle et al., 1986; Gaul et al., 1987), while *h* expression shifts anterior to and is lost within the new anterior *Kr* domain (Carroll et al., 1988).

According to Rosée et al. (1997), in the absence of *Kr* activity, two *h*7-*lac*Z expression domains were observed. *h*7-*lac*Z expression in the normal stripe 7 position was reduced, while a second and stronger activity of *h*7-*lac*Z expression appeared in the *Kr* expression domain found in wild-type embryos, covering the area of *h* stripes 3 and 4. The expression of these stripes was shown to be dependent on cis-acting sequences 5 to the *h*7-element, which give rise to only a single stripe in *Kr* mutant embryos (Hartmann et al., 1994).

gt In *gt* mutant embryos (Klingler and Gergen, 1993), *h* stripes 1 and 2 are barely affected, stripes 5 to 7 are fused early. According to Riddihough and Ish-Horowicz (1991), *gt* mutations expand displaced stripe 5' posteriorly, but abolish displaced stripe 6'. Displaced stripe 3'-4' and 7' are unaffected by *gt* mutation. Similarly in Langeland et al. (1994), stripe 5 expands posteriorly when *gt* is removed, putative binding sites for the gt protein have also been localized in stripe 5 regulatory sequences (Langeland and Carroll, 1993). In

Rosée et al. (1997), the spatial limit of *h*7-*lac*Z expression is unaffected in *gt* mutant embryos.

kni In *kni* mutant embryos (Carroll and Vavra, 1989; Hooper et al., 1989), *h* stripes 1, 2, and 3 appear normal but stripe 4 is missing and stripes 5-7 are fused in a wide band. In *kni* mutant embryos (Klingler and Gergen, 1993), *h* shows normal stripe 3, no broad domain, and stripe 7 is affected. According to Riddihough and Ish-Horowicz (1991), *kni* mutations reduce displaced stripe 5', abolish stripe 6', and expand stripe 7'. Displaced stripe 3'-4' is broadened in *kni* embryos, where the *Kr* domain is expanded (Gaul et al., 1987; Jäckle et al., 1986). *Kr* expression expands posteriorly, while *h* expression spreads out posterior to, and is lost within, the new posterior *Kr* domain (Carroll et al., 1988). In *kni* ectopic expression (Kosman and Small, 1997), unexpectedly, there was no detectable effect on the initial *h* pattern. In Rosée et al. (1997), the *h*7-*lac*Z expression also expands anteriorly in *kni* mutant embryos.

tll Stripe 1 expanded anteriorally and displaced stripe 6' expanded posteriorly in *tll* mutant embryos (Riddihough and Ish-Horowicz, 1991). Displaced stripe 7' is completely abolished in *tll* mutant embryos, and the *h*7-*lac*Z expression is also absent (Rosée et al., 1997). In *tll* mutant embryo (Mahoney and Lengyel, 1987; Hooper et al., 1989), *h* stripe 7 is missing. In embryos homozygous for the *tll* mutation (Hooper et al., 1989), the *h* pattern is only affected at the posterior end, showing a broad domain in the 6-7' region plus a faint posterior stripe outside the area where *h* protein is normally expressed.

double mutants From Rosée et al. (1997), in the absence of either *cad* or *bcd* activity, *h*7 expression is still activated. Even if both activities are

deleted from the embryo, activation occurs. In embryos lacking both *bcd* and *cad* activities, where *kni* activity is absent (Rivera-Pomar et al., 1995), an anterior border of the *h*7-*lac*Z expression is established in a position slightly more anterior than in wild-type. *h*7-*lac*Z expression in *kni*, *tll* double mutant embryos expands into the posterior pole region.

From Carroll and Vavra (1989), in the absence of *hb* and/or *kni* activity, loss of *h* expression occurs in the region where the *Kr* domain expands. In *hb kni* double mutant embryo, *h* is not expressed over most of the anterior segment primordia (about 40-65 % egg length) but has spread out on the posterior part of the *kni+* domain (about 20-35 % egg length). Removing *Kr+* along with *hb+* and *kni+* in the triple mutant embryo derepresses *h* expression over the posterior two-thirds of the embryo; that is, in the absence of these three gap genes, the hairy pattern is nearly uniform and the gene is strongly active because hairy expression expands at high levels across a *hb–, kni–, Kr–* embryo.

From Hooper et al. (1989), in both *kni* hb double mutant embryos, and *kni hb tll* triple mutant embryos. Interpretation is difficult due to an inability to assign stripe identities. Both embryos retain a head patch and a narrow displaced stripe 1' and a very weak stripe 2'. Both genotypes show a weak displaced 5' stripe and an adjacent broad posterior stripe. In *kni hb tll* triple mutant embryos, the posterior *h* expression is enhanced, extends more posteriorly, than in the single or double mutant embryos, suggesting that *h* is subject to interacting gap gene control in this region, and these genes may act negatively in regulating *h*.

eve According to Hooper et al. (1989), in embryos homozygous for *eve* mutant allele, *h* stripe 2 is greatly reduced or missing. The positions and intensities of the other stripes appear normal except that stripe 4 is of equal intensity to the other stripes and displaced towards stripe 3. From Carroll and Vavra (1989), in *eve* mutant embryos, the strongest effect on *h* involves the second stripe which is greatly reduced while the other stripes are generally narrower and irregularly spaced. In *hs-eve* ectopic expression embryos (Manoukian and Krause, 1992), there was no effect on *h* expression.

hairy No complex patterns found.

runt From Hooper et al. (1989), *h* pattern is only mildly affected in embryos homozygous for *run* allele. Stripe 1 appears somewhat broader than wild-type, and stripes 3/4 and 6/7 are only partially resolved by the end of blastoderm. This indicates that the altered pattern results from partial failure to repress *h* expression in specific interstripes. The equivalent pattern of *h* transcripts shows fusion of stripes 3 and 4, and of 5, 6 and 7, although stripe 5 is ultimately refined (Ingham and Gergen, 1988). *h* expression may also be translationally controlled as there is no *h* protein expression between stripes 5 and 6. From Riddihough and Ish-Horowicz (1991), in *run* mutant embryos, stripe 1 is broadened, displaced stripe 5' thinner, stripe 6' is expanded, and stripe 7' is unaffected.

From Tsai and Gergen (1994), in *hs-runt* ectopic expression, the most notable difference is the repression of stripes 1 and 6. Stripes 2 and 5 are also reduced in intensity. In contrast to these repressive effects, *h* stripes 3 and 4 appear to become more intense.

run and *h* patterns has precise complementarity in wild-type embryos (Ka-

nia et al., 1990). In *run* mutant embryos (Warrior and Levine, 1990), *h* pattern was found more severely disrupted than *eve*, stripe 5 of *h* is weaker than normal, as is stripe 2. Stripes 3 and 4, as well as stripes 6 and 7 are fused. *h* pattern was also found expanded (Ingham and Gergen, 1988; Hartmann et al., 1994; Carroll and Vavra, 1989; Manoukian and Krause, 1993; Warrior and Levine, 1990). In *run* null mutant embryo, *h* pattern was found overexpressed, with *h* stripes becoming variably wider (Ingham and Gergen, 1988). From Carroll and Vavra (1989), in *run* mutant embryo, the *h* pattern partly expands with the first *h* stripe spreading posteriorly, while the interband between stripes 3 and 4 accumulates some protein, and stripes 6 and 7 are stronger and nearly fused. The *h* pattern is still fairly periodic.

In *run* ectopic expression embryos (Manoukian and Krause, 1993), when heat shocked for 30-45 minutes all *h* expression are repressed. Transcripts encoded by the *h* gene were not strongly affected. Stripe 1 showed the highest sensitivity to ectopic Run. From Tsai and Gergen (1994), in *hs-runt* ectopic expression, the most notable difference is the repression of stripes 1 and 6. Stripes 2 and 5 are also reduced in intensity. In contrast to these repressive effects, *h* stripes 3 and 4 appear to become more intense.

From Hooper et al. (1989), *h* pattern is only mildly affected in embryos homozygous for *run* allele. Stripe 1 appears somewhat broader than wild-type, and stripes 3/4 and 6/7 are only partially resolved by the end of blastoderm. This indicates that the altered pattern results from partial failure to repress *h* expression in specific interstripes. The equivalent pattern of *h* transcripts shows fusion of stripes 3 and 4, and of 5, 6 and 7, although stripe 5 is ultimately refined (Ingham and Gergen, 1988). *h* expression may also be translationally controlled as there is no *h* protein expression between stripes 5 and 6.

From Riddihough and Ish-Horowicz (1991), in *run* mutant embryos, stripe 1 is broadened, displaced stripe 5' thinner, stripe 6' is expanded, and stripe 7' is unaffected.

ftz No complex patterns found.

odd In *odd* mutant embryos (Drean et al., 1998), the entire 7-stripe pattern of *h* appears to expand, both anteriorly and posteriorly. The first stripes of *h* appear to expand, and head defects occur in structures normally derived from adjacent regions (Nüsslein-Volhard et al., 1985; Coulter and Wieschaus, 1988).

In ectopic *hs-odd* embryos, stripe 1 of *h* is efficiently repressed by ectopic Odd. Repression of *h* stripe 1 continues in older embryos from stage 5 and is accompanied by weaker repression of stripes 2-6. The earliest observed effects of ectopic Odd (late stage 4/early stage 5) are on the anterior-most stripes.

double mutants In *run eve* double mutant embryos (Carroll and Vavra, 1989), the *h* protein pattern exhibits elements of both single mutants, for example, loss of stripe 2 and fusion of stripes 6 and 7. The periodicity is only moderately perturbed and the remaining spatial restriction suggests that there are possibly other negative regulatory functions for gap genes.

A.4.3 *run* complex mutant patterns

bcd In *bcd* mutant embryo, *run* is de-repressed over a large anterior region, about 30% of the embryo (Klingler and Gergen, 1993). The de-repression is apparent at the earliest stages of detectable *run* transcript accumulation. Subsequently one posterior stripe (corresponding to stripe 6 in wild type) is formed, and a broad domain of expression, spanning almost half of the length of the embryo is formed at the anterior. Later, a stripe corresponding to stripe 7 emerges, and between the well-formed stripes (6 and 7) and the anterior domain, 1 or 2 imperfectly formed stripes arise. as cellularization proceeds, the anterior domain shrinks to some extent, but it never resolves into distinct stripes.

cad No complex patterns found.

hb According to Klingler and Gergen (1993), the posterior domain of *hb* has little effect on the *run* pattern: stripes 4 to 7 are formed perfectly in *hb* mutant embryo. A slight effect is observed at the very end of cellularization, when a low level of *run* transcript builds up between stripes 6 and 7. The effect of the absence of the anterior *hb* domain on *run* is more dramatic; early in the blastoderm, stripes 2 and 3 are replaced by one domain of expression, about the size of two stripes combined. Later this domain moves to the anterior and forms a sharp anterior border, such that only a very narrow gap is left with stripe 1, while a large gap is formed with stripe 4.

Kr In *Kr* mutant embryo (Klingler and Gergen, 1993), stripes 2 to 5 are replaced by one large domain. Expression within this domain subsequently

fades, and breaks up into a broad anterior and a more narrow posterior stripe. Stripes 3 and 4 are also narrower in *Kr−/+*.

gt In *gt* mutant embryo (Klingler and Gergen, 1993), the *run* pattern is strongly affected early in the cellular blastoderm: stripes 1 and 2 are fused and form a band of intense expression at the anterior, stripes 4 to 7 are not fully resolved; as the nuclei elongate, the first two stripes begin to separate; at this time, stripes 5 and 6 form a strongly stained band when cellularization approaches completion, the pattern of *run* improves to a surprising degree: stripes 1 and 2 resolve perfectly, with only a slight difference in spacing of stripe 2 between 1 and 3 remaining; at the posterior, stripes 5 and 6 also show signs of separation, although stripe 6 is abnormally weak. Although the early effects of *gt−* are dramatic, the *run* pattern recovers surprisingly well during these later stages.

kni In *kni* mutant embryo (Klingler and Gergen, 1993), it is stripes 3 to 6 that are affected. At early stages stripe 3 is fused to the de-repression domain. Later this stripe partially separates from the domain, indicating that its posterior border is not formed solely by *kni* late in the blastoderm stage, the domain weakens further, similarly as in *Kr−*, and an additional faint stripe may be observed. Stripe 5 is also narrower in *kni−/+* .

In *kni* ectopic expression experiments (Kosman and Small, 1997), *eve stripe 2-kni* constructs caused disruptions of *run* stripes 2 and 3, but had no effect on stripe 1. Early in cycle 14, low levels of ectopic *kni* repressed *run* stripe 2 quite strongly, but stripe 3 only mildly. At the same age, higher levels increased repression of both stripes: stripe 2 is absent and stripe 3 is severely reduced. *run* stripes 2 and 3 respond differently to changing the levels of *kni* at

the position of *eve* stripe 2. The repression of stripe 3 increases in proportion to the level of ectopic *kni*, a response similar to that seen for *eve* stripe 3. For stripe 2, all levels cause repression early in cycle 14, but there is a restoration of expression in this region that increases with the level of ectopic *kni*.

tll In *tll* mutant embryo (Klingler and Gergen, 1993), stripe 7 is not formed at all. Stripe 6 appears belatedly (in wild type, stripe 6 appears very early), and this stripe as well as stripe 5 are shifted posteriorly.

eve According to Klingler and Gergen (1993), in *eve* mutant embryo, the earliest pattern abnormality detectable is a ventral gap in the first stripe; otherwise at this stage (nuclear elongation) all stripes are perfectly formed. When cellularization has progressed halfway (cell membranes extended to just below the nuclei), the ventral gap in the first stripe becomes partially restored, but now the intensity and the spacing of the other stripes becomes affected. Stripes 1 and 2 as well as 3 and 4 are closer together, and all stripes but 2 and 6 are less intense than in wild type. Towards the end of cellularization, the stripes become fainter and wider with badly defined stripe boundaries. At later stages *run* becomes expressed almost homogenously throughout the extending germband of the embryo. This later more uniform effect fits well with the evolution of *run* and *eve* expression patterns observed in wild-type embryos. the stripes initially overlap by about 2 cells and then as they are refined they come to abut each other in a way suggesting that *eve* may be directly involved in stabilizing the anterior borders of the *run* stripes at these later stages.

hairy According to Lardelli and Ish-Horowicz (1993), ectopic *h* only affects *run* near the margins of endogenous *h* expression where *h* concentrations are highest (Ish-Horowicz and Pinchin, 1987; Klingler and Gergen, 1993).

According to Klingler and Gergen (1993) in *h* mutant embryo, at mid-cellularization, *run* is ectopically expressed in the inter-stripes. This ectopic expression is at a low level, and the 7 *run* stripes are still clearly visible above this basic expression. Indeed the stripes are formed concisely and with perfect spacing. The stripes become less distinct later, but they still can be detected at the onset of gastrulation when the transition to the 14 stripe pattern still occurs. It is notable that the cells anterior to *run* stripe 1 are not de-repressed in *h*–.

runt In *run* mutant embryos (Goto et al., 1989), stripes 2, 3, 4, 6 and 7 bifurcate into sets of two sharply defined stripes while stripes 1 and 5 are incompletely split. According to Tsai and Gergen (1994), in *hs-runt* ectopic expression, stripe-specific defects are observed.

According to Klingler and Gergen (1993), in amorphic *run* alleles that express an mRNA transcript, stripes 4 and 6 exceed normal levels of expression, more intense and broader than in wild-type, during earlier stages, while stripes 3 and 5 are abnormally weak, less intense and narrower. Towards the end of the blastoderm stage and through gastrulation, stripes 4 and 7, and also to a lesser degree stripe 1, all continue to be expressed at high levels; the other stripes progressively degenerate. As in *eve*–, the first *run* stripe develops a ventral gap at the mid-cellularization stage in *runt*– embryos.

ftz In *ftz* mutant embryos (Klingler and Gergen, 1993), the pattern develops normally until the onset of gastrulation. The stripes expand posteriorly,

similar to wild-type, but at a full level of intensity and they do not split into 14 stripes. These stripes are broader than the interstripes and persist during germ-band extension.

odd In stage 6 embryos (Drean et al., 1998), all seven stripes of *run* are moderately repressed by ectopic Odd. This correlates with what appears to be a slight broadening and strengthening of *run* stripes in *odd* mutant embryos. According to Klingler and Gergen (1993), mutations in *odd* cause relatively minor defects. The 14 stripe pattern of *run* forms, but the additional set of stripes that form between the 7 original ones fail to gain full width and intensity.

double mutants In *eve slp* double mutant embryo (Jaynes and Fujioka, 2004), *run* has low level expression throughout the *eve* domain.

A.4.4 *ftz* complex mutant patterns

bcd According to Klingler and Gergen (1993), in *bcd* mutant embryo, *ftz* differs in forming a separate stripe at the anterior pole, apparently a duplicated stripe 7. Duplication of the posterior *ftz* stripe in *bcd* mutant embryo was also found by (Hooper et al., 1989; Frohnhöfer and Nüsslein-Volhard, 1987).

cad No complex patterns found.

hb According to Klingler and Gergen (1993), in *hb* mutant embryo, the position of *ftz* stripe 4 is unaffected, and stripes 6 and 7 are partially fused. It has been shown that the *ftz* expression pattern is strongly altered in *hb*– embryos (Frasch and Levine, 1987; Carroll and Scott, 1986; Carroll et al., 1988). Comparison of the altered *eve* and *ftz* patterns reveals that they show reciprocal defects. Regions in *hb*– embryos where *eve* proteins are expressed coincide with regions where *ftz* proteins are not expressed, and vice versa.

Kr *ftz* expression patterns are compressed in *Kr* heterozygotes (Frasch and Levine, 1987); this region includes the third *eve* stripe through the fourth *ftz* stripe. According to Klingler and Gergen (1993), *ftz* form one broad domain in *Kr* mutant embryos.

According to Carroll and Vavra (1989); Carroll et al. (1988), in *Kr* mutant embryo , *h* and *ftz* transcript assume complementary patterns, indicating that the effect of *Kr* upon *ftz* may be mediated indirectly through *h* (Ingham et al., 1986).

gt According to Klingler and Gergen (1993); Reinitz and Levine (1990), *ftz* stripes 1 and 2 fused early, but resolve perfectly later on. Only stripes 5 and

6 are fused.

kni According to Klingler and Gergen (1993), in *kni* mutant embryo, *ftz* stripe 3 fused to broad expression domain, while stripe 7 remain normal. In *kni* mutants, there is also a posterior expansion of reporter gene expression driven by the stripe 3 enhancer (Small et al., 1996). According to Kosman and Small (1997), different levels of ectopic *kni* caused disruptions of *ftz* stripes 2 and 3, but had no effect on the expression of *ftz* stripe 1.

According to Frasch and Levine (1987), *kni*– embryos show abnormal *eve* and *ftz* patterns that closely correspond to the segments deleted in advanced stage mutants. The patterns of *eve* and *ftz* expression show reciprocal defects. The third through sixth *ftz* expression stripes are fused into a single broad band (Carroll and Scott, 1986), which coincides with the region where *eve* staining is absent.

A one nucleus anterior expansion of *ftz* stripe 3 can be detected in some embryos containing low levels of ectopic *kni* (Kosman and Small, 1997). Increasing the levels of ectopic *kni* first turns off the expression in the one cell expansion, and then represses the stripe itself. There is a strong correlation between high levels of ectopic *kni* at *eve* stripe 2 and the repression of *ftz* stripe 3.

tll No complex patterns found.

double mutants According to Frasch and Levine (1987), in *hb*–, *kni*– double mutant embryos, *ftz* proteins are uniformly distributed along the a-p axis of cellular blastoderm stage; lack segment boundaries and show a continuous lawn of denticle hairs, which is a phenotype similar to strong *eve*– embryos.

The altered patterns of *ftz* expression observed in such mutants do not appear to represent a simple addition of the *ftz* expression patterns seen in *hb*– and *kni*– embryos. Within the *ftz* expression limit in the mutant embryos, from 74% to 13% egg length, there are regions that show somewhat reduced levels of expression.

eve According to Frasch et al. (1988), in *eve* mutant embryo, *ftz* pattern appears nearly normal (Carroll and Scott, 1986; Harding et al., 1986). In each *eve* mutant the seven *ftz* stripes are shifted to more anterior regions (see also Warrior and Levine (1990)), thereby bringing adjacent *eve* and *ftz* stripes closer together. The degree of this shift correlates with the strength of the *eve* allele, with weak mutants causing relatively minor shifts and stronger mutants causing more severe shifts. In *eve* null mutant embryo, several abnormalities are detected by the onset of gastrulation, including the loss of the first *ftz* stripe and unequal spacing in the locations of the remaining six stripes. This anterior shifting appears even more severe than that observed for *eve* hypomorphs, and the anterior margins of adjacent *eve* and *ftz* stripes are separated by only one or two cells. It is not clear whether this shift of the anterior margin results in broader *ftz* stripes. It appears that *ftz* stripes of normal widths are shifted in their entirety to more anterior positions.

According to Yu and Pick (1995), the earliest abnormal *ftz* patterns were observed only after seven *ftz* stripes had formed. The first abnormality is apparent in a loss of *ftz* expression from the ventral portion of *ftz* stripe 1. Later, expression decreases throughout stripe 1 and the remaining stripes appear to be slightly less regular and weaker than in wild type embryos. The clearest requirement for *eve* is for the maintenance of *frz* stripe 1, a requirement that

is displayed differentially ventrally to dorsally.

According to Carroll and Vavra (1989), in *eve* mutant embryo, *ftz* expression is lost in *eve*– embryos from the region where the first stripe would normally form and there are shifts in the regularity of stripe width and spacing. There is a gap about 8 nuclei in width where little or no *ftz* protein accumulates, posterior to this gap the combined pattern is largely periodic. After cellularization *ftz* patterns decay rapidly in an *eve*– embryo (Carroll and Scott, 1986).

Ectopic *eve* expression was found to repress gene *ftz* (Manoukian and Krause, 1992, 1993). Stripes of *ftz* expression diminished in intensity and width as the abundance of ectopic Eve increased. Total repression of *ftz* transcription occurred when heat shocks were 4 min or longer. A very short temporal delay between the rise in levels of Eve and the subsequent loss of *ftz* transcripts would favor a direct interaction between the two genes. The expression patterns of *ftz* promoter-*lac*Z fusion genes were also repressed within a similar time frame.

hairy In *h* mutant embryo (Howard and Ingham, 1986; Carroll and Scott, 1986; Ish-Horowicz and Pinchin, 1987; Ingham and Gergen, 1988; Carroll and Vavra, 1989; Tsai and Gergen, 1995), *ftz* was found broadened and ectopically expressed in nearly all of the nuclei where it is normally absent, except that no *ftz* protein is seen in the anterior 30% or posterior tip of the embryo. *ftz* stripes expand, and fail to narrow properly (Ingham and Gergen, 1988). However the effect of loss *ftz* interstripe repression (Tsai and Gergen, 1995) may also come from the de-repression of *run* expression in these same embryos (Klingler and Gergen, 1993).

According to Yu and Pick (1995), in *h* mutant embryo, the broadening of *ftz* stripes (Howard and Ingham, 1986) is not entirely uniform along the anterior-posterior axis; a larger gap remains between broadened *ftz* stripes 3 and 4 than the other stripes. While mutations in the *h* gene clearly affect the *ftz* striped pattern, no defects in stripe establishment were observed.

Ectopic *h* expression suppresses *ftz* expression (Howard and Ingham, 1986; Carroll and Scott, 1986; Ingham and Gergen, 1988; Carroll and Vavra, 1989; Lardelli and Ish-Horowicz, 1993). According to Ish-Horowicz and Pinchin (1987); Lardelli and Ish-Horowicz (1993), expression of *h* under the control of heat-inducible *hsp70* promoter completely abolished the expression of *ftz*.

runt In *run* mutant embryo (Frasch and Levine, 1987), there is a premature narrowing, and loss, of the *ftz* expression stripes. *ftz* products disappear prematurely in gastrulating embryos. According to Carroll and Vavra (1989), *ftz* expression is reduced in *run* mutant embryos with the first, third, fifth, and sixth stripes narrowing or almost disappearing. The *ftz* protein pattern complements the *h* protein pattern and is likely to result from the initial effect of *runt*– on the *h* pattern and the subsequent effect of *h* on *ftz* (Howard and Ingham, 1986; Carroll and Scott, 1986).

According to Jaynes and Fujioka (2004), in *run* mutant embryo, relatively narrow and weak *ftz* expression were observed (Carroll and Scott, 1986). *ftz* stripes 1, 4, and 5 remain relatively broad, while others are reduced (Lawrence and Johnston, 1989). The *ftz* domains are incompletely organized. In *run* null mutant, there is weaker than normal *ftz* expression. Even *ftz* stripes 1, 4, and 5 appear weaker than normal, although they remain broad.

According to Tsai and Gergen (1995), in *run* mutant embryo, alterations

in *ftz* expression are apparent by the time the seven-striped pattern emerges. The initial difference is reduced intensity of stripe 3. The expression of this stripe as well as stripes 1 and 6 becomes greatly reduced as cellularization proceeds. By the completion of cellularization only stripes 4 and 7 remain. *ftz* *lac*Z expression was also reduced.

According to Yu and Pick (1995), in *run* mutant embryo, by the end of cellularization (when nuclei are fully elongated), and during gastrulation, the seven striped pattern became very abnormal. Stripes decayed in *run* embryos in a variable order. Stripes 1, 3 and 6 appeared to be the most sensitive to loss of *run* activity, while stripes 7 and 4 were the most resistant. *ftz* pattern initiate normally in *run* mutant embryos but decay rapidly at the end of cellularization (Ingham and Gergen, 1988).

According to Manoukian and Krause (1993), in *run* mutant embryo, *ftz* stripes initiate weakly and are prematurely lost (Ingham and Gergen, 1988). Normally, *ftz* stripes narrow at their posterior edges, beginning at gastrulation. In *run*– embryos, premature loss of *ftz* expression begins at about the same time, but is no longer limited to the posterior domains of expression (Ingham and Gergen, 1988).

In a *hs-runt* ectopic expression experiment (Tsai and Gergen, 1995, 1994), transient heat-shock treatment induces uniform accumulation of Runt in all somatic cells (Tsai and Gergen, 1994) which in turn leads to activation of *ftz*. Short heat-shock treatment during the early blastoderm stage leads to stable, broadened *ftz* stripes. More extreme treatment causes *ftz* to be expressed in a broad band that extends from 15% to 65% egg length. Interestingly, *hs/runt* treatment does not lead to significant *ftz* expression outside this region. *ftz* *lac*Z was also found overexpressed.

In *hs-run* ectopic expression experiment from Manoukian and Krause (1993), expression of the *ftz* gene did not appear to be affected prior to 30 minutes after initiation of heat shock (AHS). However, starting at 30 minutes AHS, ftz stripes widened dramatically. In embryos that had been heat shocked prior to *ftz* stripe resolution, and fixed 30-45 minutes later, *ftz* was often expressed in a single solid stripe that filled the entire trunk of the embryo. When these embryos were permitted to develop for another 15-30 minutes prior to fixation, this solid pattern of *ftz* expression began to split into a pattern of seven, segment-wide stripes. In embryos where *ftz* had already resolved into stripes prior to the time of *run* induction, the seven stripe pattern could no longer be consolidated into a solid band of expression. Nevertheless, at 30-45 minutes AHS, *ftz* stripes were abnormally wide.

ftz No complex patterns found.

odd *ftz* stripes fail to narrow properly in *odd* mutant embryos (Mullen and DiNardo, 1995). *ftz* stripes are broad and persistent. The seven *ftz* stripes resolve from the early broad domain similar to wildtype (Carroll and Scott, 1986), but the first difference occurs at cellular blastoderm when stripes 1 and 2 appear to span virtually the entire parasegment. As germ band extension begins, the broad *ftz* stripes fail to retract and thus remain three to four cells wide. The posterior edge of each *ftz* stripe extends closer to the anterior edge, and has lower level.

According to Drean et al. (1998), activation of *ftz* occurs when ectopic Odd is expressed prior to the completion of cellularization and is most pronounced at the beginning of cellularization. This positive relationship between Odd and *ftz* is consistent with the expression patterns of the two genes at this

stage: *odd* and *ftz* stripes overlap perfectly, except for stripe 7 of *odd* which is missing at this stage (Manoukian and Krause, 1993). Beginning at stage 6, *odd* and *ftz* stripes begin to resolve into non-overlapping patterns and it is at this later time that Odd becomes a repressor of *ftz*.

double mutants In *run*– *h*– double mutant embryo (Carroll and Vavra, 1989; Tsai and Gergen, 1995), *ftz* pattern is de-repressed compared to patterns in embryos mutant only for *run*, and similar to that of *h*– mutant embryo. In *run*– *eve*– double mutant embryo, the *ftz* pattern is also strongly affected (Carroll and Vavra, 1989).

A.4.5 *odd* complex mutant patterns

gap and maternal genes No complex patterns found.

eve In *eve* mutant embryo, *odd* expression remains from the anterior-most cells of each Ftz-stripe (Jaynes and Fujioka, 2004).

hairy No complex patterns found.

runt In *run* null mutant embryo (Jaynes and Fujioka, 2004), primary *odd* stripes disappear essentially completely. *odd* comes on in broad stripes in the *eve* domain in place of *slp*, and is lost from the *ftz* domains.

ftz No complex patterns found.

odd No complex patterns found.

double mutants According to Jaynes and Fujioka (2004), in *eve slp* double mutant embryo, *odd* stripes are extensively broadened, failing to retract from the posterior of the *ftz* domains as they normally do, as well as from the anterior of the *ftz* domains due to the absence of *eve*. In *run slp* double mutant embryo, *odd* expression is lost from the *ftz* domains. In *run eve* double mutant embryo, there is no *odd* expression in the trunk region during gastrulation.

A.5 Regulatory Phasing Analysis

A.5.1 *eve* regulatory phasing analysis

According to Appendix Table A.1, for *Kr* repression on the *eve* stripe 3 anterior border, as shown in the phasing portrait (Fig. A.2 (D)), the repression input increases toward the peak of the total regulatory input for *eve* stripe 3. For *Kr* repression on the stripe 4 posterior border (Fig. A.2 (B)), the repression input increases toward the peak of the total regulatory input for stripe 4. Hence both regulations do not fit in the simple phasing rule, and are considered as regulatory balancers. The other gap gene regulations on *eve*, predicted in Fig.4.1, that fit in the simple phasing rule are shown in Fig. A.1 and A.2.

According to Appendix Table A.2, for *h* activation on *eve*, as shown in the phasing portrait (Fig. A.3 (A, B)), *h* is placed in an anteriorly overlapping position to *eve*, hence the activating role of *h* fits in the simple phasing rule. The *h* activation input (Fig. A.3 (C)) increases toward the peak of the total regulatory input for *eve* in a more anterior position, which helps shape the stripe and also shift it forward anteriorly.

According to Appendix Table A.2, for *odd* repression on *eve*, as shown in the phasing portrait (Fig. A.4 (A, B)), *odd* is placed in a more complementary position to *eve*, with residual expression remaining between the two borders, hence the repressor role of *odd* fits in the simple phasing rule. The *odd* repression input increases toward the limit of the two borders of the total regulatory input for *eve*, which helps set the two borders of *eve* (Fig. A.4 (C)).

According to Appendix Table A.2, for *ftz* activation on *eve*, as shown in the phasing portrait (Fig. A.5 (A, B)), *ftz* is also in a more complementary position to *eve*, with residual expression remaining between the two borders, hence the

activator role of *ftz* does not fit in the simple phasing rule. The *ftz* activation input increases toward the limit of the two borders of the total regulatory input for *eve*, which serves as a regulatory balancer for the refinement of the two *eve* borders (Fig. A.5 (C)).

According to Appendix Table A.2, for *run* repression on *eve*, particularly on the posterior border, as shown in the phasing portrait (Fig. A.6 (A, B)), *run* is placed in a posteriorly overlapping position to *eve*, hence the repressor role of *run* fits in the simple phasing rule. The *run* repression input increases toward the limit of the posterior border (Fig. A.6 (C)), which helps set the posterior border, and in this case shift the posterior border forward in the refinement phase.

According to Appendix Table A.2, for *eve* auto-activation, particularly on the posterior border, as shown in the phasing portrait (Fig. A.7 (A)), the *eve* activation input increases toward the peak of the total regulatory input for *eve*, which helps form and maintain *eve* stripes in the late refinement phase.

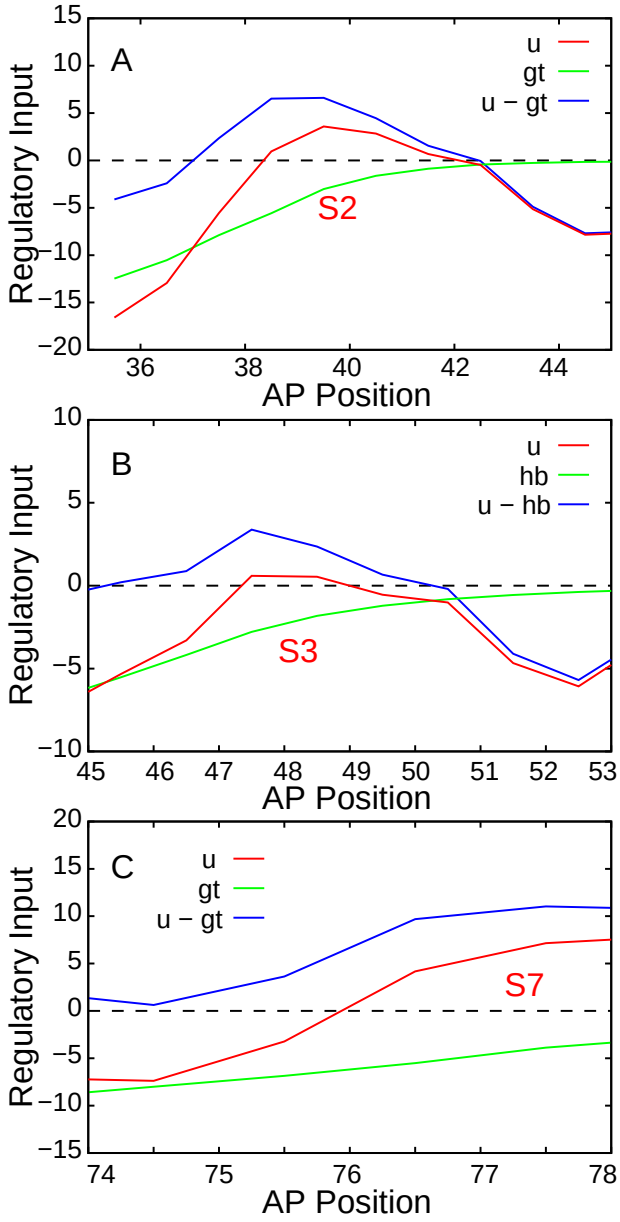

Figure A.1: *hb* and *gt* regulation on *eve*. (**A**) *gt* repression on *eve* stripe 2 anterior border at t7 in circuit A1. The total regulatory input for *eve* stripe 2 (u^{eve} from Eq. 3.1), *gt* regulatory input on *eve* stripe 2, and the total regulatory input subtracts (without) *gt* input on *eve* stripe 2 (key $u - gt$ denotes the value of $u^{eve} - E^{eve \leftarrow gt} v^{gt}(t)$). (**B**) *hb* repression on *eve* stripe 3 anterior border at t7 in circuit A2. (**C**) *gt* repression on *eve* stripe 7 anterior border at t7 in circuit A1.

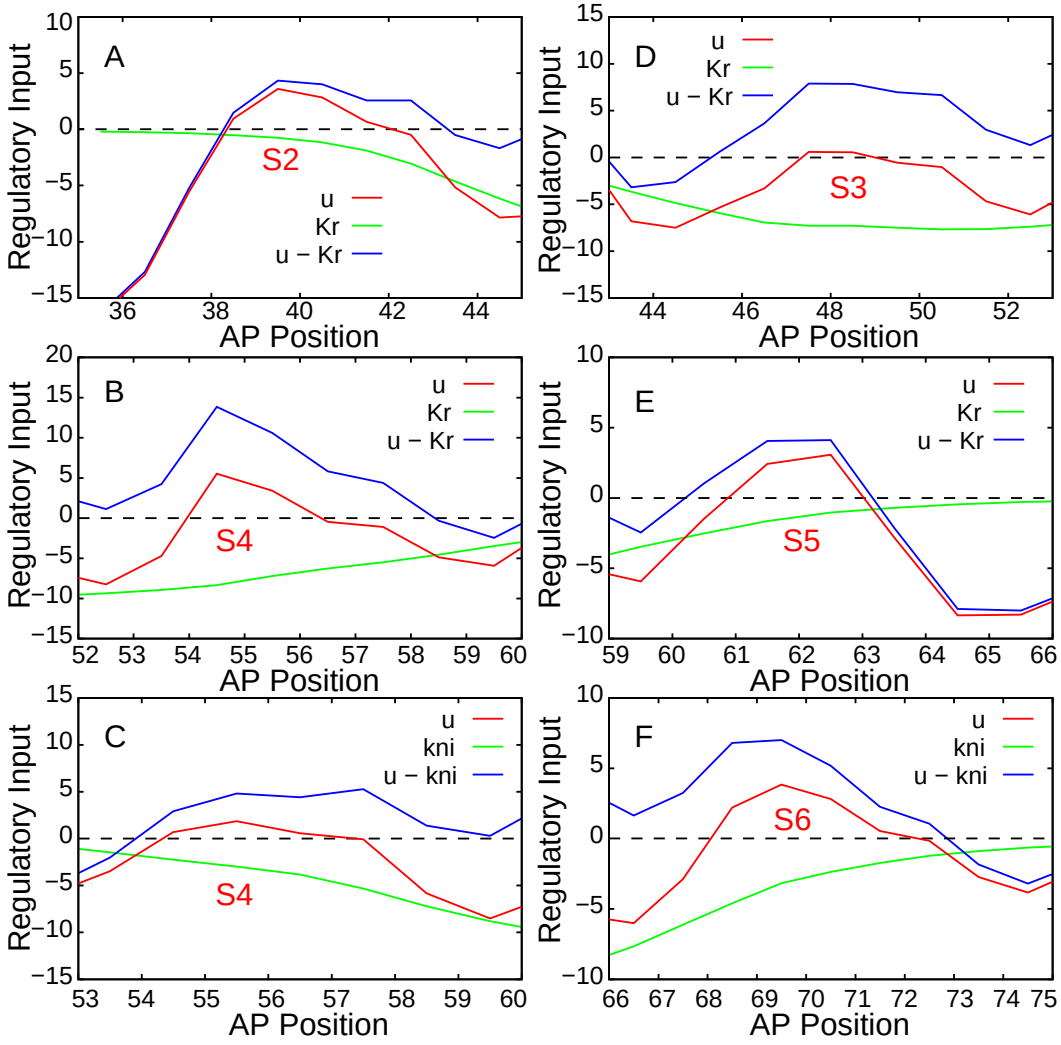

Figure A.2: *Kr* and *kni* regulation on *eve*. (**A**) *Kr* repression on *eve* stripe 2 posterior border at t7 in circuit A1. The total regulatory input for *eve* stripe 2 (u^{eve} from Eq. 3.1), *Kr* regulatory input on *eve* stripe 2, and the total regulatory input subtracts (without) *Kr* input on *eve* stripe 2 (key $u - Kr$ denotes the value of $u^{eve} - E^{eve \leftarrow Kr} v^{Kr}(t)$). (**B**) *Kr* repression on *eve* stripe 4 posterior border at t7 in circuit A1. (**C**) *kni* repression on *eve* stripe 4 posterior border at t7 in circuit A2. (**D**) *Kr* repression on *eve* stripe 3 anterior border at t7 in circuit A2. (**E**) *Kr* repression on *eve* stripe 5 anterior border at t7 in circuit A1. (**F**) *kni* repression on *eve* stripe 6 anterior border at t7 in circuit A2.

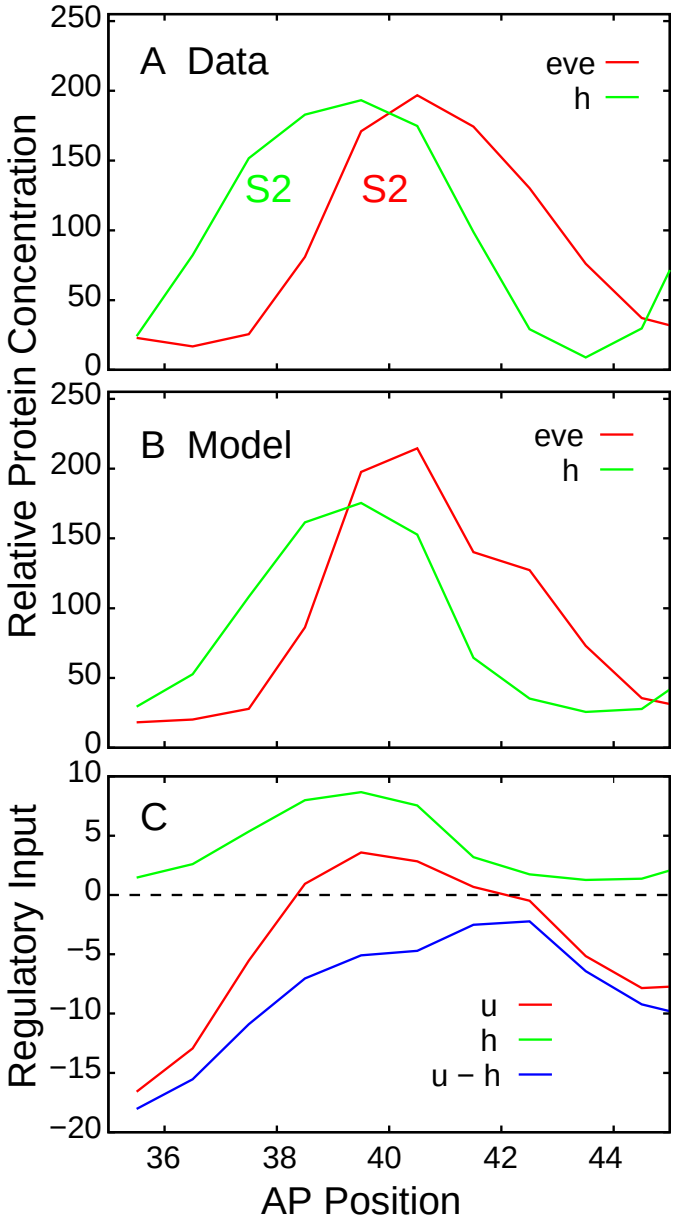

Figure A.3: h regulation on *eve* stripe 2 at t7 in circuit A1. (**A**) *eve* and h stripe 2 at t7 from data (Fig. 1.3). (**B**) *eve* and h stripe 2 at t7 in circuit A1. (**C**) The total regulatory input for *eve* stripe 2 (u^{eve} from Eq. 3.1), h regulatory input on *eve* stripe 2, and the total regulatory input subtracts (without) h input on *eve* stripe 2 (key $u - h$ denotes the value of $u^{eve} - T^{eve \leftarrow h} v^h$).

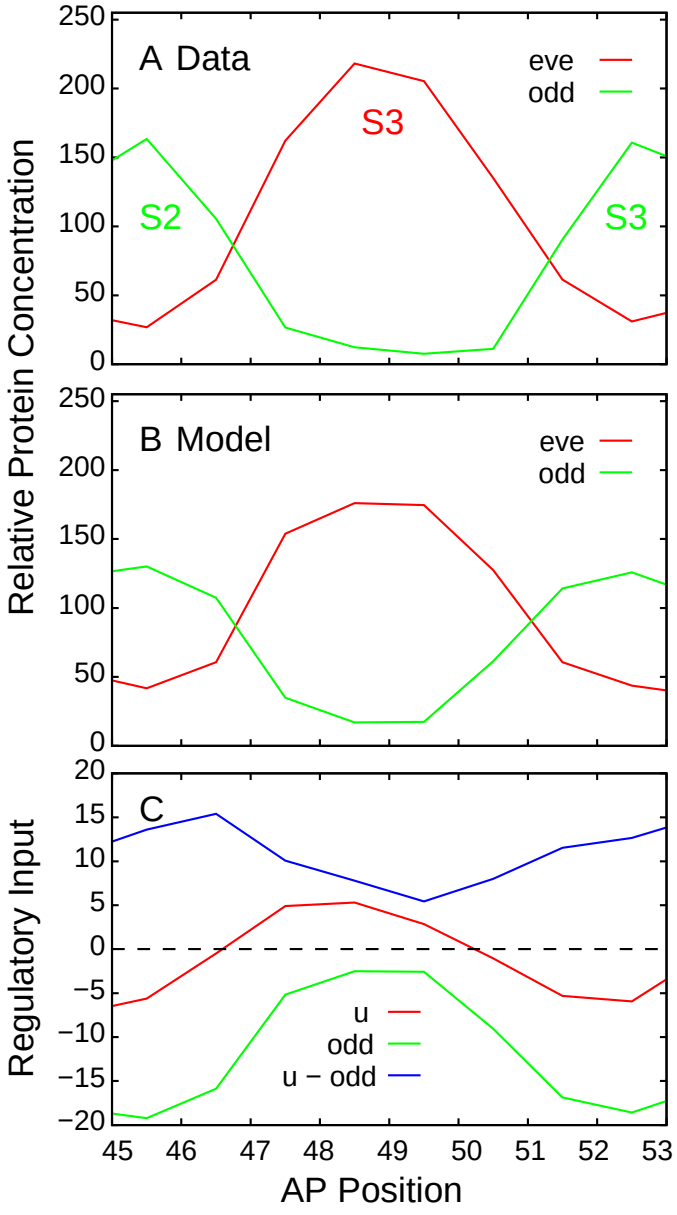

Figure A.4: *odd* regulation on *eve* stripe 3 at t7 in circuit B1. (**A**) *eve* stripe 3 and *odd* stripe 2 and 3 at t7 from data (Fig. 1.3), and in circuit B1 (**B**). (**C**) The total regulatory input for *eve* stripe 3 (u^{eve} from Eq. 3.1), *odd* regulatory input on *eve* stripe 3, and the total regulatory input subtracts (without) *odd* input on *eve* stripe 3 (key $u - odd$ denotes the value of $u^{eve} - T^{eve \leftarrow odd} v^{odd}$).

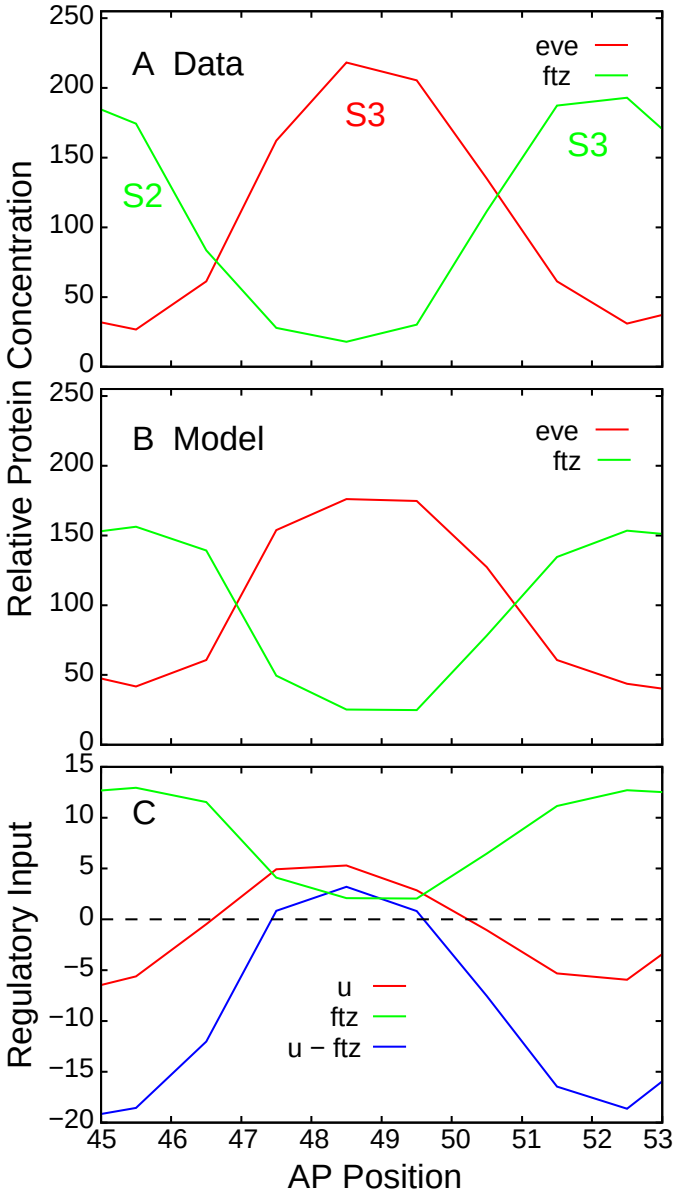

Figure A.5: *ftz* regulation on *eve* stripe 3 at t7 in circuit B1. (**A**) *eve* stripe 3 and *ftz* stripe 2 and 3 at t7 from data (Fig. 1.3), and in circuit B1 (**B**). (**C**) The total regulatory input for *eve* stripe 3 (u^{eve} from Eq. 3.1), *ftz* regulatory input on *eve* stripe 3, and the total regulatory input subtracts (without) *ftz* input on *eve* stripe 3 (key $u - ftz$ denotes the value of $u^{eve} - T^{eve \leftarrow ftz} v^{ftz}$).

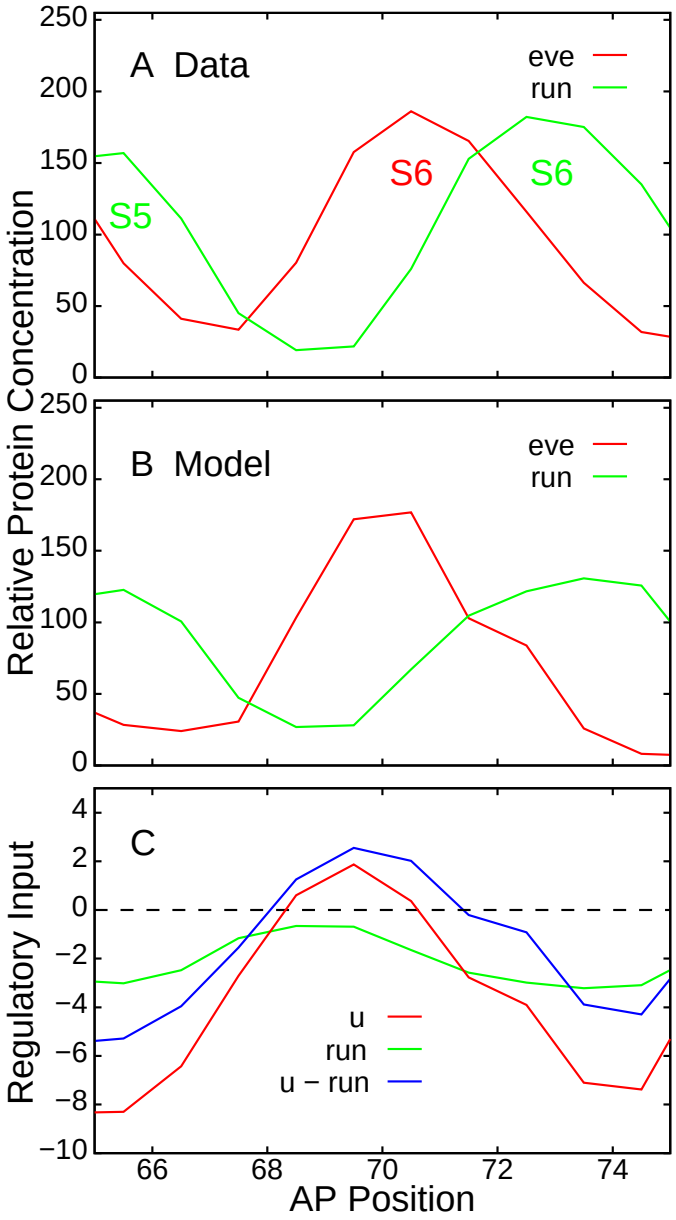

Figure A.6: *run* regulation on *eve* stripe 6 at t7 in circuit A1. (**A**) *eve* stripe 6, *run* stripe 6 and stripe 5 at t7 from data (Fig. 1.3), and in circuit A1 (**B**). (**C**) The total regulatory input for *eve* stripe 6 (u^{eve} from Eq. 3.1), *run* regulatory input on *eve* stripe 6, and the total regulatory input subtracts (without) *run* input on *eve* stripe 6 (key $u - run$ denotes the value of $u^{eve} - T^{eve \leftarrow run} v^{run}$).

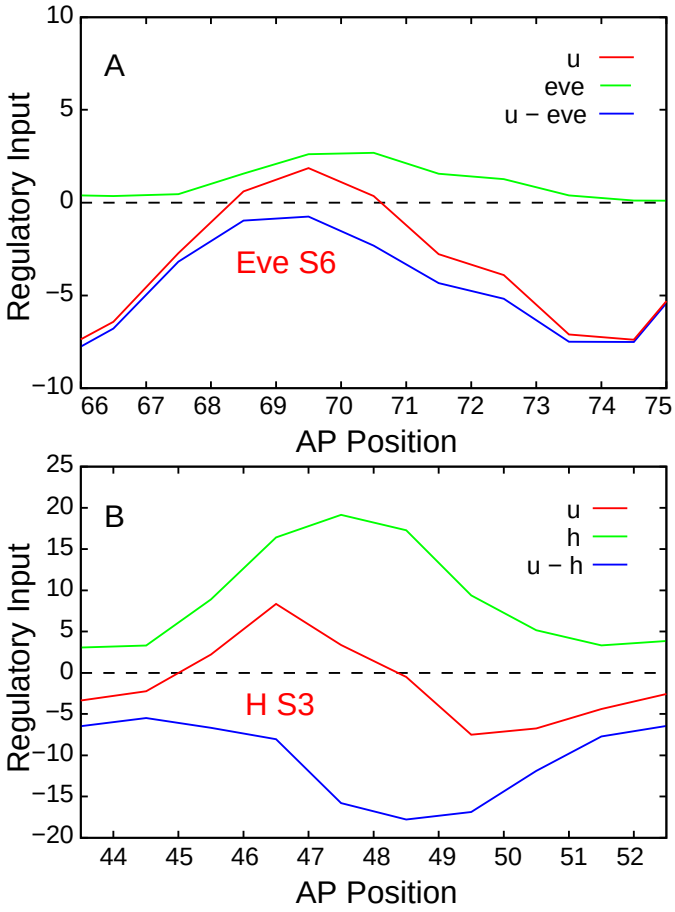

Figure A.7: *eve* and h auto-activation. (**A**) *eve* auto-activation on stripe 6 at t7 in circuit A1. The total regulatory input for *eve* stripe 6 (u^{eve} from Eq. 3.1), *eve* regulatory input on *eve* stripe 6, and the total regulatory input subtracts (without) *eve* input on *eve* stripe 6 (key $u - eve$ denotes the value of $u^{eve} - T^{eve \leftarrow eve} v^{eve}$). (**B**) h auto-activation on stripe 3 at t7 in circuit B1.

A.5.2 *h* regulatory phasing analysis

According to Appendix Table A.3, for *Kr* repression on *h* stripe 3 anterior border, as shown in the phasing portrait (Fig. A.8 (B)), the repression input increases toward the peak of the total regulatory input for stripe 3, which does not fit in the phasing rule. Hence *Kr* repression on stripe 3 anterior border is considered as a regulatory balancer. The other gap gene regulations on *h*, predicted in Fig.4.1, that fit in the simple phasing rule are shown in Fig. A.8.

According to Appendix Table A.4, for *run* repression on *h*, as shown in the phasing portrait (Fig. A.10 (A, B)), *run* is placed in a complimentary and slightly more posteriorly overlapping position to *h*, with residual expression remaining between the two borders, hence the repressor role of *run* fits in the simple phasing rule. The *run* repression input increases toward the limit of both borders of the total regulatory input for *h* (Fig. A.10 (C)), which helps set both borders of each *h* stripe.

According to Appendix Table A.4, for *eve* activation on *h*, as shown in the phasing portrait (Fig. A.9 (A, B)), *eve* is placed in a posteriorly overlapping position to *h*, hence the activator role of *eve* does not fit in the simple phasing rule. The *eve* activation input on *h* (Fig. A.9 (C)) increases toward the peak of the total regulatory input for *h* in a more posterior position, hence even though it helps establish both *h* borders through activation, it does not shift the stripe forward anteriorly and violates the shifting constraints.

According to Appendix Table A.4, for *ftz* activation on *h*, as shown in the phasing portrait (Fig. A.11 (A, B, D, E)), *ftz* is placed in a more anteriorly overlapping position to *h*, hence the activator role of *ftz* fits in the simple phasing rule. The *ftz* activation input increases toward the peak of the total regulatory input for *h* stripe 5 and 6 in a more anterior position in circuit B1.

For other stripes in circuits B1 and A1, however, the *ftz* input on the anterior *h* border is more of a plateau. In Fig. A.11 (C, F), *ftz* helps set both *h* borders through activation, except for the plateau input on stripe 4 anterior border, and helps shift the *h* stripe forward anteriorly.

According to Appendix Table A.4, for *odd* regulation on *h*, as shown in the phasing portrait (Fig. A.12 (A, B, D, E)), *odd* is positioned in an anteriorly overlapping position to *h*, hence the repressor role of *odd* does not fit in the simple phasing rule, *odd* may be considered as a regulatory balancer for refinement in the late phase in circuit B1. The *odd* repression input increases toward the peak of the total regulatory input for *h* (Fig. A.4 (F)), and is a plateau on the anterior border, except for *h* stripe 7 anterior border. *odd* may also serve as an activator in the early phase, which would fit in the simple phasing rule. However in circuit A1, *odd* activation input is still more plateau on the anterior border (Fig. A.4 (C)), except for stripe 2 and 7 anterior border.

According to Appendix Table A.4, for *h* auto-activation in circuit B1, as shown in the phasing portrait (Fig. A.7 (B)), the *h* activation input is increasing toward the peak of the total regulatory input for *h*, which fits in the simple phasing rule. While for *h* auto-repression in circuit A1, the repression increases toward the peak of the total regulatory input for *h*, which does not fit in the simple phasing rule.

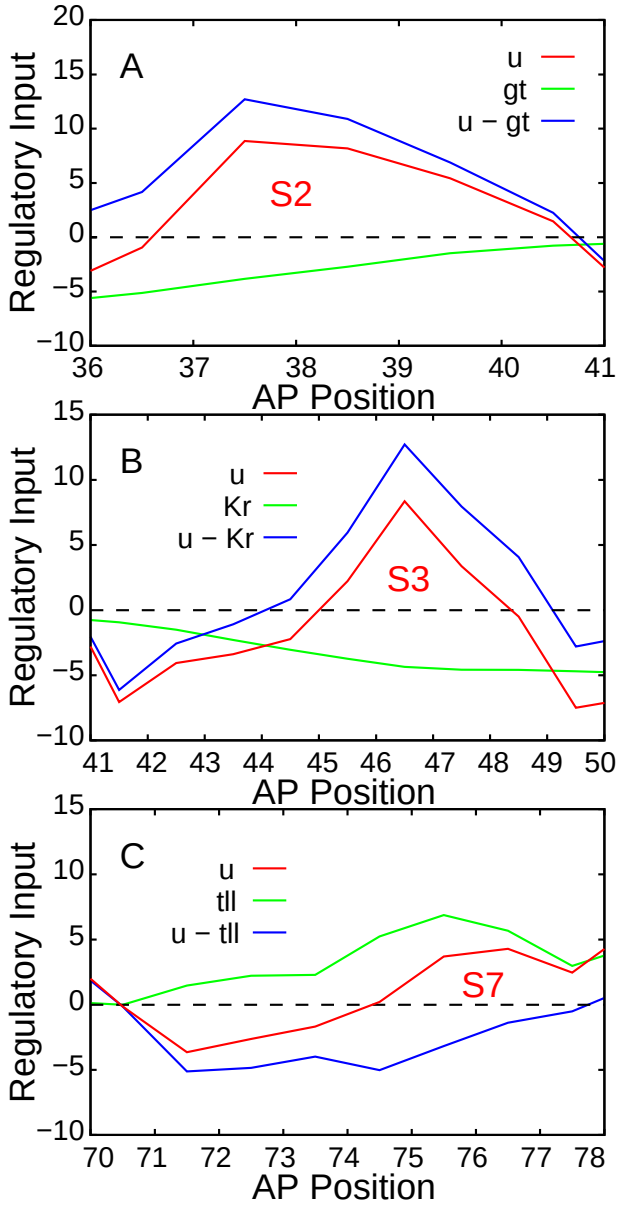

Figure A.8: *Kr*, *gt* and *tll* regulation on h. (**A**) *gt* repression on h stripe 2 anterior border at t7 in circuit B1. The total regulatory input for h stripe 2 (u^h from Eq. 3.1), *gt* regulatory input on h stripe 2, and the total regulatory input subtracts (without) *gt* input on h stripe 2 (key $u - gt$ denotes the value of $u^h - E^{h \leftarrow gt} v^{gt}(t)$). (**B**) *Kr* repression on h stripe 3 anterior border at t7 in circuit B1. (**C**) *tll* activation on h stripe 7 anterior border at t7 in circuit A1.

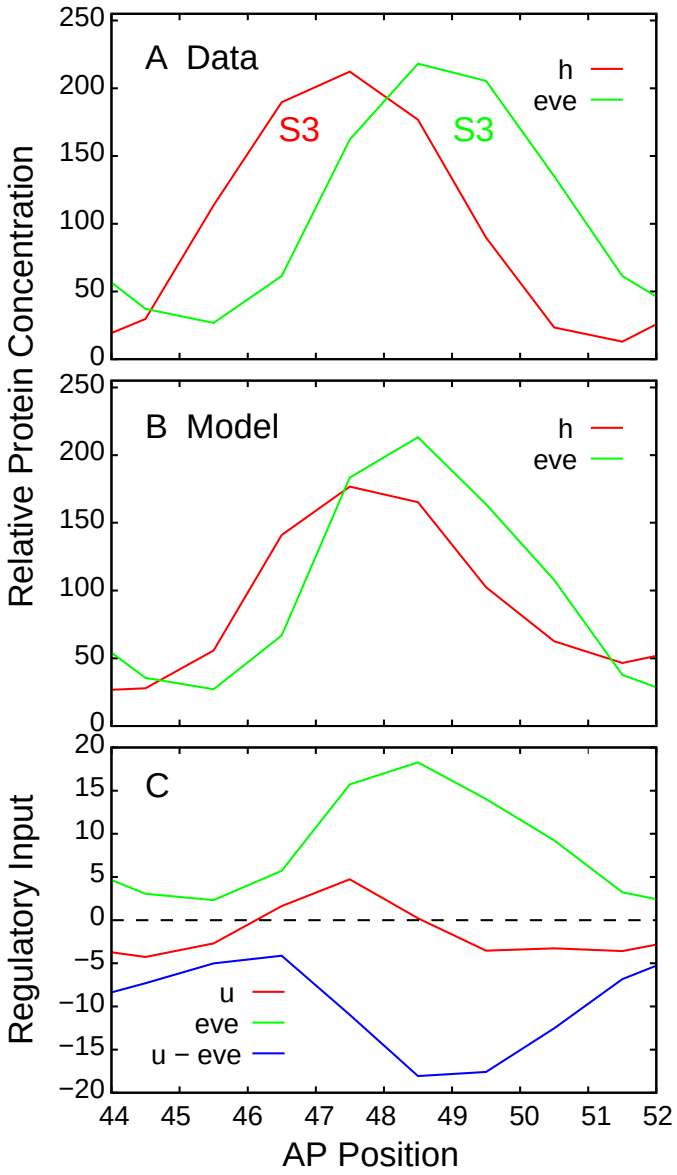

Figure A.9: *eve* regulation on h stripe 3 at t7 in circuit A1. (**A**) h stripe 3 and *eve* stripe 3 at t7 from data (Fig. 1.3), and in circuit A1 (**B**). (**C**) The total regulatory input for h stripe 3 (u^h from Eq. 3.1), *eve* regulatory input on h stripe 3, and the total regulatory input subtracts (without) *eve* input on h stripe 3 (key $u - eve$ denotes the value of $u^h - T^{h \leftarrow eve} v^{eve}$).

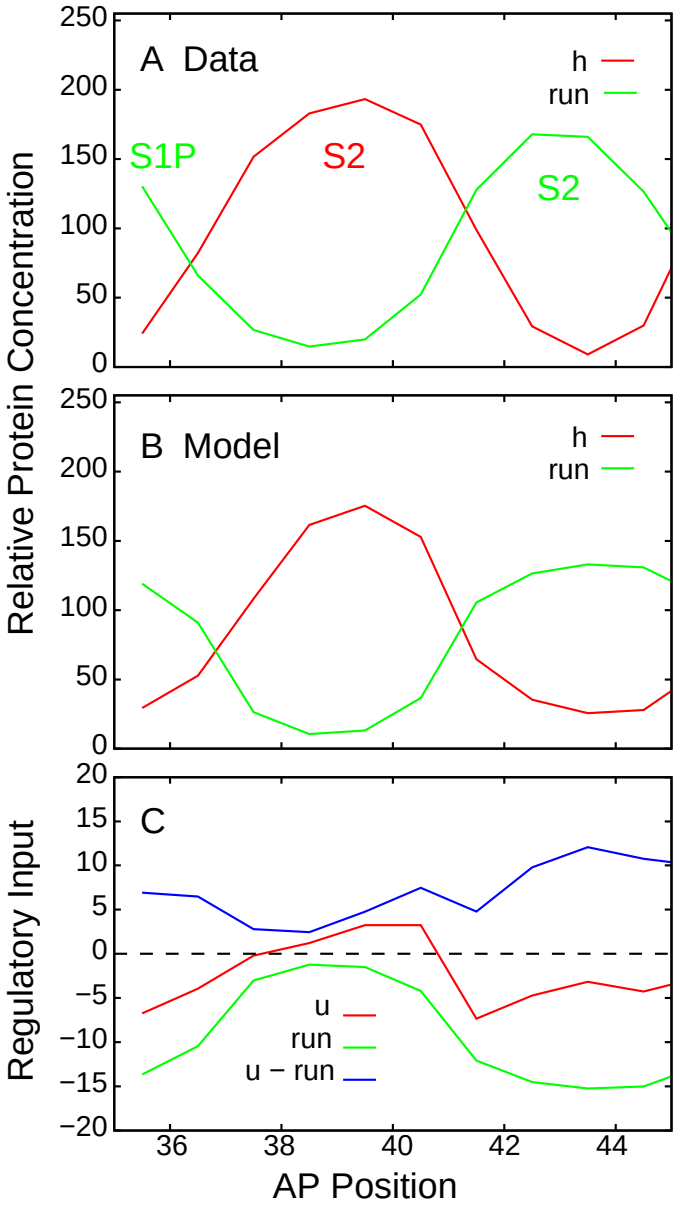

Figure A.10: *run* regulation on h stripe 2 at t7 in circuit A1. (**A**) h stripe 2, *run* stripe 1 posterior border and stripe 2 at t7 from data (Fig. 1.3), and in circuit A1 (**B**). (**C**) The total regulatory input for h stripe 2 (u^h from Eq. 3.1), *run* regulatory input on h stripe 2, and the total regulatory input subtracts (without) *run* input on h stripe 2 (key $u - run$ denotes the value of $u^h - T^{h \leftarrow run} v^{run}$).

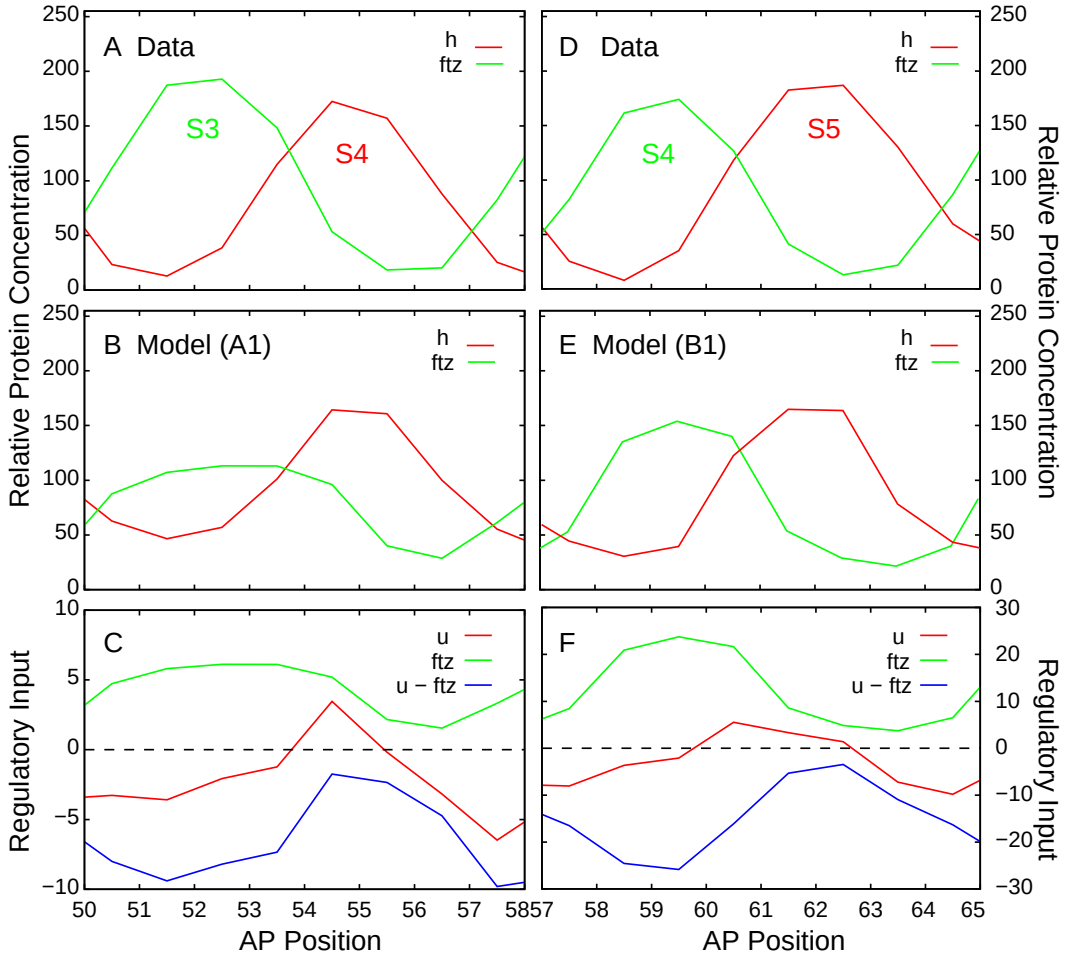

Figure A.11: *ftz* regulation on *h* stripe 4 and 5 at t7 in circuit A1 and B1. (**A**) *h* stripe 4 and *ftz* stripe 3 at t7 from data (Fig. 1.3), and in circuit A1 (**B**). (**D**) *h* stripe 5 and *ftz* stripe 4 at t7 from data, and in circuit B1 (**E**). (**C**, **F**) The total regulatory input for *h* stripe 4 and 5 (u^h from Eq. 3.1), *ftz* regulatory input on *h* stripe 4 and 5, and the total regulatory input subtracts (without) *ftz* input on *h* stripe 4 and 5 (key $u - ftz$ denotes the value of $u^h - T^{eve \leftarrow ftz} v^{ftz}$).

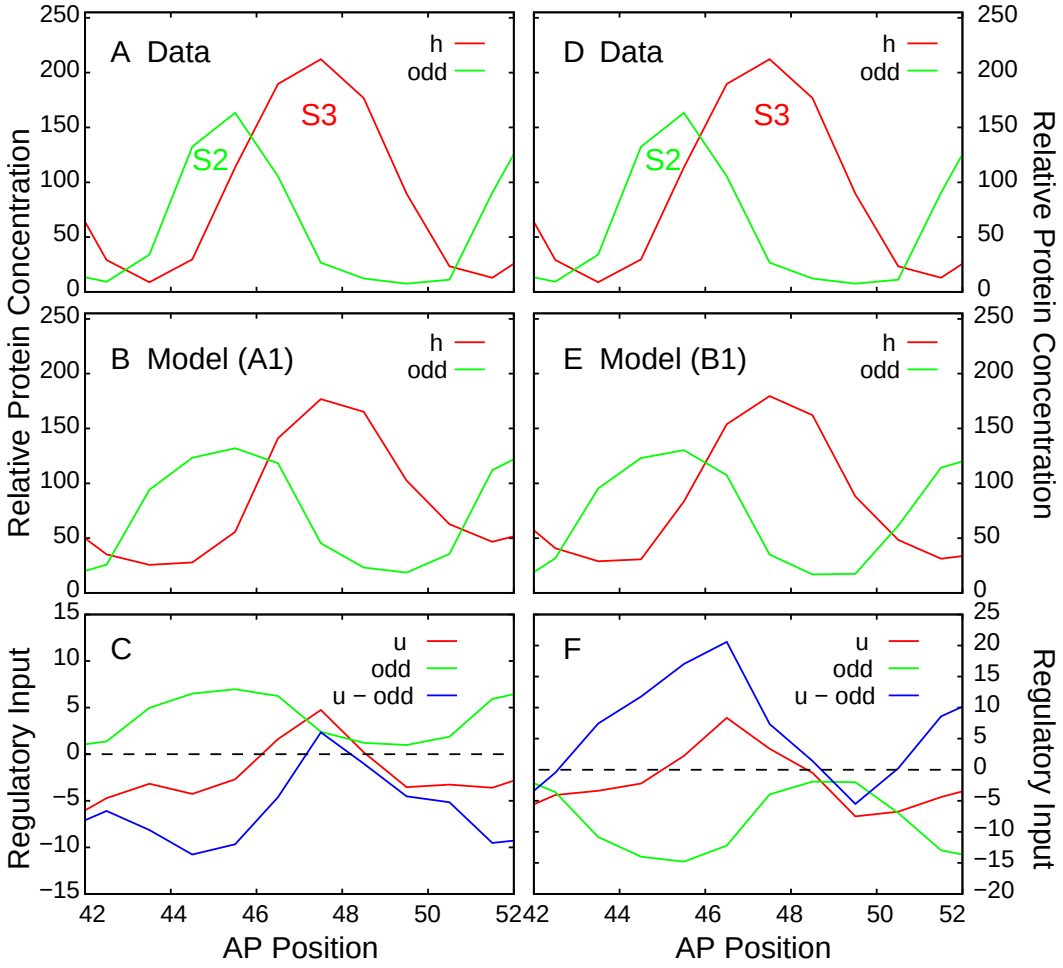

Figure A.12: *odd* regulation on h stripe 3 at t7 in circuit A1 and B1. (**A**, **D**) h stripe 3 and *odd* stripe 2 at t7 from data (Fig. 1.3), and in circuit A1 (**B**) and B1 (**E**). (**C**, **F**) The total regulatory input for h stripe 3 (u^h from Eq. 3.1), *odd* regulatory input on h stripe 3, and the total regulatory input subtracts (without) *odd* input on h stripe 3 (key $u - odd$ denotes the value of $u^h - T^{h \leftarrow odd} v^{odd}$).

A.5.3 *run* regulatory phasing analysis

According to Appendix Table A.5, for *Kr* activation on *run* stripe 2 posterior border, as shown in the phasing portrait (Fig. A.13 (D)), the activation input increases toward the limit of the posterior border of the total regulatory input for *run*. For *Kr* activation on stripe 4 anterior border (Fig. A.13 (B)), the activation input increases toward the limit of the anterior border of the total regulatory input for *run*. For *gt* activation on stripe 5 posterior border (Fig. A.13 (C)), the activation input increases toward the limit of the posterior border of the total regulatory input for *run*. Hence all of the above regulations do not fit in the simple phasing rule, and are considered as regulatory balancers. The other gap gene regulations on *run*, predicted in Fig.4.1, that fit in the simple phasing rule are shown in Fig. A.13 and A.14.

Repression between *h* and *run* has previously been proposed on the basis of their approximately reciprocal, complementary, domains of expression in the literature (Ingham and Gergen, 1988; Kania et al., 1990; Jiménez et al., 1996; Frasch and Levine, 1987; Carroll and Vavra, 1989) (see also Fig. A.10 (A, B)). Hence the repressor role of *h* fits in the simple phasing rule. According to Appendix Table A.6, the *h* repression input increases toward the limit of both borders of the total regulatory input for *run* (Fig. A.14 (B)), which sets both borders of *run* stripes.

According to Appendix Table A.6, for *eve* repression on *run*, as shown in the phasing portrait (Fig. A.15 (A, B)), *eve* is placed in an anteriorly overlapping position to *run*, hence the repressor role of *eve* does not fit in the simple phasing rule. The *eve* repression input is a plateau on the anterior border of the total regulatory input for *run*(Fig. A.15 (C)), and is increasing toward the peak of the total regulatory input on the posterior border of the total

regulatory input for *run*, except for *run* stripe 1 posterior border in circuit A2. The *eve* repression input hence does not help shift the *run* stripe forward anteriorly.

According to Appendix Table A.6, for *ftz* repression on *run*, as shown in the phasing portrait (Fig. A.16 (A, B, D, E)), *ftz* is placed in a posteriorly overlapping position to *run*, hence the repressor role of *ftz* fits in the simple phasing rule. The *ftz* repression input increases toward the limit of both borders of the total regulatory input for *run* (Fig. A.16 (C, F)), which helps set both borders for *run* stripes and shift the stripe forward anteriorly.

According to Appendix Table A.6, for the stripe specific *odd* repression on *run* stripe 6, as shown in the phasing portrait (Fig. A.17 (A, B, D, E)), *odd* is placed in a posteriorly overlapping position to *run* stripe 6, hence the repressor role of *odd* fits in the simple phasing rule. The *odd* repression input is more of a plateau and increases toward the limit of both borders of the total regulatory input for *run* (Fig. A.17 (C, F)), which helps set both borders and push the stripe forward anteriorly.

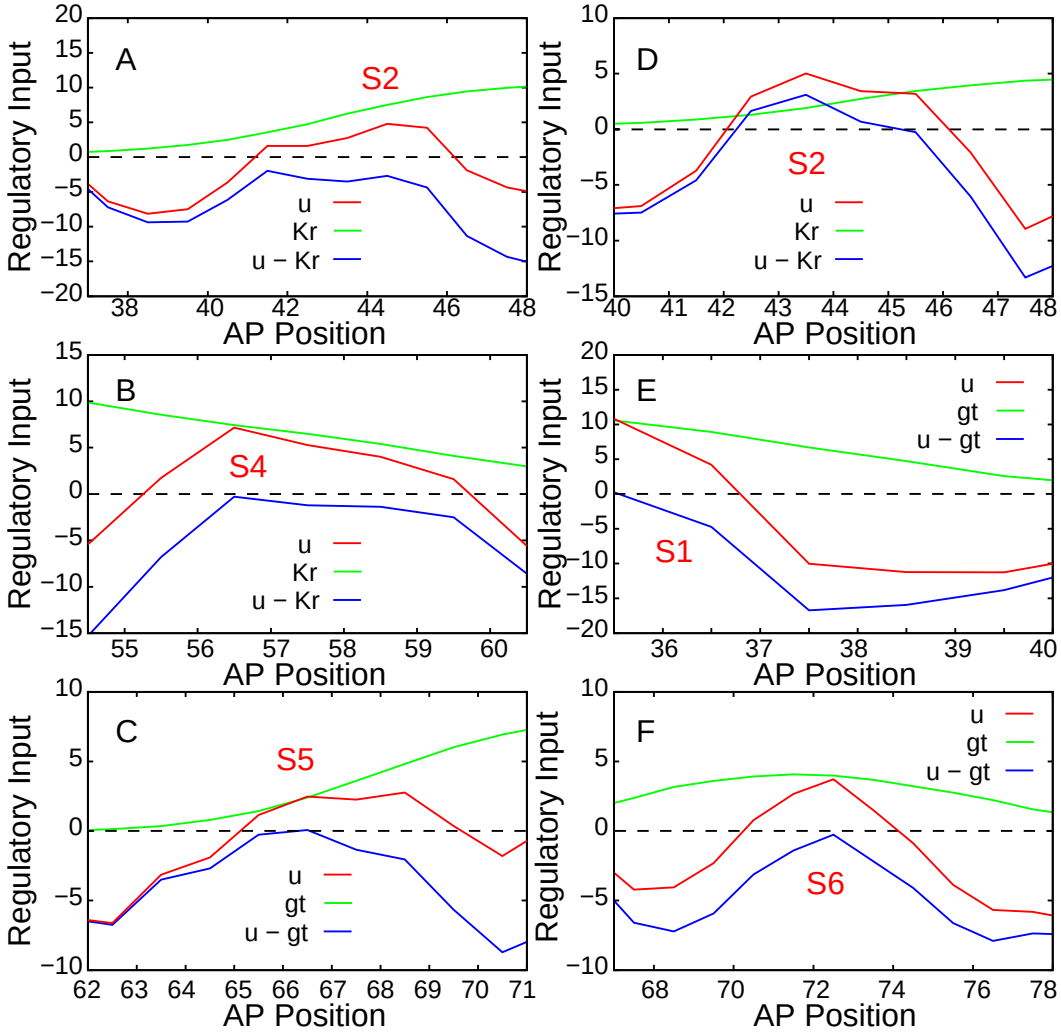

Figure A.13: *Kr* and *gt* regulation on *run*. (**A**) *Kr* activation on *run* stripe 2 anterior border at t4 in circuit A1. The total regulatory input for *run* stripe 2 (u^{run} from Eq. 3.1), *Kr* regulatory input on *run* stripe 2, and the total regulatory input subtracts (without) *Kr* input on *run* stripe 2 (key $u - Kr$ denotes the value of $u^{run} - E^{run \leftarrow Kr} v^{Kr}(t)$). (**B**) *Kr* activation on *run* stripe 4 at t7 in circuit A1. (**C**) *gt* activation on *run* stripe 5 posterior border at t4 in circuit B1. (**D**) *Kr* activation on *run* stripe 2 posterior border at t5 in circuit B1. (**E**) *gt* activation on *run* stripe 1 posterior border at t7 in circuit B1. (**F**) *gt* activation on *run* stripe 6 at t7 in circuit A2.

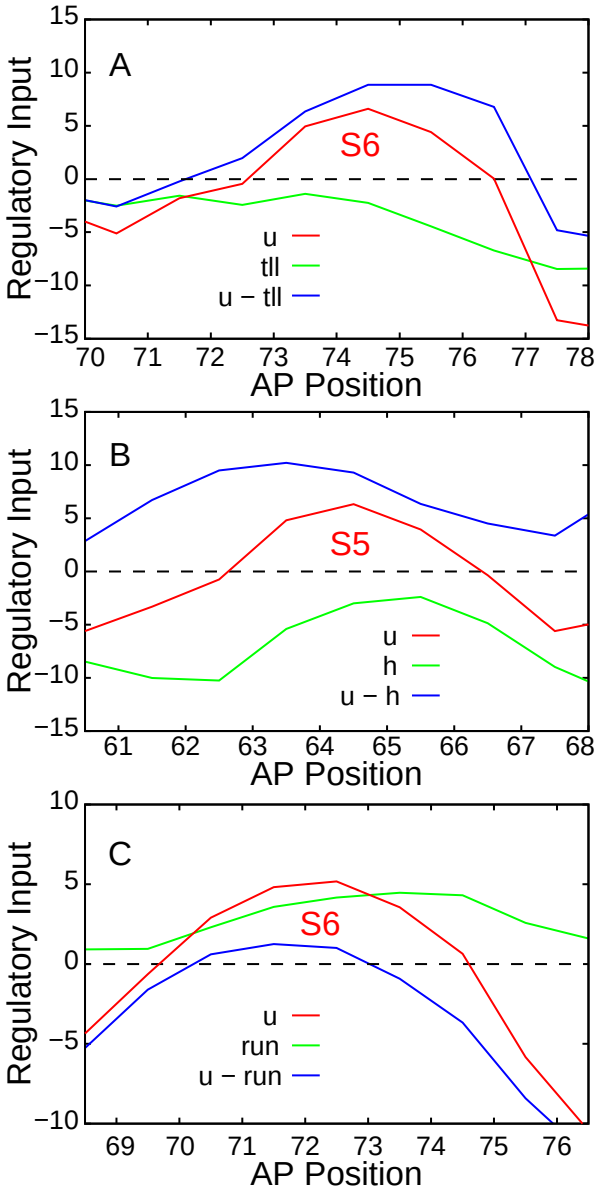

Figure A.14: *tll*, *h* and *run* regulation on *run*. (**A**) *tll* repression on *run* stripe 6 posterior border at t5 in circuit B1. The total regulatory input for *run* stripe 6 (u^{run} from Eq. 3.1), *tll* regulatory input on *run* stripe 6, and the total regulatory input subtracts (without) *tll* input on *run* stripe 6 (key $u - tll$ denotes the value of $u^{run} - E^{run \leftarrow tll} v^{tll}(t)$). (**B**) *h* repression on *run* stripe 5 at t7 in circuit A1. (**C**) *run* auto-activation on stripe 6 at t7 in circuit A1.

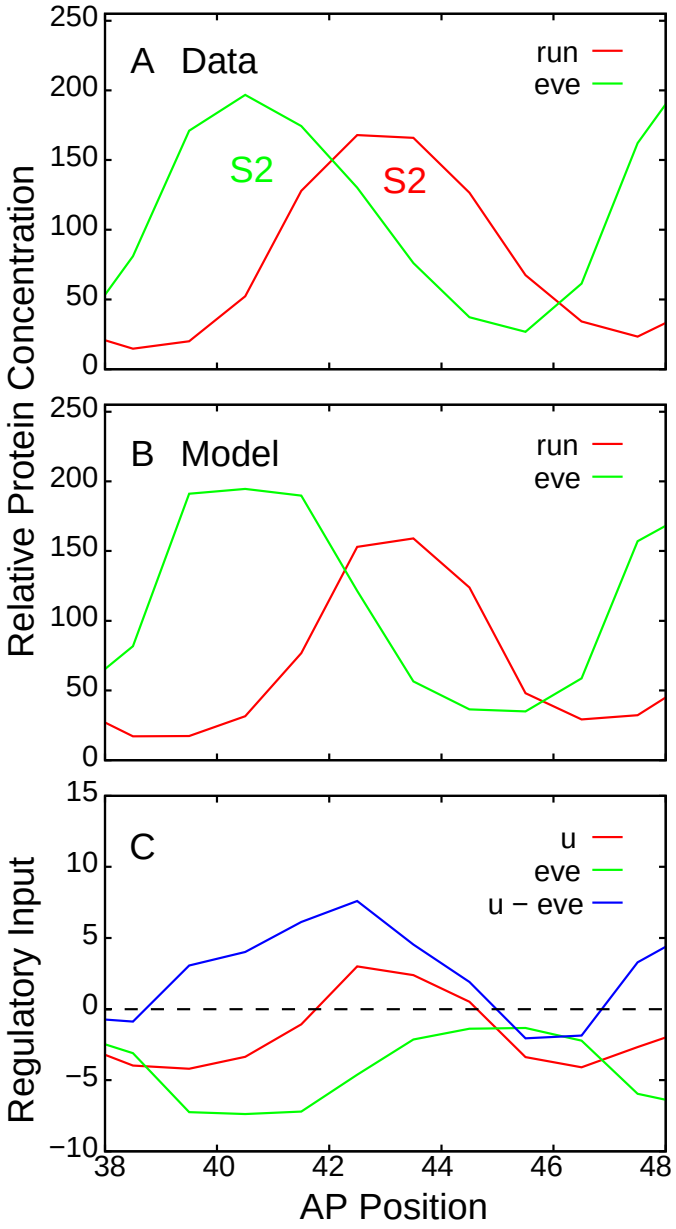

Figure A.15: *eve* regulation on *run* stripe 2 at t7 in circuit A2. (**A**) *eve* and *run* stripe 2 at t7 from data (Fig. 1.3), and in circuit A2 (**B**). (**C**) The total regulatory input for *run* stripe 2 (u^{run} from Eq. 3.1), *eve* regulatory input on *run* stripe 2, and the total regulatory input subtracts (without) *eve* input on *run* stripe 2 (key $u-eve$ denotes the value of $u^{run} - T^{run \leftarrow eve} v^{eve}$).

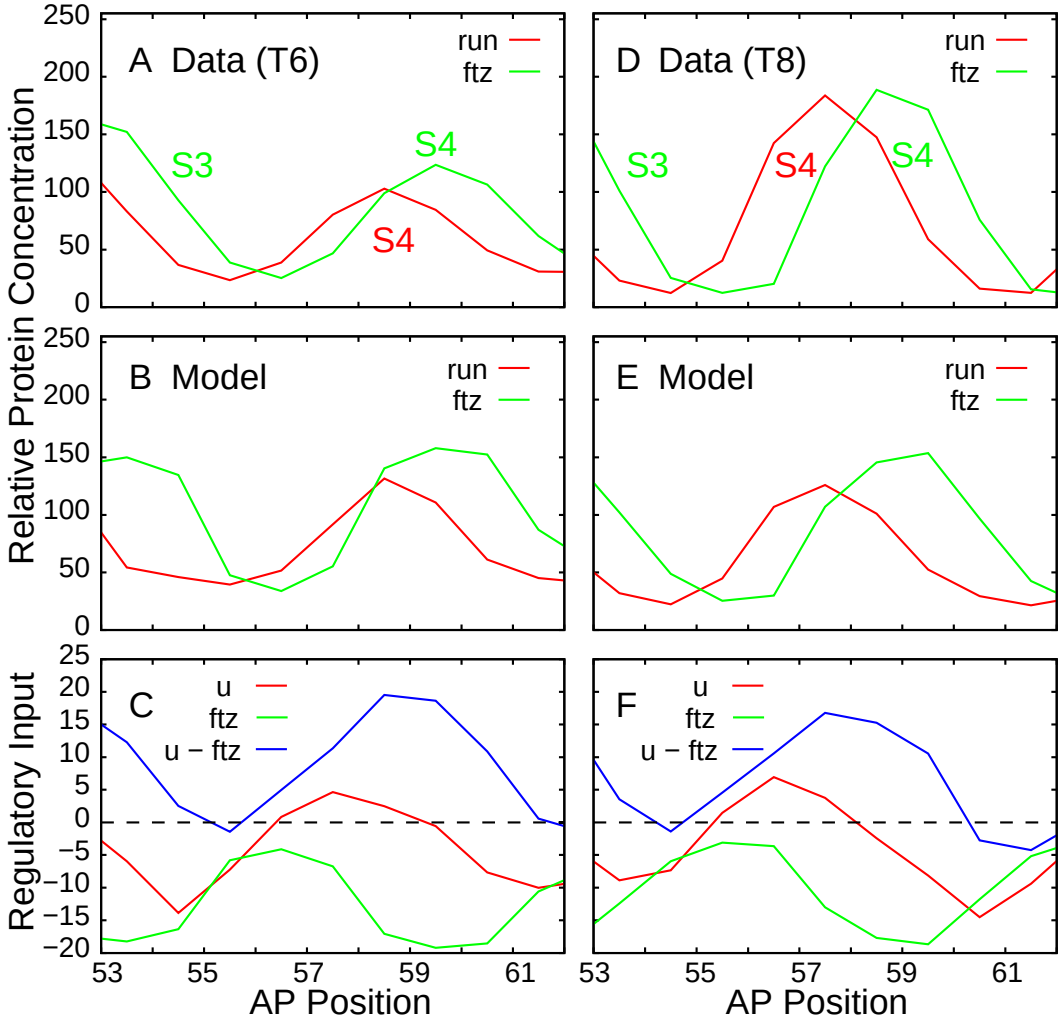

Figure A.16: *ftz* regulation on *run* stripe 4 at t6 and t8 in circuit B1. (**A**, **D**) *run* stripe 4 and *ftz* stripe 3 and 4 at t6 and t8 from data (Fig. 1.3), and in circuit B1 (**B**, **E**). (**C**, **F**) The total regulatory input for *run* stripe 4 (u^{run} from Eq. 3.1), *ftz* regulatory input on *run* stripe 4, and the total regulatory input subtracts (without) *ftz* input on *run* stripe 4 (key $u - ftz$ denotes the value of $u^{run} - T^{run \leftarrow ftz} v^{ftz}$).

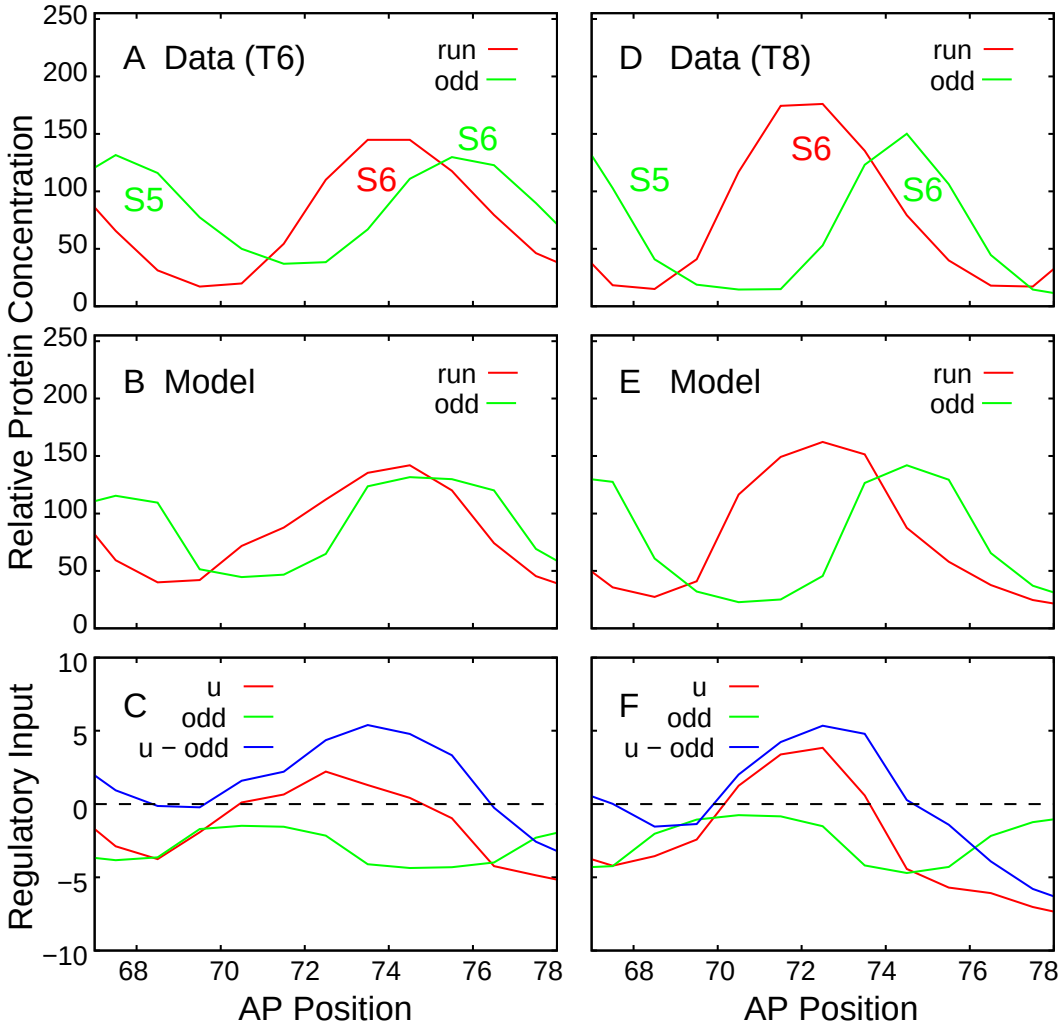

Figure A.17: *odd* regulation on *run* stripe 6 at t6 and t8 in circuit A2. (**A**, **D**) *run* stripe 6 and *odd* stripe 5 and 6 at t6 and t8 from data (Fig. 1.3), and in circuit A2 (**B**, **E**). (**C**, **F**) The total regulatory input for *run* stripe 6 (u^{run} from Eq. 3.1), *odd* regulatory input on *run* stripe 6, and the total regulatory input subtracts (without) *odd* input on *run* stripe 6 (key $u - odd$ denotes the value of $u^{run} - T^{run \leftarrow odd} v^{odd}$).

A.5.4 *ftz* regulatory phasing analysis

According to Appendix Table A.7, for *Kr* activation on stripe 4 anterior border, as shown in the phasing portrait (Fig. A.18 (A)), the activation input increases toward the limit of the anterior border of the total regulatory input for *ftz* stripe 4. For *gt* activation on stripe 5 posterior border (Fig. A.18 (C)), the activation input increases toward the limit of the posterior border of the total regulatory input for stripe 5. Hence the above regulations do not fit in the simple phasing rule, and are considered as regulatory balancers. The other gap gene regulations on *ftz*, predicted in Fig.4.1, that fit in the simple phasing rule are shown in Fig. A.18.

According to Appendix Table A.8, for stripe specific *h* activation on *ftz* stripe 3 posterior border (Fig. 4.5), as shown in the phasing portrait (Fig. A.19 (A, B)), *h* is placed in a complimentary and more posteriorly overlapping position to *ftz*, with high residual expression remaining between the two borders, hence the activator role of *h* does not fit in the simple phasing rule. The *h* activation input is increasing toward the limit of the posterior border of the total regulatory input for *ftz* (Fig. A.19 (C)), which serves as a regulatory balancer for refinement of *ftz* and does not shift the *ftz* stripe forward anteriorly.

According to Appendix Table A.8, for *odd* regulation on *ftz*, as shown in the phasing portrait (Fig. A.20 (A, D, G)), *odd* is placed in a posteriorly overlapping position to *ftz* in data, however in the 3 major circuits *odd* is almost overlapping with *ftz* (Fig. A.20 (B, E, H)), which is an artifact and can result in false critical auto-activation from *odd*, for example in circuit A2 (Fig. A.20 (F)). The artifact auto-regulatory effect from *odd* in circuit A1 and B1 is limited (Fig. A.20 (I, C)). According to data, the repressor role of *odd* would actually, authentically, fit in the simple phasing rule.

According to Appendix Table A.8, for *eve* repression on *ftz*, *eve* is placed in a more complimentary position to *ftz* (see also Fig. A.5 (A, B)), with residual expression remaining between the two borders, hence the repressor role of *eve* fits in the simple phasing rule. The *eve* repression input increases toward the limit of the two borders of the total regulatory input for *ftz* (Fig. A.21 (A)), which helps set both borders.

According to Appendix Table A.8, for *run* activation on *ftz*, *run* is placed in an anteriorly overlapping position to *ftz* (see also Fig. A.16 (A, B, D, E)), hence the activator role of *run* fits in the simple phasing rule. The *run* activation input increases toward the peak of the total regulatory input for *ftz* in a more anterior position (Fig. A.21 (B)), which helps shape the stripe and also shift the stripe forward anteriorly.

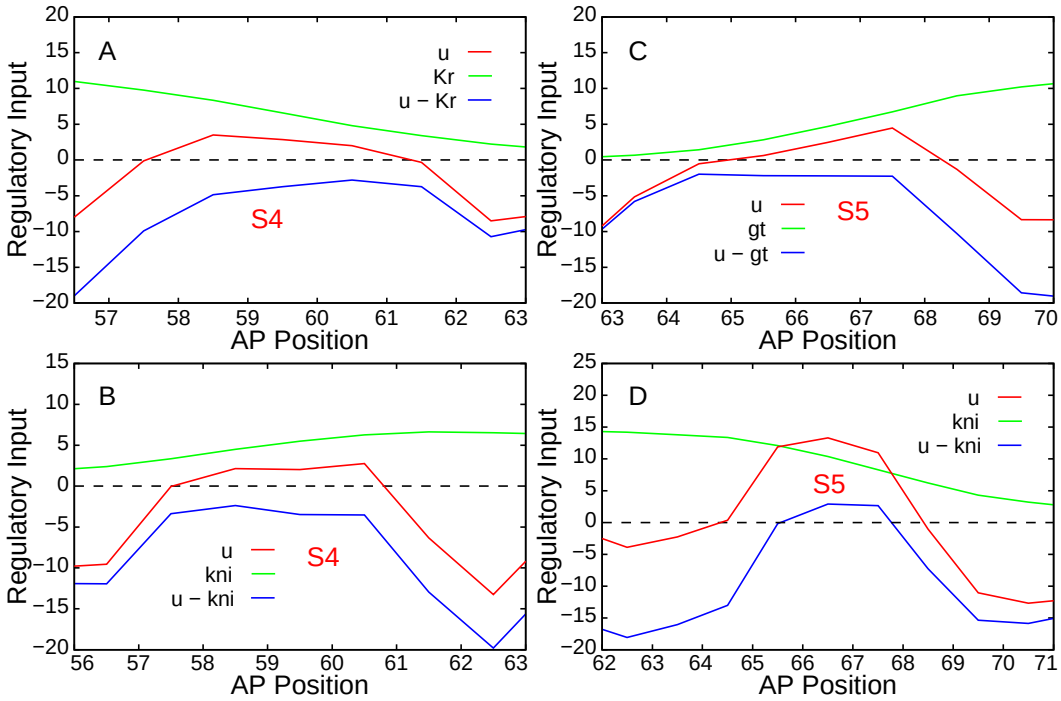

Figure A.18: *Kr*, *gt* and *kni* regulation on *ftz*. (**A**) *Kr* activation on *ftz* stripe 4 anterior border at t6 in circuit A1. The total regulatory input for *ftz* stripe 4 (u^{ftz} from Eq. 3.1), *Kr* regulatory input on *ftz* stripe 4, and the total regulatory input subtracts (without) *Kr* input on *ftz* stripe 4 (key $u - Kr$ denotes the value of $u^{ftz} - E^{ftz \leftarrow Kr} v^{Kr}(t)$). (**B**) *Kni* activation on *ftz* stripe 4 at t7 in circuit A1. (**C**) *gt* activation on *ftz* stripe 5 at t7 in circuit A1. (**D**) *kni* activation on *ftz* stripe 5 posterior border at t7 in circuit A2.

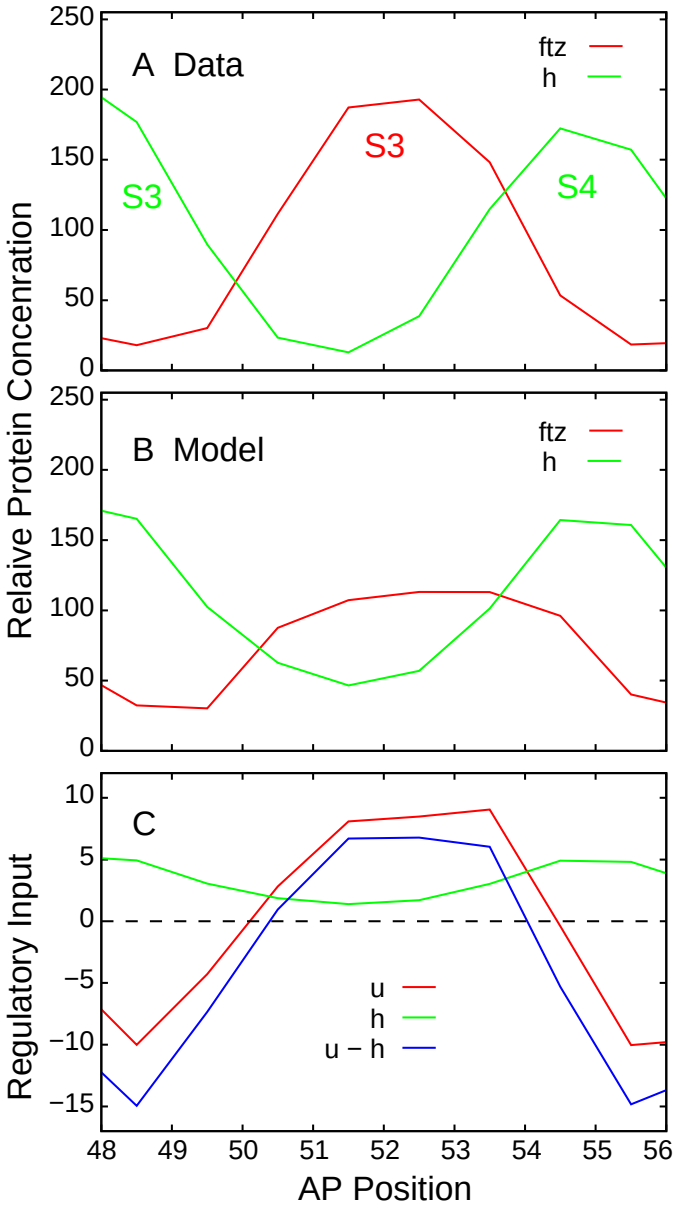

Figure A.19: h regulation on *ftz* stripe 3 at t7 in circuit A1. (**A**) *ftz* stripe 3 and h stripe 3 and 4 at t7 from data (Fig. 1.3), and in circuit A1 (**B**). (**C**) The total regulatory input for *ftz* stripe 3 (u^{ftz} from Eq. 3.1), h regulatory input on *ftz* stripe 3, and the total regulatory input subtracts (without) h input on *ftz* stripe 3 (key $u - h$ denotes the value of $u^{ftz} - T^{ftz \leftarrow h} v^h$).

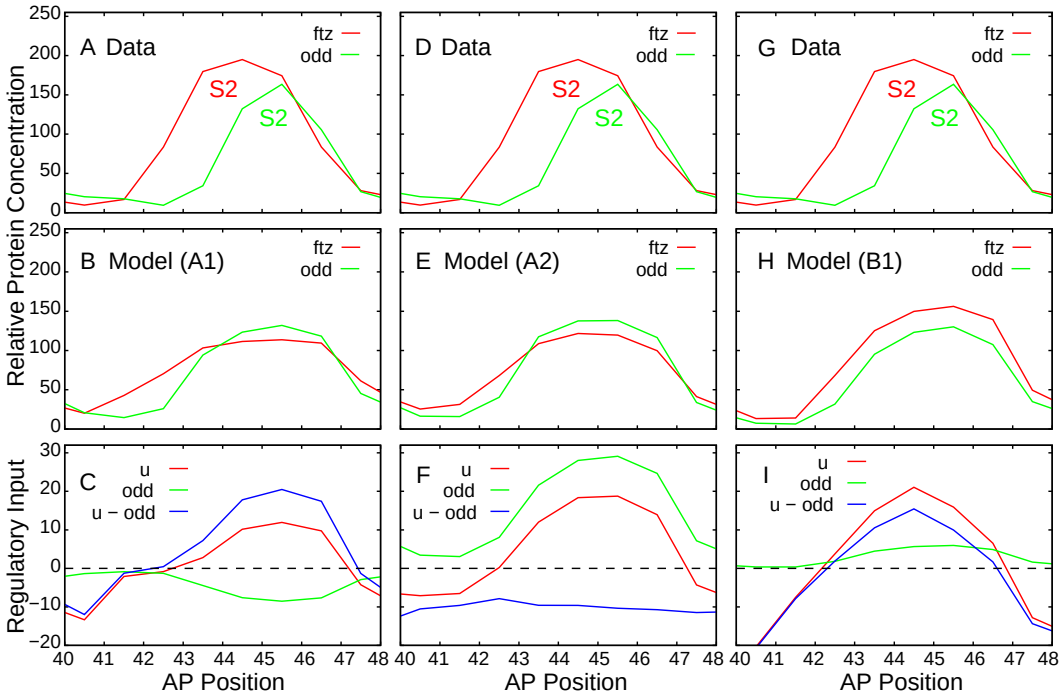

Figure A.20: *odd* regulation on *ftz* stripe 2 at t7 in circuit A1, A2 and B1. (**A**, **D**, **G**) *ftz* stripe 2 and *odd* stripe 2 at t7 from data (Fig. 1.3), and in circuit A1, A2 and B1 (**B**, **E**, **H**). (**C**, **F**, **I**) The total regulatory input for *ftz* stripe 2 (u^{ftz} from Eq. 3.1), *odd* regulatory input on *ftz* stripe 2, and the total regulatory input subtracts (without) *odd* input on *ftz* stripe 2 (key $u - odd$ denotes the value of $u^{ftz} - T^{ftz \leftarrow odd} v^{odd}$).

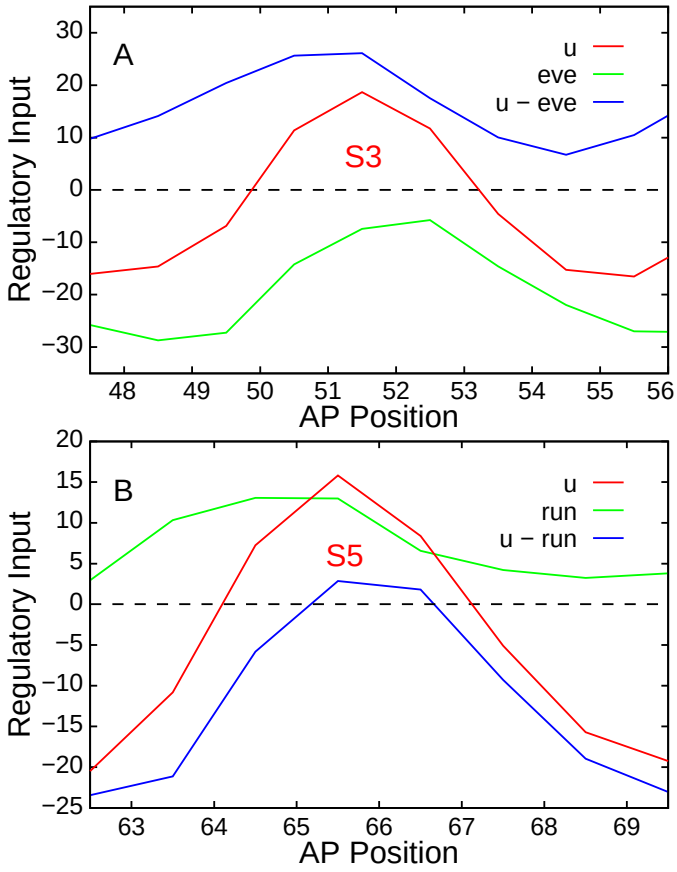

Figure A.21: *eve* and *run* regulation on *ftz*. (**A**) *eve* repression on *ftz* stripe 3 at t8 in circuit B1. The total regulatory input for *eve* stripe 3 (u^{ftz} from Eq. 3.1), *eve* regulatory input on *ftz* stripe 3, and the total regulatory input subtracts (without) *eve* input on *ftz* stripe 3 (key $u - gt$ denotes the value of $u^{ftz} - E^{ftz \leftarrow gt} v^{gt}(t)$). (**B**) *run* activation on *ftz* stripe 5 at t8 in circuit B1.

A.5.5 *odd* regulatory phasing analysis

According to Appendix Table A.9, for *Kr* activation on the stripe 4 anterior border, as shown in the phasing portrait (Fig. A.23 (C)), the activation input increases toward the limit of the anterior border of the total regulatory input for *odd*. For *gt* activation on the stripe 5 posterior border (Fig. A.22 (B)), the activation input increases toward the limit of the posterior border of the total regulatory input for *odd*. Hence the above regulations do not fit in the simple phasing rule, and are considered as regulatory balancers. The other gap gene regulations on *odd*, predicted in Fig.4.1, that fit in the simple phasing rule are shown in Fig. A.22 and A.23.

According to Appendix Table A.10, for *h* repression on *odd*, as shown in the phasing portrait (Fig. A.24 (A, B)), *h* is placed in a posteriorly overlapping position to *odd*, hence the repressor role of *h* fits in the simple phasing rule. The *odd* repression input increases toward the limit of both borders of the total regulatory input for *odd* (Fig. A.24 (C)), which helps set both borders for *odd* stripes and shift the stripe forward anteriorly.

According to Appendix Table A.10, for *run* activation on *odd*, as shown in the phasing portrait (Fig. A.25 (A, B)), *run* is placed in an anteriorly overlapping position to *odd*, hence the activator role of *run* fits in the simple phasing rule. The *run* activation input increases toward the peak of the total regulatory input for *odd* in a more anterior position (Fig. A.25 (C)), which helps shape both borders and shift the stripe forward anteriorly.

According to Appendix Table A.10, for *eve* repression on *odd*, *eve* is placed in a complimentary position to *odd* (see also Fig. A.4 (A, B)), with residual expression remaining between the two borders, hence the repressor role of *eve* fits in the simple phasing rule. The *eve* repression input increases toward the

limit of both borders of the total regulatory input for *odd* (Fig. A.26 (A)), which helps set both borders.

According to Appendix Table A.10, for *ftz* activation on *odd*, *ftz* is placed in an anteriorly overlapping position to *odd* in data (see also Fig. A.20 (A, D, G)), however in the major circuits *odd* and *ftz* are almost overlapping (Fig. A.20 (B, E, H)). In either position the main activator role of *ftz* on *odd* fits in the simple phasing rule. The *ftz* activation input increases toward the peak of the total regulatory input for *odd* (Fig. A.26 (B)), which helps elevate the *odd* stripes.

According to Appendix Table A.10, for *odd* auto-activation (Fig. A.26 (C)), the *odd* activation input increases toward the peak of the total regulatory input for *odd*, which fits in the simple phasing rule and helps elevate the *odd* stripes.

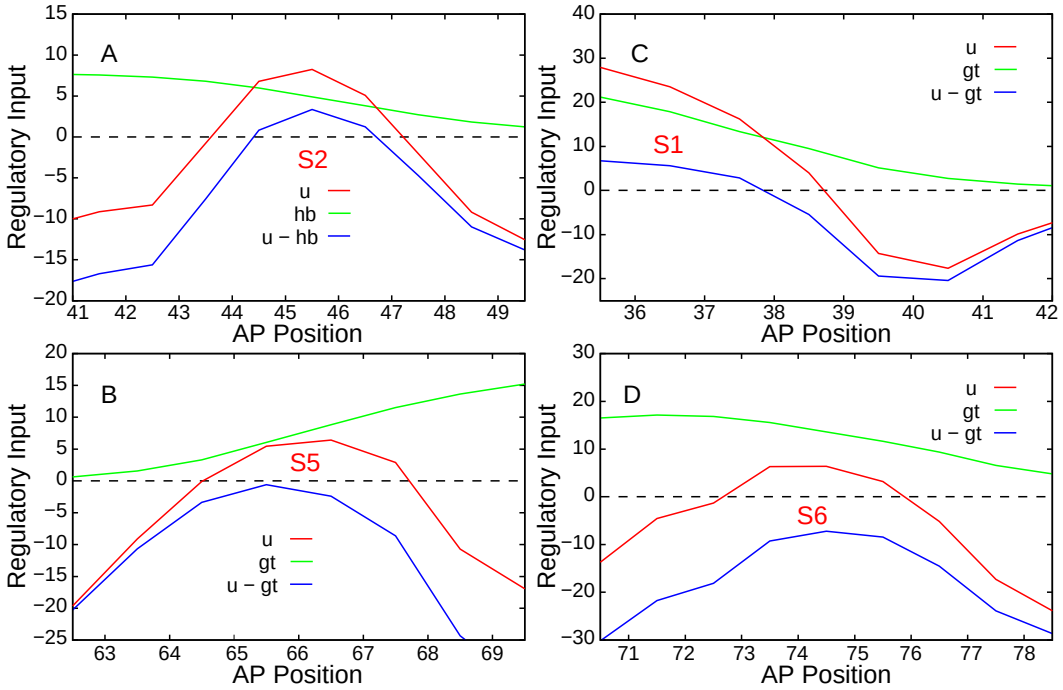

Figure A.22: *hb* and *gt* regulation on *odd*. (**A**) *hb* activation on *odd* stripe 2 posterior border at t5 in circuit A1. The total regulatory input for *odd* stripe 2 (u^{odd} from Eq. 3.1), *hb* regulatory input on *odd* stripe 2, and the total regulatory input subtracts (without) *hb* input on *odd* stripe 2 (key $u - hb$ denotes the value of $u^{odd} - E^{odd \leftarrow hb} v^{hb}(t)$). (**B**) *gt* activation on *odd* stripe 5 at t8 in circuit A1. (**C**) *gt* activation on *odd* stripe 1 posterior border at t7 in circuit A1. (**D**) *gt* activation on *odd* stripe 6 posterior border at t7 in circuit A1.

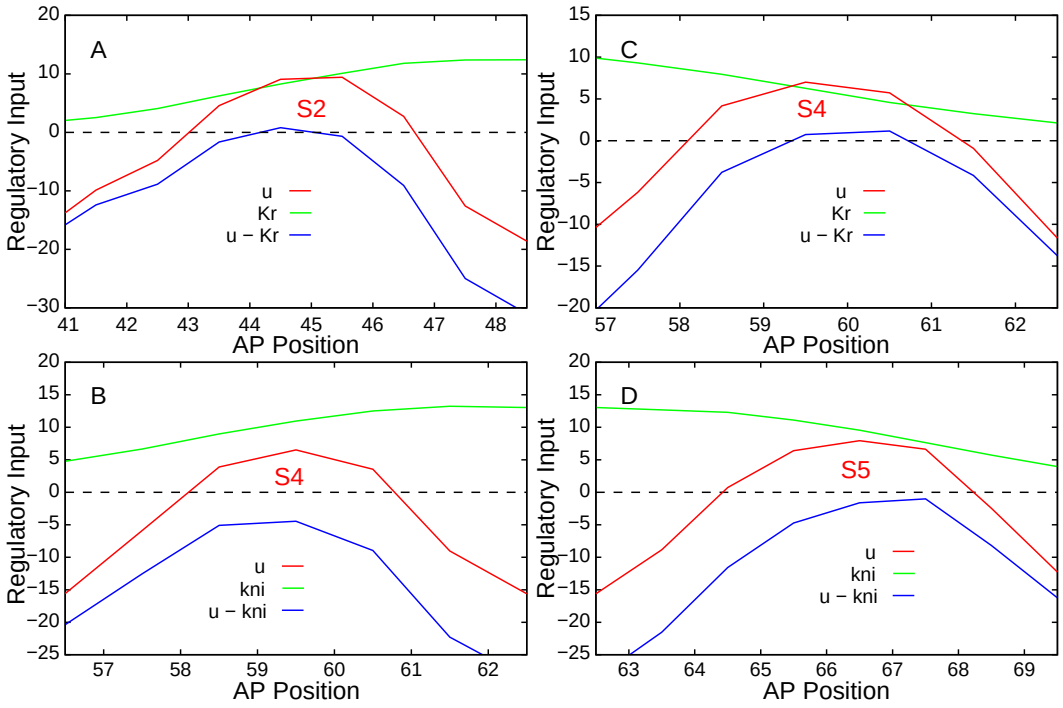

Figure A.23: *Kr* and *kni* regulation on *odd*. (**A**) *Kr* activation on *odd* stripe 2 anterior border at t7 in circuit A1. The total regulatory input for *odd* stripe 2 (u^{odd} from Eq. 3.1), *Kr* regulatory input on *odd* stripe 2, and the total regulatory input subtracts (without) *Kr* input on *odd* stripe 2 (key $u - Kr$ denotes the value of $u^{odd} - E^{odd \leftarrow Kr} v^{Kr}(t)$). (**B**) *kni* activation on *odd* stripe 4 anterior border at t7 in circuit A1. (**C**) *Kr* activation on *odd* stripe 4 at t6 in circuit A1. (**D**) *kni* activation on *odd* stripe 5 posterior border at t7 in circuit A1.

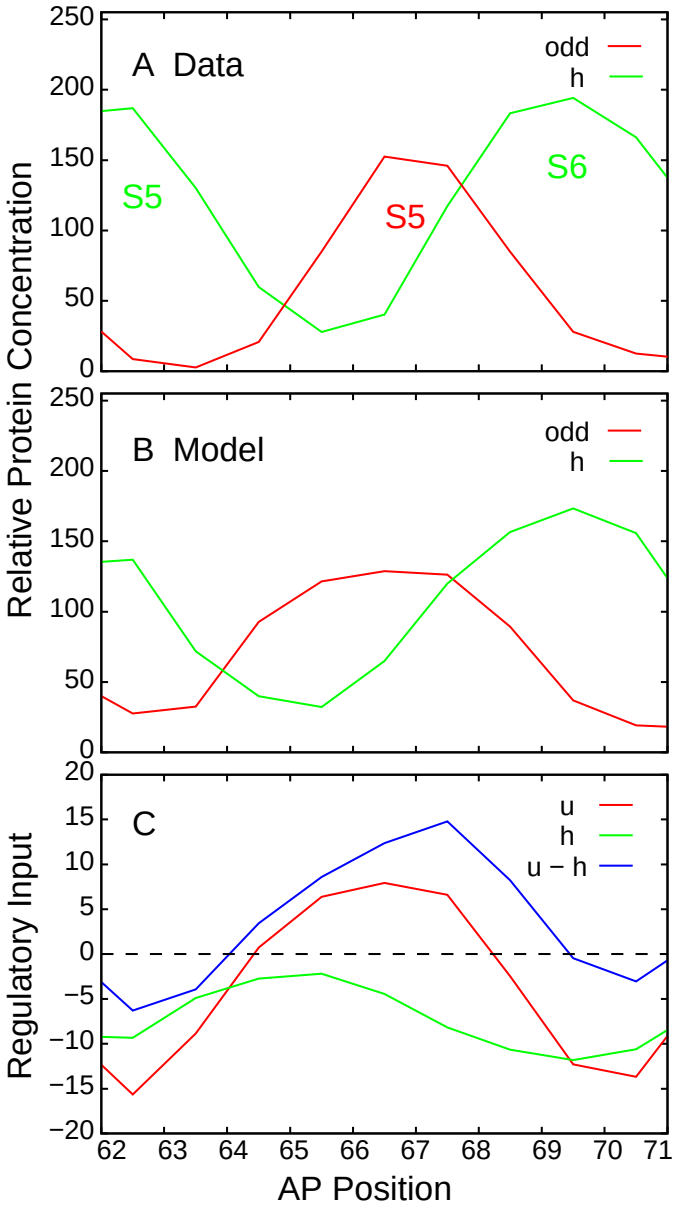

Figure A.24: h regulation on *odd* stripe 5 at t7 in circuit A1. (**A**) *odd* stripe 5, h stripe 5 and 6 at t7 from data (Fig. 1.3), and in circuit A1 (**B**). (**C**) The total regulatory input for *odd* stripe 5 (u^{odd} from Eq. 3.1), h regulatory input on *odd* stripe 5, and the total regulatory input subtracts (without) h input on *odd* stripe 5 (key $u - h$ denotes the value of $u^{odd} - T^{odd \leftarrow h} v^h$).

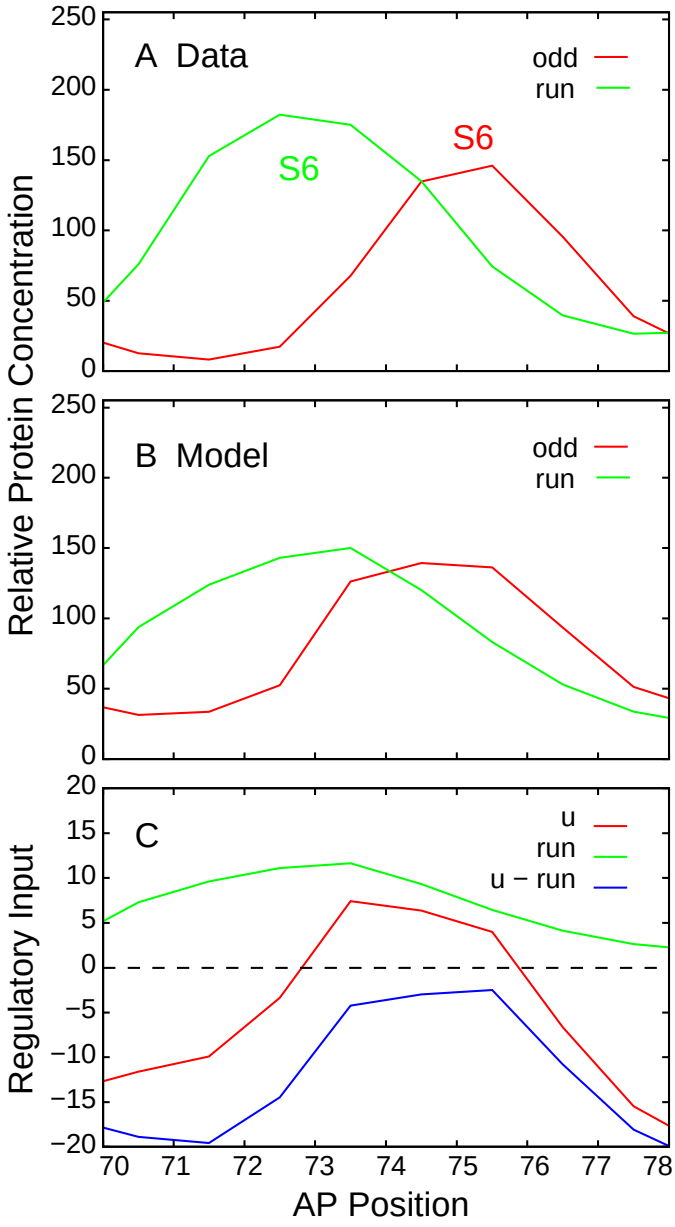

Figure A.25: *run* regulation on *odd* stripe 6 at t7 in circuit A2. (**A**) *odd* and *run* stripe 6 at t7 from data (Fig. 1.3), and in circuit A2 (**B**). (**C**) The total regulatory input for *odd* stripe 6 (u^{odd} from Eq. 3.1), *run* regulatory input on *odd* stripe 6, and the total regulatory input subtracts (without) *run* input on *odd* stripe 6 (key $u - run$ denotes the value of $u^{odd} - T^{odd \leftarrow run} v^{run}$).

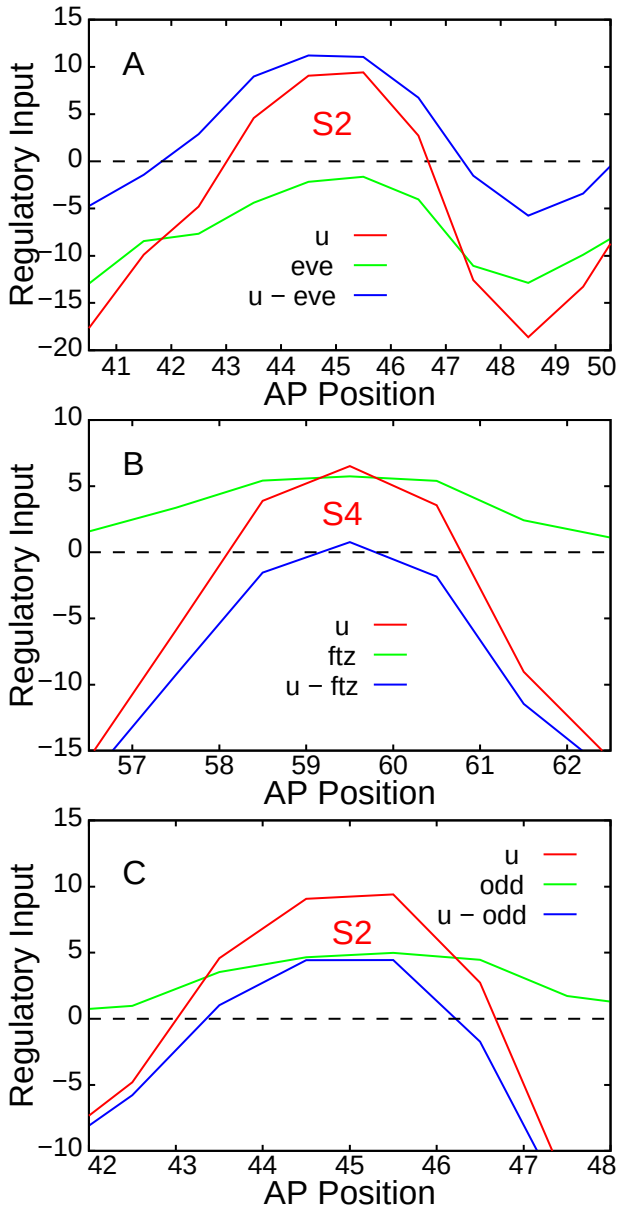

Figure A.26: *eve*, *ftz* and *odd* regulation on *odd*. (**A**) *eve* repression on *odd* stripe 2 at t7 in circuit A1. The total regulatory input for *odd* stripe 2 (u^{odd} from Eq. 3.1), *eve* regulatory input on *odd* stripe 2, and the total regulatory input subtracts (without) *eve* input on *odd* stripe 2 (key $u - eve$ denotes the value of $u^{odd} - T^{odd \leftarrow eve} v^{eve}$). (**B**) *ftz* activation on *odd* stripe 4 at t7 in circuit A1. (**C**) *odd* auto-activation on stripe 2 at t7 in circuit A1.

Appendix B

Pair-Rule Gene Regulation

B.1 *even-skipped* regulation

In the literature, *eve* regulation by gap genes were best understood from the *eve* stripe 2 enhancer (Small et al., 1991) and stripe 3 enhancer study (Small et al., 1996). Experimental implementations include DNA binding assays (Stanojevic et al., 1989), transient cotransfection assays (Small et al., 1991), P-transformation experiments (Stanojevic et al., 1991; Small et al., 1992, 1993; Arnosti et al., 1996), promoter fusion studies and genetic analyses (Frasch and Levine, 1987; Goto et al., 1989; Small et al., 1993).

In the early literature of Frasch and Levine (1987); Carroll and Vavra (1989), using the strongest available mutant alleles for all the pair-rule genes found only mild perturbation to the establishment of the wild-type *eve* expression pattern during cleavage cycle 14 development. Only relatively mild alterations in the spacing and intensity of expression are detected in cellular blastoderm stage embryos. A general proposition were made that the expression of the primary pair-rule gene *eve* is modulated only by the primary

pair-rule genes *h* and *run*, yet remains unaffected by the remaining, secondary and tertiary, pair-rule genes.

B.1.1 *eve* regulation by gap and maternal genes

bcd In the literature (Table A.17), findings from the *eve* stripe 2 and stripe 3 enhancer study suggest that *bcd* may activate *eve* stripe 2 and repress the *eve* stripe 3 anterior border. In *bcd* mutant embryos, anterior expansion and shift of the stripe 3 pattern were observed (Small et al., 1996), also the stripe 7 staining seems reduced. Although the anterior expansion is usually attributed to release of *hb* repression.

In the major circuits (Table A.1), *bcd* only has biased, plateau, input on the anterior-embryo *eve* stripes, hence is not essential, slope determining, for *eve* border formation in the dynamical model. The biological relevance of the *bcd* input is therefore indeterminable from the model. In the parameter consensus table (Table A.13), both classes of circuits are biased toward repression on *eve*.

cad No literature were found for *cad* regulation on *eve*.

In the major circuits (Table A.1), *cad* has small biased, near plateau, input on the posterior-embryo *eve* stripes, hence is also not essential, slope determining, for *eve* border formation in the dynamical model. The biological relevance of the *cad* input is therefore also indeterminable from the model. In the parameter consensus table (Table A.13), both classes of circuits are biased toward repression on *eve*.

hb *hb* was found to activate *eve* stripe 2 (Table A.17) from the *eve* stripe 2 enhancer study (Small et al., 1991). It was also suggested recently as a

repressor on *eve* stripe 3 anterior border from the *eve* stripe 3 enhancer study (Small et al., 1996). Mutations in *hb* were found to expand the initial limits of the stripe 3 pattern (Small et al., 1996). Further observations include the study of Goto et al. (1989), with a *lac*Z stripe 2, 3, 7 construct, which indicated that in *hb* mutants, stripes 2 and 3 are fused and stripe 7 is reduced.

In the major circuits (Table A.1), only circuit A2 has *hb* as a critical repressor on the stripe 3 anterior border, which supports recent literature finding. However *hb* is not essential on the remaining borders and in the other circuits. The biased plateau input on the *eve* stripe 2 can not be determined whether it is biologically relevant in the dynamical model. In the parameter consensus table (Table A.13), both classes of circuits have consensus toward repression on *eve*. Hence I conclude *hb* is more likely a repressor on the stripe 3 anterior border with priority level black as the first level regulation in the ensemble regulatory map (Fig. 4.1).

Kr *Kr* was found to repress *eve* stripe 2 posterior border (Table A.17) from the *eve* stripe 2 enhancer study (Small et al., 1991). In *Kr*– embryos, *eve* stripes 2 and 3 are fused, replaced by a composite band of expression (Goto et al., 1989). Further observations in homozygous mutant embryos (Warrior and Levine, 1990) found the stripes 2 and 3 were completely fused as were the stripes 4 and 6, while stripe 5 was reduced or absent, the stripes 1 and 7 were normal.

In 2 of the major circuits A1 and A2 (Table A.1), *Kr* is a critical repressor of the *eve* stripe 2 posterior border, which supports the literature. In circuit A1, *Kr* is also a critical repressor of the stripe 4 posterior border and the stripe 5 anterior border. In circuit A2, *Kr* is also an essential repressor of

the stripe 3 anterior border. In circuit B1, however, *Kr* is not required. I believe the class B circuits are more representative of the late maintenance and refinement phase, and *Kr* is more required in the early phase of the *eve* stripe formation. The early phase is better captured by the class A circuits, with more gap gene regulations involved. In the parameter consensus table (Table A.13), class A circuits have stronger consensus toward repression on *eve*, while class B circuits are more neutral toward *Kr* regulation on *eve*. Only the second priority set in the class B circuits have stronger consensus toward repression.

Given the above comparison I conclude *Kr* repressing the posterior border of the *eve* stripe 2 in black as the first level regulation, *Kr* repression on the *eve* stripe 3 and 5 anterior border, and the stripe 4 posterior border in blue as the second level regulation in the ensemble regulatory map (Fig. 4.1).

gt *gt* was found to repress *eve* stripe 2 anterior border (Table A.17) from the *eve* stripe 2 enhancer study (Small et al., 1991). Mutations in *gt* causes severe anterior expansion of the stripe 2 pattern, but have no effect on the stripe 3 expression (Small et al., 1996). Further observations in Goto et al. (1989), early *eve* stripe 2 is abnormally broad. And from Klingler and Gergen (1993), *eve* stripes 1 and 2 fused early, stripes 5 and 6 fused early.

In the major circuit A1 (Table A.1), *gt* is an essential repressor of the *eve* stripe 2 anterior border, which supports the literature, and also a critical repressor to set the stripe 7 anterior border, relevant to the observations from Frasch and Levine (1987). However in circuit A2 and B1, there is no dependence on *gt*. In the parameter consensus table (Table A.13) I see strong dependence on *gt* repression to set *eve* stripes in the class A circuits, in the

class B circuits the dependence is weaker, perhaps because it is more representative of the late refinement phase. Hence from the above comparison I put *gt* repressing the *eve* stripe 2 anterior border in black as the first level regulation, and *gt* repression on the stripe 7 anterior border in blue as the second level regulation in the ensemble regulatory map (Fig. 4.1).

kni *kni* was found to repress the *eve* stripe 3 posterior border (Table A.17) and the stripe 6 anterior border from the stripe 3 enhancer study (Small et al., 1996). In mutants that lack *kni* function, there is a posterior expansion of endogeous *eve* and the reporter gene expression driven by the stripe 3 enhancer, the stripe 3 fused to form a broad expression domain. There is no effect on the stripe 2 expression. Further observations include that from Kosman and Small (1997), in embryos with the highest levels of ectopic *kni* expression, the *eve* stripe 3 was completely abolished early in cycle 14, but reappeared later in cycle 14 in a more posterior position. Compared with the stripe 3, other *eve* stripes were not as severely affected.

In both of my major circuits A1 and A2 (Table A.1), *kni* is a critical repressor for both the *eve* stripe 4 posterior border and the stripe 6 anterior border. It is however not required in circuit B1, which is likely more representative of the late refinement phase. Our circuitry results support the literature findings of *kni* repressing the stripe 6 anterior border (Small et al., 1996), it however does not support the direct repression role on *eve* stripe 3 posterior border. This is more pertinent to the observations made in Frasch and Levine (1987) that the stripe 3 is unaffected. The repression role on the stripe 4 posterior border is also reproducible in the earlier application of the gene circuit method Reinitz and Sharp (1995). In the parameter consensus table (Table A.13), *eve*

stripe formation is strongly dependent on *kni* repression in the class A circuits. In the class B circuits, the dependence is weaker.

Given the above comparison, I put both *kni* repression on the stripe 6 anterior border and the stripe 4 posterior border in priority level black as the first level regulation in the ensemble regulatory map (Fig. 4.1).

tll *tll* was found to activate *eve* stripe 7 (Table A.17) from the *eve* stripe 3 enhancer study (Small et al., 1996). *eve* stripe 7 were found abolished in embryos that lack *tll*+ function. Further observations from studies with a *lac*Z stripe 2, 3, 7 construct also indicated that in *tll*– mutants stripe 7 is missing while stripes 2 and 3 are unaffected (Goto et al., 1989).

In the major circuits (Table A.1), *tll* has biased, plateau, input on *eve* stripe 7 formation. Hence it is not essential, slope determining, to the stripe 7 border formation in the dynamical model. Therefore I was unable to determine whether its effect on *eve* stripe 7 is biologically relevant. In the parameter consensus table (Table A.13), both classes of circuits are biased toward repression on *eve*.

B.1.2 *eve* regulation by gap and maternal genes summary

First level regulations (black) The higher consensus *eve* regulations by gap genes in Fig. 4.1 include *gt* repression on the *eve* stripe 2 anterior border, *Kr* repression on the stripe 2 posterior border, *hb* repression on the stripe 3 anterior border, *kni* repression on the stripe 4 posterior border, and *kni* repression on the stripe 6 anterior border. All of these interactions are repressive interactions.

In the literature (Table A.17), *gt* repression on the *eve* stripe 2 anterior border and *Kr* repression on the stripe 2 posterior border were supported by the *eve* stripe 2 enhancer studies (Small et al., 1991, 1992, 1993). Mutations in *gt* causes severe anterior expansion of the stripe 2 pattern (Small et al., 1996), early *eve* stripe 2 was found abnormally broad (Goto et al., 1989), and the *eve* stripes 1 and 2 were found fused early (Klingler and Gergen, 1993). In *Kr*– embryos, *eve* stripes 2 and 3 are fused (Goto et al., 1989; Warrior and Levine, 1990). *hb* repression on *eve* stripe 3 anterior border was supported by the *eve* stripe 3 enhancer study (Klingler and Gergen, 1993; Small et al., 1996; Kosman and Small, 1997). Mutations in *hb* were found to expand the initial limits of the stripe 3 pattern (Small et al., 1996). Studies with a *lac*Z stripe 2, 3, 7 construct indicated that stripes 2 and 3 are fused (Goto et al., 1989). *kni* repression on the stripe 4 posterior border was reproduced in the early application of the gene circuit method based on less quantitative data (Reinitz and Sharp, 1995), and *kni* mutant was found to affect the *eve* stripe 4 posterior border in an early literature of Frasch and Levine (1987). *kni* repression on the stripe 6 anterior border was supported by Small et al. (1996) from the *eve* stripe 3 enhancer study.

In the major circuits (Fig. 4.2), *gt* repression on the *eve* stripe 2 anterior border is supported by circuit A1. *hb* repression on the stripe 3 anterior border is supported by circuit A2. *Kr* repression on the stripe 2 posterior border, *kni* repression on the stripe 4 posterior border, and *kni* repression on the stripe 6 anterior border are supported by both circuit A1 and A2. All interactions are supported as critical repressors, except *gt* repression on *eve* stripe 2 anterior border is supported as an essential repressor. In the parameter distribution analysis (Table A.13), *gt*, *Kr* and *kni* repression on *eve* are supported by

strong consensus in the class A circuits. *hb* repression on *eve* is supported by significant consensus of both class A and class B circuits.

Second level regulations (blue) The second level *eve* regulations by gap genes in color blue in Fig. 4.1, indicating strong predictions made by circuits but may not be directly supported by literature, which include *Kr* repression on the stripe 3 anterior border, *Kr* repression on the stripe 4 posterior border, *Kr* repression on the stripe 5 anterior border and *gt* repression on the stripe 7 anterior border.

In the literature (Table A.17), observations in homozygous *Kr* mutant embryos (Warrior and Levine, 1990) found the stripes 2 and 3 were completely fused, as were the stripes 4 and 6, while the stripe 5 was reduced or absent. *gt* repression on the stripe 7 anterior border was supported by Frasch and Levine (1987), in *gt* mutants the seventh stripe is strongly reduced, and never reaches wild-type levels of expression.

In the major circuits (Fig. 4.2), *Kr* repression on the stripe 3 anterior border is supported by circuit A2 as an essential repressor. *Kr* repression on the stripe 4 posterior border, the stripe 5 anterior border, and *gt* repression on the stripe 7 anterior border are supported by circuit A1 as critical repressors. In the parameter distribution analysis (Table A.13), *gt* repression on *eve* is supported by strong consensus in the class A circuits.

Fifth level regulations (green) The fifth level of *eve* regulations by gap genes in green in Fig. 4.1, indicating interactions in the circuits that are considered as minor (insignificant), indeterminable or irrelevant during analysis, but are supported by literature. These interactions include *bcd* activation on *eve* stripe 2 anterior border, *hb* activation on *eve* stripe 2, *Kr* repression on the

stripe 3 posterior border and the stripe 4 anterior border, and *tll* activation on the stripe 7 anterior border.

In the literature (Table A.17), *bcd* and *hb* activation on *eve* stripe 2, *Kr* repression on *eve* stripe 3 posterior border and the stripe 4 anterior border were all supported by the *eve* stripe 2 and stripe 3 enhancer study (Small et al., 1991, 1992, 1993). *tll* activation on the stripe 7 anterior border were supported by the *eve* stripe 3 enhancer study (Small et al., 1996), *eve* stripe 7 were found abolished in embryos that lack *tll*+ function. Studies with a *lac*Z stripe 2, 3, 7 construct also indicated that in *tll*– mutants stripe 7 is missing (Goto et al., 1989).

Sixth level regulations (yellow) The sixth level *eve* regulations by gap genes in yellow in Fig. 4.1, indicating interactions supported by literature but are totally absent (do not have any input) in the circuits. These interactions include *kni* repression on *eve* stripe 3 posterior border, *hb* repression on the stripe 6 posterior border and *kni* repression on the stripe 7 anterior border.

In the literature (Table A.17), *kni* repression on *eve* stripe 3 posterior border were supported by the *eve* stripe 3 enhancer study (Small et al., 1996). In mutants that lack *kni* function, there is a posterior expansion of endogeous *eve* and the reporter gene expression driven by the stripe 3 enhancer, the stripe 3 fused to form a broad expression domain. In embryos with the highest levels of ectopic *kni* expression Kosman and Small (1997), *eve* stripe 3 was completely abolished early in cycle 14, but reappeared later in cycle 14 in a more posterior position. *hb* repression on the stripe 6 posterior border was supported by Fujioka et al. (1999). *kni* repression on the stripe 7 anterior border was supported by the *eve* stripe 3 enhancer study (Small et al., 1996).

B.1.3 *eve* regulation by pair-rule genes

eve *eve* was found to have auto-activating effect (Table A.18). The *eve* promoter was found to contain Eve-binding sites that when mutated dramatically affect expression of gene *eve* (Frasch et al., 1988; Goto et al., 1989). Further observations include, in *eve* mutant embryos, all seven stripes fail to refine, and are prematurely lost (Frasch et al., 1988; Lawrence and Johnston, 1989). Each of the *eve* mutants shows an abnormal spacing during blastoderm stages, and the sharpening of the pattern is abnormal during gastrulation. In *eve* null mutants, there is a premature loss of expression.

In the major circuits (Table A.2), only circuit A1 shows essential dependence on *eve* auto-activation, particularly on the posterior *eve* borders. In the parameter consensus table (Table A.13), there is no clear dependence on *eve* auto-activation in the high priority set. In the lower priority set there is even consensus toward weak repression. Hence the circuits do not support auto-activation well. Given the above results, I still put *eve* auto-activation in black as the first level regulation in the ensemble regulatory map (Fig. 4.1).

hairy *hairy* was found to activate *eve* in the late refinement phase (Table A.18). In *h* mutant embryos (Frasch and Levine, 1987; Ingham and Gergen, 1988), *eve* expression is lost prematurely. In heat shock *hairy* embryos (Warrior and Levine, 1990), the *eve* pattern is strongly altered despite the low level of ectopic *h* expression. In all cases, the brief expression of *h* in all nuclei led to a broadening of the *eve* stripes and in some cases to partial fusions between stripes.

In all three of the major circuits (Table A.2), *hairy* is a critical activator of *eve*. In the parameter consensus analysis (Table A.13), both classes of circuits

have strong consensus toward *hairy* activation on *eve*. Hence my circuitry results are very strong support for the literature, and I put the corresponding regulation in priority level black as the first level regulation with weighted width in the ensemble regulatory map (Fig. 4.1).

runt *run* was found to be repressing *eve* in the late refinement phase (Table A.18), particularly on the posterior border. In *run* mutant embryos, *eve* stripes expanded (Manoukian and Krause, 1993; Frasch and Levine, 1987; Ingham and Gergen, 1988; Warrior and Levine, 1990). The early, broad *eve* stripes persist longer than normal (Frasch and Levine, 1987; Ingham and Gergen, 1988). Late *eve* expression also persists abnormally (Jaynes and Fujioka, 2004). Ectopic expression of *run* causes loss of *eve* expression (Manoukian and Krause, 1993; Tsai and Gergen, 1994; Hooper et al., 1989), *eve* is rapidly repressed in *hs-runt* embryos.

In three of the major circuits (Table A.2), only circuit A1 depends on *run* as an essential repressor on the posterior border, which supports the literature finding. In the parameter consensus table (Table A.13), there is no strong consensus toward *run* repression in the high priority set, however in the lower priority sets there is stronger dependence on *run* repression. Given the above results I put *run* repression on *eve* posterior border in black as the first level regulation in the ensemble regulatory map (Fig. 4.1).

ftz In the literature survey (Table A.18), there is no specific conclusion drawn about *ftz* regulation on *eve*. In *ftz* mutant embryos, *eve* gene expression was found to be normal (Frasch et al., 1988; Frasch and Levine, 1987; Carroll and Scott, 1986).

In the three major circuits (Table A.2), however, *ftz* is an essential activa-

tor. In the parameter consensus table (Table A.13), there is weaker consensus toward activation in the higher priority set of the class A circuits, and stronger consensus in the class B circuits. Given the above results I put *ftz* activation on *eve* in magenta as the third level regulation in the ensemble regulatory map (Fig. 4.1).

odd *odd* was found to repress *eve* (Table A.18). In *odd* mutant embryos (Drean et al., 1998), the entire 7-stripe pattern appears to expand, both anteriorly and posteriorly. The effect was more significant at the later developmental stages. In ectopic *hs-odd* embryos, *eve* is the most dramatically affected among the so called primary pair-rule genes at the later stages. All 7 *eve* stripes are strongly repressed.

Further arguments on mutant observations were made in Drean et al. (1998), suggesting the above changes may have been missed in the earlier studies, for example Mullen and DiNardo (1995); Coulter and Wieschaus (1988); Frasch and Levine (1987) observed unaffected *eve* patterns in *odd* mutant embryos, due to their subtle nature in certain stage embryos. The full effect of these actions may also be masked by the redundant actions of other segmentation genes.

In all three of the major circuits (Table A.2), *odd* is a critical repressor of *eve*, which strongly supports the literature. In the parameter consensus table (Table A.13), both classes of circuits have clear consensus toward *odd* repression on *eve*. Given the above results, I put *odd* as a repressor on both borders of *eve* in black as the first level regulation in the ensemble regulatory map (Fig. 4.1).

B.1.4 *eve* regulation by pair-rule genes summary

First level regulations (black) The high consensus *eve* regulations by pair rule genes in black in Fig. 4.1 as the first level regulations, include *h* activation on *eve*, *odd* repression on *eve*, *run* repression on the posterior *eve* borders and *eve* auto-activation in the late refinement phase.

In the literature (Table A.18), *h* activation on *eve* in the late refinement phase were supported by Frasch and Levine (1987); Kosman and Small (1997); Warrior and Levine (1990); Carroll and Scott (1986); Ingham and Gergen (1988). In *h* mutant embryos (Frasch and Levine, 1987; Ingham and Gergen, 1988), *eve* expression is lost prematurely. In heat shock *h* embryos (Warrior and Levine, 1990), the *eve* pattern is strongly altered despite the low level of ectopic *h* expression. In all cases, the brief expression of *h* in all nuclei led to a broadening of the *eve* stripes and in some cases to partial fusions between stripes. *odd* repression on *eve* in the late refinement phase was supported by Jaynes and Fujioka (2004); Drean et al. (1998). In *odd* mutant embryos (Drean et al., 1998), the entire 7-stripe pattern appears to expand, both anteriorly and posteriorly. In ectopic *hs-odd* embryos, *eve* is the most dramatically affected among the so called primary pair-rule genes (*eve*, *h*, *run*) at the later stages. All 7 *eve* stripes are strongly repressed. *run* repression on *eve* in the late refinement phase was supported by Carroll and Vavra (1989); Manoukian and Krause (1993); Jaynes and Fujioka (2004); Jiménez et al. (1996); Ingham and Gergen (1988), particularly on the posterior borders (Warrior and Levine, 1990; Frasch and Levine, 1987; Fujioka et al., 1996). In *run* mutant embryos, *eve* stripes expanded (Manoukian and Krause, 1993; Frasch and Levine, 1987; Ingham and Gergen, 1988; Warrior and Levine, 1990). The early, broad *eve* stripes persist longer than normal (Frasch and Levine, 1987; Ingham and Ger-

gen, 1988). Late *eve* expression also persists abnormally (Jaynes and Fujioka, 2004). Ectopic expression of *run* causes loss of *eve* expression (Manoukian and Krause, 1993; Tsai and Gergen, 1994; Hooper et al., 1989), *eve* is rapidly repressed in *hs-run* embryos. *eve* auto-activation was supported by Goto et al. (1989); Ingham and Gergen (1988); Frasch and Levine (1987). The *eve* promoter was found to contain Eve-binding sites that when mutated dramatically affect expression of gene *eve* (Frasch et al., 1988; Goto et al., 1989). In *eve* mutant embryos, all seven stripes fail to refine, and are prematurely lost (Frasch et al., 1988; Lawrence and Johnston, 1989). Each of the *eve* mutants shows an abnormal spacing during the blastoderm stages, and the sharpening of the pattern is abnormal during gastrulation. In *eve* null mutants, there is a premature loss of expression.

In the major circuits (Fig. 4.2), both *h* activation on *eve* and *odd* repression on *eve* are supported by all three circuits A1, A2 and B1. Both *h* and *odd* are supported as a critical regulator. Both *run* repression on *eve* posterior border and *eve* auto-activation are supported by circuit A1 as an essential regulator. In the parameter distribution analysis (Table A.13), both *h* activation on *eve* and *odd* repression on *eve* are supported by strong consensus from both the class A and class B circuits. *run* repression on *eve* posterior border is supported by higher consensus in the lower priority sets of both the class A and class B circuits.

Third level regulations (magenta) The third level *eve* regulations by pair rule genes in magenta in Fig. 4.1, indicating interactions predicted by circuits but may contradict to literature. The interactions include *ftz* activation on *eve*.

In the literature (Table A.18), *ftz* regulation on *eve* is more concluded toward no direct effect. In *ftz* mutant embryos, *eve* gene expression was found to be normal (Frasch et al., 1988; Frasch and Levine, 1987).

In the major circuits (Fig. 4.2), *ftz* activation on *eve* is supported by all three circuits A1, A2 and B1, as an essential activator. In the parameter distribution analysis (Table A.13), *ftz* activation on *eve* is supported by stronger consensus in the class B circuits and the lower priority sets of the class A circuits.

Fourth level regulations (cyan) The fourth level *eve* regulations by pair rule genes in cyan in Fig. 4.1, indicating stripe specific pair rule cross regulations in the circuits. The interaction includes *eve* activation on the stripe 2 anterior border.

Fifth level regulations (green) The fifth level *eve* regulations by pair rule genes in green in Fig. 4.1, indicating interactions in the circuits that are considered as minor (insignificant), indeterminable or irrelevant during analysis but are supported by literature. The interactions include *eve* auto-activation on the anterior borders and *run* repression on the anterior *eve* borders in general.

B.2 *hairy* regulation

B.2.1 *h* regulation by gap and maternal genes

bcd *bcd* was found to activate *h* stripe 1 (Howard and Struhl, 1990; Riddihough and Ish-Horowicz, 1991) and the stripe 7 (Rosée et al., 1997), and may also repress the stripe 4 (Howard and Struhl, 1990; Riddihough and Ish-Horowicz, 1991). No individual gap gene abolishes the stripe 1 expression (Hooper et al., 1989), only mutations that abolish or reduce *bcd* concentrations cause loss of the stripe 1 (Riddihough and Ish-Horowicz, 1991).

In the major circuits (Table A.3), *bcd* is not the essential input for the stripe 2 anterior border, and has biased, plateau, input on the other borders. In the parameter consensus table (Table A.14), the class A circuits are biased toward repression on *h*.

cad *cad* was found to be possibly activating *h* stripes 6 and 7 (Rosée et al., 1997). In the absence of *cad*, *h*7-*lac*Z expression is strongly affected.

In the major circuits (Table A.3), *cad* has small biased, near plateau, input on the posterior-embryo *h* stripes. Hence is not essential, slope determining, for *h* border formation in the dynamical model. In the parameter consensus table (Table A.14), the class A circuits have more consensus toward repression on *h*.

hb *hb* was found to activate *h* stripe 3 (Hartmann et al., 1994). In *hb* mutant embryos, *h* stripe 3 is missing. It may also repress *h* (Carroll and Vavra, 1989), on the stripe 3 (Howard and Struhl, 1990; Riddihough and Ish-Horowicz, 1991) and the stripe 6 posterior border (Langeland et al., 1994).

In the major circuits (Table A.3), however, there is no input from *hb* to *h*. There is also no strong consensus for *hb* regulation on *h* of both classes of circuits (Table A.14).

Kr *Kr* was found to repress *h* (Carroll and Vavra, 1989), on the stripe 2 and 6 (Riddihough and Ish-Horowicz, 1991), stripe 5 (Langeland and Carroll, 1993), stripe 5 and 6 anterior borders (Langeland et al., 1994), and the stripe 7 (Rosée et al., 1997). *Kr* may also activate *h* stripe 4 (Howard and Struhl, 1990; Riddihough and Ish-Horowicz, 1991).

In the major circuit B1 (Table A.3), *Kr* is an essential repressor on the stripe 3 anterior border. There is no dependence on *Kr*, however, in circuit A1 and A2. In the parameter distribution analysis (Table A.14), there is also stronger consensus toward *Kr* repression on *h* in the class A circuits. Hence I conclude *Kr* repression on *h* stripe 3 anterior border in magenta as the third level regulation in the ensemble regulatory map (Fig. 4.1).

gt *gt* was found to repress *h* stripe 5 on the posterior border (Riddihough and Ish-Horowicz, 1991; Langeland and Carroll, 1993; Langeland et al., 1994), and may act as a local activator of the stripe 6.

In the major circuit B1 (Table A.3), *gt* is a critical repressor of *h* stripe 2 anterior border. However in circuit A1 and A2, there is no essential dependence on *gt*. In the parameter consensus table (Table A.14), there is very strong consensus toward *gt* repression on *h*. Hence I conclude *gt* repression on *h* stripe 2 anterior border in blue as the second level regulation (Fig. 4.1).

kni *kni* was found to activate *h* stripe 6 (Riddihough and Ish-Horowicz, 1991; Langeland et al., 1994), and the stripe 5 (Riddihough and Ish-Horowicz, 1991;

Langeland and Carroll, 1993; Langeland et al., 1994). *kni* may also repress *h* stripe 4 (Riddihough and Ish-Horowicz, 1991; Hartmann et al., 1994), and the stripe 7 anterior border (Howard and Struhl, 1990; Riddihough and Ish-Horowicz, 1991; Rosée et al., 1997).

In all three of the major circuits (Table A.3), *kni* is not an essential regulator. In the parameter distribution analysis (Table A.14), there is stronger consensus toward *kni* repression on *h* in the first priority sets.

tll *tll* was found to repress *h* stripe 1 (Howard and Struhl, 1990; Riddihough and Ish-Horowicz, 1991), stripe 2 and 6 (Riddihough and Ish-Horowicz, 1991), and the stripe 7 posterior border (Rosée et al., 1997).

In the major circuit A1 (Table A.3), *tll* is a critical activator for the stripe 7 anterior border. In circuit A2 and B1, however, it is not required. In the parameter distribution analysis (Table A.14), there is stronger consensus for *tll* activation on *h* in the class A circuits and the lower priority sets of the class B circuits. In the first priority set of the class B circuits, however, there is stronger consensus for *tll* repression on *h*. Given the above results, I put *tll* activation on *h* stripe 7 anterior border in magenta as the third level regulation.

B.2.2 *h* regulation by gap and maternal genes summary

Second level regulations (blue) The second level *h* regulations by gap genes in blue in Fig. 4.1, indicating strong predictions made by circuits but may not be directly supported by literature. The interactions include *gt* repression on the stripe 2 anterior border.

In the literature (Table A.19), there is no direct support for *gt* repression on the stripe 2 anterior border. In the major circuits (Fig. 4.3), *gt* repression on

the stripe 2 anterior border is supported by circuit B1 as a critical repressor. In the parameter distribution analysis (Table A.14), *gt* repression on *h* is supported by very strong consensus in both the class A and class B circuits.

Third level regulations (magenta) The third level *h* regulations by gap genes in magenta in Fig. 4.1, indicating interactions predicted by circuits but may contradict to literature. These interactions include *Kr* repression on the stripe 3 anterior border and *tll* activation on the stripe 7 anterior border.

In the literature (Table A.19), *Kr* repression on *h* is supported by Carroll and Vavra (1989), there is no specific support for repression on the stripe 3 anterior border. In *Kr* mutant embryos (Carroll and Vavra, 1989; Hooper et al., 1989), only four broad *h* stripes are seen roughly in the positions of the stripe 1, a fused stripe 2/3/4, a fused stripe 5/6, and the stripe 7. In *Kr* homozygous mutant embryo (Warrior and Levine, 1990), the stripes 2 and 3 are fused. *tll* activation on *h* stripe 7 anterior border is contradicted by Rosée et al. (1997) as indirect effects. Displaced *h* stripe 7' is completely abolished in *tll* mutant embryos, and the *h*7-*lac*Z expression is also absent (Rosée et al., 1997). In *tll* mutant embryo (Mahoney and Lengyel, 1987; Hooper et al., 1989), *h* stripe 7 is missing.

In the major circuits (Fig. 4.3), *Kr* repression on *h* stripe 3 anterior border is supported by circuit B1 as an essential repressor. *tll* activation on the stripe 7 anterior border is supported by circuit A1 as a critical activator. In the parameter distribution analysis (Table A.14), *Kr* repression on *h* is supported by stronger consensus in the class A circuits. *tll* activation on *h* is supported by stronger consensus in the class A circuits and the lower priority sets of the class B circuits.

Fifth level regulations (green) The fifth level of *h* regulations by gap genes in green in Fig. 4.1, indicating interactions in the circuits that are considered as minor (insignificant), indeterminable or irrelevant during analysis, but are supported by literature. These interactions include *tll* repression on *h* stripe 2, *Kr* activation on the stripe 4, *Kr* repression on the stripe 5 anterior border, *kni* activation on the stripe 5, *gt* and *cad* activation on the stripe 6, *tll* repression on the stripe 6 posterior border, *bcd* and *cad* activation on the stripe 7 anterior border.

In the literature (Table A.19), *tll* repression on *h* stripe 2 is supported by Riddihough and Ish-Horowicz (1991). *Kr* activation on the stripe 4 is supported by Howard and Struhl (1990); Riddihough and Ish-Horowicz (1991). In ectopic *hs-Kr* expression (Langeland et al., 1994), all *h* stripes are extinguished except for the stripes 3 and 4, which normally fall within the wild-type *Kr* domain. *Kr* repression on the stripe 5 anterior border is supported by Langeland and Carroll (1993); Langeland et al. (1994). *h* stripe 5 displays significant anterior expansion when *Kr* is removed (Langeland et al., 1994). Several binding sites for the *Kr* repressor were identified in the stripe 5 regulatory sequences. In *Kr* homozygous mutant embryo, *h* stripes 4-6 are fused. *kni* activation on the stripe 5 is supported by Riddihough and Ish-Horowicz (1991); Langeland and Carroll (1993); Langeland et al. (1994). *kni* mutations were found to reduce the displaced stripe 5'(Riddihough and Ish-Horowicz, 1991). *gt* activation on the stripe 6 is supported by Riddihough and Ish-Horowicz (1991). *gt* mutations were found to abolish the displaced stripe 6' (Riddihough and Ish-Horowicz, 1991). In *gt* mutant embryos (Klingler and Gergen, 1993), *h* stripes 5 to 7 are fused early. *cad* activation on the stripe 6 is supported by Rosée et al. (1997). Caudal-binding sites were found to be present in the *h*

stripe 6-element (Häder et al., 1998). *tll* repression on the stripe 6 posterior border is supported by Riddihough and Ish-Horowicz (1991). Displaced stripe 6' expanded posteriorly in *tll* mutant embryos (Riddihough and Ish-Horowicz, 1991). *bcd* activation on the stripe 7 is supported by Rosée et al. (1997). In embryos lacking *bcd* as the key component of the anterior organizer system (Rosée et al., 1997), the *h*7-*lac*Z expression domain is duplicated. The normal posterior expression domain appears irregular and is shifted anteriorly. *cad* activation on the stripe 7 anterior border is supported by Rosée et al. (1997). In the absence of *cad*, *h*7-*lac*Z expression is strongly affected.

Sixth level regulations (yellow) The sixth level *h* regulations by gap genes in yellow in Fig. 4.1, indicating interactions supported by literature but are totally absent (do not have any input) in the circuits. These interactions include *Kr* repression on the *h* stripe 2, *hb* activation on the stripe 3, *kni* repression on the stripe 4, *gt* repression on the stripe 5 posterior border, *Kr* repression on the stripe 5 posterior border, *kni* activation on the stripe 6, *Kr* repression on the stripe 6, *hb* repression on the stripe 6 posterior border, *Kr* and *kni* repression on the stripe 7 anterior border.

In the literature (Table A.19), *Kr* repression on the *h* stripe 2 is supported by Riddihough and Ish-Horowicz (1991). According to Warrior and Levine (1990), in *Kr* heterozygous mutant embryos, *h* stripe 2 is expanded posteriorly while the distance between the stripes 2 and 3 is reduced. *hb* activation on the stripe 3 is supported by Hartmann et al. (1994). In *hb* mutant embryos, *h* stripe 3 is missing. Contradicting literature results were found in Carroll and Vavra (1989), suggesting *hb* may also repress *h*, on the stripe 3 (Howard and Struhl, 1990; Riddihough and Ish-Horowicz, 1991). *kni* repression on the

stripe 4 is supported by Riddihough and Ish-Horowicz (1991); Hartmann et al. (1994). In *kni* mutant embryos (Carroll and Vavra, 1989; Hooper et al., 1989), *h* stripe 4 is missing. According to Riddihough and Ish-Horowicz (1991), the displaced stripe 3'-4' is broadened in *kni*– embryos, where the *Kr* domain is expanded (Gaul et al., 1987; Jäckle et al., 1986). *gt* repression on the stripe 5 posterior border is supported by Riddihough and Ish-Horowicz (1991); Langeland and Carroll (1993); Langeland et al. (1994). *gt* mutations expand the displaced stripe 5' posteriorly (Riddihough and Ish-Horowicz, 1991). Similarly in Langeland et al. (1994), the stripe 5 expands posteriorly when *gt* is removed, putative binding sites for the gt protein have also been localized in the stripe 5 regulatory sequences (Langeland and Carroll, 1993). *Kr* repression on the stripe 5 posterior border is supported by Langeland and Carroll (1993). In *Kr* homozygous mutant embryo, the *h* stripes 4-6 are fused. *kni* activation on the stripe 6 is supported by Riddihough and Ish-Horowicz (1991); Langeland et al. (1994). In *kni* mutant embryos (Carroll and Vavra, 1989; Hooper et al., 1989), the *h* stripes 5-7 are fused in a wide band. According to Riddihough and Ish-Horowicz (1991), *kni* mutations abolish the displaced stripe 6'. *Kr* repression on the stripe 6 is supported by Riddihough and Ish-Horowicz (1991). In *Kr* homozygous mutant embryo, the *h* stripes 4-6 are fused. The *h* stripe 6 display significant anterior expansion when *Kr* is removed (Langeland et al., 1994). Several binding sites for the *Kr* repressor were also identified in the *h* stripe 6 regulatory sequences. *hb* repression on the stripe 6 posterior border is supported by Langeland et al. (1994). THe stripe 6 expands posteriorly when *hb* is removed (Langeland et al., 1994). Several putative *hb*-binding sites were also found in the stripe 6 regulatory sequence. The stripe 6 is also flanked by the posterior domain of *hb*. *Kr* repression on the stripe 7 is supported by

Rosée et al. (1997). In the absence of *Kr* activity, two *h*7-*lac*Z expression domains were observed. *h*7-*lac*Z expression in the normal stripe 7 position was reduced. *kni* repression on the stripe 7 anterior border is supported by Howard and Struhl (1990); Riddihough and Ish-Horowicz (1991); Rosée et al. (1997). In *kni* mutant embryos (Klingler and Gergen, 1993), the *h* stripe 7 is affected, stripes 5-7 are fused in a wide band (Carroll and Vavra, 1989; Hooper et al., 1989). In Rosée et al. (1997), the *h*7-*lac*Z expression also expands anteriorly in *kni* mutant embryos. According to Riddihough and Ish-Horowicz (1991), *kni* mutations expand the displaced stripe 7'.

B.2.3 *h* regulation by pair-rule genes

eve *eve* was found to be only required for *h* stripe 2 maintenance (Hooper et al., 1989; Carroll and Vavra, 1989), and perhaps have activating effect in the early phase of *h* stripe formation (Ingham and Gergen, 1988).

In the major circuit A1 (Table A.4), *eve* is a critical activator of all *h* borders, however in circuit A2 *eve* is in a reducible set. In circuit B1, *eve* is also not required. In the parameter consensus table (Table A.14), there is moderate consensus toward *eve* activation on *h* in the low priority sets and consensus toward *eve* repression on *h* in the higher priority sets of the class B circuits. Given the above results, I put *eve* activation on *h* in blue as the second level regulation in the ensemble regulatory map (Fig. 4.1).

hairy *h* was found to have no autoregulatory effect (Hooper et al., 1989; Parkhurst and Ish-Horowicz, 1991; Jiménez et al., 1996; Riddihough and Ish-Horowicz, 1991). Normal *h* patterning occurs in the absence of active *h* protein. In particular, levels of *h* expression are independent of *h* function. From

Riddihough and Ish-Horowicz (1991), *h-lac*Z expression is unaltered in an *h* mutant background.

In the major circuit A1 (Table A.4), *h* is an essential repressor for all the borders, while in circuit A2, *h* is not required, and in circuit B1, *h* is a critical activator for all the borders. It is possible that *h* has transient repression effect in the early stripe formation phase, and auto-activation effect in the late refinement phase. In the parameter consensus analysis (Table A.14), there is stronger consensus toward *h* auto-activation in the class B circuits. However, based on the controversial results, I conclude no convincing support for *h* auto-activation in the ensemble regulatory map (Fig. 4.1).

runt *run* was found to repress *h* (Carroll and Vavra, 1989; Warrior and Levine, 1990; Manoukian and Krause, 1993; Jiménez et al., 1996), especially in the late phase (Jaynes and Fujioka, 2004). *h* may also be independent of *run* (Hooper et al., 1989), or only has stripe specific repression on *h* stripe 1 (Manoukian and Krause, 1993; Tsai and Gergen, 1994), or stripe 3/4 and 6/7 (Hooper et al., 1989).

In both of the major circuits A1 and A2 (Table A.4), *run* is a critical repressor for all the *h* borders, which is a very strong support for the literature. In circuit B1, however, *run* is not required. The stripe specific *run* regulations in the literature are not supported in the major circuits. In the parameter consensus table (Table A.14), there is strong consensus toward *run* repression of both classes of circuits. Given the above results I put *run* repression on *h* in black as the first level regulation with weighted width in the ensemble regulatory map (Fig. 4.1).

ftz *ftz* was found to have no influence on *h* (Howard and Ingham, 1986).

In the major circuits A1 (Table A.4), *ftz* is an essential activator for the stripe 2 anterior border and all the posterior borders except the stripe 2. In the major circuit A2, *ftz* is in a reducible set for all the stripes. In circuit B1, *ftz* is a critical activator for both the stripe 5 and stripe 6 anterior borders, and for all the posterior borders. In the parameter distribution analysis (Table A.14), there is stronger consensus toward activation in the class B circuits and the high priority set of the class A circuits. *ftz* activation may be more required in the late refinement phase. Given the above results, I conclude *ftz* activation on all the posterior borders in magenta as the third level regulation in the ensemble regulatory map (Fig. 4.1).

odd *odd* was found to repress *h* (Drean et al., 1998).

In the major circuit A1 (Table A.4), *odd* is an essential activator on the stripe 2 and stripe 7 anterior borders, and on all the posterior borders except for the stripe 2. In circuit A2, however, *odd* is not required. In circuit B1, *odd* is a critical repressor on the stripe 7 anterior border, and an essential repressor on all the posterior borders except for the stripe 2. The contradiction is also reflected in the parameter distribution analysis (Table A.14), the class A circuits have strong consensus toward *odd* activation while the class B circuits have strong consensus toward *odd* repression. Based on the above complex results, and since the class A circuits are more representative of the early stripe formation phase, I conclude *odd* may have transient activation effect on the stripe 2 and stripe 7 anterior borders and on all the posterior borders except for the stripe 2. And *odd* is likely required for repression on *h* in the late refinement phase on the stripe 7 anterior border and on all the posterior borders, except for stripe 2, in blue as the second level regulations in Fig. 4.1.

B.2.4 *h* regulation by pair-rule genes summary

First level regulations (black) The high consensus, first level, *h* regulations by pair rule genes in black in Fig. 4.1 include *run* repression on *h*.

In the literature (Table A.20), *run* repression on *h* is supported by Carroll and Vavra (1989); Warrior and Levine (1990); Manoukian and Krause (1993); Jiménez et al. (1996), especially in the late phase (Jaynes and Fujioka, 2004). In *run* mutant embryos, *h* pattern was found expanded (Ingham and Gergen, 1988; Hartmann et al., 1994; Carroll and Vavra, 1989; Manoukian and Krause, 1993; Warrior and Levine, 1990). In *run* null mutant embryo, *h* pattern was found overexpressed, with *h* stripes becoming variably wider (Ingham and Gergen, 1988).

In the major circuits (Fig. 4.3), *run* repression on *h* is supported by both circuit A1 and A2 as a critical repressor. In the parameter distribution analysis (Table A.14), *run* repression on *h* is supported by strong consensus of both the class A and class B circuits.

Second level regulations (blue) The second level *h* regulations by pair rule genes in blue in Fig. 4.1, indicating strong predictions made by circuits but may not be directly supported by literature. These interactions include *eve* activation on *h* and *odd* repression on *h* posterior borders.

In the literature (Table A.20), *eve* activation on *h* is supported for *h* stripe 2 maintenance (Hooper et al., 1989; Carroll and Vavra, 1989), and perhaps in the early phase of *h* stripe formation (Ingham and Gergen, 1988). In *hs-eve* ectopic expression embryos (Manoukian and Krause, 1992), there was even no effect on *h* expression. *odd* repression on *h* is supported by Drean et al. (1998). In *odd* mutant embryos (Drean et al., 1998), the entire 7-stripe pattern of *h*

appears to expand, both anteriorly and posteriorly. In ectopic *hs-odd* embryos, the earliest observed effects are on the anterior-most stripes.

In the major circuits (Fig. 4.3), *eve* activation on *h* is supported by circuit A1 as a critical activator. *odd* repression on *h* posterior borders is supported by circuit B1 as an essential repressor, except for the stripe 2. In the parameter distribution analysis (Table A.14), *eve* activation on *h* is supported by consensus in the low priority sets of the circuits. *odd* repression on *h* is supported by strong consensus in the class B circuits.

Third level regulations (magenta) The third level *h* regulations by pair rule genes in magenta in Fig. 4.1, indicating interactions predicted by circuits but may contradict to literature. The interactions include *ftz* activation on *h* and transient *odd* activation on the posterior *h* borders in the early stripe formation phase.

In the literature (Table A.20), *ftz* was also found to have no influence on *h* (Howard and Ingham, 1986; Carroll and Scott, 1986).

In the major circuits (Fig. 4.3), *ftz* activation on *h* is supported by circuit A1 as an essential activator and by circuit B1 as a critical activator. There are also stripe specific effects mostly on the anterior borders. *odd* activation on the posterior *h* borders is supported by circuit A1 as an essential activator, except for the stripe 2. In the parameter distribution analysis (Table A.14), *ftz* activation on *h* is supported by stronger consensus in the class B circuits and in the high priority set of the class A circuits, which may imply *ftz* activation is more required in the late refinement phase. *odd* activation on *h* is supported by strong consensus in the class A circuits.

Fourth level regulations (cyan) The fourth level *h* regulations by pair rule genes in cyan in Fig. 4.1 indicating stripe specific pair rule cross regulations found in the circuits (only the critical regulators are shown in Fig. 4.1 to Fig. 4.7). The interactions include transient *odd* activation on the stripe 2 anterior border in the early phase, *ftz* activation on the stripe 2 anterior border, *ftz* activation on the stripe 5 anterior border, *ftz* activation on the stripe 6 anterior border, transient *odd* activation on the stripe 7 anterior border and *odd* repression on the stripe 7 anterior border.

In the major circuits (Fig. 4.3), transient *odd* activation on the stripe 2 anterior border and the stripe 7 anterior border is supported by circuit A1 as an essential activator. *odd* repression on the stripe 7 anterior border is supported by circuit B1 as a critical repressor. *ftz* activation on the stripe 2 anterior border is supported by circuit A1 as an essential activator. *ftz* activation on the stripe 5 anterior border and the stripe 6 anterior border is supported by circuit B1 as a critical activator.

Fifth level regulations (green) The fifth level *h* regulations by pair rule genes in green in Fig. 4.1 indicating interactions in the circuits that are considered as minor (insignificant), indeterminable or irrelevant during the circuit analysis, but are supported by literature. The interactions include *odd* repression on the anterior *h* borders.

B.3 *runt* regulation

According to Klingler and Gergen (1993), all of the gap gene mutations (except *cad*) have clear effects at the earliest stages when the 7 *run* stripes become apparent. Mutations in the gap genes *Kr* and *kni* had the most dramatic effects: in both cases only 3 well-formed stripes remained. The anterior border of stripe 1 of *run* is not affected by any of the gap genes here (the situation is similar for *h*, *eve* and *ftz*).

According to Klingler and Gergen (1993), while the *run* pattern in gap mutations is abnormal from the very beginning, 7 stripes are initially formed in all pair-rule mutations. In embryos mutant for the primary pair rule genes (*eve*, *h*, *run*), the *run* pattern is already affected when the blastoderm cell membranes have extended about half-way. We find that mutations in all of the secondary pair-rule genes (except *slp*) also alter *run*'s expression, however these defects are not apparent until the very end of the cellular blastoderm stage, or even the onset of gastrulation and involve the transition from 7 to 14 stripes. The remaining pair-rule genes (*odd*, *prd*) affect the *run* pattern only at the end or after the cellular blastoderm. Mutations in secondary pair-rule genes do not affect the initial 7 stripe patterns of *run* or the other primary pr genes. *run*'s 14 stripe pattern does depend on the secondary pair-rule genes. Mutations in the three primary pair-rule genes (*eve*, *h*, *run*) all lead to patterning defects that are observable during the blastoderm stage.

B.3.1 *run* regulation by gap and maternal genes

bcd *bcd* was found to repress *run* in the anterior region of an early broad *run* expression field (Klingler and Gergen, 1993; Tsai and Gergen, 1994).

In the major circuits (Table A.5), there is no essential dependence on *bcd*. *bcd* only has biased plateau input which is indeterminable with respect to its biological relevance. In the parameter consensus table (Table A.15), there is strong bias toward *bcd* repression in the class A circuits.

cad No literature were found here for *cad* regulation on *run* pattern.

In the major circuits (Table A.5), there is no essential dependence on *cad*. *cad* has biased, near plateau, input on the posterior-embryo stripes, which is indeterminable to its biological relevance. In the parameter consensus table (Table A.15), there is strong bias toward *cad* repression in the class A circuits.

hb *hb* was found to be repressing *run* stripe 3 anterior border (Klingler and Gergen, 1993; Small et al., 1996).

In the major circuits (Table A.5), however, there is no dependence on *hb*. In the parameter consensus table (Table A.15), there is also no specific consensus of both classes of circuits.

Kr *Kr* was found to repress *run* on the stripe 2 posterior and stripe 5 anterior border (Klingler and Gergen, 1993).

In the major circuit A1 (Table A.5), *Kr* is a critical activator on *run* stripe 4 and an essential activator on the stripe 2 anterior border. In circuit A2, however, there is no dependence on *Kr*. In circuit B1, *Kr* is an essential activator on the stripe 2 posterior border and stripe 4 posterior border. In the parameter consensus table (Table A.15), there is mild consensus toward *Kr* activation on *run* of both classes of circuits. I conclude *Kr* activation on *run* stripe 4 in blue as the second level regulation, and activation on the stripe 2 in magenta as the third level regulation in the ensemble regulatory map

(Fig. 4.1).

gt *gt* was found to repress *run* on the stripe 2 anterior and stripe 5 posterior border (Klingler and Gergen, 1993).

In the major circuits (Table A.5), *gt* is a critical activator on the stripe 1 posterior border in all circuits. *gt* is also an essential activator on the stripe 5 posterior border in circuit A1 and B1, and a critical activator on the stripe 6 posterior border and the stripe 6 in circuit A1 and A2. In the parameter consensus table (Table A.15), there is significant consensus toward *gt* activation on *run* of both classes of circuits. Given the above results, I conclude *gt* activation on *run* stripe 1 posterior border and stripe 6 in blue as the second level regulation, and activation on the stripe 5 posterior border in magenta as the third level regulation in the ensemble regulatory map (Fig. 4.1).

kni *kni* was found to repress *run* on the stripe 3 posterior border (Carroll and Scott, 1986; Klingler and Gergen, 1993; Small et al., 1996; Kosman and Small, 1997) and the stripe 6 anterior border (Klingler and Gergen, 1993).

In the major circuits (Table A.5), however, there is no dependence on *kni*. In the parameter consensus table (Table A.15), there is also no specific consensus of both classes of circuits.

tll *tll* was found to repress *run* on the stripe 6 posterior boundary (Klingler and Gergen, 1993), and may also activate the stripe 7 anterior border.

In the major circuits (Table A.5), *tll* is an essential repressor on the stripe 6 posterior border in circuit B1. In circuit A1 and A2, however, there is no dependence on *tll*. In the parameter consensus table though (Table A.15), there is very strong consensus toward *tll* repression in both classes of circuits.

I conclude *tll* repression on *run* stripe 6 posterior border in black as the first level regulation in the ensemble regulatory map (Fig. 4.1).

B.3.2 *run* regulation by gap and maternal genes summary

First level regulations (black) The high consensus, first level, *run* regulations by pair rule genes in black in Fig. 4.1, include regulations of *tll* repression on the *run* stripe 6 posterior border.

In the literature (Table A.21), *tll* repression on *run* stripe 6 posterior border is supported by Klingler and Gergen (1993). In *tll* mutant embryo (Klingler and Gergen, 1993), the stripe 7 is not formed at all, stripe 6 appears belatedly, and this stripe as well as the stripe 5 are shifted posteriorly.

In the major circuits (Fig. 4.4), *tll* repression on the *run* stripe 6 posterior border is supported by circuit B1 as an essential repressor. In the parameter distribution analysis (Table A.15), *tll* repression on *run* is supported by very strong consensus of both classes of circuits.

Second level regulations (blue) The second level *run* regulations by gap genes in blue in Fig. 4.1, indicating strong predictions made by circuits but may not be directly supported by literature, which include *gt* activation on the stripe 1 posterior border, *Kr* activation on the stripe 4 and *gt* activation on the stripe 6.

In the literature (Table A.21), there is no specific conclusion for *gt* activation on *run* stripe 1 posterior border. In *gt* mutant embryo (Klingler and Gergen, 1993), *run* stripes 1 and 2 are fused only in the early phase before cellularization. There is no specific reference for *Kr* activation on the stripe

4. *run* stripes 3 and 4 are narrower in *Kr*−/+ (Klingler and Gergen, 1993). There is no specific reference for *gt* activation on the stripe 6. In *gt* mutant embryo (Klingler and Gergen, 1993), the stripe 6 is abnormally weak.

In the major circuits (Fig. 4.4), *gt* activation on *run* stripe 1 posterior border is supported by all circuits as a critical activator. *Kr* activation on the stripe 4 is supported by circuit A1 as a critical activator, and as an essential activator on the stripe 4 posterior border in circuit B1. *gt* activation on the stripe 6 is supported as a critical activator in circuit A2, and as a critical activator on the stripe 6 posterior border in circuit A1. In the parameter distribution analysis (Table A.15), *gt* activation on *run* is supported by significant consensus of both classes of circuits. *Kr* activation on *run* is supported by mild consensus of both classes of circuits.

Third level regulations (magenta) The third level *run* regulations by gap genes in magenta in Fig. 4.1, indicating interactions predicted by circuits, but may contradict to literature. The interactions include *Kr* activation on *run* stripe 2 and *gt* activation on the stripe 5 posterior border.

In the literature (Table A.21), *Kr* repression on *run* stripe 2 posterior border is supported by Klingler and Gergen (1993). In *Kr* mutant embryo (Klingler and Gergen, 1993), the stripes 2 to 5 are replaced by one large domain. *gt* repression on the stripe 5 posterior border is supported by Klingler and Gergen (1993). In *gt* mutant embryo (Klingler and Gergen, 1993), *run* stripes 5 and 6 form a strongly stained band when cellularization approaches completion.

In the major circuits (Fig. 4.4), *Kr* activation on *run* stripe 2 is supported by circuit A1 as an essential activator on the anterior border, and by circuit B1

on the posterior border. *gt* activation on stripe 5 posterior border is supported by circuit A1 and B1 as an essential activator.

Sixth level regulations (yellow) The sixth level *run* regulations by gap genes in yellow in Fig. 4.1, indicating interactions supported by literature, but are totally absent (do not have any input) in the circuits. These interactions include *hb* repression on the stripe 3 anterior border, *Kr* repression on the stripe 5 anterior border, *gt* repression on the stripe 2 anterior border, *kni* repression on the stripe 3 posterior border and *kni* repression on the stripe 6 anterior border.

In the literature (Table A.21), *hb* repression on *run* stripe 3 anterior border is supported by Klingler and Gergen (1993); Small et al. (1996). In *hb* mutant embryo (Klingler and Gergen, 1993), the stripes 2 and 3 are replaced by one domain of expression early in the blastoderm. *Kr* repression on the stripe 5 anterior border is supported by Klingler and Gergen (1993). In *Kr* mutant embryo (Klingler and Gergen, 1993), the stripes 2 to 5 are replaced by one large domain in the early phase. *gt* repression on the stripe 2 anterior border is supported by Klingler and Gergen (1993). In *gt* mutant embryo (Klingler and Gergen, 1993), *run* stripes 1 and 2 are fused and form a band of intense expression early in the cellular blastoderm. *kni* repression on the stripe 3 posterior border is supported by Carroll and Scott (1986); Klingler and Gergen (1993); Small et al. (1996); Kosman and Small (1997). In *kni* mutant embryo (Klingler and Gergen, 1993), the stripe 3 is fused to the de-repression domain in the early stage. In *kni* ectopic expression experiments (Kosman and Small, 1997), the stripe 3 is severely reduced. *kni* repression on the stripe 6 anterior border is supported by Klingler and Gergen (1993). In *kni* mutant embryo

(Klingler and Gergen, 1993), it is the stripes 3 to 6 that are affected.

B.3.3 *run* regulation by pair-rule genes

eve *eve* was found to repress *run* (Manoukian and Krause, 1992, 1993; Jaynes and Fujioka, 2004; Ingham and Gergen, 1988; Fujioka et al., 1996; Klingler and Gergen, 1993). *eve* may also activate *run* in the early phase (Carroll and Vavra, 1989). In *eve* mutant embryo (Jaynes and Fujioka, 2004), late *run* expression expands throughout the *eve* domain (Fujioka et al., 1995). Ectopic *eve* expression at high level was found to repress *run* (Manoukian and Krause, 1992).

In the major circuits (Table A.6), *eve* is an essential repressor on *run* posterior borders in circuit A2, but is not required in the other circuits. In the parameter consensus table (Table A.15), there is stronger consensus in the class B circuits toward *eve* activation on *run*. I conclude *eve* repression on *run* posterior borders in black as the first level regulation in the ensemble regulatory map (Fig. 4.1).

hairy *h* was found to repress *run* (Read et al., 1992; Jaynes and Fujioka, 2004; Howard and Ingham, 1986; Carroll and Scott, 1986; Ish-Horowicz and Pinchin, 1987; Ingham and Gergen, 1988; Carroll and Vavra, 1989; Klingler and Gergen, 1993; Jiménez et al., 1996). Repression between *h* and *run* has previously been proposed on the basis of their approximately reciprocal domains of expression (Ingham and Gergen, 1988; Kania et al., 1990; Jiménez et al., 1996; Frasch and Levine, 1987; Carroll and Vavra, 1989). Their stripes are roughly complementary at the blastoderm stage (Kania et al., 1990). In *h* mutant embryo (Jaynes and Fujioka, 2004), *run* expression expands and is

ectopically expressed (Ingham and Gergen, 1988; Carroll and Vavra, 1989).

In the major circuits (Table A.6), *h* is a critical repressor on all borders and in all circuits, except the posterior borders in circuit A2. In the parameter consensus analysis (Table A.15), there is very strong consensus of both classes of circuits toward *h* repression on *run*. Hence I conclude *h* repression on *run* in black as the first level regulation in the ensemble regulatory map (Fig. 4.1).

runt There is no specific conclusions found in the literature regarding *run* auto-activation.

In the major circuits (Table A.6), *run* is an essential auto activator on all borders except the stripe 2 posterior border in circuit A1, and a critical activator on the stripe 2, 5, and 6 anterior borders in circuit A1, and the stripe 1, 5, and 6 posterior borders in circuit A1. *run* is a critical auto activator in the circuit A2 except on the stripe 3 anterior border and the stripe 1 and 3 posterior borders. In the parameter consensus table (Table A.15), there is stronger consensus toward *run* auto-activation in the high priority set of the class A circuits. Based on the major circuits, I conclude *run* auto-activation in blue as the second level regulation in the ensemble regulatory map (Fig. 4.1).

ftz *ftz* was found to be a negative regulator of *run* in the late phase during the transition from 7 to 14 stripe patterns (Klingler and Gergen, 1993). In *ftz* mutant embryos (Klingler and Gergen, 1993), the pattern develops normally until the onset of gastrulation.

In the major circuits (Table A.6), *ftz* is a critical repressor on all anterior borders in circuit A1. In circuit A2, *ftz* is an essential repressor on all anterior borders except the stripe 2, and on the stripe 1 posterior border, it is also a critical repressor on the stripe 6 anterior border. *ftz* is an essential repressor on

all borders except the stripe 1 posterior border in circuit B1, and it is a critical repressor on all borders except the stripe 2 anterior border, and the stripe 1 and 6 posterior border. In the parameter consensus table (Table A.15), there is stronger consensus toward *ftz* repression on *run* in the class B circuits and in the high priority set of the class A circuits. I conclude *ftz* repression on *run* in blue as the second level regulation in the ensemble regulatory map (Fig. 4.1).

odd *odd* was found to be repressing *run* (Drean et al., 1998), in the late phase (Klingler and Gergen, 1993).

In the major circuits (Table A.6), *odd* is a critical repressor on the stripe 6, and an essential repressor on the stripe 1 posterior border. In circuit A1 and B1, however, there is no dependence on *odd*. In the parameter consensus table (Table A.15), there is stronger consensus toward *odd* repression in the class A circuits and the lower priority sets of the class B circuits, while there is consensus toward activation in the high priority set of the class B circuits.

B.3.4 *run* regulation by pair-rule genes summary

First level regulations (black) The first level *run* regulations by pair rule genes in black in Fig. 4.1, indicating interactions with high level consensus between circuits and literature. The interactions includes *h* repression on *run* and *eve* repression on *run* posterior borders.

In the literature (Table A.22), *h* repression on *run* is supported by Read et al. (1992); Jaynes and Fujioka (2004); Howard and Ingham (1986); Carroll and Scott (1986); Ish-Horowicz and Pinchin (1987); Ingham and Gergen (1988); Carroll and Vavra (1989); Klingler and Gergen (1993); Jiménez et al. (1996). Repression between *h* and *run* has previously been proposed on the

basis of their approximately reciprocal, complementary, domains of expression (Ingham and Gergen, 1988; Kania et al., 1990; Jiménez et al., 1996; Frasch and Levine, 1987; Carroll and Vavra, 1989). In *h* mutant embryo (Jaynes and Fujioka, 2004), *run* expression expands and is ectopically expressed (Ingham and Gergen, 1988; Carroll and Vavra, 1989; Klingler and Gergen, 1993). *eve* repression on *run* is supported by Manoukian and Krause (1992, 1993); Jaynes and Fujioka (2004); Ingham and Gergen (1988); Fujioka et al. (1996); Klingler and Gergen (1993). In *eve* mutant embryo (Jaynes and Fujioka, 2004), late *run* expression expands throughout the *eve* domain (Fujioka et al., 1995). Ectopic *eve* expression at high level was found to be repressing *run* (Manoukian and Krause, 1992).

In the major circuits (Fig. 4.4), *h* repression on *run* is supported by all circuits as a critical repressor. *eve* repression on *run* posterior borders is supported by circuit A2 as an essential repressor. In the parameter distribution analysis (Table A.15), *h* repression on *run* is supported by very strong consensus of both classes of circuits. There is, however, no clear consensus toward *eve* repression on *run*.

Second level regulations (blue) The second level *run* regulations by pair rule genes in blue in Fig. 4.1, indicating strong predictions made by circuits but may not be directly supported by literature. These interactions include *ftz* repression on *run* and *run* auto-activation.

In the literature (Table A.22), *ftz* repression on *run* is supported by Klingler and Gergen (1993), only during the transition from 7 to 14 stripe patterns. In *ftz* mutant embryos (Klingler and Gergen, 1993), the pattern develops normally until the onset of gastrulation. *run* auto-activation is not supported by

any specific reference in the literature. In *run* mutant embryos (Goto et al., 1989; Klingler and Gergen, 1993) and *hs-runt* ectopic expression (Tsai and Gergen, 1994), complex stripe-specific defects are observed.

In the major circuits (Fig. 4.4), *ftz* repression on *run* is supported by circuit A1 as a critical repressor, and by circuit A2 and B1 with stripe specific effects. *run* auto-activation is supported by circuit A1 and A2 as an essential and critical activator with complex stripe specific effects. In the parameter distribution analysis (Table A.15), *ftz* repression on *run* is supported by stronger consensus in the class B circuits and the high priority set of class A circuits. *run* auto-activation is supported by stronger consensus in the high priority set of class A circuits.

Fourth level regulations (cyan) The fourth level *run* regulations by pair rule genes in cyan in Fig. 4.1, indicating stripe specific pair rule cross regulations found in the circuits (only the critical regulators are shown in Fig. 4.1 to Fig. 4.7). The interactions include *eve* repression on the *run* stripe 1 posterior border, *odd* repression on the stripe 1 posterior border and stripe 6.

In the literature (Table A.22), in *eve* mutant embryo (Klingler and Gergen, 1993), the earliest pattern abnormality detectable is a ventral gap in the first stripe. When cellularization has progressed halfway, stripes 1 and 2 are closer together.

Fifth level regulations (green) The fifth level *run* regulations by pair rule genes in green in Fig. 4.1, indicating interactions in the circuits that are considered as minor (insignificant), indeterminable or irrelevant during analysis, but are asserted by literature. The interactions include *odd* repression on *run* and *eve* repression on *run* anterior borders.

In the literature (Table A.22), *odd* repression on *run* is supported by Drean et al. (1998) and in the late phase Klingler and Gergen (1993). In *odd* mutant embryos (Drean et al., 1998), all seven stripes of *run* are moderately repressed by ectopic Odd. This correlates with what appears to be a slight broadening and strengthening of the *run* stripes in *odd* mutant embryos.

In the major circuits (Fig. 4.4), there are only stripe specific effects found for *odd* repression on *run*. In the parameter distribution analysis (Table A.15), *odd* repression on *run* is supported by stronger consensus in the class A circuits and the lower priority sets of class B circuits.

B.4 *fushi-tarazu* regulation

B.4.1 *ftz* regulation by gap and maternal genes

ftz pattern was found to form correctly in all three primary pair-rule mutants (Yu and Pick, 1995). Primary pair-rule genes are more involved in the refinement rather than establishment phase of the *ftz* stripes.

run and *h* were found important for maintenance and refinement of the *ftz* pattern (Kania et al., 1990; Tsai and Gergen, 1995; Kosman and Small, 1997), their stripes overlap the anterior and posterior borders of each *ftz* stripe respectively, consistent with this hypothesis (Ingham and Gergen, 1988; Kania et al., 1990). However, the initial pattern of *ftz* stripes is correctly established in *h* and *run* mutant embryos (Ingham and Gergen, 1988; Yu and Pick, 1995), suggesting that these genes may only be important for maintaining and refining pattern. Thus, the initial *ftz* stripes may be regulated by aperiodic cues, which may include the gap genes (Yu and Pick, 1995).

bcd *bcd* was found to be repressing *ftz* in the anterior pole of the embryo (Yu and Pick, 1995; Vavra and Carroll, 1989).

In the major circuits (Table A.7), *bcd* only has biased, plateau, input on the anterior-embryo *ftz* stripes. In the parameter consensus table (Table A.16), the class B circuits are biased toward repression on *ftz*.

cad *cad* was found to be activating *ftz* (Dearolf et al., 1989a). The posterior *ftz* expression is drastically reduced in *cad* mutant embryos. Caudal binding site was also found required for the posterior expression in *ftz-lac*Z fusion constructs.

In the major circuits (Table A.7), *cad* is an essential repressor on the stripe 2 anterior border in circuit B1. There is no essential dependence on *cad* in circuit A1 and A2. In the parameter consensus table (Table A.16), both classes of circuits are biased toward repression on *ftz*.

hb *hb* was found repress *ftz* stripe 3 anterior border (Hülskamp et al., 1994). The *hb* PS4 stripe has been shown to be important for establishing the inter-stripe between *ftz* stripes 2 and 3.

In the major circuits (Table A.7), there is no essential dependence on *hb*. In the parameter consensus table (Table A.16), however, both classes of circuits are biased toward activation on *hb*.

Kr In *Kr* mutant embryo, *ftz* pattern was found to be strongly disrupted (Carroll and Scott, 1986; Ingham et al., 1986).

In the major circuits (Table A.7), *Kr* is a critical and essential activator on *ftz* stripe 4 anterior border in circuit A1 and B1 respectively. However in circuit A2 *Kr* is in a reducible set on the stripe 4 anterior border. In the parameter consensus table (Table A.16), both classes of circuits have strong consensus toward *Kr* activation on *ftz*. Hence I conclude *Kr* activation on the stripe 4 anterior border in blue as the second level regulation in the ensemble regulatory map (Fig. 4.1).

gt *ftz* expression pattern is found strongly altered in *gt* mutant embryos (Carroll and Scott, 1986; Frasch and Levine, 1987).

In the major circuits (Table A.7), *gt* is an essential activator on *ftz* stripe 5 in circuit A1, and on *ftz* stripe 1 posterior border in circuit B1. However in circuit A2 there is no dependence on *gt*. In the parameter consensus table

(Table A.16), there is strong consensus of *gt* activation on *ftz* in both classes of circuits. I conclude *gt* activation on *ftz* stripe 5 in blue as the second level regulation in the ensemble regulatory map (Fig. 4.1).

kni *kni* was found to repress *ftz* (Frasch and Levine, 1987) on the stripe 3 posterior border (Carroll and Scott, 1986; Klingler and Gergen, 1993; Small et al., 1996; Kosman and Small, 1997).

In the major circuit A1 (Table A.7), *kni* is a critical activator on the stripe 4 anterior border, and an essential activator on the stripe 5. In circuit A2, *kni* is an essential activator on the stripe 5 posterior border, but in a reducible set for the stripe 4 anterior border. In circuit B1, however, there is no essential dependence on *kni*. In the parameter consensus table (Table A.16), there is significant consensus toward *kni* activation on *ftz* of both classes of circuits. Hence I conclude *kni* activation on the stripe 4 anterior border and the stripe 5 posterior border in magenta as the third level regulation in the ensemble regulatory map (Fig. 4.1).

tll There is no literature found here for *tll* regulation on *ftz* patterns.

In the major circuits (Table A.7), there is no essential dependence on *tll* regulation. In the parameter consensus table (Table A.16), however, there is consensus toward *tll* repression on *ftz*.

B.4.2 *ftz* regulation by gap and maternal genes summary

Second level regulations (blue) The second level *ftz* regulations by gap genes in blue in Fig. 4.1, indicating strong predictions made by circuits but may not be directly supported by literature. These interactions include *Kr*

activation on the stripe 4 anterior border and *gt* activation on the stripe 5.

In the literature (Table A.23), there is no specific conclusion for *Kr* activation on *ftz* stripe 4 anterior border in the literature. In *Kr* mutant embryos, the *ftz* pattern was found to be strongly disrupted (Carroll and Scott, 1986; Ingham et al., 1986). *ftz* expression patterns are compressed in *Kr* heterozygotes (Frasch and Levine, 1987); this region includes the third *eve* stripe through the fourth *ftz* stripe. There is no specific conclusion for *gt* activation on the stripe 5 in the literature. The *ftz* expression pattern is found to be strongly altered in *gt* mutant embryos (Carroll and Scott, 1986; Frasch and Levine, 1987). According to Klingler and Gergen (1993); Reinitz and Levine (1990), in *gt* mutant embryos, the *ftz* stripes 5 and 6 are fused.

In the major circuits (Fig. 4.5), *Kr* activation on the stripe 4 anterior border is supported by circuit A1 and B1 as a critical and essential activator respectively. *gt* activation on the stripe 5 is supported by circuit A1 as an essential activator. In the parameter distribution analysis (Table A.16), *gt* activation on *ftz* is supported by strong consensus of both classes of circuits. *Kr* activation on *ftz* is also supported by strong consensus of both classes of circuits.

Third level regulations (magenta) The third level of *ftz* regulations by gap genes in magenta in Fig. 4.1, indicating interactions predicted by circuits but may contradict to literature. The interactions include *kni* activation on the stripe 4 anterior border and *kni* activation on the stripe 5 posterior border.

In the literature (Table A.23), *kni* repression on *ftz* is supported by Frasch and Levine (1987). In *kni*– embryos, the third through sixth *ftz* expression stripes are fused into a single broad band (Carroll and Scott, 1986).

In the major circuits (Fig. 4.5), *kni* activation on the stripe 4 anterior border is supported by circuit A1 as a critical activator. *kni* activation on the stripe 5 posterior border is supported by circuit A1 and A2 as an essential activator on the posterior border. In the parameter distribution analysis (Table A.16), *kni* activation on *ftz* is supported by significant consensus of both classes of circuits.

Sixth level regulations (yellow) The sixth level *ftz* regulations by gap genes in yellow in Fig. 4.1, indicating interactions supported by literature but are totally absent (do not have any input) in the circuits. These interactions include *hb* repression on the stripe 3 anterior border and *kni* repression on the stripe 3 posterior border.

In the literature (Table A.23), *hb* repression on the stripe 3 anterior border is supported by Hülskamp et al. (1994). In *hb* mutant embryos, *ftz* stripes 2 and 3 are fused Hülskamp et al. (1994). *kni* repression on the stripe 3 posterior border is supported by Carroll and Scott (1986); Klingler and Gergen (1993); Small et al. (1996); Kosman and Small (1997). In *kni* mutant embryo (Klingler and Gergen, 1993; Carroll and Scott, 1986), *ftz* stripe 3 fused to broad expression domain, there is also a posterior expansion of the reporter gene expression driven by the stripe 3 enhancer (Small et al., 1996). Different levels of ectopic *kni* expression (Kosman and Small, 1997) also caused disruptions of *ftz* stripes 2 and 3.

B.4.3 *ftz* regulation by pair-rule genes

eve *eve* was found to repress *ftz* (Frasch et al., 1988; Tsai and Gergen, 1995; Manoukian and Krause, 1993; Parkhurst and Ish-Horowicz, 1991; Ingham and

Gergen, 1988; Jiménez et al., 1996), at intermediate to higher level of *eve* expression (Fujioka et al., 1995; Jaynes and Fujioka, 2004; Manoukian and Krause, 1992), on the anterior border (Ish-Horowicz et al., 1989). *eve* may also activate *ftz*, maintaining *ftz* stripe 1, in the earlier phase (Yu and Pick, 1995; Carroll and Scott, 1986; Carroll and Vavra, 1989; Frasch and Levine, 1987; Frasch et al., 1988; Lawrence and Johnston, 1989).

In the major circuits (Table A.8), *eve* is a critical repressor on all borders in both circuit A1 and B1. In circuit A2, however, *eve* is in a reducible set. In the parameter consensus table (Table A.16), there is strong consensus toward *eve* repression on *ftz* of both classes of circuits. Given the above results I conclude *eve* repression on *ftz* in black as the first level regulation in the ensemble regulatory map (Fig. 4.1).

hairy *h* was found to repress *ftz* in the late refinement and maintenance phase (Carroll and Vavra, 1989; Jaynes and Fujioka, 2004; Howard and Ingham, 1986; Howard et al., 1988; Carroll and Scott, 1986; Carroll et al., 1988; Carroll, 1990; Ish-Horowicz and Pinchin, 1987; Ingham and Gergen, 1988; Yu and Pick, 1995; Dearolf et al., 1990; Tsai and Gergen, 1995; Manoukian and Krause, 1993; Hiromi and Gehring, 1987; Frasch and Levine, 1987; Frasch et al., 1988; Lardelli and Ish-Horowicz, 1993).

In the major circuits (Table A.8), *h* is an essential activator on the stripe 3 posterior and stripe 5 posterior border in circuit A1. There is however no essential dependence on the other borders and in the other circuits. In the parameter consensus analysis (Table A.16), there is strong consensus toward *h* repression on *ftz* in the class B circuits, but only mild consensus of the class A circuits.

runt *run* was found to be activating *ftz* (Tsai and Gergen, 1995; Manoukian and Krause, 1993; Yu and Pick, 1995; Ingham et al., 1988; Frasch and Levine, 1987; Swantek and Gergen, 2004).

In the major circuits (Table A.8), *run* is an essential activator on all *ftz* borders in circuit B1, and a critical activator on the stripe 5 in circuit B1. In the other circuits, however, *run* is not required. In the parameter consensus table (Table A.16), there is strong consensus toward *run* activation on *ftz* of both classes of circuits. I conclude *run* activation on *ftz* in black as the first level regulation in the ensemble regulatory map (Fig. 4.1).

ftz *ftz* was found to auto-activate itself in the late refinement and maintenance phase (Pick et al., 1990; Hiromi et al., 1985; Hiromi and Gehring, 1987; Ish-Horowicz et al., 1989; Schier and Gehring, 1992; Tsai and Gergen, 1995). *ftz* protein was found to directly bind and regulate expression of its own gene. According to Riddihough and Ish-Horowicz (1991), in contrast to the extensive promoters of the primary pair-rule genes, *ftz* includes a small 600-bp "zebra" regulatory element that suffices to drive seven-striped expression of a *lac*Z reporter gene (Hiromi et al., 1985; Hiromi and Gehring, 1987; Dearolf et al., 1989b).

In the major circuits (Table A.8), however, there is no essential dependence on *ftz*. *ftz* is in a reducible set in circuit A2. In the parameter consensus table (Table A.16), there is minor consensus toward *ftz* auto-repression in certain sets of circuits.

odd *odd* was found to repress *ftz* (Jaynes and Fujioka, 2004; Manoukian and Krause, 1993), on the posterior edge (Mullen and DiNardo, 1995). *odd* may also activate *ftz* before and in the beginning of cellularization, while repressing

ftz in the late phase (Drean et al., 1998; Manoukian and Krause, 1992).

In the major circuits (Table A.8), *odd* is a critical activator on all borders in circuit A2, and an essential activator in circuit B1, especially on the stripe 4 anterior and stripe 5 anterior borders. While in circuit A1, *odd* is an essential repressor. In the parameter consensus table (Table 3.4), there is mild consensus toward *odd* activation on *ftz* in the higher priority sets of the class B circuits. Given the contradicting results, I conclude *odd* repression on *ftz* posterior borders in magenta as the third level regulation in the ensemble regulatory map (Fig. 4.1).

B.4.4 *ftz* regulation by pair-rule genes summary

First level regulations (black) The first level of *ftz* regulations by pair rule genes in black in Fig. 4.1, indicating interactions with high level consensus between circuits and literature, include *eve* repression on *ftz* and *run* activation on *ftz*.

In the literature (Table A.24), *eve* repression on *ftz* is supported by Frasch et al. (1988); Tsai and Gergen (1995); Manoukian and Krause (1993); Parkhurst and Ish-Horowicz (1991); Ingham and Gergen (1988); Jiménez et al. (1996), at intermediate to higher level of *eve* expression (Fujioka et al., 1995; Jaynes and Fujioka, 2004; Manoukian and Krause, 1992), and on the anterior border (Ish-Horowicz et al., 1989). Ectopic *eve* expression was found to repress gene *ftz* (Manoukian and Krause, 1992, 1993). *run* activation on *ftz* is supported by Tsai and Gergen (1995); Manoukian and Krause (1993); Yu and Pick (1995); Ingham et al. (1988); Frasch and Levine (1987); Swantek and Gergen (2004). In *run* mutant embryo (Frasch and Levine, 1987; Manoukian and Krause, 1993; Ingham and Gergen, 1988), there is a premature narrowing, and loss, of the

ftz expression stripes. According to Jaynes and Fujioka (2004), in *run* mutant embryo, relatively narrow and weak *ftz* expression were observed (Carroll and Scott, 1986). In *hs-run* ectopic expression experiment from Manoukian and Krause (1993); Tsai and Gergen (1995, 1994), expression of the *ftz* stripes widened dramatically.

In the major circuits (Fig. 4.5), *eve* repression on *ftz* is supported by circuit A1 and B1 as a critical repressor on all *ftz* borders. *run* activation on *ftz* is supported by circuit B1 as an essential activator on all borders. In the parameter distribution analysis (Table A.16), *eve* repression on *ftz* is supported by strong consensus of both classes of circuits. *run* activation on *ftz* is also supported by strong consensus of both classes of circuits.

Third level regulations (magenta) The third level *ftz* regulations by pair rule genes in magenta in Fig. 4.1, indicating interactions found by circuits but may contradict to the literature. The interactions include *odd* repression on the posterior *ftz* borders.

In the literature (Table A.24), *odd* repression on *ftz* is supported by Jaynes and Fujioka (2004); Manoukian and Krause (1993), particularly on the posterior edge (Mullen and DiNardo, 1995). *odd* may also activate *ftz* before and in the beginning of cellularization, while repressing *ftz* in the late phase (Drean et al., 1998; Manoukian and Krause, 1992). *ftz* stripes fail to narrow properly in *odd* mutant embryos (Mullen and DiNardo, 1995).

In the major circuits (Fig. 4.5), *odd* repression on the posterior *ftz* borders is supported by circuit A1 as an essential repressor. While *odd* activation on *ftz* is supported by circuit A2 as a critical activator and by circuit B1 as an essential activator. In the parameter distribution analysis (Table A.16), there

is more consensus toward activation in the class B circuits.

Fourth level regulations (cyan) The fourth level *ftz* regulations by pair rule genes in cyan in Fig. 4.1, indicating stripe specific pair rule cross regulations found in the circuits (only the critical regulators are shown in Fig. 4.1 to Fig. 4.7). The interactions include *h* activation on the stripe 3 posterior border, *odd* repression on the stripe 4 anterior border, *odd* repression on the stripe 5 anterior border, *h* activation on the stripe 5 posterior border and *run* activation on the stripe 5.

In the major circuits (Fig. 4.5), *h* activation on the stripe 3 posterior border and the stripe 5 posterior border are supported by circuit A1 as essential activators. *odd* repression on the stripe 4 anterior border and the stripe 5 anterior border are supported by circuit B1 as essential activators. *run* activation on the stripe 5 is supported by circuit B1 as critical activators.

Fifth level regulations (green) The fifth level *ftz* regulations by pair rule genes in green in Fig. 4.1, indicating interactions in the circuits that are considered as minor (insignificant), indeterminable or irrelevant during analysis but are supported by literature. These interactions include *ftz* auto-activation, *h* repression on *ftz* and *odd* repression on the anterior *ftz* borders.

In the literature (Table A.24), *ftz* auto-activation in the late refinement phase is supported by Kauffman and Goodwin (1990); Pick et al. (1990); Hiromi et al. (1985); Hiromi and Gehring (1987); Ish-Horowicz et al. (1989); Schier and Gehring (1992); Tsai and Gergen (1995). *ftz* protein was found to directly bind and regulate expression of its own gene. According to Riddihough and Ish-Horowicz (1991), in contrast to the extensive promoters of the primary pair-rule genes, *ftz* includes a small 600-bp "zebra" regulatory element that

suffices to drive seven-striped expression of a *lac*Z reporter gene (Hiromi et al., 1985; Hiromi and Gehring, 1987; Dearolf et al., 1989b). *h* repression on *ftz* in the late refinement phase is supported by Carroll and Vavra (1989); Jaynes and Fujioka (2004); Howard and Ingham (1986); Howard et al. (1988); Carroll and Scott (1986); Carroll et al. (1988); Carroll (1990); Ish-Horowicz and Pinchin (1987); Ingham and Gergen (1988); Yu and Pick (1995); Dearolf et al. (1990); Tsai and Gergen (1995); Manoukian and Krause (1993); Hiromi and Gehring (1987); Frasch and Levine (1987); Frasch et al. (1988); Lardelli and Ish-Horowicz (1993). In *h* mutant embryo (Howard and Ingham, 1986; Carroll and Scott, 1986; Ish-Horowicz and Pinchin, 1987; Ingham and Gergen, 1988; Carroll and Vavra, 1989; Tsai and Gergen, 1995), *ftz* was found broadened and ectopically expressed. Ectopic *h* expression suppresses *ftz* expression (Howard and Ingham, 1986; Carroll and Scott, 1986; Ingham and Gergen, 1988; Carroll and Vavra, 1989; Lardelli and Ish-Horowicz, 1993).

In the parameter distribution analysis (Table A.16), *h* repression on *ftz* is supported by strong consensus in the class B circuits, but only mild consensus of the class A circuits.

B.5 *odd-skipped* regulation

B.5.1 *odd* regulation by gap and maternal genes

No literature were found here for gap genes regulation on *odd* pattern. The following is only based on circuitry results.

bcd In the major circuits (Table A.9), *bcd* only has biased, plateau, input on the anterior-embryo *odd* stripes. Hence it is not essential, slope determining, for *odd* border formation in the dynamical model. In the parameter consensus table (Table 3.4), both classes of circuits are biased toward activation on *odd*.

cad In the major circuits (Table A.9), *cad* has small biased, near plateau, input on the posterior-embryo *odd* stripes. Hence it is also not essential, slope determining, for *odd* border formation in the dynamical model. In the parameter consensus table (Table 3.4), both classes of circuits are biased toward repression on *odd*.

hb In the major circuits (Table A.9), *hb* is an essential activator for the stripe 2 posterior border in circuit A1. In circuit A2, however, *hb* is not required, and there is no essential dependence on *hb* in circuit B1. In the parameter consensus table (Table 3.4), both classes of circuits have consensus toward *hb* activation on *odd*. Hence I conclude *hb* activation on the *odd* stripe 2 posterior border in magenta as the third level regulation in the ensemble regulatory map (Fig. 4.1).

Kr In the major circuit A1 (Table A.9), *Kr* is a critical activator for the stripe 2 anterior border. *Kr* is also an essential activator for the stripe 4. In

circuit A2 *Kr* is not required, and there is no essential dependence on *Kr* in circuit B1. In the parameter consensus table (Table 3.4), both class A and class B circuits have stronger consensus toward activation on *odd*. I conclude *Kr* repression on the stripe 2 anterior border in blue as the second level regulation, and *Kr* repression on stripe 4 in magenta as the third level regulation in the ensemble regulatory map (Fig. 4.1).

gt In all three major circuits (Table A.9), *gt* is an essential activator on the stripe 1 posterior border. In both circuit A1 and A2, *gt* is a critical activator on the stripe 6 posterior border. *gt* is also a critical activator for the stripe 5 posterior border and an essential activator for the stripe 5 anterior border in circuit A1. *gt* is an essential activator for the stripe 5 posterior border in circuit A2. In the parameter consensus table (Table 3.4) there is strong consensus toward *gt* activation on *odd* of both classes of circuits. From the circuitry results I put *gt* activation on the stripe 1 posterior border and the stripe 5 in blue as the second level regulation, also activation on the stripe 6 posterior border in black as the first level regulation in the ensemble regulatory map (Fig. 4.1).

kni In the major circuit A1 (Table A.9), *kni* is a critical activator for the stripe 4 anterior border and the stripe 5 posterior border. In circuit A2, *kni* is an essential activator for the same borders of the stripe 4 anterior border and the stripe 5 posterior border. In the parameter consensus table (Table 3.4), there is strong consensus toward *kni* activation on *odd* in both class A and class B circuits. I conclude *kni* activation on the stripe 4 anterior border in black as the first level regulation, and activation on the stripe 5 posterior border in blue as the second level regulation in the ensemble regulatory map (Fig. 4.1).

tll In the major circuits (Table A.9), *tll* only has biased, plateau, input on *odd*, hence it is not essential, slope determining in the dynamical model. In the parameter consensus table (Table 3.4), there is strong consensus toward *tll* activation on *odd* in the class B circuits.

B.5.2 *odd* regulation by gap and maternal genes summary

First level regulations (black) The first level, high consensus, *odd* regulations by gap genes in black in Fig. 4.1 include *kni* activation on the stripe 4 anterior border and *gt* activation on the stripe 6 posterior border.

In the major circuits (Fig. 4.6), *kni* activation on the stripe 4 anterior border is supported by circuit A1 as a critical activator and by circuit A2 as an essential activator. *gt* activation on the stripe 6 posterior border is supported by circuit A1 and A2 as a critical activator. In the parameter distribution analysis (Table 3.4), both *kni* activation on *odd* and *gt* activation on *odd* are supported by strong consensus of both classes of circuits.

Second level regulations (blue) The second level *odd* regulations by gap genes in blue in Fig. 4.1 indicating strong predictions made by circuits but may not be directly supported by literature, which include *gt* activation on the stripe 1 posterior border, *Kr* activation on the stripe 2 anterior border, *gt* activation on the stripe 5 and *kni* activation on the stripe 5 posterior border.

In the major circuits (Fig. 4.6), *gt* activation on stripe 1 posterior border is supported by all three major circuits as an essential activator. *Kr* activation on the stripe 2 anterior border is supported by circuit A1 as a critical activator. *gt* activation on the stripe 5 anterior border is supported by circuit A1 as an

essential activator, and activation on the stripe 5 posterior border is supported by both circuit A1 and A2 as a critical and essential activator respectively. *kni* activation on the stripe 5 posterior border is supported by both circuit A1 and A2 as a critical and an essential activator respectively. In the parameter distribution analysis (Table 3.4), *Kr* activation on *odd* is supported by strong consensus of both classes of circuits.

Third level regulations (magenta) The third level of *odd* regulations by gap genes in magenta in Fig. 4.1 indicate interactions found by circuits but may contradict to the literature. The interactions include *hb* activation on the stripe 2 posterior border and *Kr* activation on the stripe 4.

In the major circuits (Fig. 4.6), *hb* activation on the stripe 2 posterior border is supported by circuit A1 as an essential activator. *Kr* activation on the stripe 4 is supported by circuit A1 as an essential activator. In the parameter distribution analysis (Table 3.4), *hb* activation on *odd* is supported by significant consensus of both classes of circuits.

B.5.3 *odd* regulation by pair-rule genes

eve *eve* was found to be repressing *odd* (Jaynes and Fujioka, 2004; Fujioka et al., 1995; Manoukian and Krause, 1992; Kobayashi et al., 2001). Ectopic expression of *eve* in *hs-eve* embryo rapidly repressed *odd* (Manoukian and Krause, 1992).

In all three major circuits (Table A.10), *eve* is a critical repressor on *odd*. There are stripe specific effects in circuit A1 on the stripe 2, 6 anterior borders and stripe 1, 2, 5 posterior borders. In the parameter consensus analysis (Table 3.4), there is very strong consensus toward *eve* repression on *odd* in

both class A and class B circuits. Based on the above results I conclude *eve* repression on *odd* in black as the first level regulation in the ensemble regulatory map (Fig. 4.1).

hairy *h* was found to be repressing *odd* (Jiménez et al., 1996). In *h* mutant embryo, broadening of *odd* expression is observed.

In the major circuit A1 (Table A.10), *h* is an essential repressor on all borders, and a critical repressor on the stripe 6 anterior and stripe 5 posterior borders. In circuit A2 and B1, however, *h* is not required. In the parameter consensus analysis (Table 3.4), there is only consensus toward *h* repression on *odd* in the lower priority sets of class B circuits. Based on the above results I conclude *h* repression on *odd* in black as the first level regulation in the ensemble regulatory map (Fig. 4.1).

runt *run* was found to be repressing *odd* (Jaynes and Fujioka, 2004). In *run* null mutant embryos, primary *odd* stripes disappear essentially completely.

In the major circuit A2 (Table A.10), *run* is a critical activator on the stripe 5 and 6 anterior borders, and the stripe 3, 4 and 6 posterior borders. In circuit B1, *run* is a critical activator on all borders. In the parameter consensus analysis (Table 3.4), there is strong consensus toward *run* activation on *odd* in the higher priority set of circuits. Based on the above results I conclude *run* activation on *odd* in magenta as the third level regulation in the ensemble regulatory map (Fig. 4.1).

ftz *ftz* was found to be activating *odd* (Jaynes and Fujioka, 2004; Nasiadka and Krause, 1999). In a *ftz* mutant embryo, *ftz* is found to be required in order to maintain *odd* expression. In a *hs-ftz* embryo, *odd* is rapidly activated.

In the major circuit A1 (Table A.10), *ftz* is a critical activator for all borders. In the parameter consensus analysis (Table 3.4), there is significant consensus toward *ftz* activation on *odd* of both classes of circuits. Based on the above results I conclude *ftz* activation on *odd* in black as the first level regulation in the ensemble regulatory map (Fig. 4.1).

odd No literature were found here for *odd* auto-regulation.

In the major circuit A1 (Table A.10), *odd* is an essential auto-activator for all borders. In the parameter consensus analysis (Table 3.4), there is consensus toward *odd* auto-repression in the lower priority sets of the class A circuits, and moderate consensus toward auto-activation in the other sets of circuits. Hence I conclude *odd* auto-activation in magenta as the third level regulation in the ensemble regulatory map (Fig. 4.1).

B.5.4 *odd* regulation by pair-rule genes summary

First level regulations (black) The first level of *odd* regulations by pair rule genes in black in Fig. 4.1 indicating interactions with high level consensus between circuits and literature. The interactions include *eve* repression on *odd*, *h* repression on *odd* and *ftz* activation on *odd*.

In the literature (Table A.25), *eve* repression on *odd* is supported by Jaynes and Fujioka (2004); Fujioka et al. (1995); Manoukian and Krause (1992); Kobayashi et al. (2001). In *eve* mutant embryo, *odd* expression remains from the anterior-most cells of each Ftz-stripe (Jaynes and Fujioka, 2004). Ectopic expression of *eve* in *hs-eve* embryo also rapidly repressed *odd* (Manoukian and Krause, 1992). *h* repression on *odd* is supported by Jiménez et al. (1996). In *h* mutant embryo, broadening of *odd* expression is observed. *ftz* activation on

odd is supported by Jaynes and Fujioka (2004); Nasiadka and Krause (1999). In *ftz* mutant embryo, *ftz* is found required to maintain *odd* expression. In *hs-ftz* embryo, *odd* is rapidly activated.

In the major circuits (Fig. 4.6), *eve* repression on *odd* is supported by all three major circuits as a critical repressor. *h* repression on *odd* is supported by circuit A1 as an essential repressor. *ftz* activation on *odd* is supported by circuit A1 as a critical activator. In the parameter distribution analysis (Table 3.4), *eve* repression on *odd* is supported by strong consensus of both classes of circuits. *h* repression on *odd* is supported by consensus in the lower priority sets of class B circuits. *ftz* activation on *odd* is supported by significant consensus of both classes of circuits.

Third level regulations (magenta) The third level of *odd* regulations by pair rule genes in magenta in Fig. 4.1, indicating interactions found by circuits, but may contradict to literature. The interactions include *run* activation on *odd* and *odd* auto-activation.

In the literature (Table A.25), *run* repression on *odd* is supported by Jaynes and Fujioka (2004). In *run* null mutant embryo, primary *odd* stripes disappear essentially completely. There is no literature conclusions for *odd* auto-activation.

In the major circuits (Fig. 4.6), *run* activation on *odd* is supported by circuit B1 as a critical activator. *odd* auto-activation is supported by circuit A1 as an essential activator. In the parameter distribution analysis (Table 3.4), *run* activation on *odd* is supported by strong consensus of the higher priority set of circuits.

Fourth level regulations (cyan) The fourth level *odd* regulations by pair rule genes in cyan in Fig. 4.1, indicating stripe specific pair rule cross regulations found in the circuits (only the critical regulators are shown in Fig. 4.1 to Fig. 4.7). The interactions include *run* activation on the stripe 3 posterior border, *run* activation on the stripe 4 posterior border, *run* activation on the stripe 5 anterior border, *h* activation on the stripe 5 posterior border, *run* activation on the stripe 6 anterior border, *h* repression on the stripe 6 anterior border and *run* activation on the stripe 6 posterior border.